

Gel effect induced by mucilage in the pore space and consequences on soil physical properties

by

Mathilde Brax (MSc.)

from Paris, France

Accepted dissertation thesis for the partial fulfilment of the requirements for a

Doctor of Natural Sciences

Fachbereich 7: Natur- und Umweltwissenschaften

Universität Koblenz-Landau

Thesis examiners:

Prof. Dr. Gabriele E. Schaumann, Landau in der Pfalz, Germany

Prof. Dr. Andrea Carminati, Bayreuth, Germany

Prof. Dr. Paul Hallett, Aberdeen, United Kingdom

Date of the oral examination: 18.09.2019

DECLARATION

I hereby declare that I autonomously conducted the work presented in this PhD thesis entitled “Gel effect induced by mucilage in the pore space and consequences on soil physical properties”. All used assistances and involved contributors are clearly declared. This thesis has never been submitted elsewhere for an exam, as thesis or for evaluation in a similar context; to any department of this university or any scientific institution.

Landau in der Pfalz,

Place, Date

Signature

The following parts of this thesis are published or submitted for publications:

Chapter 2: Brax, M., Buchmann, C., Schaumann, G.E., (2017) *Biohydrogel induced soil–water interactions: how to untangle the gel effect? A review*. Journal of Plant Nutrition and Soil Science 180, 121–141.

The literature was reviewed by M. Brax except for sections 3.2, 3.3, 4.3.4 and 4.3.4, which were written by C. Buchmann. G. E. Schaumann reviewed the manuscript.

Chapter 3: Brax, M., Buchmann, C., Schaumann, G.E., (2018). *Effect of mucilage on water properties in the rhizosphere monitored by ¹H-NMR relaxometry*. Microporous and Mesoporous Materials, Proceedings of the 13th International Bologna Conference on Magnetic Resonance in Porous Media (MRPM13) 269, 47–50.

M. Brax conceived, designed and conducted the experiments. The model for the data analysis was planned by M. Brax and G. E. Schaumann. All authors contributed to the writing of the article.

Chapter 4: Brax, M., Köhne, M., Kroener, E., Schaumann, G. E. (2019): *Potential of NMR relaxometry to unravel the properties of mucilage in several pore sizes*. Geoderma 340, 269–278.

M. Brax conceived, designed and conducted the experiments except for the micro-CT analysis, which was conducted and analyzed by M. Köhne. All authors contributed to the writing of the article.

Chapter 5: Brax, M., Schaumann, G. E., Diehl, D. (2019): *Gel formation mechanism and gel properties controlled by Ca²⁺ in chia seed mucilage and model substances*. J. Plant Nutr. Soil Sci. 182, 92–103.

M. Brax conceived, designed and conducted most of the experiments. All authors contributed to the writing of the article.

Chapter 6:

Brax, M., Buchmann, C., Kenngott, K., Schaumann, G., Diehl, D., (accepted in Biogeochemistry): *Influence of the physico-chemical properties of root mucilage and model substances on the microstructural stability of sand.*

M. Brax conceived, designed and conducted most of the experiments except the yield stress measurements (by C. Buchmann) and the GC measurements (by K. Kenngott). All authors contributed to the writing of the article.

In addition, M. Brax contributed to the following publications:

Banfield, C., Brax M., Dippold M. A., Vetterlein D., (in preparation) *Chemical characterization of neutral and acidic carbohydrates in root mucilage of wheat, maize, lupin and bean seedlings.*

M. Brax carried out the chemical analysis of the sugars and contributed to the writing of the article.

Benard, P., Zarebanadkouki, M., Brax, M., Kaltenbach, R., Jerjen, I., Marone, F., Couradeau, E., Felde, V., Kaestner, A., Carminati, A. (2019) *Micro-hydrological niches in soils: how mucilage and EPS alter the biophysical properties of the rhizosphere and other biological hot spots.* Vadose Zone J. 18:180211. doi:10.2136/vzj2018.12.0211

M. Brax carried out the ESEM measurements and contributed to the writing of the article.

Buchmann, C., Steinmetz Z., Brax M., Peth S., Schaumann G. E., (submitted to Geoderma) *Effect of matric potential on biohydrogel-induced soil microstructural stability and soil-water interactions.*

M. Brax contributed to the writing of the article, in particularly the section about alginate swelling.

A mes parents, Catherine et Jacques...

ACKNOWLEDGEMENTS

It is beyond words to express my gratitude to my parents, Catherine and Jacques: because I owe it all to you. Many thanks! A very special gratitude goes also out to Sebastian for his unutterable support. Your love, care and happiness guide me through life.

I gratefully acknowledge Prof. Dr. Gabriele Ellen Schaumann, who believed in me since the beginning and led me patiently through all ups and downs of my work. She taught me to think, work and write scientifically. She supervised me intelligently, always pushing me to give the best of myself. The mutual trust and respect we have for each other was always a motivation and I appreciated enormously debating about new creative ideas with her. Despite her function as a vice-president she always found time when needed for discussions and always supported me.

I am thankful to Prof. Dr. Andrea Carminati for his creative and inspiring ideas over our joint project MUCILAGE. Thank you also for accepting being the external reviewer of my PhD thesis.

My special thanks to Angelika Holderle, whose door is always always open and who helped me through all administrative and organizational issues I had all these years. She lightens and enlightens everybody and is a very precious person.

I am also very grateful to Dr. Dörte Diehl for her unfailing support in the last stretch of my thesis. As an outstanding scientist she contributed to increase the quality of my work. She is a wonderful source of motivation in search for excellence.

I also thank Jun. Prof. Dr. Eva Kroener, whom I am happy to collaborate closely with since she arrived in Landau. We shared fruitful discussions about mucilage, pores, NMR, soil physics and more ethereal or bizarre subjects. As much as me she enjoys working on interdisciplinary interconnected concepts.

I am thankful to Dr. Christian Buchmann for his unfailing and patient support in the introduction, use and reparation of the various devices I used and also for our fruitful discussions concerning gels, soils, NMR, rheometry and all what goes beyond and underneath.

To my friends and colleagues Abd, Markus, Mina, Robin, Sandra and to the rest of the group, I thank you for making of my time at the university a stimulating and cheerful experience.

I gratefully acknowledge the technicians, especially Karin, Wolfgang and Silvia, whose skills and professional commitment as well as kindness enabled me to do good and reliable measurements.

I thank all my students and HiWis, who worked for and with me with great enthusiasm and who were an inspiring source for my work. I am also grateful to my siblings and friends who have supported me along the way.

Last but not least, I am very grateful to the Deutsche Forschungsgemeinschaft for providing me funding within the framework of MUCILAGE (SCHA849/20).

ABSTRACT

Water uptake, respiration and exudation are some of the biological functions fulfilled by plant roots. They drive plant growth and alter the biogeochemical parameters of soil in the vicinity of roots, the rhizosphere. As a result, soil processes such as water fluxes, carbon and nitrogen exchanges or microbial activity are enhanced in the rhizosphere in comparison to the bulk soil. In particular, the exudation of mucilage as a gel-like substance by plant roots seems to be a strategy for plants to overcome drought stress by increasing soil water content and soil unsaturated hydraulic conductivity at negative water potentials. Although the variations of soil properties due to mucilage are increasingly understood, a comprehensive understanding of the mechanisms in the pore space leading to such variations is lacking.

The aim of this work was to elucidate the gel properties of mucilage in the pore space, i.e. interparticulate mucilage, in order to link changes of the physico-chemical properties in the rhizosphere to mucilage. The fulfilment of this goal was confronted to the three following challenges: The lack of methods for *in situ* detection of mucilage in soil; The lack of knowledge concerning the properties of interparticulate mucilage; The unknown relationship between the composition and the properties of model substances and root mucilage produced by various species. These challenges are addressed in several chapters.

In a first instance, a literature review picked information from various scientific fields about methods enabling the characterization of gels and gel phases in soil. The variation of soil properties resulting from biohydrogel swelling in soil was named the gel effect. The combined study of water entrapment of gels and gel phases in soil and soil structural properties in terms of mechanical stability or visual structures proved promising to disentangle the gel effect in soil.

The acquired methodical knowledge was used in the next experiments to detect and characterize the properties of interparticulate gel. ^1H NMR relaxometry allows the non-invasive measure of water mobility in porous media. A conceptual model based on the equations describing the relaxation of water protons in porous media was developed to integrate the several gel effects into the NMR parameters and quantify the influence of mucilage on proton relaxation. Rheometry was additionally used to assess mucilage viscosity and soil microstructural stability and ESEM images to visualize the network of interparticulate gel. Combination of the results enabled to identify three main interparticulate gel properties: The spider-web effect restricts the elongation of the polymer chains due to the grip of the polymer network to the surface of soil particles. The polymer network effect illustrates the organization of the polymer network in the pore space according to the environment. The microviscosity effect describes the increased viscosity of interparticulate gel in contrast to free gel. The impact of these properties on soil water mobility and microstructural stability were investigated. Consequences on soil hydraulic and soil mechanical properties found in the literature are further discussed.

The influence of the chemical properties of polymers on gel formation mechanism and gel properties was also investigated. For this, model substances with various uronic acid content, degree of esterification and amount of calcium were tested and their amount of high molecular weight substances was measured. The substances investigated included pectic polysaccharides and chia seed mucilage as model polymers and wheat and maize root mucilage. Polygalacturonic acid and low-methoxy pectin proved as non-suitable model

polymers for seed and root mucilage as ionic interactions with calcium control their properties. Mucilage properties rather seem to be governed by weak electrostatic interactions between the entangled polymer chains. The amount of high molecular weight material varies considerably depending on mucilage's origin and seems to be a straight factor for mucilage's gel effect in soil. Additionally to the chemical characterization of the high molecular weight compounds, determination of their molecular weight and of their conformation in several mucilages types is needed to draw composition-property profiles. The variations measured between the various mucilages also highlight the necessity to study how the specific properties of the various mucilages fulfill the needs of the plant from which they are exuded.

Finally, the integration of molecular interactions in gel and interparticulate gel properties to explain the physical properties of the rhizosphere was discussed. This approach offers numerous perspectives to clarify for example how water content or hydraulic conductivity in the rhizosphere vary according to the properties of the exuded mucilage. The hypothesis that the gel effect is general for all soil-born exudates showing gel properties was considered. As a result, a classification of soil-born gel phases including roots, seeds, bacteria, hyphae and earthworm's exuded gel-like material according to their common gel physico-chemical properties is recommended for future research. An outcome could be that the physico-chemical properties of such gels are linked with the extent of the gel effect, with their impact on soil properties and with the functions of the gels in soil.

ZUSAMMENFASSUNG

Wasseraufnahme, Atmung und Exsudation sind biologische Schlüsselfunktionen der Wurzeln höherer Pflanzen. Sie steuern das Pflanzenwachstum, indem sie die biogeochemischen Parameter des Bodens in unmittelbarer Nähe der Wurzeln, der Rhizosphäre, verändern. Folglich sind Bodenprozesse wie beispielsweise Wasserflüsse, Kohlen- und Stickstoffaustausch oder mikrobielle Aktivitäten in der Rhizosphäre im Vergleich zu freiem Boden begünstigt. Insbesondere die Exsudation von Mucilage durch die Pflanzenwurzeln scheint ein wichtiger Mechanismus zu sein, um Trockenstress vorzubeugen. Durch diese gelartige Substanz wird bei negativen Wasserpotentialen sowohl der Bodenwassergehalt als auch die ungesättigte hydraulische Leitfähigkeit erhöht. Die Veränderung der Bodeneigenschaften durch Mucilage ist Gegenstand aktueller Forschung. Ein umfassendes Verständnis der Mechanismen im Porenraum der Rhizosphäre ist bisher allerdings noch unzureichend.

Ziel dieser Arbeit war die Aufklärung der Gel-Eigenschaften von Mucilage im Porenraum der Rhizosphäre, um Veränderungen der physiko-chemischen Eigenschaften der Rhizosphäre auf dieses interpartikuläre Mucilage zurückzuführen. Dabei stellten sich drei Herausforderungen: Zunächst einmal mangelte es an Methoden zur *in situ* Detektion von Mucilage im Boden. Außerdem fehlten detaillierte Kenntnisse bezüglich der Eigenschaften von interpartikulärem Mucilage. Desweiteren war die Beziehung zwischen der Zusammensetzung und den Eigenschaften von Modellsustanzen und wurzelstämmigem Mucilage verschiedener Spezies unbekannt. Diese Fragen werden in den verschiedenen Kapiteln der Arbeit thematisiert.

Zunächst erfolgte eine Literaturrecherche, um Informationen aus verschiedenen Wissenschaftsbereichen über Methoden zur Charakterisierung von Gelen und Gel-Phasen im Boden zusammenzustellen. Die Änderung von Bodeneigenschaften aufgrund vorhandener Biohydrogelphasen im Boden kann als „Gel-Effekt“ bezeichnet werden. Die kombinierte Studie von Wassereinschlüssen in Gelen und Boden-Gel-Phasen mit der Untersuchung struktureller Eigenschaften von Boden hinsichtlich der mechanischen Stabilität und visueller Strukturen, zeigte sich als vielversprechend, um den Gel-Effekt im Boden zu charakterisieren.

Das erworbene methodische Wissen wurde in den nächsten Untersuchungen angewendet, um die Eigenschaften von interpartikulären Gelen zu detektieren und zu charakterisieren. ¹H NMR Relaxometrie erlaubt die nicht-invasive Bestimmung der Wassermobilität in porösen Medien. Ein konzeptuelles Modell wurde aus Gleichungen entwickelt, welche die Proton-Relaxation in gelhaltigen porösen Medien beschreiben. Dieses Modell berücksichtigt den beschriebenen Gel-Effekt bei der Wahl der NMR Parameter und quantifiziert den Einfluss von Mucilage auf die Proton-Relaxation. Darüber hinaus wurde mithilfe von Rheometrie die Viskosität von Mucilage sowie die mikrostrukturelle Bodenstabilität bestimmt. Mittels Rasterelektronenmikroskopie wurde die Netzwerkstruktur von interpartikulärem Gel visualisiert. Die kombinierte Auswertung dieser Ergebnisse identifizierte drei wichtige Eigenschaften von interpartikulärem Gel: Der „Spinnennetz-Effekt“ schränkt die Dehnung der Polymerketten aufgrund der Verbindung zwischen dem Polymer Netzwerk und der Oberfläche von Bodenpartikeln ein. Der „Polymer-Netzwerk-Effekt“ veranschaulicht die Anordnung des Polymernetzwerks im Porenraum gemäß der räumliche Umgebung. Der „Mikroviskositäts-Effekt“ beschreibt die erhöhte Viskosität von interpartikulärem Gel im Vergleich zu freiem Gel. Die Auswirkungen dieser Eigenschaften auf die Wassermobilität und auf die mikrostrukturelle

Stabilität des Bodens wurden untersucht und daraus resultierende Konsequenzen für hydraulische und mechanische Eigenschaften des Bodens diskutiert.

Der Einfluss von den chemischen Eigenschaften von Polymeren auf Gel-Bildungsmechanismen und Gel-Eigenschaften wurde untersucht. Dafür wurden Modellschubstanzen mit verschiedenen Uronsäure-Gehalt, Veresterungsgrade und Calcium-Gehalt getestet und die Menge an Materialanteil mit hohem Molekulargewicht quantifiziert. Die untersuchten Modellschubstanzen waren verschiedenen Pektin Polymeren und Chia Samen Mucilage. Darüber hinaus wurde Mucilage aus Winterweizen und Mais Wurzeln isoliert und untersucht. Polygalakturonsäure und Niedermethyliertes Pektin erwiesen sich als nicht geeignete Modelpolymere für Samen und Wurzel mucilage, da ionische Wechselwirkungen mit Calcium ihre Eigenschaften dominieren. Die dem Mucilage zuzurechnenden Eigenschaften scheinen eher durch schwache elektrostatische Wechselwirkungen zwischen verstrickten Polymerketten beherrscht zu sein. Die Menge an Material mit hohem Molekulargewicht variiert deutlich, abhängig von dem Ursprung des Mucilages. Dies scheint ein bedeutender Faktor für den Gel-Effekt von Mucilage im Boden zu sein. Zusätzlich zu der chemischen Charakterisierung der hochmolekulargewichtigen Polymere ist die exakte Bestimmung der Molekularmassen und der Konformation in verschiedenen Mucilagesorten notwendig, um Zusammensetzungs-Eigenchafts-Profile aufzeichnen zu können. Die Abweichungen zwischen den verschiedenen Mucilagestypen, welche sich durch die Messungen ergeben, haben die Notwendigkeit weiterer Untersuchungen unterstrichen. Nur so lässt sich die Frage klären, wie die spezifischen Eigenschaften von verschiedenen Mucilagestypen auf die Bedürfnisse der Pflanze abgestimmt sind, der sie entstammen.

Schließlich wurde diskutiert, wie die Betrachtung von molekularen Wechselwirkungen im Gel und interpartikulären Gel-Eigenschaften das Verständnis über die physikalischen Eigenschaften der Rhizosphäre erweitert. Dieser Ansatz ist vielversprechend, um zum Beispiel der Wassergehalt oder die hydraulische Leitfähigkeit entsprechend die Eigenschaften vom exudierten Mucilage zu klären. Darüber hinaus liegt die Vermutung nahe, dass der Gel-Effekt allgemein für alle Bodenexsudate mit Gel-Charakter Gültigkeit besitzt. Eine Klassifizierung natürlicher Boden-Gel-Phasen einschließlich der von Wurzeln, Samen, Bakterien, Hyphen oder Regenwürmern exsudierten, gelartigen Materialien nach ihren gemeinsamen physiko-chemischen Gel-Eigenschaften wird für die zukünftige Forschung empfohlen. Als Ergebnis könnten die physiko-chemische Eigenschaften von solchen Gelen zum Gel-Effekt den Auswirkungen auf die Bodeneigenschaften und den Funktionen von den Gelen im Boden zugeschrieben werden.

TABLE OF CONTENTS

Declaration	1
Acknowledgements	4
Abstract	5
Zusammenfassung	7
Table of Contents	9
1. Introduction	10
1.1. Root exudation in the rhizosphere	10
1.2. Modulation of soil physical properties induced by mucilage gel properties	11
1.3. Necessity to clarify interparticulate gel properties	12
1.4. Water mobility measured with ¹ H NMR relaxometry as a tool to detect and characterize interparticulate gel	13
1.5. Use of model substances to investigate the properties of interparticulate mucilage	15
1.6. Objectives and structure of the dissertation	17
2. Biohydrogel induced soil-water interactions: how to untangle the gel effect?	21
3. Effect of mucilage on water properties in the rhizosphere monitored by ¹ H-NMR relaxometry	43
4. Potential of NMR relaxometry to unravel the properties of mucilage in several pore sizes	48
5. Gel formation mechanism and gel properties controlled by Ca ²⁺ in chia seed mucilage and model substances	59
6. Influence of the physico-chemical properties of root mucilage and model substances on the microstructural stability of sand	72
7. Synthesis and conclusions	94
7.1. Possibilities, limits and outlook of mucilage detection in soil with ¹ H NMR relaxometry	94
7.2. A stepwise approach to explain the gel effect: from the mucilage polymers to soil physical properties	95
7.3. Bringing together the three main interparticulate gel properties	98
7.4. Significance of the physico-chemical composition of mucilage on the rhizosphere microstructural and hydraulic properties	100
7.5. Soil-born gel phases, a strategy of nature?	102
8. References	104
9. Annexes	111
9.1. List of abbreviations	111
9.2. Picturing the network of “free” chia seed mucilage	111
9.3. Supporting information of chapter 4	112
10. Curriculum Vitae	117

1. INTRODUCTION

1.1. Root exudation in the rhizosphere

A range of key biological functions of plant roots such as water uptake, respiration and exudation considerably alter the biogeochemical parameters of soil in the vicinity of the roots, i.e. the rhizosphere (*Hinsinger et al.*, 2006). Soil processes involving water fluxes, carbon and nitrogen exchanges or microbial activity are accordingly enhanced in the rhizosphere in comparison to the bulk soil. Rhizosphere processes are also important drivers for plant growth, soil organic matter decomposition and nutrient release at the ecosystem scale (*Finzi et al.*, 2015). Still, a comprehensive understanding of these processes remains restricted as long as all significant mechanisms taking place in the pore space are not all resolved.

Hiltner was in 1904 pioneer in the rhizosphere research, as he identified it as the volume of soil around living roots influenced by root activity and shared with bacteria (*Hiltner*, 1904). Root activity comprehends root growth, water and nutrient uptake, respiration and rhizodeposition (*Gregory*, 2006). Root activity turns the soil-root interface in a pole of dynamic reactions, whose consequences are felt on a range of temporal and spatial scales (*Hinsinger et al.*, 2009). The size and shape of the rhizosphere are not definable due to the inherent complexity and diversity of plant root systems and rather consist of a gradient of chemical, physical and biological properties, which change both radially and longitudinally along the root (*McNear Jr.*, 2013). For example, volatile compounds released from roots affect soil up to tens of millimetres, whereas microbial populations and immobile compounds are found at a fraction of millimetre distant from the root (*Hinsinger et al.*, 2009).

Root exudation is part of the rhizodeposition process, which is a major source of soil organic carbon (*Haichar et al.*, 2014). Plants invest 5 to 21% of their photosynthetically-fixed carbon in root exudation (*Haichar et al.*, 2014). Root exudates can be categorized into secretions, which are actively released by the root, and diffusates, which are passively released due to osmotic differences between soil solution and cell (*Bais et al.*, 2006). The secretions include low molecular weight (LMW) and high molecular weight (HMW) material. LMW compounds comprehend organic acids, amino acids, sugar, proteins, phenolics and other secondary metabolites generally easily used by microorganisms (*Nguyen*, 2003). Several excellent reviews have been published recently and give an overview about the chemical diversity, the functions of LMW exudates and their interactions with the root microbiome (*Haichar et al.*, 2014; *Pieterse et al.*, 2016; *Sasse et al.*, 2018). HMW compounds consist of heterogeneous polysaccharides, distinct proteins and extracellular DNA released by root cap cells at the root tip and identified as root mucilage (*Oades*, 1978; *Sasse et al.*, 2018). The mucilaginous layer around the roots can expand in volume up to 1000-fold after exudation through water uptake (*Shannon and Steer*, 1984) and varies from 1 to 10 μm in thickness (*Oades*, 1978).

Root mucilage is suspected to fulfill several functions supporting the life cycle of plants. These include the lubrication of growing root tips (*McCully*, 1999; *Traoré et al.*, 2000), the exchange of ions between carboxyl groups and soil minerals (*Ghanem et al.*, 2010) or the immobilization of toxic metal cations (*Watanabe et al.*, 2008). Further, root mucilage is suggested to insure the perennity of root-soil contact (*McCully*, 1999), increase the stability of soil microaggregates (*Traoré et al.*, 2000), or protect roots from desiccation (*Carminati et al.*, 2010).

1.2. Modulation of soil physical properties induced by mucilage gel properties

Gel definition and gel properties of root mucilage

A gel is composed over 90% of water entrapped in a three-dimensional polymer network. Root mucilage attests typical gel properties, which include high water content, water holding capacity, shrinking and swelling and viscoelasticity (*Almdal et al.*, 1993). For example, both root mucilage of maize and lupin seedlings show a higher viscosity than water and a viscoelastic behavior at concentrations inferior to 1 wt% (*Read and Gregory*, 1997). Further, maize root mucilage is able to retain water up to a certain field capacity and to absorb water once dried (*McCully and Boyer*, 1997; *Read et al.*, 1999).

Modulation of soil physical properties attributed to mucilage gel properties...

The gel properties of root mucilage affect soil hydraulic properties in the rhizosphere: The increase of soil water content toward the roots in the rhizosphere of chickpea, white lupin and maize, even when the roots take up water, is attributed to the swelling properties and water holding capacity of root mucilage (*Carminati et al.*, 2010; *Moradi et al.*, 2011). After drying, the rewetting of the rhizosphere of lupin is delayed and then followed by an increase of the water content larger than in the bulk soil (*Carminati et al.*, 2010). This delay was explained by the presence of phospholipids, measured by *Read et al.* (2003) in root mucilage, which would decrease soil wettability after a period of drying. The increase of the water content was explained by the ability of mucilage to reswell once dried (*Carminati et al.*, 2010; *Hallett et al.*, 2003). Root mucilage may also affect soil water retention and local water fluxes in the rhizosphere. Chia seed mucilage amendment of a sandy soil increases its water holding capacity at any matric potentials (*Ahmed et al.*, 2014), which lets suppose a similar effect of root mucilage at the soil-root interface. Increasing concentrations of chia seed mucilage also decrease the saturated hydraulic conductivity of a sandy soil (*Kroener et al.*, 2014). This effect is primarily attributed to the higher viscosity of mucilage in comparison to water.

Root mucilage of maize also positively influences soil stability (*Traoré et al.*, 2000), as the viscosity and elasticity of mucilage increase the resistance to movement of any soil particles in contact with mucilage. Enhancement of soil stability promotes in the long term soil aeration, root growth, prevents soil erosion and thus improves soil structure (*Jones et al.*, 2009).

Viscosity, water retention capacity, shrinking and swelling ability are the gel properties of mucilage at the origin of complex and time-dependent processes in the rhizosphere as they affect root water uptake and relevant properties including water content, water fluxes and soil structural stability (*Carminati and Vetterlein*, 2013; *Kroener et al.*, 2014; *Kroener et al.*, 2015). Still, the modification of soil physical properties by mucilage results from several gel-induced mechanisms happening in the pore space.

... and explained by gel-induced mechanisms in the pore space

According to its porosity, the polymer network is suspected to create an additional matrix in the rhizosphere, which can therefore hold more water than the bulk soil upon negative matric potentials. The elasticity of the polymer network enables its swelling, and hydrogel swelling can increase maximal water content in soil and modify soil particle size. Indeed, swelling of released EPS and of soil organic matter (SOM) is suggested to induce changes in soil pore size

distributions (Jaeger *et al.*, 2006; Meyer *et al.*, 2018), although the mechanism is not clear. Being also able to swell, root mucilage may also affect soil pore sizes in the rhizosphere.

In general, the gluing of soil particles by hydrogel-forming polymers and the cementation of soil particles upon drying/remoistening events explain the additional soil stabilizing effects of hydrogels (Albalasmeh and Ghezzehei, 2014; Buchmann *et al.*, 2015; Liu *et al.*, 2009). The polymer network increases soil particle interconnectivity and interparticle forces as a function of the polymer properties (for example type and amount of functional groups).

Still, information is lacking concerning the supramolecular mechanisms leading to mucilage network formation. The organization of the mucilage network in the pore space, the variations of this network properties with various environmental conditions (plant specie or soil solution) and the variations of the pore size according to this network (extension, shrinking) are also unknown. Investigations on mucilage polymer network in the pore space are therefore necessary to link the macroscopic properties measured for the rhizosphere with mechanisms in the pore space attributed to mucilage.

1.3. Necessity to clarify interparticulate gel properties

Lack of methods to detect and characterize mucilage in situ

The lack of comprehensive knowledge on the spatial and temporal patterns of mucilage and on its physico-chemical properties in the rhizosphere represents a major bottleneck in our understanding of plant-water-soil interactions (Figure 1.1). One reason is the lack of available methods capable to detect and characterize the properties of interparticulate gel. In contrast to a free or bulk gel, which has no physical constraint, interparticulate gel is situated in the pore space and is limited by the pore walls.

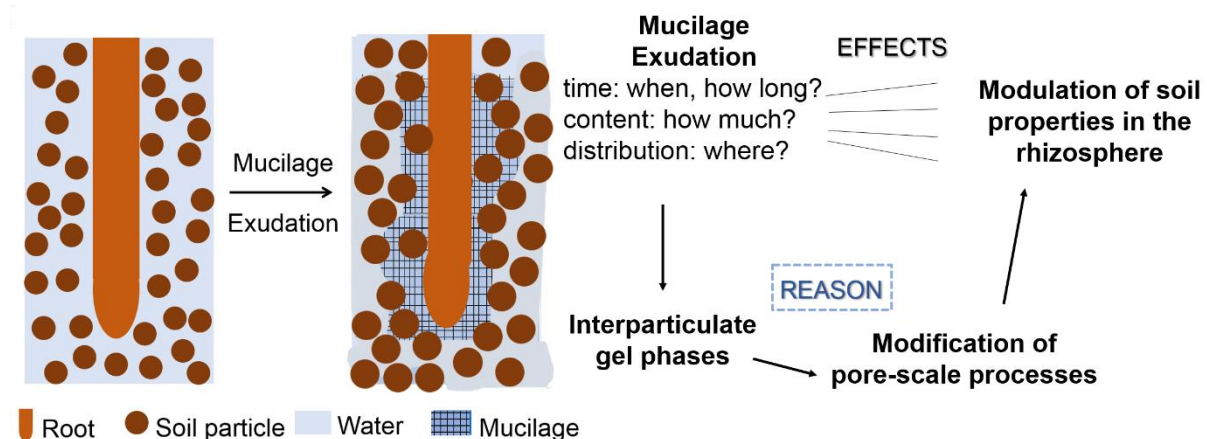


Figure 1.1. Schematic exudation of mucilage, its effects and their reasons.

A solution to detect root mucilage in the rhizosphere is the imaging of mucilage *in situ* with non-destructive three-dimensional techniques such as neutron imaging, magnetic resonance imaging and X-ray computer tomography. Recent progress in imaging techniques provide detailed images of water content, water fluxes and soil structure in the rhizosphere (Metzner *et al.*, 2015; Oswald *et al.*, 2015). Still, the detection of mucilage with these techniques faces a methodical problem: high water content and low carbon content result in low attenuation contrasts of mucilage in comparison to water. Infrared spectroscopy (Holz *et al.*, 2018) and combination of imaging techniques (van Veelen *et al.*, 2018) obtained encouraging results to measure the spatial

distribution of mucilage in the rhizosphere, but still require further development. To date, no experimental method allows to non-invasively and quantitatively characterize the spatio-temporal distribution of mucilage in the pore space of the rhizosphere, or to measure the properties of interparticulate gels.

Lack of knowledge about the properties of interparticulate gels

Usually, the properties of free gels such as water absorption, water retention or viscosity are measured to assess the properties of soil amended with gels, i.e. their swelling ratio, water retention or structural stability (*Andry et al.*, 2009; *Chenu and Roberson*, 1996; *Naveed et al.*, 2017). For example, the effect of xanthan, used as exopolysaccharide (EPS) analog, could be quantified by linear superposition of the non-treated soil and of the xanthan retention curves (*Rosenzweig et al.*, 2012). However, the properties of interparticulate gels differ from them of free gels: in most cases, dependencies are distinctly nonlinear, for example in the case of the dependency between hydrogel swelling and increase of water-holding capacity of sandy soils (*Kazanskii and Dubrovskii*, 1992).

Little literature has been published about the properties of interparticulate gels and how they vary in contrast to those of free gels. A previous study developed a theory of constrained swelling for gels subjected to the constraint of hard boundaries (*Marcombe et al.*, 2010). According to this theory, the constraint causes a field of stress in a gel, often leading to an inhomogeneous swelling. It is not clear how the hard boundary constraint may affect the properties of interparticulate mucilage.

Composition-property relationship of various root mucilage unknown

The relationships linking the chemical composition of exuded mucilage and its gel properties are of high interest to get a comprehensive understanding of mucilage exudation depending on the plant specie and the environment. Indeed, the amounts and types of rhizodeposits remain highly context specific (*Jones et al.*, 2009) and studies show that the gel properties of root mucilage vary in function of the plant specie (*Naveed et al.*, 2017; *Read and Gregory*, 1997). At the present time, the dependence on environmental conditions (type and age of the plant, time of the day, drying period ect...) on the amount of mucilage produced in soil remains unknown.

The chemical composition has already been characterized for several root mucilage: wheat and cowpea root mucilage (*Moody et al.*, 1988), maize root mucilage (*Bacic et al.*, 1986; *Osborn et al.*, 1999; *Read et al.*, 2003), rice root mucilage (*Chaboud and Rougier*, 1984). However, beyond their uncontemporary realization, these studies mostly focus on the sugar composition of root mucilage and do not consider the supramolecular mechanisms leading to gel formation. They also mostly discard the other possible components present in root mucilage, which potentially affect its gel properties such as the presence of phospholipids or proteins. Until now, the relationships between the chemical composition of mucilage and its physical gel properties have therefore remained poorly researched.

1.4. Water mobility measured with ^1H NMR relaxometry as a tool to detect and characterize interparticulate gel

Measurement of the water mobility

One solution to detect and characterize interparticulate mucilage in situ could be the measurement of the water mobility, which is different in interparticulate gel phases and pore water. Water mobility can be defined by the translational motion and by the rotational motion of water molecules (*Buchmann and Schaumann, 2017*), which can be restricted by molecular interactions (binding) or by physical barriers (within a pore) (*Götz and Hinrichs, 2008*). NMR relaxation has been developed over many years as a tool for the characterization of water mobility in porous media (*Bayer et al., 2010; Dunn et al., 2002*). In gels, interactions between the entrapped water molecules and the surrounding polymer chains alter the mobility of water (*Belton, 1997*). As an interparticulate gel (gel situated in a soil pore), the properties of water in interparticulate mucilage are different from those of water in soil pore. The method has two clear advantages in our field of study: first it is non-destructive and non-invasive, and second, water, being itself a primary constituent of mucilage, is also the primary probe.

The principle and applications of NMR relaxometry are exhaustively detailed in several excellent texts (*Callaghan, 1993; Callaghan et al., 1992; Kimmich, 2012*) and in later chapters, so that we give here only a short introduction to the method to understand the principles and foresee its potential concerning detection of mucilage in soil. Hydrogen nuclei align parallel and anti-parallel to an applied magnetic field B_0 according to a Boltzmann distribution, thus creating a bulk nuclear magnetisation. Short radiofrequency (RF) pulses transmitted to the samples at the Larmor frequency disturb the equilibrium Boltzmann population and cause the spins to flip into an angle to B_0 . The spins then relax back to their equilibrium orientation along B_0 within a coherent precession. This means that all nuclei turn together in phase, what results in a rotating macroscopic magnetisation that can be detected by a radio receiver. The magnetic field experienced by the nuclei does not confined to the applied laboratory field. It is enhanced by small local fields within the sample itself, for example due to neighbouring nuclei and unpaired electrons in chemical bonds. According to their chemical environment, different nuclei experience different local fields.

There are two principles of relaxation, each characterized by a relaxation time: T_1 and T_2 . T_2 is the spin-spin relaxation time and can be viewed as the time required for the nuclei initially precessing together in phase to lose coherence due to local magnetic fields in their environment. There is no net energy exchange between the nuclei and the lattice, thus no change in the distribution of the Boltzmann population. In contrast, T_1 is the spin-lattice relaxation time and characterizes the return of the nuclei alignment within the magnetic field and the recover of the thermal equilibrium with the lattice through exchange of energy. Measurement of both relaxation times provides information on molecular dynamics and water movement in gels over a wide range of length and time scales (*de Celis Alonso et al., 2010; Hills et al., 2000; Průšová et al., 2013*).

Recent investigations using the water mobility to detect and characterize interparticulate gels and their limits

Soil-water interactions are defined by the water distribution in the porous soil matrix and by the various bindings of water in the porous soil matrix, which for example differentiate clay-associated water from mineral soil pore water and from gel-associated water (*Buchmann and Schaumann, 2018; Schaumann and Bertmer, 2014*). ^1H -NMR relaxometry is widely used to measure water distribution and water binding in porous media (*Dunn et al., 2002; Kleinberg, 1999*). It allows to assess soil wetting kinetics (*Schaumann et al., 2005*), pore-size distribution in various soils (*Meyer et al., 2018*), influence of microbial activity (*Codd et al., 2011; Jaeger et al., 2006*) and soil organic matter swelling (*Bayer et al., 2010; Jaeger et al., 2010*). In recent studies,

soil samples were mixed with polyacrylic acid as a hydrogel-forming polymer and the water mobility was measured with ^1H NMR relaxometry. The NMR signal corresponding to polymer-associated water was successfully distinguished from the NMR signal of pure pore water (Buchmann *et al.*, 2015b, 2015a; Buchmann and Schaumann, 2017). The results allowed an estimation of the quantity of water trapped in the hydrogel and the expression of hydrogel swelling as function of clay content in soils with various clay contents. What is more, the structural stability of the soil samples could be linked with the content of polymer-associated water. Thus, ^1H -NMR relaxometry represents a promising method to detect and characterize mucilage in soil *via* the difference of mobility between pure water and mucilage water in soil pores.

Polyacrylic acid is a grateful polymer to lead NMR studies on polymer-amended soil due to a strong shift of the relaxation time to larger values corresponding to polymer-associated water (Buchmann and Schaumann, 2017). Until now, no study reports about the measurement of the water mobility in mucilage or mucilage amended soil, but ^1H NMR relaxometry has been used to detect biofilm in porous media. Biofilm consists in proteins, polymers and DNA material excreted by bacteria and forms a biohydrogel composed of more than 90% water (Sutherland, 2001). Yet, the NMR signal of water trapped in biofilm in porous media is not trivial to distinguish from the one of “pure” water trapped in porous media (Codd *et al.*, 2011; Sanderlin *et al.*, 2013). Several studies showed a decrease of the relaxation time due to the presence of biomacromolecules in biofilm (Codd *et al.*, 2011; Vogt *et al.*, 2013). Those enhance spin relaxation as protons bound to the polymers and dissolved organics rapidly exchange with free protons on the liquid molecules (Hills *et al.*, 1991). However, the shift of the relaxation time in biofilm in porous media is relatively low (Kirkland *et al.*, 2015), so that a quantitative evaluation of the amount of biofilm and of the concentration of the polymers has not been possible yet with ^1H NMR relaxometry. What is more, the mechanisms leading to shifts in relaxation times and the criteria allowing the distinction between biohydrogel water and non-biohydrogel water in soil pores have neither been fully identified until now. Although equations allow to measure the pore size distribution in soil by means of the relaxation time (Brownstein and Tarr, 1979; Godefroy *et al.*, 2001), the presence of biofilm or swellable organic matter in the pores unvalidate these equations (Meyer *et al.*, 2018).

1.5. Use of model substances to investigate the properties of interparticulate mucilage

Challenge to collect root mucilage

The little body of research providing data about the physico-chemical characterization of root mucilage is largely due to the difficulty to collect it in sufficient amounts. One collection method is the extraction of axenic root mucilage from seedlings by centrifugation (Zickenrott *et al.*, 2016) or by vacuum suction (Holz *et al.*, 2018) after aeroponic or hydroponic (Watanabe *et al.*, 2008) growth of the seedlings. Another method collects brace root mucilage (Ahmed *et al.*, 2015) or nodal root mucilage (Ahmed *et al.*, 2018) from several weeks-old maize plants. The aeroponic method yielded for maize 16 μg dry mucilage per root tip after 3 days germination (Zickenrott *et al.*, 2016), and the collection of root mucilage from grown-up maize plants provided around 0.5 mg of dry mucilage per root per day (Ahmed *et al.*, 2015). Both methods have different strengths and weaknesses, but both are time-intensive and provide small yields.

The use of model substances is therefore necessary to conduct experiments aiming at understanding fundamental physical mechanisms in soil, which require substantial amounts of mucilage. Still, to transfer the knowledge gained about the mechanisms, properties or processes

of soil amended with model substances to the rhizosphere, the model substances used must share chemical composition and/or physical properties with real root mucilage. Disparities between the properties of root mucilage and model substances should also be clear to assess how far the mechanisms, properties or processes found with the model substances are comparable to root mucilage. Polygalacturonic acid and chia seed mucilage have both been used to conduct studies on physical soil parameters requiring higher amount of mucilage material (Barré and Hallett, 2009; Kroener et al., 2014).

Polygalacturonic acid as a model substance for root mucilage

The choice of polygalacturonic acid (PGA) as a model substance relies on one side on the high content of uronic acid measured in maize root mucilage (Morel et al., 1986) and on the other side on the similarities of the patterns built by dried root mucilage and dried calcium-polygalacturonate on garlic roots (Gessa and Deiana, 1992, 1990). Out of these measurements, the authors concluded that the gel formation mechanism of root mucilage is similar to the one of PGA: the polymer chains are bound together by ionic bonds between calcium and deprotonated carboxylic groups (Figure 1.2). A range of studies use PGA as a model substance of root mucilage to investigate the effect of mucilage on soil microstructural stability, water transport and rewetting (Albalasmeh and Ghezzehei, 2014; Barré and Hallett, 2009; Czarnes et al., 2000; Peng et al., 2011; Zhang et al., 2008).

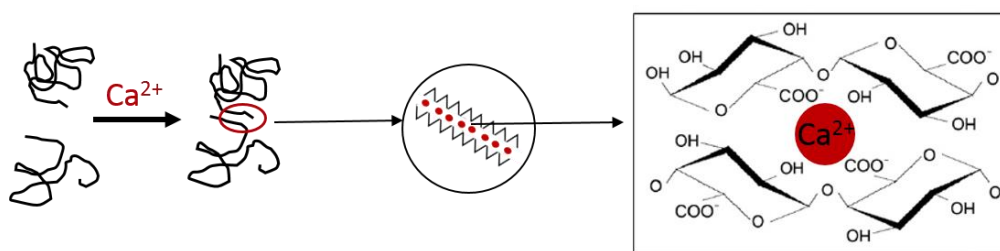


Figure 1.2. Idealized representation of calcium cross-linking of galacturonate residues in the egg-box model, modified from Kirtil et al. (2014).

Only, the viability of PGA as a model of root mucilage can be set into question, as well as the existence of one model of root mucilage for all species. For example, root exudates from rice contain 5 wt% (based on the total carbohydrate content) uronic acid (Bacilio-Jiménez et al., 2003), root mucilage from pea and from wheat consist of 13 wt% (Knee et al., 2001) and 11.5 wt% (Moody et al., 1988) uronic acid respectively, and 48 wt% uronic acid were measured for three days-old cress root mucilage (Ray et al., 1988). Thus, the content of uronic acid in root mucilage of different species is far below the 100 wt% of PGA and varies greatly depending on the species. The uronic acid content between various studies is also difficult to compare quantitatively as it depends on the method of collection, plant specie and age and biotic and abiotic external factors such as the presence of microorganisms or the nutrient status. For example, the uronic acid content measured in maize root mucilage varies from 3 wt% to 34 wt% (Bacic et al., 1986; Morel et al., 1986). Thus, the influence of various uronic acid content on the gel formation mechanism and gel properties of root mucilage needs to be clarified.

Chia seed mucilage as another model substance for root mucilage

Besides the use of a chemically defined polymer such as PGA, another approach is the use of chia seed mucilage as a model substance for root mucilage. Although the exudation mechanism of chia seed mucilage and its function for the plant are different from root mucilage (Capitani *et al.*, 2013; Muñoz *et al.*, 2012), it has comparable chemico-physical properties to root mucilage: Chia seed mucilage is mostly composed of polysaccharides, which are to around 20 wt% composed of uronic acids (Lin *et al.*, 1994; Timilsena *et al.*, 2015). Chia seed mucilage also has a high water content, viscous properties and reswells once dried (Capitani *et al.*, 2015; Goh *et al.*, 2016; Muñoz *et al.*, 2012). Thus, being easily producible and in great quantities, chia seed mucilage is an appropriate model to study the influence of the gel properties of root mucilage on soil properties (Ahmed *et al.*, 2014; Kroener *et al.*, 2018).

Still, it is not clear how far both types of mucilage are comparable as the viscosity of chia seed mucilage is clearly higher than the one of maize and wheat root mucilage for the same concentration (Naveed *et al.*, 2017). It is also not known how the gel properties of chia seed mucilage and root mucilage vary according to different chemical conditions. Also, the role of root mucilage chemistry on gel formation mechanism and gel properties is still to elucidate. It is further unclear how root mucilage with various gel properties differently affects soil properties.

1.6. Objectives and structure of the dissertation

Goals of the multidisciplinary project MUCILAGE

This PhD thesis is part of the multidisciplinary project MUCILAGE, financed by the German research foundation (DFG). MUCILAGE aims at understanding the mechanistic role of root mucilage for the regulation of water supply to plants. The main working hypothesis of MUCILAGE illustrated in Figure 1.3 is that root mucilage alters the physical properties of the rhizosphere and that these alterations affect the water flow across the rhizosphere.

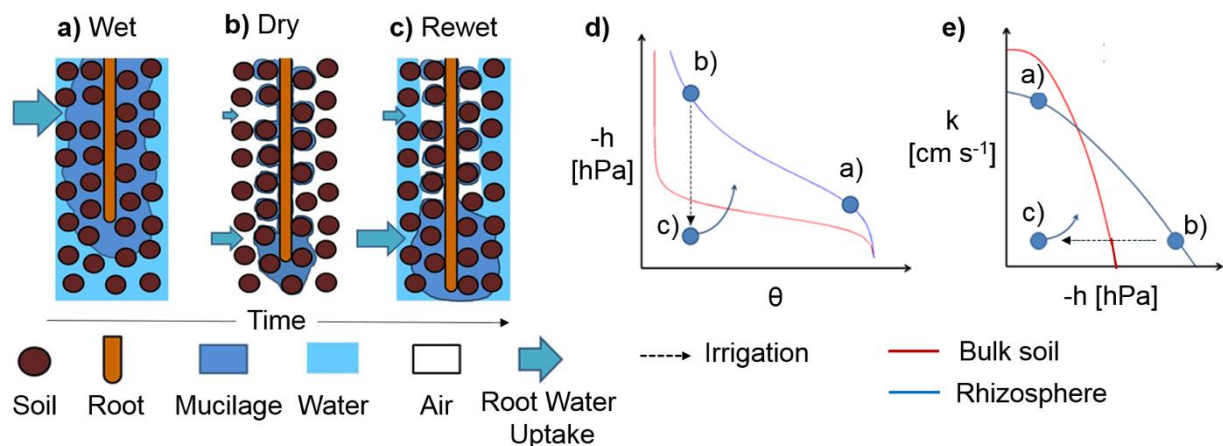


Figure 1.3. Illustration of the water distribution in the rhizosphere during a drying (a-b) and wetting (c) cycle, expected retention curve (d) and hydraulic conductivity (e) of the rhizosphere (blue) and the adjacent bulk soil (red) during a drying-wetting cycle. The figure is modified from the MUCILAGE DFG research proposal.

The expected effects of root mucilage in the rhizosphere are to increase water content θ at given soil water potential h (Figure 1.3 d) thanks to mucilage water holding capacity, and to decrease the saturated hydraulic conductivity k (Figure 1.3 e) thanks to mucilage's higher viscosity than water. During drying, the rhizosphere is expected to stay wetter than the adjacent bulk soil (Figure

1.3 a-b, d). Thus, the unsaturated hydraulic conductivity of the rhizosphere may become higher than that of the bulk soil at negative water potentials (Figure 1.3 e). As a result, mucilage would extend the range of water potentials in which roots and soil are hydraulically connected and would act as a “hydraulic bridge” in the rhizosphere. This way, mucilage exudation may be a plant strategy to attenuate the effects of drought. The hypothesized effects of mucilage on root water uptake are illustrated with blue arrows on Figure 1.3 (a-c).

Dried mucilage is also supposed to become hydrophobic and to make the rhizosphere temporary water repellent, what hinders the rewetting of the rhizosphere upon rehydration. After a drying/wetting cycle, root water uptake is supposed to be reduced at the root segments covered with dry old mucilage and to shift to young root segments covered with freshly exuded mucilage.

Three subprojects were designed to test these hypotheses and link stepwise the effect of mucilage properties on rhizosphere soil properties (main responsibility G.E. Schaumann, University Koblenz-Landau) (Figure 1.4 a-c), the hydraulic properties of soil-gel mixtures and of the rhizosphere (main responsibility A. Carminati, BayCEER) (Figure 1.4 c-d), and the interrelation between root water uptake and soil moisture dynamics in the rhizosphere (main responsibility D. Vetterlein, UFZ Halle) (Figure 1.4 d).

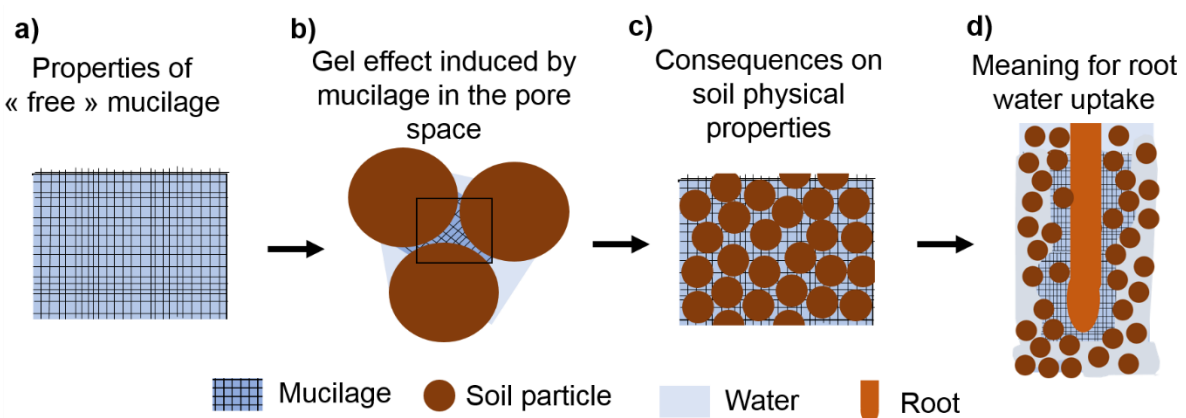


Figure 1.4. Research strategy of the MUCILAGE project: The characterization of mucilage gel properties (a) helps to elucidate the gel properties of mucilage in the pore space and to clear the underlying mechanisms (b), which lead to modulations of soil physical properties (c). With this information, relationships between root water uptake and moisture dynamics can be established (d). The stripes chosen for the representation of mucilage highlight the polymer network constituting mucilage.

The main objective of this PhD thesis was therefore to identify the gel properties of mucilage and how they induce changes in soil physical properties (Figure 1.4 a-c). This included the elucidation of mucilage gel formation, its supramolecular arrangement and the measurement of mucilage gel properties (Figure 1.4 a). The constraint of pore walls also needs clarification, as it may affect the properties of interparticulate gel in contrast to free gel, which has no physical constraint. As the gel leading to changes in soil physical properties is interparticulate and not free, the mechanisms in the pore space induced by interparticulate mucilage also needed to be clarified (Figure 1.4 b-c). With this PhD study, we intend to relate the findings of our partners about hydraulic processes with gel-induced mechanisms in the pore space.

Structure of the dissertation

The fulfilment of the goals set by MUCILAGE to this PhD thesis was confronted to three main challenges already introduced in subchapters 1.3, 1.4 and 1.5. They are the lack of methods to detect and characterize mucilage in situ, the lack of knowledge about the properties of interparticulate gels and the unknown relationship between the composition and the properties of model substances and root mucilage produced by various species. The next five chapters (2-6) of this dissertation aim at creating the knowledge needed to address these challenges. Chapter 7 brings the knowledge gained in the previous chapters together and proposes explanations, which clarify the properties of interparticulate gel in the pore space and their effect on soil physical properties.

In a first instance, the objective of this work was confronted to a lack of systematic methods to characterize gels and their mechanistic effect on soil properties, which we defined as the “gel effect”. This was surely due to the little awareness concerning the presence of gel phases in soil, and their ability to change soil properties by affecting processes at the pore-scale. In order to fill this gap, chapter 2 evaluated the potential of methods analysing gel properties developed by food research and polymer science for their application in soil science. Chapter 2 further critically reviews the currently available methods for their potential to characterize the spatio-temporal distribution of biohydrogel phases in soil. The gained knowledge served to orientate the approach and the choice of the methods to address the remaining challenges.

Water properties in soil pores are key factors affecting soil physical properties. Chapters 3 and 4 therefore focus on the development of ^1H NMR relaxometry to detect and to characterize mucilage gel phases in soil by measurement of the water mobility. The properties of interparticulate gel as a contrast to free gel are also considered. Chapter 3 aims at identifying the mechanisms leading to a shift of the relaxation rate for biohydrogel-associated water, considering the NMR parameters governing the relaxation rate in porous media defined by Brownstein and Tarr. Two-dimensional T_1 - T_2 measurements were conducted on pure mucilage and on artificial soils of several particle sizes mixed with one concentration of mucilage.

The quantitative distinction between biohydrogel-associated pore water and “pure” pore water is further developed in chapter 4. The effect of particle pore size and of mucilage concentration are particularly considered. A conceptual model integrating the “gel effect” on the NMR parameters identified in chapter 3 is proposed based on the equations of Brownstein and Tarr (1979). The results obtained with the two-dimensional T_1 - T_2 NMR experiments are combined with visual characterization of the samples with the electron microscope and image analysis from μCT images. The difficulty to create homogeneous and defined mucilage-amended samples to quantify the NMR parameters complicates the exact quantification of the several “gel effects” affecting the NMR parameters and is discussed in this chapter.

To fully assess the influence of mucilage on the properties of the rhizosphere, the physico-chemical properties of mucilage need to be characterized. Chapter 5 focuses on the control of the chemical properties of the polymer on the gel formation mechanism and on the resulting gel properties relevant for soil hydraulic properties, such as water content, water mobility or water holding capacity. Until now, the hypothesis has been accepted that the gel formation of mucilage is driven by cross-links between uronic acids and calcium and thus is comparable to the one of polygalacturonic acid (PGA). We put this hypothesis into question and investigate the role of the uronic acid and Ca^{2+} content on the gel formation mechanism and gel properties of chia seed mucilage and other model substances.

The relationship between the chemical and physical properties of several root mucilage and model substances are investigated in chapter 6, as well as how they variously affect soil structural stability. For this, several chemical conditions including free uronic acids, calcium adsorption and content of high molecular weight (HMW) material are measured for maize and wheat RM, chia seed mucilage and low-methoxy pectin. The control of these chemical conditions on the viscosity of the substances is investigated. Then, the influence of these substances on the microstructural stability of artificial soils is examined. Sand and glass beads were used as artificial soils with defined water content to measure the microstructural stability of the samples and to picture the structure of the interparticulate gel networks. Unfortunately, measurement of the water mobility at the time of the experiment was not possible due to a long-term technical failure of the NMR relaxometer.

The systematic study of fundamental mechanisms conducted in this thesis requires the use of artificial and homogeneous soil samples to limit the unavoidable heterogeneity present in disturbed soils. Glass beads and sand are therefore used as artificial soils to discard the influence of chemical interactions between the polymers and the particles, the swelling of soil particles or the non-controlled effect of soil solution. Although the artificial soil-gel systems studied in this thesis are simple in comparison to “real” soils and far from the reality, they permit the elucidation of several properties of interparticulate gel in the pore space. Those provide explanation for gel-induced changes of soil physical properties and help to understand further processes in the highly complex system which is the rhizosphere.

2. BIOHYDROGEL INDUCED SOIL-WATER INTERACTIONS: HOW TO UNTANGLE THE GEL EFFECT?

Review Article

Biohydrogel induced soil–water interactions: how to untangle the gel effect? A review

Mathilde Brax¹, Christian Buchmann¹, and Gabriele Ellen Schaumann^{1*}¹ University Koblenz-Landau, Institute for Environmental Sciences, Group of Environmental and Soil Chemistry, Fortstrasse 7, 76829 Landau, Germany

Abstract

Biohydrogels such as microbial exudates and root-derived mucilage are soil-born cross-linked polymers, able to form porous three-dimensional networks during water uptake. The gel effect is the variation of soil properties, such as soil hydrology and soil structural stability, resulting from biohydrogel swelling in soil. Conventionally, soil–water–hydrogel interactions are investigated by measuring soil bulk properties such as water retention curves and porosity, without further analyzing the effect of biohydrogel phases in soil on a quantitative basis. Therefore, the evaluation of advanced and novel methods for the characterization of biohydrogel phases in soil and soil–water–hydrogel interactions is necessary. This review evaluates currently available methods for their potential to analyze processes associated to the gel effect.

A promising approach to investigate the spatio-temporal distribution of biohydrogel phases in porous media is based on Nuclear Magnetic Resonance (NMR) such as ¹H-NMR relaxometry, as well as on imaging techniques such as Environmental Scanning Electron Microscopy (ESEM). Especially NMR techniques enable the identification of different water populations based on their differences in the relaxation, and thus the mobility of water molecules in biohydrogels and non-gel water in soil pores.

Rheology measures the flow behavior of biohydrogels, providing information on the structural behavior of the hydrogel network and its gelling mechanism. Soil rheology further quantifies the effect of the biohydrogel phases on the interactions between soil particles, and thus the impact on soil microstructural stability. However, rheology does not elucidate the spatio-temporal distribution and structural state of biohydrogel phases in soil.

All in all, a systematic combination of rheology, NMR and suitable imaging methods seems promising and necessary in order to elucidate the still widely unknown gel effect in soil.

Key words: rheology / imaging techniques / ¹H NMR relaxometry / diffusion coefficient / differential scanning calorimetry / biohydrogel / mucilage / polysaccharides

Accepted December 08, 2016

1 Introduction

Soil–water interactions determine the structural and hydrological properties of soil and are modulated by the soil water content and soil physicochemical properties such as mineral composition, grain size distribution and soil organic matter (SOM) content. Natural organic substances derived from vegetal residues in soil are around 95% composed of biopolymers, namely polysaccharides, lignin and proteins (Haider, 1999). They comprise microbial exudates (Flemming and Wingender, 2010), root-derived mucilage (Czames et al., 2000; Deng et al., 2015), and other naturally swellable organic structures, such as polysaccharidic biopolymer (e.g., starch or cellulose), being part of SOM (Paul, 2014; Kögel-Knabner, 2002). In the presence of water, these organic substances swell, which results in the formation of three-dimensional gel networks, able to take up water several times their own

weight (Czames et al., 2000; Kögel-Knabner, 2002; Schaumann et al., 2005). In this review, soil-born organic substances in their swollen state are referred to as “biohydrogels” and dried as “dry biopolymers”, while the term “hydrogel” comprises both synthetic and biohydrogels.

It is currently unknown to what extent biohydrogels are present in soil as separate biohydrogel phases. Part of the water in soil can be incorporated in biohydrogel phases between soil particles (Fig. 1). Such biohydrogel phases represent a microporous matrix in which, complementing the usual capillary forces, water is structured by interactions with the biohydrogel polymer chains. Soil biohydrogels are increasingly drawing scientific interest as their specific properties, such as water holding capacity, swelling, shrinking or viscoelasticity, are acknowledged to affect soil-relevant processes such as structural stability, water retention, and soil-



*Correspondence: G. E. Schaumann;
e-mail: schaummann@uni-landau.de

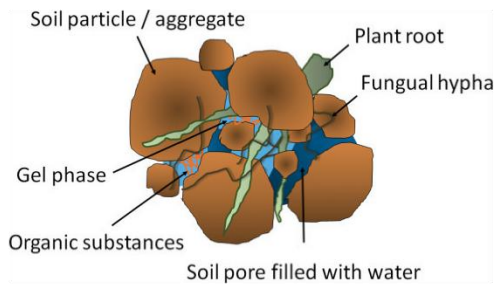


Figure 1: Schematic representation of gel phases (lighter areas between the soil particles) in saturated soil pores.

water repellency (Carminati, 2012; Rosenzweig et al., 2012; Kroener et al., 2014; Mizuta et al., 2015). Gel-induced variations of soil properties are defined here as the “gel effect”. Characterization of biohydrogels, e.g., their water holding capacity, is necessary to apprehend how they modify soil properties. For example, the effect of xanthan, used as exopolysaccharide (EPS) analog, on the hydraulic properties of sandy soils could be quantified by linear superposition of the original pure soil and the xanthan retention curves (Rosenzweig et al., 2012). Generally, swelling and wetting of biohydrogels are complex processes and they are expected to additionally induce changes in pore size distribution, sorbent properties of SOM and soil hydraulic properties (Schaumann et al., 2005). Drying is suspected to transport and deposit dry biopolymers towards the surface of particles, where they then can serve as gluing agent between soil particles and thus affect soil aggregation (Albalasmeh and Ghezzehei, 2014). As non-Newtonian fluids due to their viscoelastic nature, gels affect soils response to mechanical stress otherwise than minerals do (Buchmann and Schaumann, 2016).

Water stored in expanded biohydrogel structures may serve as water reservoir for plant growth, especially in regions with reduced water availability or periodic dry periods (Bouranis et al., 1995; Agaba et al., 2011; Mazen et al., 2015). Root, microbial and fungal biohydrogels have been demonstrated to stabilize the soil structure (Watt et al., 1994; Zhang et al., 2008; Barré and Hallett, 2009; Peng et al., 2011; Albalasmeh and Ghezzehei, 2014; Buchmann et al., 2014). This process is complex and depends on the nature of exudates (Barré and Hallett, 2009; Peng et al., 2011), clay content (Barré and Hallett, 2009; Buchmann et al., 2015), soil structure rigidity (Peng et al., 2011), amount of organic matter (Albalasmeh and Ghezzehei, 2014; Buchmann et al., 2015, 2014), and moisture dynamics (Peng et al., 2011). Swelling–shrinking of biohydrogels induced by moisture dynamics is supposed to increase bond strength between particles (Czarnes et al., 2000) and to influence a reorientation of soil particles and their gluing by organic structures (Peng et al., 2011; Buchmann et al., 2015).

Root biohydrogels, such as mucilage, have been suspected for a long time to increase the water-holding capacity of the rhizosphere (Morel et al., 1991; Young, 1995). Although recent studies have confirmed such effects of mucilage (Deng et al., 2015; Peng et al., 2011; Rosenzweig et al., 2012; Kroener et al., 2014), laboratory experiments revealed

a restricted rewetting of dried soil and model rhizosphere containing biological exudates as result of hydrophobic properties of root exudates in their dry state (Peng et al., 2011; Carminati, 2012; Ahmed et al., 2015). A first attempt to describe the rewetting of dry rhizosphere has been done by using a percolation model in which the impermeability of dry rhizosphere relies on a critical mucilage concentration, depending itself on the soil texture and the soil matric potential (Kroener et al., 2015). These results show the versatile effect of mucilage on soil and outline the need to characterize the properties of pure biohydrogels in order to forecast their behavior in soil. Once the properties of pure biohydrogels, such as swelling degree, viscosity, shrinking or reswelling ability, are well-characterized under different conditions, their behavior and their effects in soil can be better estimated.

The ability of hydrogels to modify soil physicochemical properties, such as water holding capacity, soil structural stability and thus soil productivity, has already been employed with the use of soil amendments such as synthetic hydrogels for agricultural purposes (Hedrick and Mowry, 1952; Johnson, 1984; Guilherme et al., 2015). Current approaches assessing interactions between synthetic hydrogels and the mineral soil body are based either on soil hydrological properties, e.g., its hydraulic conductivity or water storage (Al-Darby, 1996; Santos and Serralheiro, 2000; Andry et al., 2009; Levy and Warrington, 2015;), or on mechanical properties defined by the soil microstructure and its stability against external forces (Bai et al., 2010; Mamedov et al., 2007; Peng et al., 2011; Buchmann et al., 2015). Although these studies provide some information on the interaction between hydrogels and soil and their impact on soil properties, they rather focus on the effects on soil properties than on the processes governing these properties. As most limiting factor, the knowledge on synthetic hydrogel–soil interactions cannot be directly transferred to biohydrogel-rich soils, as many of the biohydrogels properties, such as the gelling mechanism or the types and amounts of functional groups, may differ fundamentally from the ones of synthetic hydrogels.

Due to the synergistic processes of hydrogel swelling itself and the simultaneously induced changes of the mineral soil pore system coming along with it, the swelling degree of the hydrogel is not necessarily reflected in the expansion of the soil on a larger scale (Buchmann et al., 2015). This complicates the direct transfer of hydrogel-adapted physicochemical methods to hydrogel-rich soil. Although an increasing number of studies have shown that biohydrogels are highly contributing to manifold soil physicochemical properties, detailed mechanisms have not been considered and remain still unresolved (Schaumann et al., 2002; Schaumann and Hurráß, 2003). Extraction of biohydrogel structures from soil is not appropriate, as it would change both the properties of the soil and of the biohydrogel (viscosity for example); analysis of the biohydrogel in soil should take place in situ. In situ methods should allow the identification of different water populations such as water entrapped in biohydrogel and free pore water, and their subsequent quantification. This should be generally feasible, as some properties of water entrapped in biohydrogels differ from the ones of pure water and can be described with methods such as nuclear magnetic resonance (NMR) re-

laxometry, NMR diffusometry, differential scanning calorimetry (DSC), and a variety of imaging methods such as environmental scanning electron microscopy (ESEM), X-ray computer tomography (X-ray CT), and magnetic resonance imaging (MRI).

This review aims to evaluate techniques which are suitable to assess biohydrogel swelling in soil and its effect on soil processes and soil physicochemistry on quantitative and qualitative basis. In order to achieve this goal, we will first define the term “biohydrogel” and enlighten its temporal alternation (aging) as well as its replacement by model polymers. Second, we will discuss the peculiarities of hydrogels flow properties, including shear-thinning and viscoelasticity, and how they affect the rheological properties of soil. Third, we will review how conventionally used methods analyze hydrogel-rich soils in comparison to techniques such as NMR relaxometry, NMR diffusometry, and DSC, which have the potential to identify the different types of water in hydrogels and hydrogel-rich soils. In order to link the effect of hydrogel phases on soil physicochemistry, we will point out how rheological and imaging methods may further improve our understanding of the gel effect.

2 Biohydrogels, a “new” form of matter for soil scientists

2.1 Definition and properties of hydrogels

Hydrogels are commonly defined as chemically or physically cross-linked polymers, whose hydrophilic structure allows them to absorb water into their porous three-dimensional networks and swell without dissolving (Kazanskii and Dubrovskii, 1992; Mathur et al., 1996; Gerlach and Amdt, 2010; Ahmed et al., 2015; Lauth and Kowalczyk, 2016;). Their ability to absorb water arises from hydrophilic functional groups attached to the polymer backbone, while their resistance to dissolution comes from the cross-links between network chains (Gerlach and Amdt, 2010). A hydrogel is a form of matter intermediate between liquid and solid: it has the property of both, respectively viscosity and viscoelasticity, typically measured by rheometry (see respective chapter). In this context, the viscosity η (Pa·s) of hydrogels characterizes their flow resistance because of the internal frictions of molecules in the hydrogel. Viscoelasticity describes the structural stability of hydrogels and is defined by an elastic modulus (G') and a loss modulus (G''); G' describes the energy stored by a sample during the deformation process and counts for the elastic behavior of the sample, while G'' is a measure for the lost deformation energy of a sample due to inner friction, and thus represents the viscous behavior of the investigated sample. The most commonly used definition describing hydrogels in terms of their properties refers to “gel” as a viscoelastic system with $G' > G''$ (Williams et al., 2004). There is no universal definition describing hydrogels more specifically as their properties vary widely according to their water content and to their three-dimensional (3D)-network. Since the water content

is another important parameter contributing to the structural stability of hydrogels, the water holding capacity (WHC) of hydrogels exposed to external forces, e.g., centrifugal force or osmotic pressure as used to adjust a certain matric potential in the hydrogel, can be determined according to Eq. (1) as:

$$\text{WHC} = \frac{W_{\text{rem}}}{W_i} - 1 \quad (1)$$

where W_i and W_{rem} are the initial water content and the remaining water content after external force exposition. At the equilibrium swelling (WC_{eq}), osmotic forces and elasticity are balanced out and the water content of the hydrogel is in equilibrium with the surrounding solvent (Ganji et al., 2010). A hydrogel reaches equilibrium swelling [synonymously called swelling at infinite time or maximum water-holding capacity (Ganji et al., 2010)] when there is no further hydrogel swelling. The time range it needs can be within a couple of seconds or take over several hours, depending on the chemical nature and the particle size of the polymer (Zohuriaan-Mehr and Kabiri, 2008). The several methods available to determine WC_{eq} have been described in a recent review (Zohuriaan-Mehr and Kabiri, 2008). The WC_{eq} depends on the chemical composition of the hydrogel polymer as well as on the nature and density of the network joints (Ganji et al., 2010). It is a dynamic property as it characterizes a hydrogel under specific conditions for a given time period. The 3D-structure is interconnected with the WC_{eq} , but depends directly on the gelling mechanism of the polymer as indicated in Fig. 2.

2.2 Gel formation

Hydrogel formation involves the association of dispersed polymer segments to form a 3D-network that contains water in the interstices. The associated regions are known as “junction zones” and are formed by two or more polymer chains. Hence, gelation process is essentially the formation of these “junction zones”. The physical arrangement of junction zones can be affected by various parameters such as temperature, presence and concentrations of ions, and the inherent structure of the hydrocolloid. Three main mechanisms are proposed to explain the gelation process: ionotropic gelation, cold-set gelation, and heat-set gelation (Djabourov, 1991; Burey et al., 2008). Ionotropic gelation occurs via cross-linking with ions, especially polyvalent cations such as calcium or magnesium (e.g., for pectin and alginate) (Burey et al., 2008). During cold-set gelation, hydrogel network formation results from the formation of enthalpically-stabilized interchain helices of individual chains during the cool down of hydrocolloid solutions from elevated temperatures (e.g., for gelatine, agar) (Burey et al., 2008). For heat-set gelation, native structures (e.g., for starch, methyl cellulose) are heated until

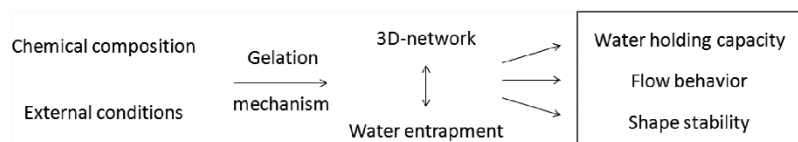


Figure 2: Influence of hydrogel formation on hydrogel properties.

unfolding/expansion of the polymer chains occur with their subsequent rearrangement into a 3D-network structure (Burey et al., 2008).

The different gelling mechanisms of pectin illustrate how gelling depends on the chemical nature of the polymer (Gamier et al., 1993); the most frequent sugar unit of pectin is D-galacturonic acid whose carboxylic group can be either methylated or deprotonated. Low-methoxy pectin has a degree of methylation < 50% and forms a hydrogel after addition of polyvalent cations. In this case, the junction zones resulting from interactions between anionic polysaccharides and cations are typically described by the egg-box model (Grant et al., 1973). The high degree of esterification of high methoxy pectin prevents the formation of such ionic network. The addition of sugar, such as galactose, lowers the water activity and promotes polymer-polymer interactions. Consequently, the formation of the hydrogel matrix rather relies on physical forces. The prevailing gelling mechanism of bacterial biofilm depends on ionic intermolecular interactions (Mayer et al., 1999). The same hypothesis is accepted for mucilage as it is principally composed of uronic acids (Gessa and Deiana, 1992; Mimmo et al., 2008).

3D-network formation by gelation and hydrogel swelling extremely depend on environmental conditions such as physical stimuli (temperature, pressure, sound, light) and chemical stimuli (solvent composition, pH, ionic strength) (Caillard et al., 2009; de Kruif et al., 2015). The type of polymer building the network structure also affects the hydrogel properties as function of the composition and concentration of cross-linker in the surrounding solution (Gerlach and Arndt, 2010). The types of bonds between the polymer chains can be either covalent chemical bonds or weaker physical bonds, and are used to label the hydrogel as a chemical or a physical hydrogel, respectively (Caló and Khutoryanskiy, 2015). Physical cross-links are electrostatic forces, hydrogen bonds, hydrophobic bonds, chain entanglements, and cation mediated cross-linking (Ottenbrite et al., 2010; Caló and Khutoryanskiy, 2015). Since chemical cross-links prevent chemical hydrogels from dissolving in the surrounding solvent, chemical hydrogels behave macroscopically solid-like. Because of their weaker nature compared to chemical cross-links, physical cross-links are found in a constant cycle of creation and destruction. At short time scale, the cross-links do not have time to dissolve, while at long time scale, physical hydrogels adapt to their environment. The concentration of cross-links is crucial as it is responsible for the swelling behavior and determines the solid-like or liquid-like properties of the hydrogel. The main components of biohydrogels are polysaccharides, which form gels by physical association of their polymer chains (Rees and Welsh, 1977). Polysaccharides have functional groups with coordinative properties, e.g., hydroxyl or carboxyl groups. The oxygen donor group may tend to form coordinative bonds with metal ions, thus, forming inner-sphere complexes which are energetically more stable than outer-sphere complexes. These hydrogels may thus have solid-like properties and can be defined as coordinative physical gels.

Contrary to well-defined hydrogels, such as pectines and alginates, mucilage primarily consists of neutral and acid poly-

saccharides (» 94%), proteins (» 6%), small amounts of phenolic acids (Bacic et al., 1986), and phospholipids (Read et al., 2003). Mucilage concentrations in the rhizosphere are estimated at » 0.1% (Carminati and Vetterlein, 2013). Besides the complex composition of mucilage in the rhizosphere, bacteria can produce EPS (Flemming and Wingender, 2010) in which polysaccharides, proteins and DNA, and in some cases extracellular lipids, are the main constituents (Schmitt and Flemming, 1999). The complexity in composition indicates the limitations to directly link physicochemical properties of well-defined hydrogels to complex soil-born biohydrogels, although several processes, such as ageing or drying/reswelling, might be comparable.

2.2.1 Hydrogel specific processes

2.2.1.1 Aging and drying/swelling processes

In this review, the physicochemical hydrogel properties changing with time are summarized as "aging". In this context, aging processes depend on specific environmental conditions (temperature, pressure, solvent composition) and include shrinking, reswelling, and syneresis over time (Diehl et al., 2014). Drying/swelling processes induced by external changes in the water potential and being constant over time once reached the equilibrium value are distinguished from aging. The following chapter shows how aging and drying/swelling processes are often inextricably combined for hydrogels. Especially for hydrogel-rich soils, experiments investigating hydrogels specific processes might help to understand how gel phases in soil will react to soil processes and how they influence soil physicochemical properties.

Hydrogels exposed to external forces (e.g., load, drying, drainage) generally loose water, which typically results in their shrinkage in terms of volume. Their tendency to shrink is characterized by their WHC. As hydrogel properties are strongly related to their water content, shrinkage leads to a higher elasticity for many polysaccharide hydrogels (Lüsse and Arnold, 1998; de Kruif et al., 2015). One particularity of hydrogels is their ability to reswell after shrinking. Reswelling can be hysteretic if the hydrogel follows a different course of rehydration over time but ends up with the same WC_{eq} as before the shrinkage (Sun et al., 2016). If the hydrogel does not reabsorb the same amount of water as at the initial WC_{eq} , the hydrogel-specific properties are changed. This can be attributed to an irreversible modification of the hydrogel network during shrinking, e.g., reduced average distances among cross-linking sites (Chang et al., 2010). Polysaccharide hydrogels are often subjected to syneresis, which describes the spontaneous release of water resulting from passive diffusion and from rearrangement of the polymer to an energy-favored conformation (Rees, 1968; Matsukawa et al., 2009). Ionic gels, such as alginate and pectate, show decreased volumetric expansion of their hydrogel network with increasing calcium concentrations upon storage due to syneresis (Hills et al., 2000; Mao et al., 2001). Syneresis is rarely taken into account during the induced dehydration of hydrogels by application of

external forces, despite this effect adds up to the other suction forces applied to the hydrogel.

2.3 Methods to quantify drying/swelling and aging

The proportion of water in hydrogels is > 90%, hence, variations of the water content lead to drastic changes in the physicochemical properties of hydrogels. Traditionally, procedures to study hydrogels artificially trigger hydrogel dehydration or rehydration, and determine the time-dependent development of WHC. These procedures are limited in their information value due to (1) the diversity of the experimental methods which prevent comparison between the results and (2) the destruction and modification of the hydrogel structure by the measuring procedures themselves (Götz and Hinrichs, 2008). However, two approaches are commonly used to study the dehydration of hydrogels: (1) the application of an external force at different degrees of load and connection of the results with a certain matric potential (Hall, 1996; Andry et al., 2009). These methods involve the application of pressure, centrifugal forces, capillary suction, osmotic pressure or water potential with subsequent measurement of the water loss; (2) the assessment of desiccation kinetics of a hydrogel under constant dehydration conditions.

For the adjustment of a certain matric potential using centrifugal dehydration, hydrogels are placed on a centrifuge filter and centrifuged at different centrifugal forces for a certain time. This method offers the advantage to be quick, but a negative side-effect is the potential destruction of the hydrogel microstructure such as phase separation of water and recreation of water compartments with distinct motion properties (Shin et al., 2002). Moreover, it is recommended to choose relative high centrifugal acceleration to avoid gravity artifacts which may result in inaccurate capillary pressure data (Chen and Ruth, 1995). Another method is the application of a matric potential by direct pressure reduction using a water column (Johnson and Veltkamp, 1985). The reproducibility of the results depends on the contact between hydrogel and the suction plate which is not self-evident (Fonteno and Bilderback, 1993). In this context, syneresis effects are an additional problem encountered for low matric potentials. Polysaccharide gels exhibit continuous water exudation, therefore, the determination of the equilibrium mass for a given matric potential cannot be based on the time-dependent constancy of the hydrogel mass. Moreover, the bacterial degradation of polysaccharides will limit the incubation time for which the hydrogel can stay unaltered (Morel et al., 1991; Mary et al., 1993; Nguyen et al., 2008). The application of osmotic pressure on a hydrogel through dialysis against polyethylene glycol (PEG) solutions can also be related to a matric potential (Williams and Shaykewich, 1969). The matric potential is adjusted for 10–15 d using a defined concentration of PEG in the dialysis solution (Chenu, 1993; Chenu and Roberson, 1996). This technique allows the adjustment of both pH and salt concentration and a soft dehydration which should exempt artefacts due to fast dehydration (Lüsse and Arnold, 1998). However, this procedure is time-consuming and chemically intensive. Even more, unexplained discrepancies in the water release for the osmotic pressure method and the pressure plates have been observed for some polyacrylamide

hydrogels (Hüttermann et al., 1999). Although the above cited methods aim to characterize the water retention of hydrogels under application of different loads, the factor time cannot be completely separated from the results due to the liquid-like properties of hydrogels.

An approach to study hydrogel aging is the investigation of desiccation kinetics which can be measured under different temperatures or vapor pressures (Hills et al., 2000; Bakass et al., 2002). Here, gentle hydrogel dehydration takes place by directly putting the hydrogel in contact with a porous, hydrophilic soil surface (Kaith et al., 2013; Buchmann et al., 2015). Dynamic de-swelling tests allow the determination of the water retention ability by placing swollen hydrogels in a desiccator containing silica gel at 37°C (Guan et al., 1996). A variation of this test is the exposure of wet samples to different relative humidities, which are generated in desiccators over saturated salt solutions (Froix and Nelson, 1975; Chenu, 1993).

Rehydration of hydrogels gives information on their aging properties; hydrogels in soil are continuously subjected to moisture dynamics, e.g., rainfall or irrigation. This typically induces their reswelling, especially when they are previously dry, e.g., due to dry periods or intensive solar radiation. The standard method to investigate hydrogel rehydration is the immersion of dry polymer in an excess of water or in saline solutions and the measurement of the water content against rehydration time (Fonteno and Bilderback, 1993; Abd El-Rehim et al., 2004). This allows the investigation of hydrogel rehydration kinetics and hysteresis process as it has been recently done for mucilage (Kroener et al., 2015).

The method of choice to study hydrogel specific processes strongly depends on the parameters involved. Application of an external force can produce artefacts, which are signaled either as discrepancies between the theoretical and real degree of load applied to the hydrogel or as destruction of the hydrogel microstructure. To avoid potential interferences with aging, one option could be to apply the external load for a defined time, e.g., when the hydrogel is subjected to different matric potentials but only three days for each potential. To simulate the aging of biohydrogels in soil, pure hydrogels are dehydrated in order to forecast how the material and structural properties of the hydrogels in soil may change under dehydration over time. Since aging of hydrogels in soil is a continuous process, the application of an external force at different degrees of load is not recommended. The ideal approach to study aging effects on hydrogels involves their gentle and continuous desiccation with a potential rehydration, especially under different environmental conditions.

2.4 Can biopolymer characteristics be mimicked by well-defined model hydrogels?

The laboratory-induced natural production of biopolymers, such as root mucilage or extracellular polymeric substances (EPS), is time-consuming and yields only small quantities (Ahmed et al., 2015). Hence, the investigation of natural biopolymer by traditional physicochemical methods seems

already a methodical challenge. The storage of the “harvested” biopolymer is further problematic since biopolymers have a fast degradation rate of $\gg 3$ d (Morel et al., 1991; Mary et al., 1993; Nguyen et al., 2008). Several authors have reported that the structure of polysaccharide hydrogels irreversibly alters during freezing with a significant loss of water during thawing (Belton et al., 1988; Hills et al., 2000; Mao et al., 2001).

Studies directly characterizing biopolymers typically use well-defined polysaccharide model substances such as polygalacturonic acid (PGA) or agarose (Gessa and Deiana, 1992; Strathmann et al., 2001, 2000). For biohydrogels-rich soils, model polymers are also used to investigate complex processes induced by biohydrogels (Buchmann et al., 2015). In soil, the use of model polymers arises from the difficulties to study the impact of one single biohydrogel property in macroscopic observations. For example, the hydrophobicity of mucilage after drying is supposed to result from the presence of amphiphilic compounds in mucilage, whereby no single compound or physicochemical property have been directly attributed to the hydrophobic effect until now (Read et al., 2003; Ahmed et al., 2015). Given that the chemical composition, the gelling mechanism and other hydrogel physicochemical properties are known, the use of model polymers with comparable properties can enable the investigation of biohydrogel-induced processes in soil in more detail, e.g., metal sorption by the root apoplast (Mimmo et al., 2008). The use of xanthan, an anionic polysaccharide, and of dextran, a neutral polysaccharide, as models for EPS allows separating the influence of EPS on soil properties from other environmental factors. In this case, clay- and sand-associated EPS showed to improve water retention on clay minerals and sand upon repetitive desiccation and rehydration (Chenu, 1993; Chenu and Roberson, 1996; Czames et al., 2000; Du et al., 2010; Henao and Mazeau, 2009). PGA is typically used as model for root mucilage since several authors have shown similarities to natural root mucilage with a favored rhizosphere formation by increasing soil microstability (Czames et al., 2000; Barré and Hallett, 2009; Zhang et al., 2008; Peng et al., 2011).

2.5 Chemical characterization of biohydrogels for the choice of model polymers

The gelling mechanism and the resulting physical properties of biohydrogels are mostly determined by their chemical structure. Hence, the first step to identify an appropriate model polymer consists in identifying the main chemical components of the biopolymer. A first indication is given by the neutral, acidic or basic nature of the biohydrogel and by the valence and concentration of cross-linking cations. Simple and standard spectrophotometric methods allow the quantification of the monomers building up the 3D-network of the biohydrogel (Dubois et al., 1956; Blumenkrantz and Asboe-Hansen, 1973). Carbon and cation content are typically measured by total organic carbon (TOC) analyzer or Inductively Coupled Plasma-Atomic Emission Spectrometry (ICP-AES) after microwave digestion (Mimmo et al., 2008).

Sugar monomers are identified with a glycosyl compositional analysis. The polysaccharides are first isolated from the

matrix in order to undergo a separation treatment governed by the fractionation between neutral and acid polymers or between high and low molecular weights (Timotiwi and Sakurai, 2002). In a next step, polysaccharides are degraded to their monomer units for the glycosyl compositional analysis per gas chromatography (Osborn et al., 1999). Further components which do not belong to the hydrogel structure, e.g., phospholipids (Read et al., 2003), phenolic acids (Bacic et al., 1986), amino acids (Ray et al., 1988), and proteins (Bradford, 1976), can even modulate the physicochemical properties of the biohydrogel and are therefore also chemically identified.

However, due to the high chemical diversity of biohydrogels, one model polymer may not cover all the characteristics of the represented biohydrogel. For root mucilage, two reasons have made PGA such a popular model: (1) uronic acid is one of the principal component of root mucilage, although it widely varies in dependence on the plant species (Tab. 1) (Ray et al., 1988; Liu et al., 2003); (2) the scanning electron microscopy (SEM) and transmission electron microscopy (TEM) images of artificially formed Ca-PGA on a root surface are similar to the ones of naturally produced root mucilage (Gessa and Deiana, 1992).

Despite the reasonability of the two criteria, other physicochemical properties of PGA, such as flow behavior or reswelling capacity, are not comparable with natural root mucilage. The yellow mustard mucilage investigated by Liu et al. (2003) has shown an interfacial activity and a shear-thinning behavior rather comparable to xanthan gum dispersions than to PGA. Moreover, depending on the degree of esterification of the uronic acids in root mucilage, the biopolymer may have another gelling mechanism than PGA. One reason for using model polymers is based on the fact that the choice of model polymers has mostly relied on past observations or general acceptance. Indeed, defined criteria to select appropriate model polymers are lacking, probably because soil scientists still miss the tools to measure the properties and direct effects of biohydrogels in more complex systems such as soil. The microbiologists Mayer et al. (1999) and Strathmann et al. (2000) have compared the physicochemical properties of biofilms formed by model polymers with those naturally formed by plants or microorganisms (Tab. 2). This approach

Table 1: Principal composition of polysaccharides in root mucilage (Ray et al., 1988; Liu et al., 2003).

	Cress (%) ^a	Maize (%)	Rice (%)	Yellow Mustard (%)
Uronic acid ^b	47.8	3	n.d	14.6
Galactose	33.3	26	20.3	13.8
Glucose	15.1	18	37.9	23.5
Arabinose	21.8	20	13.7	3.0

^aExpressed as percentage of total amount of polysaccharide carbohydrates.

^bUronic acids determined as galacturonic acid equivalents and expressed as a percentage of the total carbohydrate equivalents.

Table 2: Central studies justifying the choice of appropriate model polymers to investigate natural biopolymers.

Biopolymer	Model polymer	Justification	Source
Root mucilage	PGA	SEM and TEM showed arrangement of Ca-PGA in fibrils similar to those of plant roots. Chemical composition (large fraction of uronic acid in mucilage)	(Gessa and Deiana, 1990; Gessa and Deiana, 1992)
Bacterial biofilm	Xanthan, dextran	Chemical composition	(Chenu, 1993)
	Agarose	High water binding capacity, stability against dissolution, pore structure variable, highly hydrated gel network	(Strathmann et al., 2000; Strathmann et al., 2001)
	Polyacrylic acid	Functional group analysis (NMR spectra), Similar molecular interactions (viscosity and effect of inorganic structures on the viscosity)	(Mayer et al., 1999)

is relevant, as hydrogels formed by biopolymers and model polymers have to be characterized from different perspectives and that the choice of an appropriate model polymer has to rely on both the research question and on the behavior of the biohydrogel under the situation considered.

3 Rheometry: a tool to measure material properties

3.1 Rheological properties of hydrogels

3.1.1 Shear-thinning behavior

The flow behavior of hydrogels provides information about the arrangement of the polymer chains in the sample. Shear-thinning behavior [expressed as the viscosity η (Pa·s)] decreases with increasing degree of shear load and is described by the entanglement model (Mezger, 2014). In the absence of external forces, the polymer chains are entangled several times with each other and occupy the lowest energy state. Application of external forces, such as shearing, decreases the flow resistance because the polymer chains disentangle to a certain extent (Graessley, 1974). Polyelectrolytes like gums or mucilage are characterized by a more pronounced shear-thinning behavior when the polymer solution gets more concentrated (Smidsrød and Haug, 1971). Flow properties of mucilage are dependent on the molecular conformation of the molecules, which depends on the ionic strength, temperature, and solution pH (Medina-Torres et al., 2000; Chen and Chen, 2001; Vinod et al., 2008). At zero ionic strength, the negative charges of an anionic polyelectrolyte polymer cause strong intermolecular repulsion with an expanded molecule of high viscosity (Medina-Torres et al., 2003). Increasing the ionic strength by counter ions with no specific molecular interaction (e.g., monovalent metal ions) typically reduces the viscosity and suggests a collapse of the hydrogel network by shielding the electrostatic repulsions of the polyions (Medina-Torres et al., 2000; Medina-Torres et al., 2003; McConaughy et al., 2008b). When cation binding takes place with polyvalent cations, intermolecular and intramolecular interactions can occur. Hence, the resulting viscosity depends on the antagonistic shielding and the cross-linking effects. For example, the

viscosity of arabic, karaya or cashew tree gums decrease in the presence of NaCl, but increase in the presence of CaCl₂ and AlCl₃ (Davidson, 1980; de Paula and Rodrigues, 1995).

3.1.2 Viscoelastic behavior

As already stated, hydrogels can simultaneously show viscous and elastic behavior; therefore, viscoelasticity characterizes the solid-like or liquid-like properties of hydrogels. Variations in viscoelasticity can help to elucidate gelation mechanisms, e.g., for acid and ionic hydrogels. The formation of acid hydrogels results from the reduction of the solution pH below the pK_a of the functional groups, which allows the bonding between adjacent polymer chains. Clear differences between G' and G'' and their frequency independence indicate a more pronounced gel-like character, as shown for acidic low-methoxy pectin at low pH values (Gilsenan et al., 2000). The influence of the network density and of the water content on the hydrogel elasticity also suggests that elastic modulus and swelling pressure are closely interconnected (Kazanskii and Dubrovskii, 1992; Yoshinobu et al., 1992). For example, the higher the calcium concentration in ionic alginate augments, the higher is the strength of the hydrogel in terms of $G' >> G''$ (Jørgensen et al., 2007).

Since material properties provide a hint of the conformation of the hydrogel-forming polymer, they also allow to proof the effects of environmental conditions, such as storage, freezing, and drying on the hydrogel, as they often lead to a rearrangement of the inner molecular structure (Van Den Bulcke et al., 2000; Wang et al., 2009; Van Vlierberghe et al., 2010; León-Martínez et al., 2011). The knowledge on rheological properties of hydrogels enables the contribution of soil-water-hydrogel interactions on the structural stability of biohydrogel-rich soil.

3.2 Rheometry as tool to measure soil microstructural stability

Soil rheometry addresses the two main tasks: (1) assessing the sample microstructure by stress-strain relationships and (2) explaining the rheological properties of the sample from

the known rheological properties of its constituents (Reiner, 1960; Markgraf et al., 2006; Holthusen et al., 2010; Keller et al., 2013). Soil structural stability and soil particle interactions, e.g., induced by dynamic soil deformation processes have been recently characterized with rheology. Similarly to hydrogels, soils samples reveal viscoelastic properties with a fast recovery of the soil structure when $G' > G''$ (Markgraf and Horn, 2009). The increase in the shear stress t (Pa) and the corresponding deformation g (rad) results in an irreversible microstructural change of the soil sample due to the loss of particle-particle contact and a subsequent particle distortion. This follows a continuous decrease of both G' and G'' (Fig. 3). The yield point (cross over) implies an irreversibly destroyed inner sample structure with $G' \approx G''$.

In recent years, rheology has proven to be a sensitive technique for assessing soil structural stability, especially in the context of several soil physicochemical properties such as clay mineralogy, soil texture (Markgraf et al., 2006), menisci forces (Markgraf and Horn, 2007) and soil solution composition (Holthusen et al., 2010).

3.3 Studying the impact of biohydrogels on soil rheology

First attempts to relate soil rheological properties to swollen hydrogel phases in soil were done by Barré and Hallett (2009) and Deng et al. (2015) for model root mucilage (PGA) and fungal polysaccharide (sceroglucan) at different concentrations and soil types. The results showed significantly increased soil structural stability after biopolymer addition. An explanation for this phenomenon is the binding of soil particles by swollen gel phases. Although the additional presence of hydrogel-forming substances in soil increases soil structural stability, the spatio-temporal distribution of existing hydrogel phases and their swelling degree in soil remains unclear. Recently, Buchmann et al. (2015) started first attempts to close this research gap by combining rheology and ^1H proton nuclear magnetic resonance ($^1\text{H-NMR}$) relax-

ometry in order to assess the direct effects of hydrogel swelling on the rheological stability of an unstable, silty sand soil. The results reveal that the stabilization of the soil structure is a function of both polymer treatment and its swelling degree between the soil particles. The higher the proportion of polymer-associated water, the more stable is the soil structure as a result of its “gluing” effects and higher viscosity compared to mineral pore water. Nevertheless, several limitations of this method are pointed out in the chapter dealing with $^1\text{H-NMR}$ relaxometry. Despite the promising potential of soil rheology for the assessment of soil microstructural stability, the limited number of existing studies dealing with the effects of soil-water-hydrogel interactions points out the need of further investigations.

4 Entrapment of water in hydrogels

4.1 Overview on methods to characterize the water entrapment

The term water entrapment refers to the surroundings of water molecules when trapped in a porous structure: gel network, soil pores or a mixture of both. It is more accurate than “water bonding”, as the water molecules are not chemically or physically bond in the network, and better appropriate than water retention which has a specific meaning in soil science. Water entrapment describes both the types of interactions the water molecules have with the porous network, e.g., if they interact with a stiff or labile polymer matrix or with stable soil pores. It also depicts the intensity of the interactions, which depends on the pore dimensions.

The gravimetric methods reported in chapter 2.3 measure the maximum WHC and the WHC of hydrogels under load. They give a hint about the strong or loose entrapment of water in the gel network but give no information about the physicochemical parameters of the surroundings. Similarly, conventional methods in soil science measuring WHC_{max} and water retention curves (WRCs) of soils indicate how strongly the presence of biohydrogels influence soil hydraulic properties, but do not detect—neither qualitatively nor quantitatively—and do not characterize biohydrogels in soil. With $^1\text{H-NMR}$ relaxometry, the relaxation times of protons aligned in a magnetic field by radiofrequency (RF) pulses are measured. Thus, water molecules in an environment are characterized by their relaxation times as well as the amount of water in each environment. Pulsed field gradient spin-echo NMR (PFG-NMR) measures the self-diffusion coefficient of water, which depends on the physical barriers encountered by the water molecules during a measurement. Thus, due to differences in their chemical and physical surroundings, NMR methods have the potential to detect qualitatively and quantitatively gel water from non-gel water in soil pores. Until now, mechanism of proton relaxation in heterogeneous gel-soil mixtures is, however, little understood and has not been described by any theoretical model yet. Differential scanning calorimetry (DSC) measures the freezing and melting temperatures and enthalpies of water.

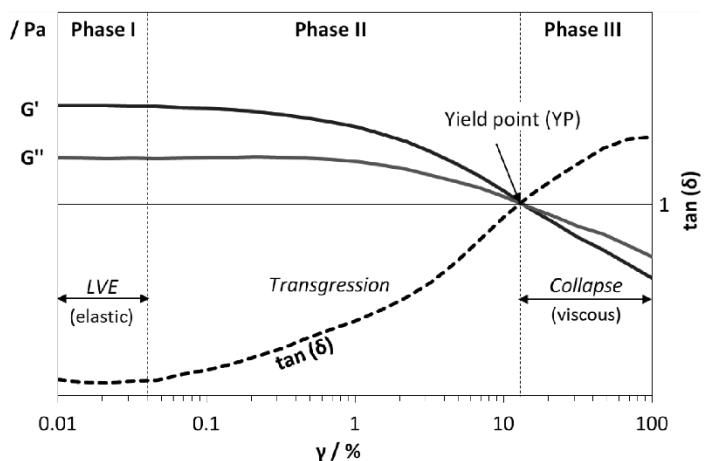


Figure 3: Typical course of a viscoelastic solid material such as soil or hydrogel during an amplitude sweep test (adapted from Mezger, 2014).

They give a hint about the degree of interaction of water molecules with the polymer or soil matrix (from bound to bulk water). Very few studies deal with the application of DSC on gel–soil mixtures, probably because the analysis of heterogeneous systems is complicated due to interactions of water in gel phase with soil constituents.

4.2 Conventional methods based on water retention of hydrogels

Maximum water holding capacity (WHC_{max}) and water-retention curves (WRCs) are typically determined in order to assess the hydrological characteristics of biohydrogel-rich soil. Generally, biohydrogels increase the water retention of soil. The WRC of a biohydrogel gives a hint about the tendency of the WRC of a soil mixed with this biohydrogel (Chenu, 1993; Rosenzweig et al., 2012). However, due to the limited number of investigations on biohydrogels, to the different ways the same biohydrogel affects the retention curve of different soils, and due to the plurality of the methods used to measure the retention curve of biohydrogels, it is difficult to make a universal quantitative relationship between the water retention curve of hydrogels and the one of soil. Among others, polymer type, polymer concentration, environmental conditions, and physicochemical soil properties are the principal parameters that define the complexity of biohydrogel-rich soil and, thus, affect soil hydrology (Fonteno and Bilderback, 1993; Muta et al., 2003; Andry et al., 2009; Narjary et al., 2012). The soil texture itself is the driving factor influencing hydrogel swelling in soil. For example, synthetic hydrogels typically increase the WHC_{max} of soils with high sand contents (e.g., sandy soil or sandy loams) more than the WHC_{max} of loamy and clayey soils (Agaba et al., 2010; Hussien et al., 2012). This is due for two reasons: (1) hydrogel swelling leads to shifts of the pore size distributions towards small, water-retaining pores with higher capillary forces than in large pores (Bhardwaj et al., 2007); (2) swollen hydrogel in pores of sandy soils retain more water as their swelling is less restricted than in clays and loams (Zohuriaan-Mehr and Kabiri, 2008; Guilherme et al., 2015). The swelling of hydrogels in heavy-textured soils, such as clays and loams, can be restricted due to the difficulty of the partly swollen hydrogel to displace and rearrange surrounding soil particles, especially in the presence of swelling clay particles (Hussien et al., 2012; Smagin et al., 2014).

Besides the manual separation of hydrogel from soil after wetting/drying cycles for proofing the hydrogel reswelling degree (Fonteno and Bilderback, 1993), the reswelling potential of biohydrogel-rich soil and artificial soil–hydrogel mixtures has been poorly investigated. This results from a lack of methods allowing the distinction between hydrogel-associated water from water confined in mineral soil pores. Indeed, it still remains unclear how hydrogels in soil contribute to a higher WHC_{max} : either hydrogels might reabsorb water after drying/rewetting or dried polymers might form a film on the surface of mineral soil pores which consequently reduces the pore diameter and hence increase the water holding against gravity. In order to investigate the water entrapment in biohydrogel-rich soil, proton nuclear magnetic

resonance (NMR) relaxometry shows a high application potential as is discussed in the following section.

4.3 Characterization of water entrapment by means of 1H -NMR relaxometry

4.3.1 Basic principle of 1H -NMR relaxometry to measure the entrapment of water

1H -NMR relaxometry allows non-invasive investigations of water populations by measuring the relaxation time of water aligned in a magnetic field by radiofrequency (RF) pulses. When a sample is placed in an outer magnetic field B_0 , water protons orientate and precess around the direction of the magnetic field with their specific Larmor frequency. A RF pulse is applied to the sample, so the spins are flipped into an angle to the external magnetic field B_0 causing a magnetization M_0 . After the RF is switched off, the spins relax back to their equilibrium orientation and the apparent magnetization induced by the RF pulse decays. Water molecules in an environment are characterized by their relaxation time, whereby two types of relaxation can be distinguished: spin-lattice or longitudinal relaxation (T_1), and spin-spin or transverse relaxation (T_2). Transverse relaxation refers to the relaxation due to variable molecular interactions in the slightly inhomogeneous magnetic field (Dunn et al., 2002). As a result of different relaxation mechanism and relaxation times of water trapped in hydrogel and water confined in soil pores, both water populations and their respective amount in each phase may be distinguished (Buchmann et al., 2015).

4.3.2 Entrapment of water in hydrogels measured with 1H -NMR relaxometry

Longitudinal relaxation of hydrogel-associated water is governed by proton chemical exchange between protons of free water and exchangeable protons of the polymer, e.g., protons from carboxylate, hydroxyl and amino groups (Belton et al., 1988; Hills et al., 1989, 1991; Belton, 1997; Calucci et al., 2008). Transverse relaxation depends on the rotational correlation time of the water molecules. Depending on the polymer itself, the mobility of water molecules will change due to different flexibility of the polymer network and water binding properties (Belton, 1997; Lüsse and Arnold, 1998). Hence, the relaxation times T_1 and T_2 of water vary according to their local environment. In hydrogels, hydration water (water molecules in close interaction with the polymer chains) has different properties than “free water” trapped in the junction zones of the hydrogel network (Hills, 1992). There is rapid exchange between “free water”, which tumbles freely and hydration water, which has a slower tumbling rate (Fyfe and Blazek, 1997; Degrassi et al., 1998; Okada et al., 2002; Calucci et al., 2008; Průšová et al., 2013). Hills et al. (1991, 1990) developed a microphase model for polysaccharide hydrogels, in which the observed relaxation time is weighted between the superjunction phase whose relaxation rate is hundred times higher than the one of the interstitial phase, e.g., 718 ms^{-1} and 5.5 ms^{-1} for agarose, respectively.

The decrease of relaxation times with increasing polymer concentration reflects the decrease in the tumbling frequency of water due to the number of hydrogen-bonding interactions with the hydroxyl groups of the polymer chains (Fyfe and Blazek, 1997). Shorter T_2 values indicate higher exchange rates of water molecules in the polymer matrix (Hills et al., 1991). For example, the hydrophilicity of the poly(HEMA-co-VP) polymer is higher than the one of poly(2-hydroxyethyl methacrylate) caused by more interactions of water molecules with hydroxyl groups in poly(HEMA-co-VP) (Ng and Swami, 2008). This observation is in agreement with $^1\text{H-NMR}$ measurements of hyaluronan-based native and sulfated-hydrogels (Barbucci et al., 2006). The type of interaction between polymer chains and water molecules further influences the measured relaxation time, i.e., methyl-ester groups in HMP restrict the mobility of water molecules due to a surrounding formation of water clathrate (Walkinshaw and Amott, 1981) but not to the extent of dipolar or hydrogen-bonded groups such as in LMP (Kerr and Wicker, 2000). Further, the chain rigidity of a gelled polymer increases due to the formation of junction zones and cross-links, which implies a significant reduction of the rotational correlation time (Shapiro, 2011) and a strong dependence of the relaxation times on the moisture content (Froix and Nelson, 1975; Kerr and Wicker, 2000).

As non-invasive tool, the degree of water entrapment in hydrogels can be investigated by $^1\text{H-NMR}$ relaxometry. This is of special interest when hydrogels undergo dynamic processes, such as drying or reswelling, as the relaxation of water molecules directly depends on the multiplicity and rigidity of the junction zones (Hills et al., 2000; de Celis Alonso et al., 2010). The relaxation time further gives an indication on the hydrogel viscosity and strength (Degrassi et al., 1998; Capitani et al., 2001; Shin et al., 2002). The characterization of water entrapment for pure hydrogels under different conditions, e.g., swollen or partly dehydrated, using $^1\text{H-NMR}$ relaxometry enables to: (1) quantify the effect of environmental conditions on the water entrapment, (2) distinct hydrogel water from mineral pore water in hydrogel-rich soils, and (3) identify the recent state of the hydrogel in soil.

4.3.3 Entrapment of water in soils measured with $^1\text{H-NMR}$ relaxometry

Water entrapment distinguishes fundamentally hydrogel-free from hydrogel-rich soil. In a simplified hydrogel-free soil, water is confined to mineral soil pores, while in a hydrogel-rich soil, water is additionally trapped in swollen hydrogel phases. The direct assessment of water entrapment in soil is important since it is conventionally indirectly measured by water retention curves or by manual sorting of hydrogels from soil-hydrogel mixtures. Fortunately, the rotational and translational mobility of water molecules confined in mineral soil pores and associated to hydrogel structures differ from each other, which enables their distinction using $^1\text{H-NMR}$ relaxometry. Although $^1\text{H-NMR}$ relaxometry cannot be easily transferred to soil due to the high complexity and heterogeneity of soil and to the poorly understood role of SOM swelling on the water entrapment in soil, several efforts have been made to apply this technique for soil specific research questions (Schaumann, 2006a, 2006b; Schaumann and Bertmer, 2014).

Soil-water interactions by $^1\text{H-NMR}$ relaxometry are commonly investigated by solely observing the transverse relaxation time T_2 , since T_1 measurements are very time-consuming (Dunn et al., 2002; Schaumann and Bertmer, 2014). The measured T_2 results from solid-fluid interactions at soil pore surfaces with fixed spins and the additional presence of paramagnetic ions or paramagnetic crystal defects (Kleinberg et al., 1994; Jaeger et al., 2008). Under the assumption of a surface-limited regime (Schaumann and Bertmer, 2014), the relaxation directly depends on the pore size of the soil sample. In porous systems, such as soil, a wide distribution of pore sizes is given, which typically results in a distribution of relaxation times and not in one single relaxation time as typically measured for bulk water (Fig. 4).

Thus, within each relaxation time distribution, the amplitude at a given relaxation time indicates a certain pore size (Schaumann et al., 2005). In recent years, $^1\text{H-NMR}$ relaxometry has been proven as reliable method to assess the pore-size distribution of soil (Jaeger et al., 2009; Costabel and Yaramanci, 2013; Meyer et al., submitted). Wetting and swelling are the two independent processes directly influencing the $^1\text{H-NMR}$ measurements of soil. Several studies proved that relaxation times of soil are often shifted towards shorter relaxation times as result of soil pore wettability and swelling processes of clay particles and organic substances such as SOM (Schaumann et al., 2005; Buchmann et al., 2015; Meyer et al., submitted). Especially the investigations done by Jaeger et al. (2010) and Buchmann et al. (2015) revealed significant changes of the relaxation time distributions by the swelling of organic substances in the soil matrix and subsequent volumetric expansion of the soil and water redistribution.

4.3.4 Swelling processes in soils measured with $^1\text{H-NMR}$ relaxometry

The fact that hydrogel swelling together with soil mineral constituents significantly affect the measured relaxation time distributions in soil demonstrates the need to clearly identify the likely existing water populations such as clay-associated

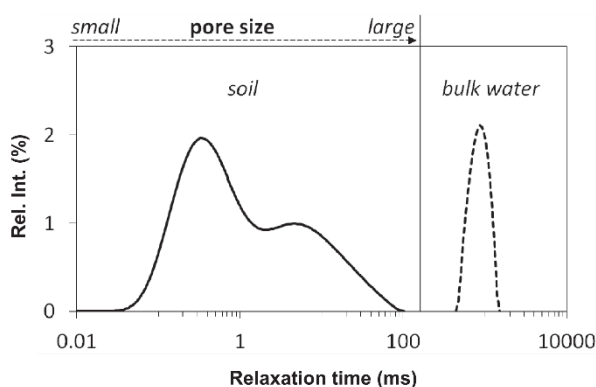


Figure 4: Transverse relaxation time distribution for soil and bulk water. The longer the relaxation time, the larger the pore size and vice versa. Bulk water typically reveals unimodal relaxation times with $T_2 \gg 1-3$ s.

water, mineral soil pore water, and hydrogel-associated water. Gradual intensity shifts towards shorter relaxation times were observed in the first applications of one-dimensional (1D) ^1H -NMR relaxometry in high organic matter soils (Schaumann et al., 2005). Nevertheless, Schaumann et al. (2005) were not able to decide from the 1D ^1H -NMR measurements if swelling and formation of biohydrogel phases were the driving mechanisms for the reduction of the T_2 , since no clear differentiation between the different water populations was possible from the measured relaxation time distributions. Recently, Buchmann et al. (2015) demonstrated the limitation of 1D ^1H -NMR relaxometry to differentiate hydrogel-associated water from pore water. The authors showed that differentiations are only possible by 1D ^1H -NMR-relaxometry measurement if the relaxation times of both hydrogel and soil are at completely different relaxation times. Yet, the observed merging of both the relaxation time distribution of hydrogel and soil has shown that it is impossible to unambiguously differentiate between hydrogel-associated water and soil pore water from 1D ^1H -NMR relaxometry measurements. Buchmann et al. (2015) concluded that 1D ^1H -NMR relaxometry should be extended by two-dimensional (2D) ^1H -NMR measurements and thermo-analytical methods, such as differential scanning calorimetry (DSC), which might discriminate the water populations due to differences in their rotational mobility and freezing behavior according to their environments.

4.4 Characterization of water entrapment by the self-diffusion coefficient of water

4.4.1 Self-diffusion coefficient of water in hydrogels

Another parameter which characterizes the water entrapment is the translational self-diffusion coefficient of water D as measured by pulsed field gradient spin-echo NMR (PFG-NMR). Contrary to relaxation time measurements, D is independent of the chemical nature of the polymer since the obtained information are rather associated to the topological structure than to the microstructure of crosslinks or interchain structure (Ohtsuka and Watanabe, 1996). D is typically determined as function of the diffusion time D and allows the calculation of the mean distance travelled by the diffusing water molecules (Cotts, 1991). The structural parameters of the surrounding are accessible between 0.3 and 30 nm (Cotts, 1991). At very short diffusion time, the diffusion coefficient is D_{SF} and depends on the viscosity of the pore fluid. At longer diffusion times, physical barriers limit the diffusion coefficient D_{SF} e.g., in network systems as for gellan gum (Ohtsuka and Watanabe, 1996) or poly[2-hydroxyethylmethacrylate] hydrogels (Peschier et al., 1993). According to Eq. (2), D_{SF} can then be related to the root-mean-square (rms) end-to-end distance r of the pore space in the hydrogel matrix:

$$\langle r^2 \rangle \gg 6D_{SF}t; \quad (2)$$

where t is the inverse of the diffusion time limiting value. Physical concepts describing the retardation effects of hydrogels affecting D are obstruction induced by the slow-moving polymer molecule, hydrodynamic interactions between water

and polymer and free-volume effects (Masaro and Zhu, 1999; Mariette et al., 2002). Several parameters characterizing the hydrogel structure can be calculated on the basis of both D_{RF} and D_{SF} , such as the critical pore radius, the tortuosity, the surface to volume ratio S/V , the pore size distribution, and the permeability (Götz and Hinrichs, 2008). These information help elucidating hydrogels morphology as exemplarily shown for Ca^{2+} cross-linked Aloe Vera polysaccharide (AvP) hydrogel. For the same calcium concentration, the diffusion profile of AvP 0.20 and 0.60 wt% relate to similar pore sizes, but a greater surface area and tortuosity for AvP 0.60 wt% (McConaughy et al., 2008a). Variation of the diffusion coefficient in function of the water content gives also information on the dynamic changes of the microstructure when facing dehydration (Topgaard and Söderman, 2002).

Measurement of D at several diffusion times is time-consuming and in many studies D is only determined for one fixed diffusion time. However, this may lead to some difficulties in the interpretation of the results as changes in the polymer mobility initiated by gelation are not evident to measure with the self-diffusion coefficient of water (Fyfe and Blazek, 1997; Mariette et al., 2002). This difficulty is illustrated by the similarity between self-diffusion coefficients measured in aqueous solution and alginate gels, and is attributed to the microporous nature of the hydrogel matrix (Hills et al., 2000). Studies of hydrogels by means of D is thus a promising and challenging approach at the same time and has not yet been much investigated, especially for hydrogel-rich soils as subsequently discussed.

4.4.2 Self diffusion coefficient of water in soil

Soil directly affects the diffusion path of water molecules by its structural properties, e.g., pore space, pore geometry, and pore interconnectivity (Stallmach and Kärger, 1999; Van As and Lens, 2001). PFG-NMR measurements of macroporous materials, such as petrophysical objects (Stallmach and Kärger, 1999), permeable sandstones (Fordham et al., 1994; Frosch et al., 2000), medium and coarse sands (Vogt et al., 2002), as well as for microporous systems such as zeolite absorbate-absorbent systems (Cavalcante et al., 1997), have provided information on the translational mobility of the fluid confined to different pore sizes. The results obtained from PFG-NMR measurements have shown an independence of the investigated fluids on the chemical properties of the fluid/grain interface (Vogt et al., 2002). Thus, D is a promising parameter to assess translational mobility of water in hydrogel-rich soils, although some difficulties exist; the conventional measurement of D is one-dimensional and gives only a weighted value for all diffusion coefficients in the sample. A two-dimensional measurement would overcome this limitation, as D could be related to another parameter, such as the relaxation time T_2 . Since hydrogels and soil have different physical barriers, D of hydrogel and soil should differ from each other. Only few data are yet available about D in hydrogels as well as in soils, thus, a demonstration whether D of both soil and hydrogel distinctively differ from each other has not been possible until now. The combination of PFG-NMR and conventional ^1H -NMR relaxometry still seems a promis-

ing approach, as it relates rotational tumbling which gives information about soil–water interactions (e.g., water binding in soil pores or swollen organic structures) to molecular diffusivity (Bayer et al., 2010; J aeger et al., 2010).

4.5 Two-dimensional measurements to characterize the water entrapment in porous media

T_1 and T_2 relaxation times are often analyzed together (McConville et al., 2002), but correlations between longitudinal and transversal relaxation time (T_1/T_2 ratio), as well as between transversal relaxation time and diffusion coefficient (T_2/D), can be combined in one single T_1 - T_2 or T_2 - D NMR relaxation experiment (Fig. 5) (Hills, 2007; Haber-Pohlmeier et al., 2010; J aeger et al., 2010; Song et al., 2012; Tang et al., 2014).

T_1 and T_2 relaxation measurements performed on different hydrogels revealed that T_2 values are more sensitive to the polymer composition and to the water content than T_1 values (Degrassi et al., 1998; Ng and Swami, 2008). In the course of water uptake and water distribution in soil, shifts in both the relaxation time distributions and T_1 - T_2 (T_2 - D) ratios allow the assessment of wetting and swelling kinetics in soils (Schaumann et al., 2005; J aeger et al., 2010; Todoruk et al., 2003), and the resulting distribution of soil pore sizes (J aeger et al., 2009; Costabel and Yaramanci, 2013). In this context, J aeger

et al. (2010) investigated the effect of SOM swelling on soil–water interactions in peat. The authors showed that SOM swelling induced significant changes in the peat structure during the course of water uptake and water drainage. Especially the rotational water mobility was significantly affected by the swollen SOM as function of the water content. The T_1/T_2 ratio at saturated conditions of the peat increased from 1.1 up to 18 at 10–20% water content, most likely due to the reduced rotation mobility of water confined in gel phases of SOM. Similar results were found for pure agar hydrogel in which the T_1/T_2 ratio increased with agar concentration (and thus decreasing water content) up to 30. Additional measurements using cryo-NMR relaxometry and differential scanning calorimetry (DSC) showed that large T_1/T_2 ratios of water in peat can be related to non-freezable water in hydrogel phases (strongly restricted in mobility) and physically immobilized water at 0°C to –5°C (partly located in hydrogel phases) (J aeger et al., 2010).

4.6 Freezing behavior of water investigated by differential scanning calorimetry (DSC)

4.6.1 Different water types distinguished in hydrogels

Differential scanning calorimetry (DSC) provides information on polymer–water interactions in terms of freezability of water in a swollen matrix (Radosta and Schierbaum, 1990; Garcia and Walter J.r., 1998; Hatakeyama and Hatakeyama, 1998). The definition of different dynamic states of water in hydrogel depends on experimental conditions such as temperature, water content, and time scale of the experiment (Roorda, 1994; Bouwstra et al., 1995; Müller-Plathe, 1998). The conventional DSC approach includes cooling and thawing of the hydrogel and allows the categorization of water into different fractions according to its behavior during the conducted cooling and heating cycles (Yoshida et al., 1993a, 1993b; Hatakeyama and Hatakeyama, 2006). The presence of a freezing/melting peak about 10–40°C below 0°C in the DSC thermogram corresponds to supercooling water (freezing bound water). Considering that pure water (bulk water) typically reveals a melting enthalpy of 333.5 J g⁻¹ and a melting temperature T_{melt} around 0°C, the amount of non-freezable water can be directly determined by the melting endotherms as the differences between the calculated water amounts from the endothermic melting peaks in the DSC thermogram and the known water amounts in the sample. The detection of small amounts of mobile water between 0 and –20°C and <–20°C using cryo-NMR underlined the categorization of the different water fractions (Leung and Steinberg, 1979; J aeger et al., 2010). The observed thermodynamic properties of water are related with the degree of interaction between water molecules and biopolymer structures (McBrierty et al., 1999). The close association of water molecules to the polymer matrix through hydrogen bonding and polar interactions causes the formation of non-freezing water, while freezing bound water is related to water with intermediate properties between those of bound and free water.

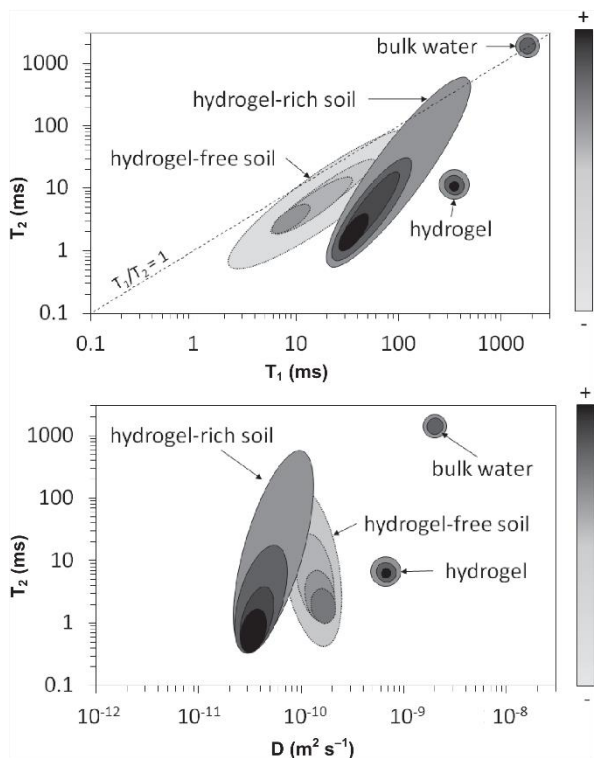


Figure 5: Schematic two-dimensional T_1 - T_2 and T_2 - D correlation spectra for water, hydrogel, hydrogel-rich soil and hydrogel-free soil.

4.6.2 A fingerprint of the polymer structure

Water uptake during hydrogel swelling can be followed by identifying different water fractions with the DSC thermogram, e.g., at different water content or polymer concentrations. At very low water contents, all water molecules are present as non-freezing water (Quinn et al., 1988). An increase in the water content comes along with increasing amounts of freezing-bound water (Takigami and Takigami, 1993). Upon an increase of the water content, the area of the endothermic peak corresponding to the melting of ice originating from freezable water with position shifts from -5°C to slightly higher values as exemplarily shown for humic acid (Kučenk et al., 2012). A peak shoulder traduces overlapping processes which may correspond to different types of freezing bound water. This indicates different kinds of interactions between polymer structures (especially polar groups) and water molecules. For hydrogels, melting enthalpy tends to increase linearly as function of the water content (Průšová et al., 2010), but does not show a linear trend for some humic acids which suggests the additional presence of hydrophobic domains at specific concentrations (Kučenk et al., 2012).

The amount of non-freezing water for polyelectrolytes depends additionally on the valence of the cross-linking ions. This relationship indicates that the structure order of polyelectrolytes strongly influences the number of water molecules tightly bound by cations (Hatakeyama et al., 1995). The quantity of non-freezing bound water gives an indication on the hydrophilicity of the polymer and on the intensity of intermolecular hydrogen bonding within the network (Guan et al., 1996). Molecular flexibility of the polysaccharide chain also affects the structural organization of water (Yoshida et al., 1993a; 1993b). Freezing-melting experiments finally allow identification of changes in the hydrated structure after hydration, aging processes or diverse drying methods (Průšová et al., 2013). Some polysaccharides revealed an alteration of their physical structure during subsequent identical freezing-melting cycles, while others were not affected (Prawitwong et al., 2007; Kučenk et al., 2012).

4.6.3 Distinction of the freezing behaviors of water in biohydrogel-rich soils

The transfer of water entrapment in hydrogel to more complex systems, such as biohydrogel-rich soil, is not trivial since the water entrapment in soil is directly influenced by interactions with soil constituents such as the organic fraction or mineral fraction. It is well-known that the hydrogen bond network of water is significantly perturbed by additional interactions with hydrophilic substrates which results in pronounced effects on the thermophysical properties of the water in soil (McBrierty et al., 1996; Schaumann, 2005). Thus, changes in the freezability of water in soil can result from both chemical interactions and local steric constraints with its identification from the amounts of freezing bound and non-freezing water (McBrierty et al., 1996). The melting of freezable water in moist soil can also be characterized by the endothermic water melting peak in the DSC thermograms. Generally, the water state in soil can range from tightly bound (non-freezable) water to more loosely bound water, and freezable bulk water as it has been

shown for peat samples and cylindrical silica materials (McBrierty et al., 1996; Jähnert et al., 2008; Jaeger et al., 2010). Tightly bound water predominantly consists of hydration water and water which chemically interacts with hydrophilic moieties in the soil matrix having transition temperature around -123°C to -83°C . Loosely bound water does not significantly differ from normal bulk water and consequently melts with increasing temperature. Contrary to freezable bulk water, the melting temperature is $< 0^{\circ}\text{C}$ (McBrierty et al., 1996; Ping et al., 2001).

In soil where swollen hydrogel phases exist, the melting peaks are broader than for pure water and can be partly separated into several overlaying peaks. First detailed attempts to identify swollen hydrogel phases in soil using DSC were done by McBrierty et al. (1996) and Schaumann (2005) for peats below WHC_{max} . The authors observed a significant splitting of the melting peaks of water in peat and traced it back to the entrapment of water in swollen gel phases. Similar observations were done in a recent study conducted by Jaeger et al. (2010). Here, the authors investigated the swelling of SOM in peat by combining several analytical techniques such as DSC, TGA, and $^1\text{H-NMR}$ relaxometry. In this case, the combination of thermal analyses and NMR relaxometry revealed an innovative method to identify processes in soil governing its physicochemical changes during hydration and hydrogel swelling.

5 Imaging three-dimensional hydrogel networks and soil structures

5.1 Imaging hydrogel networks

The visualization of the three-dimensional (3D) hydrogel network would help to link hydrogel rheological properties to the spatial arrangement of the polymer chains. As swollen hydrogels mainly consist of water, their imaging is a major challenge. Various imaging techniques are available, whereby scanning electron microscopy (SEM) is one of the rare methods which can directly picture hydrogel structures.

For example, the visualization of the hydrogel matrix using SEM enables to screen different water holding behaviors of gellan gels with and without the application of external forces. The results have revealed that two different types of microstructures exist simultaneously, whose distributions depend on the calcium concentration (Mao et al., 2001). The sample preparation is yet highly invasive due to the required drying steps, e.g., by freeze-drying, before each measurement. However, ice crystal formation during freeze-drying can distort the native microstructure of hydrogels and creates undesirable artefacts in the SEM micrographs; ice crystals forming in the interstitial spaces in the hydrogel lead to an alteration of the superjunction and interstitial microphases with the creation of a network with bigger pore distances (Belton et al., 1988; Hills et al., 2000; Mao et al., 2001). Shock-freezing with sample immersion in liquid nitrogen, directly followed by sublimation, might be an appropriate alternative to limit the artefacts, but, to our knowledge, has up to now not been tested yet.

5.2 Imaging biohydrogel-rich soils

Visualization of biohydrogel phases in soil would improve the understanding of the gel effect. Soil microstructural changes initiated by biohydrogel phases and visualized by imaging techniques could be linked to various macroscopic properties, e.g., the stability of aggregated soil structures (Liu et al., 2009). 3D-imaging of biohydrogel phases in soil could further give answers to recently unsolved questions such as: can biohydrogel phases redistribute in other soil pores or do they stay in the pore space where they have been produced? Do biohydrogel phases stick to the surface of soil particles or do they swell in the whole pore space? Furthermore, 3D-imaging of hydrogels could also give a clue about their response to environmental dynamics such as their reswelling after drying events. All in all, imaging methods must be able to distinguish between swollen biohydrogel phases and mineral pore in the soil matrix in order to answer these questions.

Contrary to the imaging of hydrogel structures, the imaging of soil samples by SEM has been done for years in order to identify structures associated to certain soil properties such as its structural stability. For example, Liu et al. (2009) demonstrated that swellable polymers ought to build membranous structures between and on the surface of polymer-treated soil aggregates, which significantly increased their structural stability. Comparable observations were done by Markgraf et al. (2012) who clearly showed how polymeric network structures derived from organic compounds (e.g., roots, fungi, and fungal hyphae) formed an external network around soil aggregates. Albalasmeh and Ghezzehei (2014) recently investigated the effects of wetting and drying on the aggregation of glass beads by a model mucilage. SEM micrographs showed that wetting and drying promoted the aggregation of glass beads by adjusting the morphology of the model mucilage during drying and rewetting. Until now, most authors investigated the polymer structures in soils on samples in their dry state. However, picturing the morphology under wet conditions, e.g., using environmental scanning electron microscopy (ESEM) is necessary to directly assess swollen hydrogel phases in soil and their contribution to the morphological and physical state of the soil structure. Furthermore, the number of existing studies using (E)SEM to assess visible effects of hydrogel swelling on soil structure is limited, which points out the need of further investigations.

5.3 Additional imaging techniques and their limitations

Besides (E)SEM, innovative and non-destructive three dimensional (3D) imaging techniques such as neutron imaging (NI), magnetic resonance imaging (MRI), and X-ray computer tomography (X-ray CT) are available and enable the observation of samples in their wet state. Although the application of these techniques is relatively new in soil science (less than two decades), they are increasingly used, especially in the context of plant-soil research. The listed techniques rely on different physical principles and hence reveal specific potentials and challenges. However, the major shortcoming of all these techniques is the low-attenuation contrast

between different types of water such as hydrogel-associated water or water confined in soil pores.

NI and MRI allow the spatio-temporal visualization of soil water distribution. NI is based on neutron transmission and maps the total proton density. It is able to detect patterns with high resolution (Oswald et al., 2015). Moradi et al. (2011) showed a water enrichment of the rhizosphere using NI and related the observations to the exertion of mucilage by the roots of the investigated plant species, as NI cannot directly distinguish hydrogel-associated water from other water types. In addition to this, the long acquisition times of about 4 h for an entire tomogram limits the use of NI for in situ measurements of fast processes associated with soil-water-hydrogel interactions (Oswald et al., 2015). In comparison to NI, MRI uses the principle of nuclear magnetic resonance to image the water protons present in the sample. Contrary to 1D and 2D $^1\text{H-NMR}$ relaxometry, the possibility of MRI to investigate samples on a three-dimensional scale involves a higher noise and a smaller number of data points (Haber-Pohlmeier et al., 2010). The contrast parameters include differences in proton density and the time constants (T_1 and T_2) of the signal decay. Image distortions and invisibility of certain water types are the major problems of MRI. They result from very short relaxation times due to the presence of ferromagnetic particles, high clay content, and low water content in the soil samples (Merz et al., 2015). Small soil pores and the presence of hydrogel phases also contribute to reduced relaxation time and can probably induce artefacts in the MRI images as observed by Oswald et al. (2015) for lupine roots; a dark zone for water depletion was observed around the root system, contradicting the results of Moradi et al. (2011) obtained with NI. The actual limitations of MRI do not yet allow the detection of biohydrogel phases in soil, but much effort is done to further develop this technique (Merz et al., 2015; Hermann et al., 2002).

The third technique, X-ray computer tomography (CT), irradiates a X-ray beam through a sample, whereby the intensity of the beam is absorbed according to the density of the sample components (Metzner et al., 2015). The differentiation between biohydrogel-associated water and other water types is rather impossible with X-ray CT as both water types have nearly the same density. However, with a relatively short measurement time, X-ray CT has the potential to examine dynamic processes, such as water movement, before and after an infiltration period or water redistribution processes during swelling and shrinkage (Mooney, 2002). This advantage could be useful in order to study water fluxes in samples in which the localization of biohydrogel phases is already known.

NI, MRI, and X-ray CT offer the exciting possibility to investigate in situ processes in the rhizosphere (Helliwell et al., 2013). Due to methods' limitations and to a missing attention for the distinction of biohydrogel phases in soil, the major shortcoming of these methods concerning our research question is the low attenuation contrast to hydrogel water. Thus, the application of these techniques to detect biohydrogel phases in soil requires further investigations and, if necessary, developments. (E)SEM offers an interesting alternative,

although the distinction of biohydrogel phases in wet samples may be the major challenge to overcome. Nevertheless, the combination of methods linking physicochemical characteristics of biohydrogel-rich soils with visual structures, e.g., as 3D pictures, is a promising approach to untangle the diverse effects of biohydrogels on soil physicochemistry.

6 Conclusion and Outlook

Biohydrogel-rich soils are complex systems as they comprise two different porous frameworks: mineral soil constituents and swollen biohydrogel structures. The combination of different methods to study water entrapment and structural properties in terms of mechanical stability or visual structures proves to be powerful by providing insights into the nature of hydrogel-induced soil-water interactions and structural stabilization mechanisms (Fig. 6).

Concerning the investigation of mechanical stability of soil structures under the impact of biohydrogel, rheology has proven to be a sensitive and innovative technique, especially in the context of microstructural stability in terms of particle-

particle interactions. However, since recent studies have not yet directly linked the swelling degree of hydrogel with the structural stability of hydrogel-rich soil, further research is needed to close this research gap.

¹H-NMR relaxometry, PFG-NMR and DSC seem the most capable methods in order to investigate the swelling degree of hydrogel structures in biohydrogel-rich soils to explain soil structural stability. They enable the study of molecular mobility of water molecules and the differentiation of several water types and degrees of water entrapment in the investigated samples. Nevertheless, the application of 1D ¹H-NMR as well as DSC on biohydrogel-rich soil seems limited due to restricted differentiability of water phases in soil and due to the lack of knowledge regarding the spatiotemporal distribution of swollen hydrogel phases within the soil matrix. 2D ¹H-NMR relaxometry is promising to overcome these limitations as it combines the measurement of the two relaxation mechanisms or the one of the diffusion coefficient. Further, imaging techniques such as (E)SEM, NI, MRI and X-ray CT might enable the visualization of biohydrogel-rich soil structures and the spatio-temporal distribution of water in the sample. Hence, imaging techniques might offer the possibility to dis-

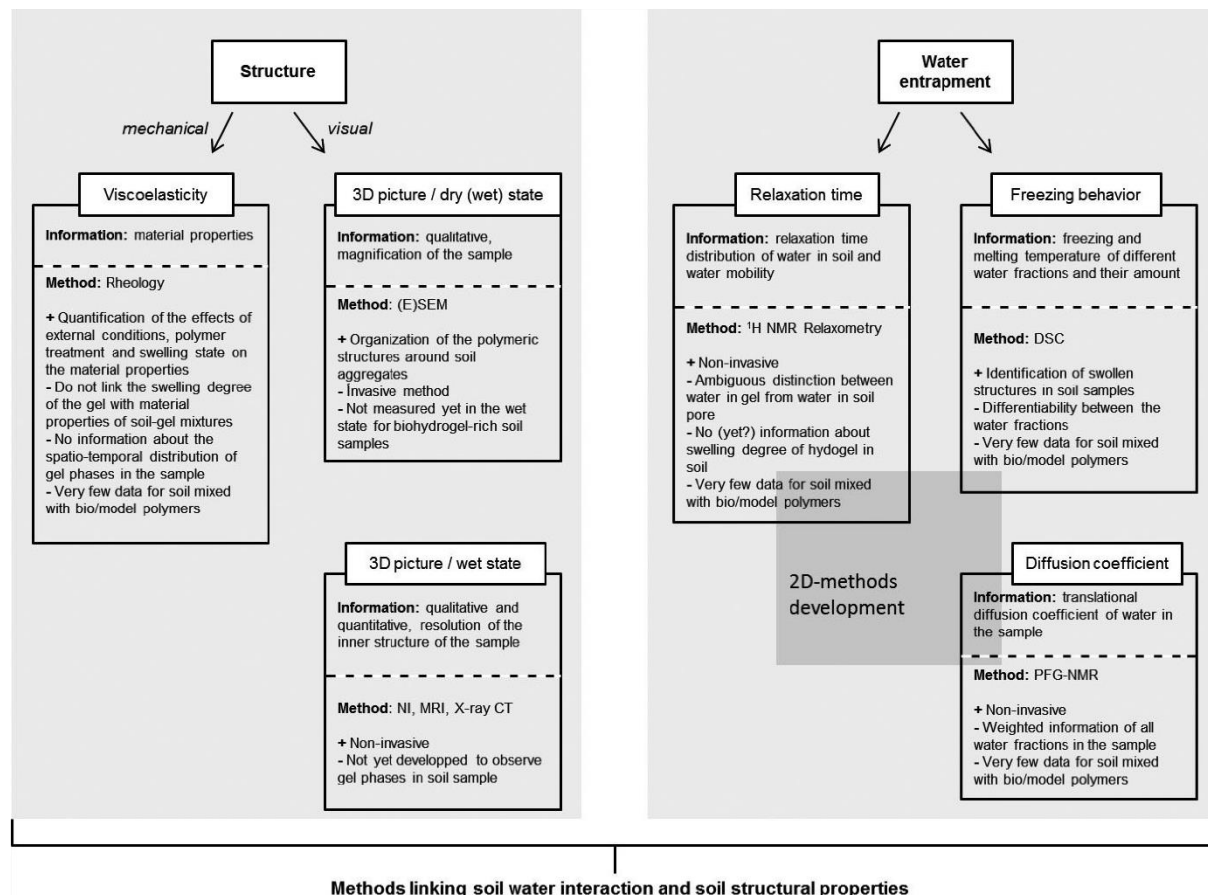


Figure 6: General overview of the different techniques allowing the disentanglement of hydrogel swelling in biohydrogel-rich soils and the associated soil-water-hydrogel interactions.

tinct between swollen biohydrogel structures and other water types, although further developments can be assumed as investigations of swollen hydrogel structures in biohydrogel-rich soil has not been investigated until now.

Acknowledgments

The authors wish to thank the DFG (German Research Foundation) for supporting this study within the project MUCILAGE (SCHA849/20).

References

- Abd El-Rehim, H. A., Hegazy, E.-S. A., Abd El-Mohdy, H. L. (2004): Radiation synthesis of hydrogels to enhance sandy soils water retention and increase plant performance. *J. Appl. Polym. Sci.* 93, 1360–1371.
- Agaba, H., Baguma Onikiriza, L. J., Esegu, O., Francis, J., Obua, J., Kabasa, J. D., Hüttermann, A. (2010): Effects of hydrogel amendment to different soils on plant available water and survival of trees under drought conditions. *Clean-Soil Air Water* 38, 328–335.
- Agaba, H., Onikiriza, L. J. B., Obua, J., Kabasa, J. D., Worbis, M., Hüttermann, A. (2011): Hydrogel amendment to sandy soil reduces irrigation frequency and improves the biomass of *Agrostis stolonifera*. *Agric. Sci.* 2, 544–550.
- Ahmed, M. A., Holz, M., Woche, S. K., Bachmann, J., Caminati, A. (2015): Effect of soil drying on mucilage exudation and its water repellency: a new method to collect mucilage. *J. Plant Nutr. Soil Sci.* 178, 821–824.
- Albalasmeh, A. A., Ghezzehei, T. A. (2014): Interplay between soil drying and root exudation in rhizosphere development. *Plant Soil* 374, 739–751.
- Al-Darby, A. M. (1996): The hydraulic properties of a sandy soil treated with gel-forming soil conditioner. *Soil Technol.* 9, 15–28.
- Andry, H., Yamamoto, T., Irie, T., Moritani, S., Inoue, M., Fujiyama, H. (2009): Water retention, hydraulic conductivity of hydrophilic polymers in sandy soil as affected by temperature and water quality. *J. Hydrol.* 373, 177–183.
- Bacic, A., Moody, S. F., Clarke, A. E. (1986): Structural analysis of secreted root slime from maize (*Zea mays* L.). *Plant Physiol.* 80, 771–777.
- Bai, W., Zhang, H., Liu, B., Wu, Y., Song, J. (2010): Effects of superabsorbent polymers on the physical and chemical properties of soil following different wetting and drying cycles. *Soil Use Manage.* 26, 253–260.
- Bakass, M., Mokhlisse, A., Lallemand, M. (2002): Absorption and desorption of liquid water by a superabsorbent polymer: Effect of polymer in the drying of the soil and the quality of certain plants. *J. Appl. Polym. Sci.* 83, 234–243.
- Barbucci, R., Leone, G., Chiumiento, A., Di Cocco, M. E., D'Orazio, G., Gianferri, R., Delfini, M. (2006): Low- and high-resolution nuclear magnetic resonance (NMR) characterisation of hyaluronan-based native and sulfated hydrogels. *Carbohydr. Res.* 341, 1848–1858.
- Barré, P., Hallett, P. D. (2009): Rheological stabilization of wet soils by model root and fungal exudates depends on clay mineralogy. *Eur. J. Soil Sci.* 60, 525–538.
- Bayer, J. V., Jaeger, F., Schaumann, G. E. (2010): Proton nuclear magnetic resonance (NMR) relaxometry in soil science applications. *Open Magn. Reson. J.* 3, 15–26.
- Belton, P. S. (1997): NMR and the mobility of water in polysaccharide gels. *Int. J. Biol. Macromol.* 21, 81–88.
- Belton, P. S., Hills, B. P., Raimbaud, E. R. (1988): The effects of morphology and exchange on proton NMR relaxation in agarose gels. *Mol. Phys.* 63, 825–842.
- Bhardwaj, A. K., Shainberg, I., Goldstein, D., Warrington, D. N., Levy, G. J. (2007): Water retention and hydraulic conductivity of cross-linked polyacrylamides in sandy soils. *Soil Sci. Soc. Am. J.* 71, 406–412.
- Blumenkrantz, N., Asboe-Hansen, G. (1973): New method for quantitative determination of uronic acids. *Anal. Biochem.* 54, 484–489.
- Bouranis, D. L., Theodoropoulos, A. G., Drossopoulos, J. B. (1995): Designing synthetic polymers as soil conditioners. *Commun. Soil Sci. Plan.* 26, 1455–1480.
- Bouwstra, J. A., Salomons-de Vries, M. A., van Miltenburg, J. C. (1995): The thermal behaviour of water in hydrogels. *Thermochim. Acta* 248, 319–327.
- Bradford, M. M. (1976): A rapid and sensitive method for the quantitation of microgram quantities of protein utilizing the principle of protein-dye binding. *Anal. Biochem.* 72, 248–254.
- Buchmann, C., Schaumann, G. E. (2016): Effect of water entrapment by a hydrogel on the microstructural stability of artificial soils with various clay content. *Plant Soil*. DOI: 10.1007/s11104-016-3110-z.
- Buchmann, C., Bentz, J., Schaumann, G. E. (2015): Intrinsic and model polymer hydrogel-induced soil structural stability of a silty sand soil as affected by soil moisture dynamics. *Soil Till. Res.* 154, 22–33.
- Buchmann, C., Meyer, M., Schaumann, G. E. (2014): Characterization of wet aggregate stability of soils by H-NMR relaxometry. *Magn. Reson. Chem.* 53, 694–703.
- Burey, P., Bhandari, B. R., Howes, T., Gidley, M. J. (2008): Hydrocolloid gel particles: formation, characterization, and application. *Crit. Rev. Food Sci. Nutr.* 48, 361–377.
- Caillard, R., Remondetto, G. E., Subirade, M. (2009): Physico-chemical properties and microstructure of soy protein hydrogels co-induced by Maillard type cross-linking and salts. *Food Res. Int.* 42, 98–106.
- Caló, E., Khutoryanskiy, V. V. (2015): Biomedical applications of hydrogels: a review of patents and commercial products. *Eur. Polym. J.* 65, 252–267.
- Calucci, L., Forte, C., Ranucci, E. (2008): Water/polymer interactions in poly (amidoamine) hydrogels by ¹H nuclear magnetic resonance relaxation and magnetization transfer. *J. Chem. Phys.* 129. DOI: 10.1063/1.2968606.
- Capitani, D., Crescenzi, V., De Angelis, A. A., Segre, A. L. (2001): Water in hydrogels. An NMR study of water/polymer interactions in weakly cross-linked chitosan networks. *Macromolecules* 34, 4136–4144.
- Caminati, A. (2012): A model of root water uptake coupled with rhizosphere dynamics. *Vadose Zone J.* 11. DOI: 10.2136/vzj2011.0106.
- Caminati, A., Vetterlein, D. (2013): Plasticity of rhizosphere hydraulic properties as a key for efficient utilization of scarce resources. *Ann. Bot.* 112, 277–290.
- Cavalcante, C. L., Brandani, S., Ruthven, D. M. (1997): Evaluation of the main diffusion path in zeolites from ZLC desorption curves. *Zeolites* 18, 282–285.
- Chang, C., Zhang, L., Zhou, J., Zhang, L., Kennedy, J. F. (2010): Structure and properties of hydrogels prepared from cellulose in NaOH/urea aqueous solutions. *Carbohydr. Polym.* 82, 122–127.
- Chen, R. H., Chen, W. Y. (2001): Rheological properties of the water-soluble mucilage of a green laver, *Monostroma nitidium*. *J. Appl. Phycol.* 13, 481–488.

- Chen, Z. A., Ruth, D. W. (1995): The effect of gravity degradation on low-speed centrifuge capillary pressure data. *AIChE J.* 41, 469–480.
- Chenu, C. (1993): Clay-or sand-polysaccharide associations as models for the interface between micro-organisms and soil: water related properties and microstructure. *Geoderma* 56, 143–156.
- Chenu, C., Roberson, E. B. (1996): Diffusion of glucose in microbial extracellular polysaccharide as affected by water potential. *Soil Biol. Biochem.* 28, 877–884.
- Costabel, S., Yaramanci, U. (2013): Estimation of water retention parameters from nuclear magnetic resonance relaxation time distributions. *Water Resour. Res.* 49, 2068–2079.
- Cotts, R. M. (1991): Diffusion and diffraction. *Nature* 351, 443–444.
- Czames, S., Hallett, P. D., Bengough, A. G., Young, I. M. (2000): Root- and microbial-derived mucilages affect soil structure and water transport. *Eur. J. Soil Sci.* 51, 435–443.
- Davidson, R. L. (1980): *Handbook of Water-Soluble Gums and Resins*. McGraw-Hill, New York, NY, USA.
- de Celis Alonso, B., Rayment, P., Ciampi, E., Ablett, S., Marciari, L., Spiller, R. C., Norton, I. T., Gowland, P. A. (2010): NMR relaxometry and rheology of ionic and acid alginate gels. *Carbohydr. Polym.* 82, 663–669.
- de Kruijf, C. K., Anema, S. G., Zhu, C., Havea, P., Coker, C. (2015): Water holding capacity and swelling of casein hydrogels. *Food Hydrocoll.* 44, 372–379.
- de Paula, R. C. M., Rodrigues, J. F. (1995): Composition and rheological properties of cashew tree gum, the exudate polysaccharide from *Anacardium occidentale* L. *Carbohydr. Polym.* 26, 177–181.
- Degrassi, A., Toffanin, R., Paoletti, S., Hall, L. D. (1998): A better understanding of the properties of alginate solutions and gels by quantitative magnetic resonance imaging (MRI). *Carbohydr. Res.* 306, 19–26.
- Deng, W., Hallett, P. D., Jeng, D.-S., Squire, G. R., Toorop, P. E., Iannetta, P. P. (2015): The effect of natural seed coatings of *Capsella bursa-pastoris* L. Medik. (shepherd's purse) on soil-water retention, stability and hydraulic conductivity. *Plant Soil* 387, 167–176.
- Diehl, D., Schneckenburger, T., Krüger, J., Goebel, M.-O., Woche, S. K., Schwarz, J., Shchegolikina, A., Lang, F., Marschner, B., Thiele-Bruhn, S., Bachmann, J., Schaumann, G. E. (2014): Effect of multivalent cations, temperature and aging on soil organic matter interfacial properties. *Environ. Chem.* 11, 709–718.
- Djabourov, M. (1991): Gelation—A review. *Polym. Int.* 25, 135–143.
- Du, C., Zhou, G., Wang, H., Chen, X., Zhou, J. (2010): Depth profiling of clay-xanthan complexes using step-scan mid-infrared photoacoustic spectroscopy. *J. Soils Sediments* 10, 855–862.
- Dubois, M., Gilles, K. A., Hamilton, J. K., Rebers, P. A., Smith, F. (1956): Colorimetric method for determination of sugars and related substances. *Anal. Chem.* 28, 350–356.
- Dunn, K.-J., Bergman, D. J., LaTorraca, G. A. (2002): *Nuclear Magnetic Resonance: Petrophysical and Logging Applications*. Pergamon, New York, NY, USA.
- Flemming, H.-C., Wingender, J. (2010): The biofilm matrix. *Nat. Rev. Microbiol.* 8, 623–633.
- Fonteno, W. C., Bilderback, T. E. (1993): Impact of hydrogel on physical properties of coarse-structured horticultural substrates. *J. Am. Soc. Hortic. Sci.* 118, 217–222.
- Fordham, E., Gibbs, S. J., Hall, L. D. (1994): Partially restricted diffusion in a permeable sandstone: observations by stimulated echo PFG NMR. *Magn. Reson. Imaging* 12, 279–284.
- Froix, M. F., Nelson, R. (1975): The interaction of water with cellulose from nuclear magnetic resonance relaxation times. *Macromolecules* 8, 726–730.
- Frosch, G. P., Tillich, J. E., Haselmeier, R., Holz, M., Althaus, E. (2000): Probing the pore space of geothermal reservoir sandstones by nuclear magnetic resonance. *Geothermics* 29, 671–687.
- Fyfe, C. A., Blazek, A. I. (1997): Investigation of hydrogel formation from hydroxypropylmethylcellulose (HPMC) by NMR spectroscopy and NMR imaging techniques. *Macromolecules* 30, 6230–6237.
- Ganji, F., Vasheghani-Farahani, S., Vasheghani-Farahani, E. (2010): Theoretical description of hydrogel swelling: a review. *Iran. Polym. J.* 19, 375–398.
- Garcia, A. M., Walter Jr., W. M. (1998): Physicochemical characterization of starch from Peruvian sweet potato selections ASA Alimentos S.S., Lima, Peru. *Starch-Stärke* 50, 331–337.
- Gamier, C., Axelos, M. A., Thibault, J.-F. (1993): Phase diagrams of pectin-calcium systems: Influence of pH, ionic strength, and temperature on the gelation of pectins with different degrees of methylation. *Carbohydr. Res.* 240, 219–232.
- Gerlach, G., Amdt, K.-F. (2010): *Hydrogel Sensors and Actuators*. Springer, Berlin, Germany.
- Gessa, C., Deiana, S. (1992): Ca-polygalacturonate as a model for a soil-root interface. *Plant Soil* 140, 1–13.
- Gessa, C., Deiana, S. (1990): Fibrillar structure of Ca Polygalacturonate as a model for a soilroot interface: I. A hypothesis on the arrangement of the polymeric chains inside the fibrils. *Plant Soil* 129, 211–217.
- Gilsenan, P. M., Richardson, R. K., Morris, E. R. (2000): Thermally reversible acid-induced gelation of low-methoxy pectin. *Carbohydr. Polym.* 41, 339–349.
- Götz, J., Hinrichs, R. (2008): *Diffusion and Relaxation in Gels*, in Webb, G. A. (ed.): *Modern Magnetic Resonance*. Springer, Amsterdam, The Netherlands, pp. 1713–1719.
- Graessley, W. W. (1974): *The Entanglement Concept in Polymer Rheology*. Springer, Berlin, Germany.
- Grant, G. T., Morris, E. R., Rees, D. A., Smith, P. J. C., Thom, D. (1973): Biological interactions between polysaccharides and divalent cations: The egg-box model. *FEBS Lett.* 32, 195–198.
- Guan, Y. L., Shao, L., Yao, K. D. (1996): A study on correlation between water state and swelling kinetics of chitosan-based hydrogels. *J. Appl. Polym. Sci.* 61, 2325–2335.
- Guilheme, M. R., Aouada, F. A., Fajardo, A. R., Martins, A. F., Paulino, A. T., Davi, M. F., Rubira, A. F., Muniz, E. C. (2015): Superabsorbent hydrogels based on polysaccharides for application in agriculture as soil conditioner and nutrient carrier: A review. *Eur. Polym. J.* 72, 365–385.
- Haber-Pohlmeier, S., Stapf, S., Van Dusschoten, D., Pohlmeier, A. (2010): Relaxation in a natural soil: comparison of relaxometric imaging, T1-T2 correlation and fast-field cycling NMR. *Open Magn. Reson. J.* 3, 57–62.
- Haider, K. (1999): Von der toten organischen Substanz zum Humus. *J. Plant Nutr. Soil Sci.* 162, 363–371.
- Hall, G. M. (1996): *Methods of Testing Protein Functionality*. Springer, New York, NY, USA.
- Hatakeyama, H., Hatakeyama, T. (1998): Interaction between water and hydrophilic polymers. *Themochim. Acta* 308, 3–22.
- Hatakeyama, T., Hatakeyama, H. (2006): *Thermal Properties of Green Polymers and Biocomposites*. Kluwer Academic Publishers, Dordrecht, The Netherlands.

- Hatakeyama, T., Hatakeyama, H., Nakamura, K. (1995): Non-freezing water content of mono- and divalent cation salts of polyelectrolyte-water systems studied by DSC. *Thermochim. Acta* 253, 137–148.
- Hedrick, R. M., Mowry, D. T. (1952): Effect of synthetic polyelectrolytes on aggregation, aeration and water relationships of soil. *Soil Sci.* 73, 427–442.
- Helliwell, J. R., Sturrock, C. J., Grayling, K. M., Tracy, S. R., Flavel, R. J., Young, I. M., Whalley, W. R., Mooney, S. J. (2013): Applications of X-ray computed tomography for examining biophysical interactions and structural development in soil systems: a review. *Eur. J. Soil Sci.* 64, 279–297.
- Henao, L. J., Mazeau, K. (2009): Molecular modelling studies of clay-exopolysaccharide complexes: Soil aggregation and water retention phenomena. *Mater. Sci. Eng. C* 29, 2326–2332.
- Herrmann, K.-H., Pohlmeier, A., Gembris, D., Vereecken, H. (2002): Three-dimensional imaging of pore water diffusion and motion in porous media by nuclear magnetic resonance imaging. *J. Hydrol.* 267, 244–257.
- Hills, B. P. (1992): The proton exchange cross-relaxation model of water relaxation in biopolymer systems. *Mol. Phys.* 76, 489–508.
- Hills, B. P. (2007): Relaxometry: Two-Dimensional Methods, in Wasylshen, R. (ed.): *eMagRes*. John Wiley & Sons, Hoboken, NJ, USA. DOI: 10.1002/9780470034590.emrstm1042.
- Hills, B. P., Cano, C., Belton, P. S. (1991): Proton NMR relaxation studies of aqueous polysaccharide systems. *Macromolecules* 24, 2944–2950.
- Hills, B. P., Godward, J., Debatty, M., Barras, L., Saturio, C. P., Ouwerx, C. (2000): NMR studies of calcium induced alginate gelation. Part II. The internal bead structure. *Magn. Reson. Chem.* 38, 719–728.
- Hills, B. P., Takacs, S. F., Belton, P. S. (1990): A new interpretation of proton NMR relaxation time measurements of water in food. *Food Chem.* 37, 95–111.
- Hills, B. P., Wright, K. M., Belton, P. S. (1989): Proton N.M.R. studies of chemical and diffusive exchange in carbohydrate systems. *Mol. Phys.* 67, 1309–1326.
- Holthusen, D., Peth, S., Horn, R. (2010): Impact of potassium concentration and matric potential on soil stability derived from rheological parameters. *Soil Till. Res.* 111, 75–85.
- Hussien, R. A., Donia, A. M., Atia, A. A., El-Sedfy, O. F., El-Hamid, A. R. A., Rashad, R. T. (2012): Studying some hydro-physical properties of two soils amended with kaolinite-modified cross-linked poly-acrylamides. *Catena* 92, 172–178.
- Hüttermann, A., Zommodi, M., Reise, K. (1999): Addition of hydrogels to soil for prolonging the survival of *Pinus halepensis* seedlings subjected to drought. *Soil Till. Res.* 50, 295–304.
- Jaeger, F., Bowe, S., Van As, H., Schaumann, G. E. (2009): Evaluation of ¹H NMR relaxometry for the assessment of pore-size distribution in soil samples. *Eur. J. Soil Sci.* 60, 1052–1064.
- Jaeger, F., Rudolph, N., Lang, F., Schaumann, G. E. (2008): Effects of soil solution's constituents on proton NMR relaxometry of soil samples. *Soil Sci. Soc. Am. J.* 72, 1694–1707.
- Jaeger, F., Shchegolikina, A., Van As, H., Schaumann, G. E. (2010): Proton NMR relaxometry as a useful tool to evaluate swelling processes in peat soils. *Open Magn. Reson. J.* 3, 27–45.
- Jähnert, S., Chávez, F. V., Schaumann, G. E., Schreiber, A., Schönhoff, M., Findenegg, G. H. (2008): Melting and freezing of water in cylindrical silica nanopores. *Phys. Chem. Chem. Phys.* 10, 6039–6051.
- Johnson, M. S. (1984): The effects of gel-forming polyacrylamides on moisture storage in sandy soils. *J. Sci. Food Agric.* 35, 1196–1200.
- Johnson, M. S., Veltkamp, C. J. (1985): Structure and functioning of water-storing agricultural polyacrylamides. *J. Sci. Food Agric.* 36, 789–793.
- Jørgensen, T. E., Sletmoen, M., Draget, K. I., Stokke, B. T. (2007): Influence of oligogulonates on alginate gelation, kinetics, and polymer organization. *Biomacromolecules* 8, 2388–2397.
- Kaith, B. S., Jindal, R., Kapur, G. S., others (2013): Enzyme-based green approach for the synthesis of gum tragacanth and acrylic acid cross-linked hydrogel: its utilization in controlled fertilizer release and enhancement of water-holding capacity of soil. *Iran. Polym. J.* 22, 561–570.
- Kazanskii, K. S., Dubrovskii, S. A. (1992): Chemistry and Physics of "Agricultural" Hydrogels, in Abe, A., Dusěk, K., Kobayashi, S. (eds.): *Polyelectrolytes Hydrogels Chromatographic Materials*. Springer, Berlin, Germany, pp. 97–133.
- Keller, T., Lamandé, M., Peth, S., Berli, M., Delenne, J.-Y., Baumgarten, W., Rabbel, W., Radjai, F., Rajchenbach, J., Selvadurai, A. P. S., Or, D. (2013): An interdisciplinary approach towards improved understanding of soil deformation during compaction. *Soil Till. Res.* 128, 61–80.
- Kerr, W. L., Wicker, L. (2000): NMR proton relaxation measurements of water associated with high methoxy and low methoxy pectins. *Carbohydr. Polym.* 42, 133–141.
- Kleinberg, R. L., Kenyon, W. E., Mitra, P. P. (1994): Mechanism of NMR relaxation of fluids in rock. *J. Magn. Reson. A* 108, 206–214.
- Kögel-Knabner, I. (2002): The macromolecular organic composition of plant and microbial residues as inputs to soil organic matter. *Soil Biol. Biochem.* 34, 139–162.
- Kroener, E., Ahmed, M. A., Carminati, A. (2015): Roots at the percolation threshold. *Phys. Rev. E* 91. DOI: 10.1103/PhysRevE.91.042706.
- Kroener, E., Zarebanadkouki, M., Kaestner, A., Carminati, A. (2014): Nonequilibrium water dynamics in the rhizosphere: How mucilage affects water flow in soils. *Water Resour. Res.* 50, 6479–6495.
- Kučenk, J., Bursáková, P., Průšová, A., Grebiková, L., Schaumann, G. E. (2012): Hydration of humic and fulvic acids studied by DSC. *J. Therm. Anal. Calorim.* 110, 451–459.
- Lauth, G. J., Kowalczyk, J. (2016): Gele: Hydrogele und Aerogele, in Lauth, G. J., Kowalczyk, J. (eds.): *Einführung in die Physik und Chemie der Grenzflächen und Kolloide*. Springer, Berlin, Germany, pp. 429–436.
- León-Martínez, F. M., Rodríguez-Ramírez, J., Medina-Torres, L. L., Lagunas, L. M., Bernad-Bernad, M. J. (2011): Effects of drying conditions on the rheological properties of reconstituted mucilage solutions (*Opuntia ficus-indica*). *Carbohydr. Polym.* 84, 439–445.
- Leung, H. K., Steinberg, M. P. (1979): Water binding of food constituents as determined by NMR, freezing, sorption and dehydration. *J. Food Sci.* 44, 1212–1216.
- Levy, G. J., Warrington, D. N. (2015): Polyacrylamide Addition to Soils: Impacts on Soil Structure and Stability, in Cirillo, G., Spizziri, U. G., Lemma, F. (eds.): *Functional Polymers in Food Science*. John Wiley & Sons, Inc., Hoboken, NJ, USA, pp. 9–32.
- Liu, H., Eskin, N. A. M., Cui, S. W. (2003): Interaction of wheat and rice starches with yellow mustard mucilage. *Food Hydrocoll.* 17, 863–869.
- Liu, J., Shi, B., Jiang, H., Bae, S., Huang, H. (2009): Improvement of water-stability of clay aggregates admixed with aqueous polymer soil stabilizers. *Catena* 77, 175–179.
- Lüsse, S., Arnold, K. (1998): Water binding of polysaccharides NMR and ESR studies. *Macromolecules* 31, 6891–6897.
- Mamedov, A. I., Beckmann, S., Huang, C., Levy, G. J. (2007): Aggregate stability as affected by polyacrylamide molecular

- weight, soil texture, and water quality. *Soil Sci. Soc. Am. J.* 71, 1909–1918.
- Mao, R., Tang, J., Swanson, B. G. (2001): Water holding capacity and microstructure of gellan gels. *Carbohydr. Polym.* 46, 365–371.
- Mariette, F., Topgaard, D., Jönsson, B., Soderman, O. (2002): ^1H NMR diffusometry study of water in casein dispersions and gels. *J. Agric. Food Chem.* 50, 4295–4302.
- Markgraf, W., Hom, R. (2007): Scanning electron microscopy–energy dispersive scan analyses and rheological investigations of South-Brazilian soils. *Soil Sci. Soc. Am. J.* 71, 851–859.
- Markgraf, W., Hom, R. (2009): Rheological Investigations in Soil Micro Mechanics: Measuring Stiffness Degradation and Structural Stability on a Particle Scale, in Gragg, L. P., Cassell, J. M. (eds.): *Progress in Management Engineering*. Nova Science Publication, New York, NY, USA, pp. 237–279.
- Markgraf, W., Hom, R., Peth, S. (2006): An approach to rheometry in soil mechanics—structural changes in bentonite, clayey and silty soils. *Soil Till. Res.* 91, 1–14.
- Markgraf, W., Watts, C. W., Whalley, W. R., Hrkac, T., Hom, R. (2012): Influence of organic matter on rheological properties of soil. *Appl. Clay Sci.* 64, 25–33.
- Mary, B., Fresneau, C., Morel, J. L., Mariotti, A. (1993): C and N cycling during decomposition of root mucilage, roots and glucose in soil. *Soil Biol. Biochem.* 25, 1005–1014.
- Masaro, L., Zhu, X. X. (1999): Physical models of diffusion for polymer solutions, gels and solids. *Prog. Polym. Sci.* 24, 731–775.
- Mathur, A. M., Moorjani, S. K., Scranton, A. B. (1996): Methods for synthesis of hydrogel networks: A review. *J. Macromol. Sci. C* 36, 405–430.
- Matsukawa, S., Sagae, D., Mogi, A. (2009): Molecular Diffusion in Polysaccharide Gel Systems as Observed by NMR, in Tokita, P. D. M., Nishinari, P. D. K. (eds.): *Gels: Structures, Properties, and Functions*. Springer Berlin, Germany, pp. 171–176.
- Mayer, C., Moritz, R., Kirschner, C., Borchard, W., Maibaum, R., Wingender, J., Flemming, H. C. (1999): The role of intermolecular interactions: studies on model systems for bacterial biofilms. *Int. J. Biol. Macromol.* 26, 3–16.
- Mazen, A. M., Radwan, D. E. M., Ahmed, A. F. (2015): Growth responses of maize plants cultivated in sandy soil amended by different superabsorbent hydrogels. *J. Plant Nutr.* 38, 325–337.
- McBrierty, V. J., Wardell, G. E., Keely, C. M., O’neill, E. P., Prasad, M. (1996): The characterization of water in peat. *Soil Sci. Soc. Am. J.* 60, 991–1000.
- McBrierty, V. J., Martin, S. J., Karasz, F. E. (1999): Understanding hydrated polymers: the perspective of NMR. *J. Mol. Liq.* 80, 179–205.
- McConaughy, S. D., Kirkland, S. E., Treat, N. J., Stroud, P. A., McCormick, C. L. (2008a): Tailoring the network properties of Ca^{2+} crosslinked Aloe vera polysaccharide hydrogels for in situ release of therapeutic agents. *Biomacromolecules* 9, 3277–3287.
- McConaughy, S. D., Stroud, P. A., Boudreaux, B., Hester, R. D., McCormick, C. L. (2008b): Structural characterization and solution properties of a galacturonate polysaccharide derived from Aloe vera capable of in situ gelation. *Biomacromolecules* 9, 472–480.
- McConville, P., Whittaker, M. K., Pope, J. M. (2002): Water and polymer mobility in hydrogel biomaterials quantified by ^1H NMR: a simple model describing both T 1 and T 2 relaxation. *Macromolecules* 35, 6961–6969.
- Medina-Torres, L., Brito-De La Fuente, E., Torrestiana-Sanchez, B., Alonso, S. (2003): Mechanical properties of gels formed by mixtures of mucilage gum (*Opuntia ficus indica*) and carrageenans. *Carbohydr. Polym.* 52, 143–150.
- Medina-Torres, L., Brito-De La Fuente, E., Torrestiana-Sanchez, B., Kalthain, R. (2000): Rheological properties of the mucilage gum (*Opuntia ficus indica*). *Food Hydrocoll.* 14, 417–424.
- Merz, S., Pohlmeier, A., Balcom, B. J., Enjilela, R., Vereecken, H. (2015): Drying of a natural soil under evaporative conditions: a comparison of different magnetic resonance methods. *Appl. Magn. Reson.* 47, 121–138.
- Metzner, R., Eggert, A., van Dusschoten, D., Pflugfelder, D., Gerth, S., Schurr, U., Uhlmann, N., Jahnke, S. (2015): Direct comparison of MRI and X-ray CT technologies for 3D imaging of root systems in soil: potential and challenges for root trait quantification. *Plant Methods* 11. DOI: 10.1186/s13007-015-0060-z.
- Mezger, T. G. (2014): *The Rheology Handbook*. Vincentz Network, Hannover, Germany.
- Mimmo, T., Marzadori, C., Gessa, C. E. (2008): Does the degree of pectin esterification influence aluminium sorption by the root apoplast? *Plant Soil* 314, 159–168.
- Mizuta, K., Taguchi, S., Sato, S. (2015): Soil aggregate formation and stability induced by starch and cellulose. *Soil Biol. Biochem.* 87, 90–96.
- Mooney, S. J. (2002): Three-dimensional visualization and quantification of soil macroporosity and water flow patterns using computed tomography. *Soil Use Manage.* 18, 142–151.
- Moradi, A. B., Caminati, A., Vetterlein, D., Vontobel, P., Lehmann, E., Weller, U., Hopmans, J. W., Vogel, H.-J., Oswald, S. E. (2011): Three-dimensional visualization and quantification of water content in the rhizosphere. *New Phytol.* 192, 653–663.
- Morel, J. L., Habib, L., Plantureux, S., Guckert, A. (1991): Influence of maize root mucilage on soil aggregate stability. *Plant Soil* 136, 111–119.
- Müller-Plathe, F. (1998): Different states of water in hydrogels? *Macromolecules* 31, 6721–6723.
- Muta, H., Kawachi, S., Satoh, M. (2003): Ion-specific swelling behavior of uncharged poly (acrylic acid) gel. *Colloid Polym. Sci.* 282, 149–155.
- Narjary, B., Aggarwal, P., Singh, A., Chakraborty, D., Singh, R. (2012): Water availability in different soils in relation to hydrogel application. *Geoderma* 187, 94–101.
- Ng, L.-T., Swami, S. (2008): NMR and texture analyses in relation to swelling kinetics of 2-hydroxyethyl methacrylate/N-vinylpyrrolidone hydrogels. *Macromol. Symp.* 264, 1–7.
- Nguyen, C., Froux, F., Recous, S., Morvan, T., Robin, C. (2008): Net N immobilisation during the biodegradation of mucilage in soil as affected by repeated mineral and organic fertilisation. *Nutr. Cycl. Agroecosys.* 80, 39–47.
- Ohtsuka, A., Watanabe, T. (1996): The network structure of gellan gum hydrogels based on the structural parameters by the analysis of the restricted diffusion of water. *Carbohydr. Polym.* 30, 135–140.
- Okada, R., Matsukawa, S., Watanabe, T. (2002): Hydration structure and dynamics in pullulan aqueous solution based on ^1H NMR relaxation time. *J. Mol. Struct.* 602, 473–483.
- Osbom, H. M. I., Lochey, F., Mosley, L., Read, D. (1999): Analysis of polysaccharides and monosaccharides in the root mucilage of maize (*Zea mays* L.) by gas chromatography. *J. Chromatogr. A* 831, 267–276.
- Oswald, S. E., Tötze, C., Haber-Pohlmeier, S., Pohlmeier, A., Kaestner, A. P., Lehmann, E. (2015): Combining neutron and magnetic resonance imaging to study the interaction of plant roots and soil. *Phys. Procedia* 69, 237–243.
- Ottenbrite, R. M., Park, K., Okano, T. (2010): *Biomedical Applications of Hydrogels Handbook*. Springer, New York, NY, USA.

- Paul, E. A. (2014): *Soil Microbiology, Ecology and Biochemistry*. Academic Press, Oxford, UK.
- Peng, X., Hallett, P. D., Zhang, B., Horn, R. (2011): Physical response of rigid and non-rigid soils to analogues of biological exudates. *Eur. J. Soil Sci.* 62, 676–684.
- Peschier, L. J. C., Bouwstra, J. A., de Bleyser, J., Junginger, H. E., Leyte, J. C. (1993): Water mobility and structure in poly[2-hydroxyethylmethacrylate] hydrogels by means of the pulsed field gradient NMR technique. *Biomaterials* 14, 945–952.
- Ping, Z. H., Nguyen, Q. T., Chen, S. M., Zhou, J. Q., Ding, Y. D. (2001): States of water in different hydrophilic polymers—DSC and FTIR studies. *Polymer* 42, 8461–8467.
- Prawitwong, P., Takigami, S., Phillips, G. O. (2007): Phase transition behaviour of sorbed water in Konjac mannan. *Food Hydrocoll.* 21, 1368–1373.
- Průšová, A., Šmejkalová, D., Chytil, M., Velebný, V., Kučenk, J. (2010): An alternative DSC approach to study hydration of hyaluronan. *Carbohydr. Polym.* 82, 498–503.
- Průšová, A., Vergeldt, F. J., Kučenk, J. (2013): Influence of water content and drying on the physical structure of native hyaluronan. *Carbohydr. Polym.* 95, 515–521.
- Quinn, F. X., Kampff, E., Smyth, G., McBrierty, V. J. (1988): Water in hydrogels. 1. A study of water in poly(N-vinyl-2-pyrrolidone/methyl methacrylate) copolymer. *Macromolecules* 21, 3191–3198.
- Radosta, S., Schierbaum, F. (1990): Polymer-water interaction of maltodextrins. Part III: Non-freezable water in maltodextrin solutions and gels. *Starch-Stärke* 42, 142–147.
- Ray, T. C., Callow, J. A., Kennedy, J. F. (1988): Composition of root mucilage polysaccharides from *Lepidium sativum*. *J. Exp. Bot.* 39, 1249–1261.
- Read, D. B., Bengough, A. G., Gregory, P. J., Crawford, J. W., Robinson, D., Scrimgeour, C. M., Young, I. M., Zhang, K., Zhang, X. (2003): Plant roots release phospholipid surfactants that modify the physical and chemical properties of soil. *New Phytol.* 157, 315–326.
- Rees, D. (1968): Structure, conformation, and mechanism in the formation of polysaccharide gels and networks. *Adv. Carbohydr. Chem. Biochem.* 24, 267–332.
- Rees, D. A., Welsh, E. J. (1977): Secondary and tertiary structure of polysaccharides in solutions and gels. *Angew. Chem. Int. Edit.* 16, 214–224.
- Reiner, M. (1960): *Lectures on Theoretical Rheology*. North-Holland Publisher, Amsterdam, The Netherlands.
- Roorda, W. (1994): Do hydrogels contain different classes of water? *J. Biomater. Sci. Polym. Ed.* 5, 381–395.
- Rosenzweig, R., Shavit, U., Furman, A. (2012): Water retention curves of biofilm-affected soils using xanthan as an analogue. *Soil Sci. Soc. Am. J.* 76, 61–69.
- Santos, F. L., Serralheiro, R. P. (2000): Improving infiltration of irrigated Mediterranean soils with polyacrylamide. *J. Agric. Eng. Res.* 76, 83–90.
- Schaumann, G. E. (2005): Matrix relaxation and change of water state during hydration of peat. *Colloid. Surface. A* 265, 163–170.
- Schaumann, G. E. (2006a): Soil organic matter beyond molecular structure Part I: Macromolecular and supramolecular characteristics. *J. Plant Nutr. Soil Sci.* 169, 145–156.
- Schaumann, G. E. (2006b): Soil organic matter beyond molecular structure Part II: Amorphous nature and physical aging. *J. Plant Nutr. Soil Sci.* 169, 157–167.
- Schaumann, G. E., Bertmer, M. (2014): Soil-Water Interactions, in Simpson, M. J., Simpson, A. J. (eds.): *NMR Spectroscopy: A Versatile Tool for Environmental Research*. John Wiley & Sons, Ltd., Chichester, UK, pp. 291–303.
- Schaumann, G. E., Hobley, E., Hurraß, J., Rotard, W. (2005): H-NMR Relaxometry to monitor wetting and swelling kinetics in high organic matter soils. *Plant Soil* 275, 1–20.
- Schaumann, G. E., Hurraß, J. (2003): Changes of porosity and soil physical chemistry due to drying and re-wetting cycles. *Mitt. Dt. Bodenkundl. Ges.* 101, 39–40.
- Schaumann, G. E., Rotard, W., Hobley, E., Hurrass, J. (2002): Colloidal properties of DOM: Changes due to drying and re-moistening cycles? *Mitt. Dt. Bodenkundl. Ges.* 99, 203–204.
- Schmitt, J., Flemming, H.-C. (1999): Water binding in biofilms. *Water Sci. Technol.* 39, 77–82.
- Shapiro, Y. E. (2011): Structure and dynamics of hydrogels and organogels: an NMR spectroscopy approach. *Prog. Polym. Sci.* 36, 1184–1253.
- Shin, J.-E., Comillon, P., Salim, L. (2002): The effect of centrifugation on agar/sucrose gels. *Food Hydrocoll.* 16, 89–94.
- Smagin, A., Sadovnikova, N., Nikolaeva, E. I. (2014): Thermodynamic analysis of the effect of strongly swelling polymer hydrogels on the physical state of soil and sediment samples. *Eurasian Soil Sci.* 47, 78–88.
- Smidsrød, O., Haug, A. (1971): Estimation of the relative stiffness of the molecular chain in polyelectrolytes from measurements of viscosity at different ionic strengths. *Biopolymers* 10, 1213–1227.
- Song, K.-M., Mitchell, J., Jaffel, H., Gladden, L. F. (2012): Monitoring water transport between pores and voids in aerated gypsum using two-dimensional nuclear magnetic resonance exchange measurements. *J. Phys. D* 45. DOI: 10.1088/0022-3727/45/10/105302.
- Stallmach, F., Kärger, J. (1999): The potentials of pulsed field gradient NMR for investigation of porous media. *Adsorption* 5, 117–133.
- Strathmann, M., Griebel, T., Flemming, H.-C. (2000): Artificial biofilm model—a useful tool for biofilm research. *Appl. Microbiol. Biotechnol.* 54, 231–237.
- Strathmann, M., Griebel, T., Flemming, H.-C. (2001): Agarose hydrogels as EPS models. *Water Sci. Technol.* 43, 169–174.
- Sun, X.-F., Feng, Y., Shi, X., Wang, Y. (2016): Preparation and property of xylan/poly (methacrylic acid) semi-interpenetrating network hydrogel. *Int. J. Polym. Sci.* 2016. DOI: 10.1155/2016/8241078.
- Takigami, S., Takigami, M. (1993): Hydration of the crosslinked hyaluronan derivativ hylan. *Carbohydr. Polym.* 22, 153–160.
- Tang, Y., Hürlimann, M., Mandal, S., Paulsen, J., Song, Y.-Q. (2014): Coaxial probe for nuclear magnetic resonance diffusion and relaxation correlation experiments. *J. Appl. Phys.* 115. DOI: 10.1063/1.4866363.
- Timotiwi, P. B., Sakurai, N. (2002): Identification of mono-, oligo-, and polysaccharides secreted from soybean roots. *J. Plant Res.* 115, 77–85.
- Todoruk, T. R., Langford, C. H., Kantzas, A. (2003): Pore-scale redistribution of water during wetting of air-dried soils as studied by low-field NMR relaxometry. *Environ. Sci. Technol.* 37, 2707–2713.
- Topgaard, D., Södeman, O. (2002): Changes of cellulose fiber wall structure during drying investigated using NMR self-diffusion and relaxation experiments. *Cellulose* 9, 139–147.
- Van As, H., Lens, P. (2001): Use of ¹H NMR to study transport processes in porous biosystems. *J. Ind. Microbiol. Biotechnol.* 26, 43–52.
- Van Den Bulcke, A. I., Bogdanov, B., De Rooze, N., Schacht, E. H., Cornelissen, M., Berghmans, H. (2000): Structural and rheological

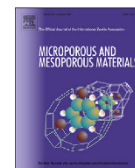
- properties of methacrylamide modified gelatin hydrogels. *Biomacromolecules* 1, 31-38.
- Van Vlierberghe, S., Dubruel, P., Schacht, E. (2010): Effect of cryogenic treatment on the rheological properties of gelatin hydrogels. *J. Bioact. Compat. Polym.* 25, 498-512.
- Vinod, V. T. P., Sashidhar, R. B., Sarma, V. U. M., Vijaya Saradhi, U. V. R. (2008): Compositional analysis and rheological properties of gum kondagogu (*Cochlospermum gossypium*): a tree gum from India. *J. Agric. Food Chem.* 56, 2199-2207.
- Vogt, C., Galvosas, P., Klitzsch, N., Stallmach, F. (2002): Self-diffusion studies of pore fluids in unconsolidated sediments by PFG NMR. *J. Appl. Geophys.* 50, 455-467.
- Walkinshaw, M. D., Amott, S. (1981): Conformations and interactions of pectins: II. Models for junction zones in pectinic acid and calcium pectate gels. *J. Mol. Biol.* 153, 1075-1085.
- Wang, Y., Wang, L.-J., Li, D., Xue, J., Mao, Z.-H. (2009): Effects of drying methods on rheological properties of flaxseed gum. *Carbohydr. Polym.* 78, 213-219.
- Watt, M., McCully, M. E., Canny, M. J. (1994): Formation and stabilization of rhizosheaths of *Zea mays* L. (Effect of soil water content). *Plant Physiol.* 106, 179-186.
- Williams, P. A., Phillips, G. O., de Vries, J. (2004): Hydrocolloid gelling agents and their applications, in Phillips, G. O., Williams, P. A. (eds.): *Gums and Stabilisers for the Food Industry* 12. Royal Society of Chemistry, Cambridge, UK, pp. 23-31.
- Williams, J., Shaykewich, C. F. (1969): An evaluation of polyethylene glycol (PEG) 6000 and PEG 20,000 in the osmotic control of soil water matric potential. *Can. J. Soil Sci.* 49, 397-401.
- Yoshida, H., Hatakeyama, T., Hatakeyama, H. (1993a): Characterization of water in polysaccharide hydrogels by DSC. *J. Therm. Anal. Calorim.* 40, 483-489.
- Yoshida, H., Hatakeyama, T., Hatakeyama, H. (1993b): Crystallization of water in the xanthan-water System. *J. Intell. Mater. Syst. Struct.* 4, 543-547.
- Yoshinobu, M., Morita, M., Sakata, I. (1992): Porous structure and rheological properties of hydrogels of highly water-absorptive cellulose graft copolymers. *J. Appl. Polym. Sci.* 45, 805-812.
- Young, I. M. (1995): Variation in moisture contents between bulk soil and the rhizosheath of wheat (*Triticum aestivum* L. cv. Wembley). *New Phytol.* 130, 135-139.
- Zhang, B., Hallett, P. D., Zhang, G. (2008): Increase in the fracture toughness and bond energy of clay by a root exudate. *Eur. J. Soil Sci.* 59, 855-862.
- Zohuriaan-Mehr, M. J., Kabiri, K. (2008): Superabsorbent polymer materials: a review. *Iran. Polym. J.* 17, 451.

*3. EFFECT OF MUCILAGE ON WATER PROPERTIES IN THE
RHIZOSPHERE MONITORED BY ^1H -NMR RELAXOMETRY*



Contents lists available at ScienceDirect

Microporous and Mesoporous Materials

journal homepage: www.elsevier.com/locate/micromesoEffect of mucilage on water properties in the rhizosphere monitored by ^1H -NMR relaxometry

Mathilde Brax, Christian Buchmann, Gabriele Ellen Schaumann*

University Koblenz-Landau, Institute for Environmental Sciences, Group of Environmental and Soil Chemistry, Fortstrasse 7, 76829 Landau, Germany

a r t i c l e i n f o

Article history:

Received 13 January 2017
 Received in revised form
 12 July 2017
 Accepted 18 July 2017
 Available online xxx

Keywords:

Mucilage
 Gel effect
 ^1H NMR relaxometry
 Hierarchical pore structure

a b s t r a c t

Mucilage produced at the root tips is a soil-born biohydrogel, whose framework is a three-dimensional polysaccharidic polymer network, which can contain over 90% water. The specific biohydrogel properties of mucilage, such as volumetric expansion and shrinkage, affect soil mechanical and hydraulic properties. Still, the physico-chemical mechanisms governing the interactions between mucilage and the porous soil system remain mostly unclear. To our best knowledge, no currently applied method allows the distinction between biohydrogel phases and pore water in the porous soil system.

In this work, we used ^1H NMR relaxometry to analyze the presence and properties of biohydrogels in soil. Mucilage in soil leads to a hierarchical pore structure, consisting of the polymeric biohydrogel network surrounded by the surface of soil particles. Water molecules entrapped in mucilage-containing soils revealed an accelerated bulk relaxation and a higher surface relaxivity in comparison with soils not containing mucilage. In model soils, we quantified the gel effect, here defined as the influence of mucilage on proton relaxation. The difference between transversal and longitudinal relaxation rates was plotted as a function of the reciprocal diameter of the model soil particles for soils containing and not containing mucilage. The gel effect was thereby characterized by an accelerated bulk relaxation and an accelerated surface relaxation, traduced respectively by an increased y -intercept and an increased linear coefficient for mucilage-containing soil.

© 2017 Elsevier Inc. All rights reserved.

1. Introduction

Mucilage is a biohydrogel produced mainly at the root tips in the rhizosphere [1]. In general, biohydrogels are soil-born three-dimensional polysaccharidic polymer networks [2]. Due to their flexible porous network, biohydrogels have specific properties including a high water holding capacity, viscosity, and the ability to undergo volumetric expansion and shrinkage [2]. In the porous soil system, biohydrogels affect soil mechanical and hydraulic properties [3,4]. Current approaches assessing the effect of biohydrogels on soil focus rather on the effects of biohydrogels on soil properties than on the processes governing soil hydrological and mechanical properties [5,6]. These processes include the spatio-temporal distribution and the water content of biohydrogels in soil [7]. In this context, the term “gel effect” is used to designate biohydrogel-induced variation of soil properties [7]. One reason for the still poorly understood biohydrogel-soil interactions is the difficulty in

identifying swollen biohydrogel phases in soil. To our best knowledge, no currently applied method has allowed yet the distinction between biohydrogel phases and pore water in soil, which is most probably due to the high water content and low density of biohydrogels [7].

As soil-water interactions determine soil physical properties [8,9], water properties in soil pores are key factors to decipher the mechanisms of the gel effect. ^1H Nuclear Magnetic Resonance (^1H -NMR) relaxometry could be a method of choice to study in situ soil-water-biohydrogel interactions: the presence of biofilm and hydrogel in soil leads to a shift of the transversal relaxation rate (TRR) or longitudinal relaxation rate (LRR), and to higher T_1/T_2 ratios [10e14]. The authors interpreted these effects by a restricted rotational mobility of water molecules. Yet, the mechanisms leading to shifts in relaxation times and the criteria allowing the distinction between biohydrogel-water in soil pores and non-biohydrogel water have neither been fully identified nor quantified until now.

This study aims to identify and quantify the gel-induced mechanisms leading to changes influencing relaxation times in mucilage-containing soil. Water in mucilage-containing soil is

* Corresponding author.

E-mail address: schaumann@uni-landau.de (G.E. Schaumann).

entrapped in a hierarchical pore structure consisting of the porous biohydrogel network, itself surrounded by soil particles. Proton relaxation in porous systems mainly depends on bulk and surface relaxation and on the pore size [15]. Proton relaxation in biohydrogel and soil pores should be analyzed separately to distinguish their contribution on proton relaxation in mucilage-containing soil. Bulk relaxation in mucilage-containing soil should correspond to proton relaxation in biohydrogel [16]. We hypothesized that proton relaxation in mucilage is concentration dependent. The gel effect in soil is thus expected to be quantifiable for non-swelling soils with the same surface relaxivity and same pore size. The influence of mucilage on the relaxation rates is expected to vary proportionally with the soil pore size.

In order to test these hypotheses, we investigated how chia seed mucilage concentration affects the relaxation rates. Glass beads of different diameters were taken as simplified model rhizosphere in order to identify the influence of the pore size, and to remove complex parameters such as soil swelling, heterogeneous soil grains sizes or paramagnetic impurities at the soil surface [17,18]. Both water-containing and mucilage-containing glass beads have the same quantity of water, which corresponds to the amount of water in water-saturated glass beads.

2. Experimental

2.1. Mucilage preparation

Mucilage from chia seeds (*Salvia hispanica* L.) was extracted similarly to Ahmed et al. [19]. The collected biohydrogel was dropped slowly in liquid nitrogen and put directly into the freeze-drier. 4 mL of distilled water were added to the freeze-dried material to prepare mucilages between 0.1 and 1.0% (w/w), estimated to be the concentration range of mucilage in the rhizosphere [4]. The samples (three replicates) were sealed and stored for 24 h.

2.2. Model rhizosphere preparation

Four types of glass beads (diameters: 40e 70 nm, 100e 200 nm, 400e 600 nm and 2000 nm) and coarse quartz sand (grain size: 0.2% 2000-630 nm, 94.9% 630-200 nm, and 4.9% 200-63 nm) were washed successively with 2 M HCl solution and distilled water, oven-dried at 105 °C for 24 h, and filled in plastic cylinders (height $\frac{1}{4}$ 4.1 cm, diameter $\frac{1}{4}$ 3.7 cm) to ca. 3.7 cm sample height. The samples (three replicates) were filled with water by capillary rise to reach the maximum water holding capacity.

Chia seed mucilage (0.50 \pm 0.05% (w/w)) was mixed homogeneously with the glass beads to reach the same water content as the water-saturated samples. The samples were closed and stored for 24 h prior to the measurements.

2.3. ^1H -NMR relaxometry measurements

Two-dimensional T_1 - T_2 ^1H -NMR relaxometry measurements were performed for all samples using a Bruker Minispec MQ at a magnetic field strength of 0.176 T. For this, the inversion recovery method was combined with a Carr-Purcell-Meiboom-Gill pulse sequence [20]. 32 steps of the inversion recovery time between 0.3 ms and 2072 ms were used to sample a T_1 relaxation decay curve. Echo time was constantly set to 0.3 ms with ranging numbers of data points. The T_1 - T_2 correlation spectra were obtained with a two-dimensional numerical inverse Laplace software based on the Schlumberger algorithm [21]. For each sample, the T_1 and T_2 were obtained by calculating the mean value of the three relaxation times with the highest intensities. Results were

statistically analyzed by linear regression and correlation analyses. Variability within the replicates was presented as the mean deviation. Calculations and figures were done using Microsoft Excel 2007 and R statistics 3.2.2.

3. Results and discussion

3.1. Pure chia seed mucilage

Fig. 1a shows the TRR ($1/T_{2,\text{muc}}$) and LRR ($1/T_{1,\text{muc}}$) of mucilage as a function of its concentration.

The TRR (correlation coefficient $r > 0.99$, P-value $P < 0.001$) as well as the LRR ($r \frac{1}{4}$ 0.93, $P < 0.05$) increased linearly over the mucilage concentration range.

Chia mucilage was considered as a porous material due to its three-dimensional polymer network. According to the model of Brownstein-Tarr, proton relaxation in mucilage should vary as a function of the surface relaxation and of the bulk relaxation. Bulk relaxation in mucilage should equal the relaxation of pure water if no paramagnetic compounds are dissolved in water. $1/T_{\text{water}}$ was subtracted from $1/T_{2,\text{muc}}$ and $1/T_{1,\text{muc}}$ (Fig. 1a). The transversal ($r > 0.99$, $P < 0.001$) as well as the longitudinal ($r \frac{1}{4}$ 0.93, $P < 0.05$) relaxation in Fig. 1a increased linearly over the mucilage concentration range.

Close to zero, the y-intercepts ($0.00 \pm 0.01 \text{ s}^{-1}$ for the LRR and $0.01 \pm 0.01 \text{ s}^{-1}$ for the TRR) indicated that bulk relaxation in mucilage indeed corresponds to $1/T_{1,2,\text{water}}$. The linear relationships suggested that the polymer network got denser with an increase of the concentration but that its arrangement did not change in this concentration range. $1/T_{1,\text{muc}}$ ($0.10 \pm 0.02 \text{ nm s}^{-1}$) was not as significantly affected by variations of the mucilage concentration as $1/T_{2,\text{muc}}$ ($0.41 \pm 0.02 \text{ nm s}^{-1}$). This observation is consistent with the proton relaxation mechanisms in biohydrogels reported in the supporting information. In comparison, Ablett et al. observed that for agarose, the LRR decreased nonlinearly with decreasing polymer concentration below 1% (w/w) [22]. Ablett et al. concluded that the super junction regions became unstable and broke into smaller units at low polymer concentrations. These ones probably depend on the polymer, as the relaxation rate for mucilage increased linearly from 0.1 to 1% (w/w). The biopolymer divided in its sugar monomers would not affect the relaxation rate as strongly: the monomers can diffuse freely in the solution, so the surface relaxation is almost non-existent for small molecules as the "rigidity" of the monomer is very small. This implies that the dependence of the relaxation rate on the polymer concentration was a gel effect, as it was due to the polymer matrix.

3.2. Glass beads and sand mixed with water and mucilage

Fig. 1b shows the LRR in glass beads mixed with water (GB-water) and mixed with mucilage (GB-mucilage) as a function of the reciprocal of the glass beads diameter ($1/D_{\text{GB}}$). The LRR ($1/T_{1,\text{GB}}$) increased linearly with $1/D_{\text{GB}}$ for GB-mucilage ($r > 0.99$, $P < 0.05$) and GB-water ($r \frac{1}{4}$ 0.98, $P < 0.05$) (Fig. 1b). Values of the y-intercept ($0.46 \pm 0.07 \text{ s}^{-1}$) and the slope for GB-mucilage ($64.78 \pm 7.35 \text{ nm s}^{-1}$) were higher than for GB-water ($0.44 \pm 0.07 \text{ s}^{-1}$ and $46.60 \pm 7.20 \text{ nm s}^{-1}$) (Fig. 1b). This suggests that the presence of mucilage accelerates the proton relaxation.

Influence of the biohydrogel on the pore size (b/D_{GB}) (see supporting information for the formula), the bulk relaxation rate ($1/T_{\text{bulk}}$) and the surface relaxivity (r_{GB}) was investigated. For this, the LRR of GB-water ($1/T_{1,\text{GB-water}}$) and of GB-mucilage ($1/T_{1,\text{GB-muc}}$) were expressed as a function of the parameters b/D_{GB} , $1/T_{\text{bulk}}$ and r_{GB} (Equ. 1 and 2).

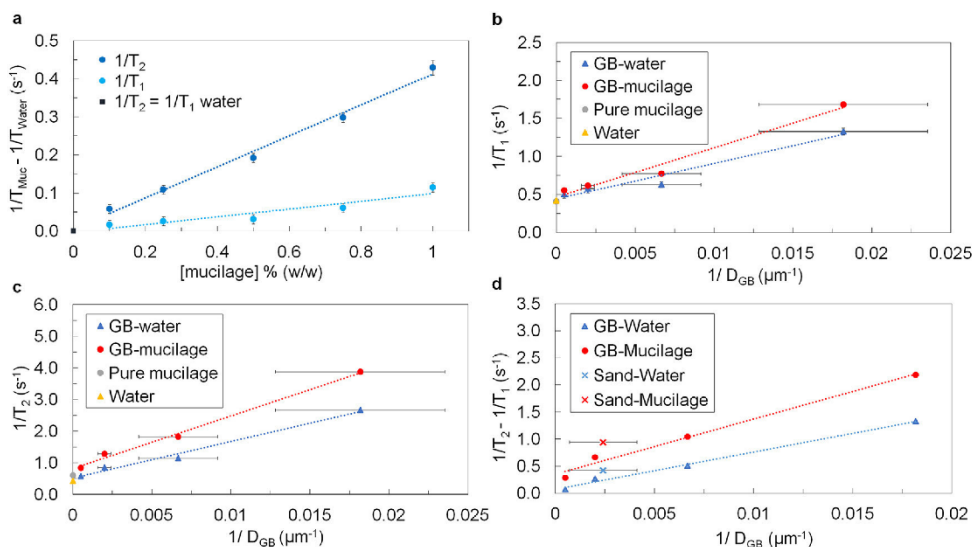


Fig. 1. (a) Linear dependence of LRR and TRR on the mucilage concentration. LRR (b) and TRR (c) for GB-mucilage and GB-water as function of the reciprocal of the GB diameter. (d) Difference between the TRR and LRR for GB-mucilage, GB-water, sand-mucilage and sand-water as function of the GB diameter reciprocal.

$$\frac{1}{T_{1\text{ GB water}}} - \frac{1}{4} \frac{1}{T_{1\text{ bulk;water}}} = \rho r_{\text{GB;water}} \frac{b}{D_{\text{GB water}}} \quad (1)$$

$$\frac{1}{T_{1\text{ GB muc}}} - \frac{1}{4} \frac{1}{T_{1\text{ bulk;muc}}} = \rho r_{\text{GB;gel}} \frac{b}{D_{\text{GB muc}}} \quad (2)$$

The y-intercept of GB-mucilage ($0.46 \pm 0.07 \text{ s}^{-1}$) (Fig. 1b) corresponds to the bulk relaxation rate of mucilage according to equation (4), and was slightly higher than the one for GB-water ($0.44 \pm 0.07 \text{ s}^{-1}$). As glass beads of the same diameter had the same water content, the total volume of the sample did not change, so the pore size was the same for GB-mucilage and GB-water. Water in gel has a longer rotational correlation time, so the water at the surface of the glass beads in GB-mucilage should have more time to relax than water in GB-water, which would lead to $r_{\text{GB;muc}} > r_{\text{GB;water}}$. This hypothesis is supported by the experimental data shown in Fig. 1b, as the slope of the regression line for GB-mucilage was larger than for GB-water.

Fig. 1c shows the TRR in GB-water ($1/T_{2\text{GB-water}}$) and in GB-mucilage ($1/T_{2\text{GB-muc}}$) as a function of $1/D_{\text{GB}}$. The TRR ($1/T_{2\text{GB}}$) was higher than the LRR ($1/T_{1\text{GB}}$) and increased linearly with $1/D_{\text{GB}}$ ($P < 0.05$). The slope and the intercept were higher for $1/T_{2\text{GB-muc}}$ ($166.84 \pm 9.32 \text{ nm s}^{-1}$; $0.81 \pm 0.09 \text{ s}^{-1}$) than for $1/T_{2\text{GB-water}}$ ($115.50 \pm 9.44 \text{ nm s}^{-1}$; $0.52 \pm 0.09 \text{ s}^{-1}$) (Fig. 1c). The value of the y-intercept in Fig. 1c corresponds to $1/T_{2\text{ bulk;water}}$ for GB-water, and to $1/T_{2\text{ bulk;muc}}$ for GB-mucilage. The difference between $1/T_{2\text{ bulk;muc}}$ and $1/T_{2\text{ bulk;water}}$ is larger than between $1/T_{1\text{ bulk;muc}}$ and $1/T_{1\text{ bulk;water}}$, and comes from the relaxation mechanism in pure mucilage (Fig. 1a).

At this point, the gel effect for $1/T_{1\text{GB-muc}}$ and $1/T_{2\text{GB-muc}}$ is traduced by an increase of the bulk relaxation rate, defined here as accelerated bulk relaxation, and by a strong increase of the surface relaxivity, defined here as accelerated surface relaxation. Unimodal relaxation in pure mucilage and uniform distribution of the mucilage in the glass beads ensured the observed accelerated bulk and surface relaxation to be pure gel effects.

However, it is difficult to determine the presence of a bio-hydrogel in an unknown sample only by examining the $1/T_1$ and $1/T_2$ values. The ratio between the slopes of $1/T_{2\text{GB-water}}$ and $1/T_{1\text{GB-water}}$ regression lines was found to be nearly the same as the ratio between the slopes of $1/T_{2\text{GB-muc}}$ and $1/T_{1\text{GB-muc}}$ regression lines (Table 1). This equality suggests that the mechanism increasing the TRR in comparison to the LRR was the same for GB-water and GB-mucilage.

The relationship between TRR and LRR (Table 1) enabled $1/T_{2\text{GB-water}}$ and $1/T_{2\text{GB-muc}}$ to be expressed as a function of $a_{T2/T1}$ according to equations (3) and (4), where $a_{T2/T1}$ is the ratio between the TRR and LRR slopes:

$$\frac{1}{T_{2\text{ GB water}}} = \frac{1}{4} \frac{1}{T_{2\text{ bulk;water}}} + \rho r_{\text{GB water}} \frac{b}{D_{\text{GB}}} a_{T2/T1} \quad (3)$$

$$\frac{1}{T_{2\text{ GB muc}}} = \frac{1}{4} \frac{1}{T_{2\text{ bulk;muc}}} + \rho r_{\text{GB muc}} \frac{b}{D_{\text{GB}}} a_{T2/T1} \quad (4)$$

The difference between the TRR and LRR highlights the accelerated bulk relaxation and the accelerated surface relaxation (Equ. 5):

$$\frac{1}{T_2} - \frac{1}{T_1} = \frac{1}{4} \frac{1}{T_{2\text{ bulk}}} - \frac{1}{T_{1\text{ bulk}}} + \rho r_{\text{GB}} \frac{b}{D_{\text{GB}}} a_{T2/T1} \quad (5)$$

Fig. 1d shows the difference between the TRR and LRR as a function of $1/D_{\text{GB}}$. The y-intercept and slope of the regression line for GB-water ($r > 0.99$, $P < 0.05$) and GB-mucilage ($r > 0.99$, $P < 0.05$) corresponded respectively to $1/T_{2\text{ bulk}} - 1/T_{1\text{ bulk}}$ and to

	$a_{T2/T1}$
GB-water	2.48
GB-mucilage	2.47

$b = (\alpha_{T_2/T_1} - 1) \tau_{GB}$ (Equ. 5). Accelerated bulk relaxation was expressed in the y-intercept of GB-mucilage ($0.35 \pm 0.08 \text{ s}^{-1}$), higher than the y-intercept for GB-water ($0.07 \pm 0.04 \text{ s}^{-1}$). As α_{T_2/T_1} and b are the same for GB-mucilage and GB-water, accelerated surface relaxation was expressed in the slope of GB-mucilage ($102.06 \pm 8.16 \text{ nm s}^{-1}$), which was stronger than the slope of GB-water ($68.90 \pm 3.66 \text{ nm s}^{-1}$). Both accelerated bulk relaxation and accelerated surface relaxation are expressions of the gel effect.

The same experiment and analysis were done for one coarse sand, whose particle size distribution was previously known. As the surface relaxivity of sand was stronger, the LRR and TRR of coarse sand were higher than the ones of glass beads for the same grain diameter. Nevertheless, $1/T_{2,sand} - 1/T_{1,sand}$ for sand-mucilage was higher than for sand-water. The highlight of the gel effect with the difference between TRR and LRR worked also for sand. Although sand is a very simplified soil system, the results set a first step for the decoding of the gel effect in natural soil samples.

4. Conclusions

Acceleration of the proton relaxation in pure mucilage led to an acceleration of the proton relaxation in mucilage-containing model soils, due to an increase of the bulk relaxation rate and of the surface relaxivity. Therefore, knowledge from proton relaxation in biohydrogels proves to be necessary to assess the influence of the biohydrogel on the proton relaxation in biohydrogel-containing soil systems. Further understanding of the gel effect in soil requires an investigation with a larger spectrum of biohydrogels. Finally, measurement of several concentrations of mucilage mixed with soil would help to clear out in which scope the polymer affected the surface relaxivity in the mucilage-containing soil system.

Acknowledgements

The authors thank the DFG (German Research Foundation) for supporting this study within the project MUCILAGE (SCHA849/20), Marcio-Fernando Cobo and Harald Todt from Bruker BioSpin for the pulse sequences of the two-dimensional ^1H -NMR measurements.

Appendix A. Supplementary data

Supplementary data related to this article can be found at <http://dx.doi.org/10.1016/j.micromeso.2017.07.044>.

References

- [1] M.A. Ahmed, M. Holz, S.K. Woche, J. Bachmann, A. Carminati, J. Plant Nutr. Soil Sci. (2015) 1e4.
- [2] K.S. Kazanskii, S.A. Dubrovskii, in: *Polyelectrolytes Hydrogels Chromatogr. Mater.*, Springer Berlin Heidelberg, 1992, pp. 97e133.
- [3] W. Deng, P.D. Hallett, D.-S. Jeng, G.R. Squire, P.E. Toorop, P.P. Iannetta, Plant Soil 387 (2015) 167e176.
- [4] A. Carminati, D. Vetterlein, Ann. Bot. 112 (2013) 277e290.
- [5] A. Al-Darby, Soil Technol. 9 (1996) 15e28.
- [6] H. Andry, T. Yamamoto, T. Irie, S. Moritani, M. Inoue, H. Fujiyama, J. Hydrol. 373 (2009) 177e183.
- [7] M. Brax, C. Buchmann, G.E. Schaumann, J. Plant Nutr. Soil Sci. 180 (2017) 121e141.
- [8] C. Buchmann, J. Bentz, G.E. Schaumann, Soil Tillage Res. 154 (2015) 22e33.
- [9] C. Buchmann, M. Meyer, G.E. Schaumann, Magn. Reson. Chem. 53 (2015) 694e703.
- [10] F. Jaeger, E. Grohmann, G.E. Schaumann, Plant Soil 280 (2006) 209e222.
- [11] F. Jaeger, A. Shchegolikhina, H. Van As, G.E. Schaumann, Open Magn. Reson. J. 3 (2010) 27e45.
- [12] C. Buchmann, G.E. Schaumann, Plant Soil (2016) 1e18.
- [13] C.M. Kirkland, R. Hiebert, A. Phillips, E. Grunewald, D.O. Walsh, J.D. Seymour, S.L. Codd, Groundw. Monit. Remediat 35 (2015) 36e44.
- [14] S.L. Codd, S.J. Vogt, J.A. Hornemann, A.J. Phillips, J.E. Maneval, K.R. Romanenko, L. Hansen, A.B. Cunningham, J.D. Seymour, Org. Geochem 42 (2011) 965e971.
- [15] K.-J. Dunn, D.J. Bergman, G.A. LaTorraca, Nuclear Magnetic Resonance: Petrophysical and Logging Applications, 2002. Pergamon, New York.
- [16] G.E. Schaumann, E. Hobbey, J. Hurraß, W. Rotard, Plant Soil 275 (2005) 1e20.
- [17] F. Jaeger, N. Rudolph, F. Lang, G.E. Schaumann, Soil Sci. Soc. Am. J. 72 (2008) 1694e1707.
- [18] Z.R. Hinedi, A.C. Chang, M.A. Anderson, D.B. Borchardt, Water Resour. Res. 33 (1997) 2697e2704.
- [19] M.A. Ahmed, E. Kroener, M. Holz, M. Zarebanadkouki, A. Carminati, Funct. Plant Biol. 41 (2014) 1129.
- [20] S. Meiboom, D. Gill, Rev. Sci. Instrum. 29 (1958) 688e691.
- [21] Y.-Q. Song, L. Venkataramanan, M.D. Hürlimann, M. Flaum, P. Frulla, C. Straley, J. Magn. Reson. 154 (2002) 261e268.
- [22] S. Ablett, P.J. Lillford, S.M.A. Baghdadi, W. Derbyshire, J. Colloid Interface Sci. 67 (1978) 355e377.

*4. POTENTIAL OF NMR RELAXOMETRY TO UNRAVEL THE
PROPERTIES OF MUCILAGE IN SEVERAL PORE SIZES*



Contents lists available at ScienceDirect

Geoderma

journal homepage: www.elsevier.com/locate/geoderma

Potential of NMR relaxometry to unravel the properties of mucilage in several pore sizes



Mathilde Brax^a, Maximilian Köhne^b, Eva Kroener^c, Gabriele Ellen Schaumann^{a,*}

^a University Koblenz-Landau, Institute for Environmental Sciences, Group of Environmental and Soil Chemistry, Fortstrasse 7, 76829 Landau, Germany

^b Helmholtz Centre for Environmental Research GmbH – UFZ, Department of Soil System Sciences, Theodor-Lieser-Strasse 4, 06120 Halle, Germany

^c University Koblenz-Landau, Institute for Environmental Sciences, Geophysics, Fortstrasse 7, 76829 Landau, Germany

ARTICLE INFO

Handling Editor: Ingrid Kögel-Knabner

Keywords:

Mucilage

Pore size

¹H NMR relaxometry

Gel effect

Water mobility

ABSTRACT

Soil-born exudates such as mucilage are known to affect soil physicochemical properties. Characterization of the gel properties of mucilage at the pore-scale is necessary to gain mechanistic understanding of the underlying processes leading to changes of soil properties. Yet, mucilage intrinsic properties' complicate its *in-situ* detection. Longitudinal and transverse magnetic relaxation rates measured with ¹H Nuclear Magnetic Resonance (NMR) relaxometry have the potential to study mucilage-water interactions *in-situ* as they are sensitive to restricted molecular motion of water protons in biohydrogels. However, the relations between water mobility and biohydrogel properties in porous media have remained unknown until now.

In this study, the mobility of water molecules in chia seed mucilage in porous systems was systematically investigated by means of ¹H NMR relaxometry. Chia seed mucilage was used as it has hydrogel properties shared by a range of biological hydrogels found in soil. Glass beads of several sizes were used to study the influence of the pore size on the NMR signal.

A conceptual model based on the equations describing the relaxation of water protons in porous media was developed to integrate these gel effects into the NMR parameters. The increased rigidity of the polymer network and its organization in the pore space, which depended on the particle size and the mucilage concentration, were assessed as the gel effects significantly affecting the bulk relaxation. Our approach, which combines the use of NMR along with other imaging methods, is a promising strategy to detect and characterize the properties of biohydrogel in porous media.

1. Introduction

Due to its gel-specific properties, mucilage can modulate several soil physicochemical properties, such as soil water holding capacity or soil hydraulic conductivity (Ahmed et al., 2014; Carminati et al., 2011). Gels are characterized by high water contents, swelling and shrinking induced by moisture dynamics and viscoelastic properties (Brax et al., 2017; Capitani et al., 2015). The complexity of biohydrogel-soil interactions requires the understanding of simple systems, and coarse sand has been mostly used as artificial soil (Ahmed et al., 2014; Carminati, 2012; Gregory, 2006; Kroener et al., 2014; Zarebanadkouki et al., 2012). Recent studies showed that the particle size plays a role in the extent to which soil-water-mucilage interactions affect the percolation threshold or the stability of aggregates (Ahmed et al., 2016; Albalasmeh and Ghezzehei, 2014; Kroener et al., 2018). To elucidate the pore-scale processes, which are at the origin of changes of soil macroscopic

properties, *in-situ* studies focusing on the properties of mucilage at the pore scale are necessary (Albalasmeh and Ghezzehei, 2014; Brax et al., 2017).

Recent advances in imaging techniques enable one to visualize the physical environment around the roots (Helliwell et al., 2013). Low-attenuation contrasts between water and biohydrogels make it difficult to image mucilage in porous systems with magnetic resonance imaging (MRI), X-ray computed microtomography (μCT) or neutron imaging (Brax et al., 2017). The addition of contrasting agents in biohydrogels is a method to overcome this limit (Davit et al., 2011), but still stays invasive. ¹H NMR relaxometry is emerging as a suitable method to differentiate mucilage from water in porous media, as biohydrogels reduce the transverse and longitudinal relaxation time of proximal water protons (Bayer et al., 2010; Brax et al., 2017; Brownstein and Tarr, 1979; Codd et al., 2011).

The asset and at the same time the difficulty of ¹H NMR relaxometry

* Corresponding author.

E-mail address: schaumann@uni-landau.de (G.E. Schaumann).

<https://doi.org/10.1016/j.geoderma.2019.01.013>

Received 13 April 2018; Received in revised form 3 January 2019; Accepted 4 January 2019

0016-7061/ © 2019 Elsevier B.V. All rights reserved.

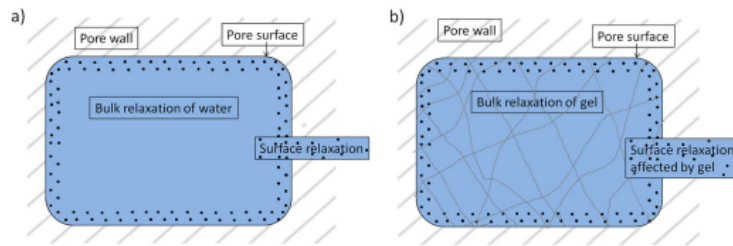


Fig. 1. Visualisation of bulk relaxation and surface relaxation in a pore filled with water (a) and the same pore filled with a polymeric network (b).

in porous systems come from the multitude of factors affecting the relaxation time, such as pore size, swelling of soil particles or paramagnetic inhomogeneity (Bayer et al., 2010). What is more, biohydrogels can change soil pore connectivity or effective pore size (Jaeger et al., 2006; Todoruk et al., 2003). Therefore, characterization of biohydrogels in porous systems first necessitates the use of simple model systems, such as glass beads or sandstone, in which the gel is homogeneously distributed (Brax et al., 2018; Sanderlin et al., 2013). Until now, most ¹H NMR relaxometry studies on biohydrogels in porous media have focused on biofilms, although some studies have been published about synthetic hydrogels in porous media (Buchmann et al., 2015a, 2015b; Buchmann and Schaumann, 2017).

NMR studies on the transverse relaxation of ¹H spins of water in porous media (Fig. 1a) typically focused on the influence of the surface relaxivity and of the diffusion gradients on the overall relaxation behavior of the medium (see supporting information for definition) (Godefroy et al., 2001; Kleinberg et al., 1994). However, the presence of biohydrogels in the pore space changes the fingerprint of the bulk relaxation, which must be taken into consideration in this case (Fig. 1a–b) (Kirkland et al., 2015). Biofilm growth within the pore space enhanced the weighted average of bound and free protons and shifted the relaxation to shorter times (Codd et al., 2011; Jaeger et al., 2010). Most studies on the influence of biofilms in porous media measured the transverse relaxation time (T_2) with one or two-dimensional experiments (Bayer et al., 2010; Codd et al., 2011; Sanderlin et al., 2013). Until now, longitudinal relaxation (T_1) distributions of biohydrogels in soil have not been much investigated, though Bayer et al. (2010) suggested helpfully the combination of T_1 and T_2 to discriminate between the effects of water mobility and the ones of pore size distribution in biohydrogel-containing porous media. In alginate, cellulose derivate or mucilage, T_2 decreased actually stronger than T_1 due to a reduced rotational mobility of the water protons in the hydrogel (Brax et al., 2018; Degrassi et al., 1998; Fyfe and Blazek, 1997).

In biohydrogel-containing porous media, water is entrapped in a hierarchical porous structure consisting of the polymer network, itself surrounded by the pore walls (Fig. 1b). As each biohydrogel has its own relaxation time fingerprint (Hills, 1992), it is necessary to characterize the relaxation of water protons in the biohydrogel in order to better assess the biohydrogel-induced shift of the relaxation time in porous media. The mucilage concentration range in the rhizosphere was estimated to vary between 0.1 and 1.0 wt% (Carminati and Vetterlein, 2013). In this range, the longitudinal relaxation rate (R_1) ($1/T_{1\text{Muc}}$) and the transverse relaxation rate (R_2) ($1/T_{2\text{Muc}}$) of free chia seed mucilage varied linearly with the mucilage concentration multiplied by a factor, which we will call $G^*_{1,2\text{B}}$ (Brax et al., 2018).

$$\frac{1}{T_{1,2\text{Muc}}} = \frac{1}{T_{1,2\text{BW}}} + G^*_{1,2\text{B}} \cdot C_{\text{Muc}} \quad (1)$$

The subscript 1,2 refers to R_1 and to R_2 respectively, the subscript BW stands for bulk water and the subscript B on the G factor indicates that mucilage is in the bulk phase. R_2 was reported to depend stronger on the mucilage concentration than R_1 , as $G^*_{2\text{B}}$ (0.41 ± 0.02 wt

$\%^{-1} \text{s}^{-1}$) was higher than $G^*_{1\text{B}}$ (0.10 ± 0.02 wt $\%^{-1} \text{s}^{-1}$) (Brax et al., 2018). The polymeric network effect $G^*_{1,2\text{B}}$ is defined as the dependence of the relaxation rate on the mucilage concentration. In the preliminary work to this study, Brax et al. (2018) studied the proton relaxation in glass beads of several sizes mixed with water and with chia seed mucilage at one mucilage concentration of 0.5 wt% (corresponding to 500 mg dry mucilage in 100 g water). The water content in the glass beads mixed with mucilage (GB-mucilage) was set the same as in the water-saturated samples (GB-water). It was shown that the influence of mucilage on the relaxation rate, also called “gel effect”, could be quantified by using the equations describing the relaxation of water protons in a porous medium. The gel effect expressed itself by an accelerated bulk relaxation and an accelerated surface relaxation (Fig. 1b) (Brax et al., 2018).

Still, it is not clear how strong these two gel effects vary with the mucilage concentration, and how relevant they are to describe mucilage at the pore scale. Our aim was to further quantify the gel effect on the NMR parameters, in order to be finally able to describe the way gel affects the molecular mobility of water in porous media. This would help us to deduce how the water mobility reflects the gel properties in porous media. Therefore, we measured R_2 and R_1 of GB-mucilage for mucilage concentrations between 0.1 and 1.0 wt%. Mucilage was mixed with glass beads of various sizes. Our approach was double-sided: on one hand, we hypothesized that the mucilage concentration influenced quantitatively and proportionally the NMR parameters. For this, we modified the equations describing the relaxation of water protons in the pore space under the assumption of a fast-diffusion regime (see below) and developed a conceptual model incorporating the gel effects identified by Brax et al. (2018) (Eq. (6)). On the other hand, we also hypothesized that the mucilage polymer network organized differently according to the pore size and expected the NMR gel effect parameters to reflect this difference.

2. Theory and conceptual model

2.1. Relaxation in porous systems

In porous systems and under the assumption of a fast-diffusion regime, R_1 and R_2 are determined by the bulk relaxation rate ($1/T_B$) and by the surface relaxation rate ($1/T_S$), and $1/T_S$ is defined by the surface relaxivity (ρ) and the surface-to-volume ratio (S/V) (Fig. 1a) (Brownstein and Tarr, 1979; Godefroy et al., 2001). In a fast-diffusion regime, water molecules can transit the pore several times before their relaxation and the magnetization decay is spatially uniform. The diffusion relaxation rate $1/T_{2D}$ originates from molecular diffusion in internal magnetic field gradients and additionally affects R_2 , but not R_1 as no energy exchange is involved (Brownstein and Tarr, 1979). Internal field gradients are negligible at small echo time t_E and small magnetic field strengths (Dunn et al., 2002).

$$\frac{1}{T_{1,2\text{WP}}} = \frac{1}{T_{1,2\text{B/WP}}} + \frac{1}{T_{1,2\text{S/WP}}} \left(+ \frac{1}{T_{2D}} \right) \quad (2)$$

The subscript *WP* refers to a porous media filled with water. The surface relaxivity describes the efficiency of the particle surface to enhance longitudinal or transverse relaxation (Brownstein and Tarr, 1979). The surface to volume ratio is a measure of the pore size and is directly connected to the diameter of the particles (D_{GB}) with the constant β for simple shapes (Eq. (3)) (Kleinberg, 1996).

$$\frac{1}{T_{1,2S/WP}} = \rho^* \frac{S}{V} = \rho^* \frac{\beta}{D_{GB}} \quad (3)$$

Low-field NMR has proven to be better adapted to the detection of biofilm in porous media than high-field NMR: the high susceptibility gradients inherent to high-field NMR dominate the T_2 distribution and prevent the detection of biofilm in porous media with strong susceptibility gradients (Codd et al., 2011; Sanderlin et al., 2013).

2.2. Relaxation in biohydrogels

The surface in biohydrogel corresponds to the polymer junction zones and cross-links (Belton et al., 1988; Chui et al., 1995). Surface relaxation is the predominant factor controlling the relaxation of water protons in hydrogels, and proton chemical exchange between the water protons and the exchangeable protons of the polymer is the most important surface relaxation mechanism (Li et al., 1999). There is a rapid exchange between the water molecules tumbling freely and the ones “chemisorbed” to the polysaccharide surface, and the measured relaxation time is weighted by the relaxation times of these two proton pools (Belton et al., 1988; Lüsse and Arnold, 1998). The transverse or spin-spin relaxation differs from the longitudinal or spin-lattice relaxation as it depends on direct interactions between the spins without energy transfer to the lattice. As it is mainly affected by the rotational correlation of the water molecules, the spin-spin relaxation monitors the conformation and mobility of the polysaccharide. The mobility of water molecules in direct vicinity to the polymer backbone is affected by reorientation processes of these water molecules, with respect to their physicochemical interactions with the polymer and to the mobility of the polymer backbone (Lüsse and Arnold, 1998). Thus, the relaxation behavior of water molecules in biohydrogels is expected to change from polymer to polymer due to different polymer mobility and water binding properties (Shapiro, 2011).

2.3. Conceptual model describing the gel effect on the NMR parameters

In a porous system, in which gel is homogeneously mixed with the particles, the gel fills the pores and covers the surface (Fig. 1b). If the gel polymer network *within* the pore has the same three-dimensional (3D) organization as the *free* gel polymer network, the bulk relaxation rate measured for the gel in porous media ($1/T_{1,2 B/GP}$) should be equal to the relaxation rate of the pure gel. As the gel is surrounded by the pore walls, the network probably reorders to better fit into the given pore space. We hypothesize that this rearrangement additionally affects the bulk relaxation rate for gel in porous media ($1/T_{1,2 B/GP}$) and call it the *matrix confinement effect* ($X_{1,2 MC}$). Accordingly, $1/T_{1,2 B/GP}$ depends on the gel relaxation rate ($1/T_{1,2 Muc}$) as expressed in Eq. (1), and on the matrix confinement effect:

$$\frac{1}{T_{1,2 B/GP}} = \frac{1}{T_{1,2 BW}} + G_{1,2 B}^* \cdot c_{Muc} + X_{1,2 MC} \quad (4)$$

The subscript *GP* indicates a porous media filled with gel, and the subscript *MC* refers to the matrix confinement effect. A biohydrogel-containing soil can hold more water than the same soil without biohydrogel at saturation and has, therefore, larger pores than its water-containing equivalent (Chenu, 1993). The type of polymer, its concentration, the soil particle size and its clay content are all factors affecting gel-induced pore expansion (Buchmann and Schaumann, 2017; Chenu, 1993; Kroener et al., 2018; Meyer et al., 2018). Besides, it is not clear how gels swell in the pore system, for example if they undergo

expansion into or movement within the pore system. Gel swelling into a cavity is subject to external pressure, which results in an increase of the gel swelling pressure but in a decrease of its equilibrium swelling degree (Kazanskii and Dubrovskii, 1992). To the best of our knowledge, it is not known yet how far external factors specific to field conditions such as confining forces restrict pore expansion coming from soil organic matter and biohydrogel swelling.

In this study, we focused on the quantitative comparison of the water mobility between porous media filled with mucilage and filled with water for several defined particle sizes. For this, the porosity of GB-water and GB-mucilage needed to be similar. For each particle size, the same volumetric amounts of water and mucilage were mixed homogeneously with the glass beads. This way, the samples were expected to be under saturated conditions with no swelling effect, and the porosity of GB-water and GB-mucilage was assumed to be similar. Consequently, we hypothesize that an increased surface relaxation in GB-mucilage results from a stronger surface relaxivity: water in gel has a longer rotational correlation time due to interactions with the polymer (Belton et al., 1988; Hills, 1992), so water protons should have more time to relax at the surface of the particles in comparison to water protons not affected by a polymer network (Brax et al., 2018). The surface relaxivity for gel in porous media ($\rho_{1,2 GP}$) was hypothesized to depend on the glass beads' surface relaxivity measured in water ($\rho_{1,2 WP}$) and on an additional parameter ($\rho_{1,2 \tau}$) depending on the increase of the rotational correlation time τ_c .

$$\rho_{1,2 GP} = \rho_{1,2 WP} + \rho_{1,2 \tau} \quad (5)$$

According to our hypotheses, the combination of Eqs. (2)–(5) describes R_1 and R_2 of biohydrogel in porous media:

$$\frac{1}{T_{1,2 GP}} = \frac{1}{T_{1,2 BW}} + G_{1,2 B}^* \cdot c_{Muc} + X_{1,2 MC} + (\rho_{1,2 WP} + \rho_{1,2 \tau}) \cdot \frac{\beta}{D_{GB}} \quad (6)$$

In order to test these hypotheses, R_1 and R_2 were plotted as a function of the GB size and of the mucilage concentration to consecutively extract and study the polymeric network effect $G_{1,2 B}^*$, the accelerated surface relaxivity $\rho_{1,2 GP}$ and the matrix confinement effect $X_{1,2 MC}$.

3. Material and methods

3.1. Mucilage preparation

Due to the experimental difficulty to isolate substantial amounts from root mucilage (Zickenrott et al., 2016), chia seed mucilage (*Salvia hispanica L.*) was used: It is easily available in great quantities and shares gel properties such as viscosity relevant to seed, root and microbial exudates in soils (Naveed et al., 2017; Sutherland, 2001). Chia seed mucilage was collected according to the method of Ahmed et al. (2014) and consecutively frozen with liquid nitrogen and freeze-dried. Distilled water was added to the freeze-dried mucilage for it to reswell at concentrations between 0.1 and 1.0 wt%. The samples were left at rest for 48 h prior to further use for the mucilage to swell completely.

3.2. Glass beads samples preparation

The particle size distribution of the four glass bead particle sizes (soda lime, MHG Strahlanlagen GmbH) was verified under the microscope. For this, glass beads were spread on a glass slide covered with double-sided adhesive tape. Diameters of the glass beads were measured by means of an ocular micrometer to get a significant statistical size distribution. The maximal water holding capacity (WHC_{max}) was measured by saturating the samples (three replicates) with the capillary force under free drainage.

The glass beads were washed successively with 2 M HCl and distilled water and were oven-dried at 105 °C for 24 h. 2 mL of water or chia seed mucilage (0.1–1.0 wt%) were mixed homogeneously with the

Table 1

Particle size and maximal water holding capacity (WHC_{max}) of the glass beads (GB).

	GB2000	GB350	GB150	GB55
Particle size (µm)	2103 ± 29	338 ± 44	157 ± 19	54 ± 10
WHC _{max} % (w/w)	24.5 ± 0.9	25.3 ± 0.8	26.2 ± 0.1	26.2 ± 0.6

glass beads in an Eppendorf tube (sample height ca 7 cm, Eppendorf diameter = 1.5 cm), in such a way that the GB-mucilage samples had the same water content as the saturated GB-water samples (Table 1). The samples (three replicates of each) were sealed and stored 48 h prior to the measurements.

3.3. ¹H NMR relaxometry measurements

3.3.1. Influence of internal field gradients on the relaxation rate

¹H NMR relaxation data were all collected with a Bruker Minispec MQ at a magnetic field of 0.176 T (proton Larmor frequency of 7.5 MHz). Mitchell et al. (2010) estimated that the largest Larmor frequency at which relaxation from spin diffusion in internal magnetic field is excluded, is 15 MHz for echo times t_E ranging from 2 to 40 ms. The magnitude of the diffusion relaxation term $1/T_{2D}$ in the NMR response of a sample can be determined by measuring the dependence of R_2 on t_E . To confirm the assumption of Mitchell et al. (2010), a preliminary test was carried out by measuring R_2 of GB350 saturated with water with a Carr-Purcell-Meiboom-Gill (CPMG) experiment as a function of increasing t_E (0.1–1.2 ms) (Keating and Knight, 2006). Number of scans was 8 and repetition time was set at 10 s to ensure that the samples had returned to thermal equilibrium prior to the start of the pulse sequence. Number of 180° pulses ranged between 50,000 and 10,000 depending on t_E . Variation of t_E did not affect R_2 , which remained constant at $0.80 \pm 0.05 \text{ s}^{-1}$. In this study, the effect of the diffusion relaxation term on R_2 in this range of t_E is negligible and agrees with the results of Keating and Knight (2006) and Mitchell et al. (2010).

3.3.2. Comparison between 1D and 2D measurements

A further preliminary test was conducted to investigate the potential for systematic errors in the results obtained with two-dimensional (2D) T_1 - T_2 correlation experiments (Song et al., 2002) in comparison to the results generated by using a conventional CPMG pulse sequence (Meiboom and Gill, 1958) and inversion recovery (IR) pulse sequence (Void et al., 1967). The measurements were performed on glass beads of two different diameters saturated with 2 mL water. For the 1D and 2D measurements, t_E was 0.3 ms, the repetition time was set at 10 s and gain was 77 such that 80% signal intensity was achieved. Number of scans was 8 for the 1D measurements to ensure a sufficiently high signal-to-noise ratio. Number of 180° pulses ranged between 15,000 (GB90) and 40,000 (GB350) for the CPMG measurement. Inversion time for the inversion recovery (IR) measurement was between 0.3 ms and 15 s with 26 values of T_1 . In the 2D correlation measurement, an IR experiment was combined with a simultaneous CPMG pulse sequence (Song et al., 2002). The number of scans was 4 to limit the measurement time to 45 min per sample. CPMG signals were collected for 34 logarithmically spaced values of T_1 with an IR time between 0.3 and 3.67 s for GB90 and 0.6 and 7.3 s for GB350. Number of 180° pulses ranged between 15,000 (GB90) and 20,000 (GB350). The results provided by the 1D and 2D measurements and subsequent data exploitation were the same in the range of the standard deviation for the long R_1 and R_2 values of GB90-water and for the short R_1 and R_2 of GB350-water (see figure in the supporting information). Therefore, no systematic error was produced from the T_1 - T_2 correlation measurement or from the 2D-ILT in this study.

3.3.3. 2D measurements of the GB-water and GB-mucilage samples

In the 2D correlation experiments carried out for the GB-water and GB-mucilage samples, the IR sequence was composed of 34 logarithmically spaced values of T_1 with an inversion recovery time between 0.6 ms and 7.3 s. Number of 180° pulses ranged between 1200 (GB55) and 9000 (GB2000) with $t_E = 0.6$ ms. For each experiment, a repetition time of 10 s, 4 scans and a gain of 77 were selected.

3.3.4. Data analysis

All samples were measured in triplicates. CPMG and IR decay curves were analysed with Inverse Laplace Transform (ILT) applied with MATLAB 7.7.0 (R2008b) using the Butler, Reeds and Dawson algorithm (Butler et al., 1981) to generate a relaxation time distribution consisting of 200 exponentially spaced time constants with their associated amplitudes set from 0.1 ms to 10 s (Jaeger et al., 2010). Residual analysis showed that the least deviation occurred for a weight factor of 0.01. The T_1 - T_2 correlation maps were obtained with a 2D numerical ILT software provided by Bruker BioSpin and based on the Schlumberger algorithm (Song et al., 2002). The weight factor was set at 1179.77. The samples were assumed to be in the fast diffusion regime so that diffusion between pores could be neglected as each sample exhibited positive signals below the diagonal (Song et al., 2014). The T_1 - T_2 maps and the relaxation time distributions from the 1D measurements were all characterized by one main narrow peak. Thus, R_1 and R_2 characterizing each sample were obtained by calculating the average of the three corresponding T_1 and T_2 with the highest signal intensities (Buchmann and Schaumann, 2017; Venkataraman et al., 2002). R_1 and R_2 were statistically analysed by linear regression and correlation analyses. Variability within the three replicates was presented as the standard deviation. Calculations and figures were made using Microsoft Excel 2007. All raw data are published in Mendeley (<http://dx.doi.org/10.17632/52f4t38d9h.1>).

3.4. Pulse-field gradient (PFG)-NMR measurements

Description and results of PFG-NMR measurements are in the supporting information.

3.5. Environmental scanning electron microscopy (ESEM)

The preparation of the ESEM samples aimed to reduce the possible changes in the structure of the polymer network. For this, GB55 and GB350 mixed with 0.1 wt% and 1.0 wt% mucilage were immersed into liquid nitrogen prior to freeze-drying to avoid a glass transition of the polymer and to preserve the original structure of the mucilage network from the wet in the dry state. ESEM images were taken with an FEI Quanta 250 ESEM (FEI Company Hillsboro, United States) under low vacuum with chamber pressures between 60 and 80 Pa. A large field detector was used with an acceleration voltage between 12.5 and 15 kV.

3.6. X-ray computed microtomography

The inner spatial structure of GB350 mixed respectively with water, 0.1 wt% and 1.0 wt% mucilage was analysed by μ CT using an industrial scanner (X-Tek XT H 225, Nikon Metrology GmbH). For preserving a good contrast, a relatively low voltage of 90 kV and a current of 205 μ A were applied and no filter was used. An entire μ CT scan comprised 2000 projections at an exposure time of 708 ms and took 25 min. The flat panel X-ray detector (PerkinElmer 1620) with 1750 by 2000 pixels captured the images at a spatial resolution of 9 μ m and 8 bit grayscale resolution. The reconstruction of three-dimensional images via filtered back projection was done using the CT Pro 3-D software package (version 3.1, Nikon Metrology). Only the middle part of the vials was captured due to the limited size of the field of view. This corresponded roughly to one third of the total sample volume of about 8 cm³, and an inner cylindrical region of interest (ROI) of 1.5 to 2 cm³ was analysed

out of it to exclude wall effects in the images.

3.7. Image processing and analysis

Image analysis was conducted to analyse the three-phase system composed of glass beads, water/mucilage and air. From the image analysis, the size distributions of particles, pores, and air bubbles within the pore space were calculated. The image processing workflow was done using the Image-J software package (Schindelin et al., 2012). Noise was first removed with a nonlocal means filter (Tristán-Vega et al., 2012). Next, the thresholds segmenting air, water/mucilage and particles were manually set based on visual comparison of the filtered grayscale image and the segmented image. This manual segmentation gave more consistent results than our usually applied combination of different histogram evaluation methods (Schlüter et al., 2014). Markov random field segmentation was then used for image segmentation (Kulkarni et al., 2012). Finally, Euclidean distance mapping as included in the “Local Thickness Plugin” in ImageJ (Dougherty and Kunzelmann, 2007) was applied to the segmented binary CT images to obtain pore size distributions.

4. Results and discussion

4.1. Structure of the mucilage network in porous media

Fig. 2 shows the ESEM pictures of N₂ (I) freeze-dried GB55 mixed with 0.1 wt% (Fig. 2a) and with 1.0 wt% mucilage (Fig. 2b).

Lone discrete polymer strands depicted by the white lines were sparsely distributed on the surface of the particles in GB55 mixed with 0.1 wt% mucilage. They appeared to be more abundant with branched structures in GB55 mixed with 1.0 wt% mucilage. Whereas no polymer network was visible in the pore space in GB55 mixed with 0.1 wt% mucilage, polymer strands linked the particles in GB55 mixed with 1.0 wt% mucilage and a porous polymer network was only observed in

the biggest pore (top left). Instead of covering the particle surface as in GB55 mixed with 0.1 wt% mucilage, the polymer agglomerated in the pore space in GB350 mixed with 0.1 wt% mucilage and formed a clear-cut network seemingly brittle. It is not clear from the picture whether it was attached to other beads or not. In GB350 mixed with 1.0 wt% mucilage, the polymer built a dense organized porous network in the pore space, whose extremities appeared to take anchor at the surface of the particles.

Imaging dry hydrogel networks with the ESEM is subject to artefacts: Ice crystal formation during the freeze-drying step and aggregation or collapse of the polymer network under vacuum cannot be discarded (Hills et al., 2000; Mao et al., 2001). Although shock-freezing directly followed by freeze-drying reduces the formation of ice crystals in comparison to slow freezing (Belton et al., 1988; Hills et al., 2000), information from the images must be considered cautiously. GB55 and GB350 had similar water content (Table 1), but GB55 had more and smaller pores than GB350. Nevertheless, mucilage was distributed homogeneously within both systems. As mucilage is a shear-thinning gel at these concentrations (Capitani et al., 2015), i.e. its viscosity decreases under shear strain, the polymer chains are flexible and deformable and have the capacity to change their conformation to adapt to the pore space. Fig. 2a–d suggested that the organization of the polymer network was pore size dependent: it extended in discrete strands at low concentrations and built bridges between the particles at higher concentrations for GB55. The higher number of pores of GB55 implies a lower amount of polymer per pore, which probably prevents polymer agglomeration and explains the absence of porous network in most pores. Another reason could be that the optimal size formed by the polymeric network is bigger than the available space between GB55 particles. In fact, already at low mucilage concentration for GB350, the polymer takes advantage of the pore space to expand and form an organized structure. The polymeric meshes gain in structure and density with increasing mucilage concentration. Finally, in GB55 and GB350 mixed with the highest mucilage concentration, the polymer strands

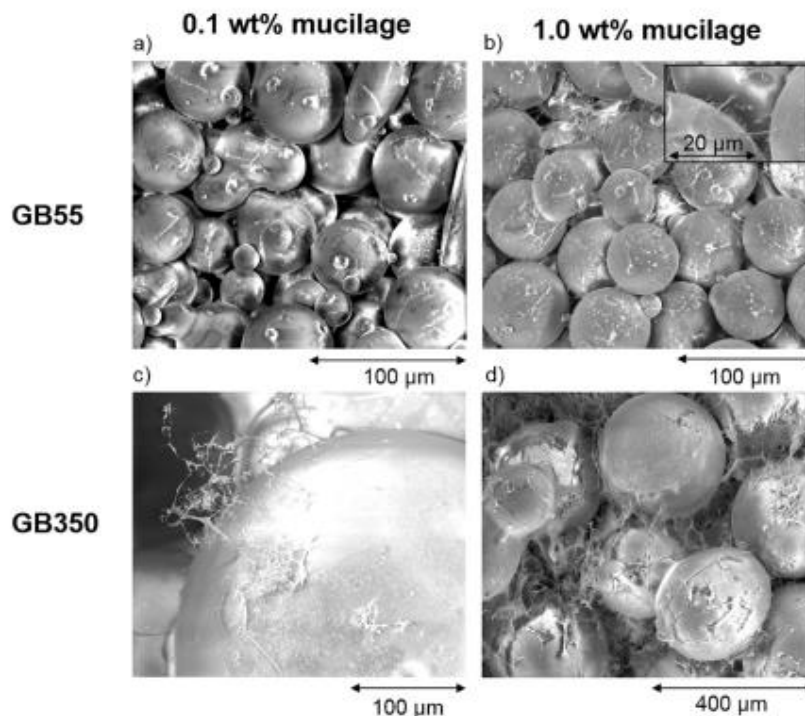


Fig. 2. ESEM pictures of GB55 mixed with 0.1% (a) and 1.0% (b) mucilage, and of GB350 mixed with 0.1% (c) and 1.0% (d) mucilage.

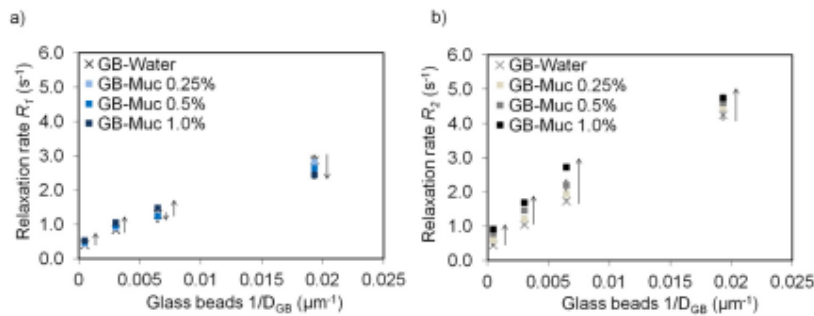


Fig. 3. Variation of the longitudinal (a) and transversal (b) relaxation rates as a function of the reciprocal GB diameter for water and mucilage at several concentrations.

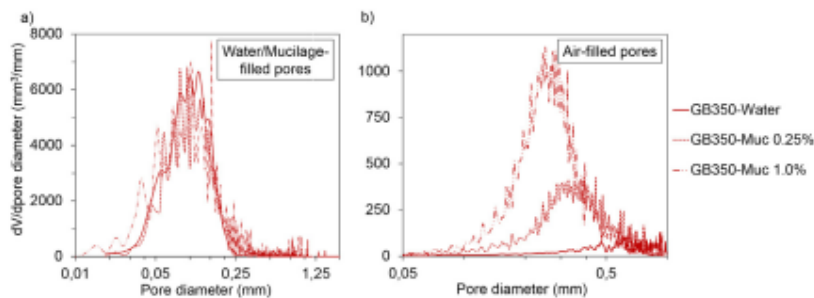


Fig. 4. Volumetric pore size distribution of water- and mucilage-filled pores in GB350 (a), and volumetric air bubbles size distribution in GB350 (b) in 2000 mm³ samples.

seemed to grip the surface of the particles and thus may have strained the network across the pore and increased its rigidity.

The ESEM pictures of the glass beads suggested qualitatively that the polymer network depends on the particle size and varies with the polymer concentration. If so, these variations of the polymer network should affect the water mobility expressed by the relaxation rate.

4.2. Water mobility in porous systems filled with water and mucilage

According to Eqs. (2) and (3), the relaxation rate is expressed as a function of the reciprocal particle diameter. R_1 (Fig. 3a) and R_2 (Fig. 3b) of GB-water and GB-mucilage from the 2D experiments were therefore plotted as a function of the reciprocal glass beads diameter. In Fig. 3a, R_1 increased with the mucilage concentration for the two larger glass beads. R_1 of GB150 decreased slightly for concentrations until 0.5 wt% and jumped to a higher relaxation rate for the highest concentration. R_1 decreased with increasing mucilage concentration for GB55. Corresponding R_2 behaved differently than R_1 : increasing mucilage concentration lead to higher R_2 for all glass beads, though the strength with which R_2 increased varied with the particles' diameter.

The two gel effects identified by Brax et al. (2018) predict higher relaxation rates when mucilage replaced water in a porous system due to an increase of the bulk relaxation and of the surface relaxivity. The diverging trends between R_1 and R_2 for the smallest glass beads suggest the existence of distinct processes affecting R_1 and R_2 differently. A solid-like relaxation behavior characterized by slow R_1 coupled with fast R_2 for the smallest beads at high mucilage concentration is unlikely: For the same volume and concentration of mucilage mixed with the glass beads, there is less polymeric material in the small pores of GB55 than in the big pores of GB350. Another explanation for the unexpected decrease of R_1 with increasing mucilage concentration might be a distortion of the pore size distribution in GB55. Swelling of biohydrogel or organic matter in soil was shown to result in an expansion of the small pores and thus to a shift of the relaxation rate (Jaeger et al., 2010;

Meyer et al., 2018; Todoruk et al., 2003). However, the effect of the increase of the polymer concentration on the pore size distribution by constant water content is not clear and has not been yet investigated to the best of our knowledge. By constant water content, mucilage at high concentration might push the beads aside to create bigger pores, in which the polymer network can expand. This distortion of the pores would affect GB55 stronger than the bigger glass beads. One reason could be that the pores in GB55 being much smaller than those of the bigger beads, the urge of mucilage to expand is stronger in the smaller pores than in the bigger pores. Another reason could be that the smaller volume and lighter weight of GB55 make it easier for mucilage to push the particles asides. This distortion of the pores would have occurred although our aim was to have the same pore size distribution for the GB-water and GB-mucilage samples at all mucilage concentrations.

In order to assess a hypothetical change of the pore size, μ CT images were scanned for GB55 and GB350 mixed with water, mucilage 0.25 wt %, and mucilage 1.0 wt%. The μ CT parameters did not permit to distinguish the particles from water for GB55 due to the limits of resolution (supporting information).

Fig. 4a characterized the volumetric pore size distribution (PSD) of water- and mucilage-filled pores in GB350, and Fig. 4b depicted the volumetric size distribution of air bubbles in GB350. The data presented refer to 2000 mm³ samples. Considering the variations within the samples, the PSD of water- and mucilage-filled pores in GB350 were similar. Although the diameter of the air bubbles decreased and the number of the air bubbles increased from GB350 mixed with water to GB350 mixed with mucilage 1.0 wt%, the air bubbles had no influence on the PSD of GB350. One effect of the air bubbles could be an additional paramagnetic relaxation from dissolved oxygen in the samples with more air bubbles. However, additional paramagnetic relaxation leads to faster R_1 (Mirhej, 1965), while the effects observed were a reduction of R_1 and an increase of R_2 . Another effect of the air bubbles can be the increase of R_2 because of magnetic susceptibility differences arising from the additional interfaces (Alexander et al., 1996). Thus, the

increase of R_2 despite the decrease of R_1 for GB55 at increasing mucilage concentration could come from the increased sensitivity of R_2 to the mucilage concentration and from the magnetic susceptibility related to the air bubbles.

Due to its viscosity, hydrated mucilage cannot be mixed with the glass beads by capillary forces as it can be done for water. Kroener et al. (2014) applied an alternative method consisting of mixing the swollen gel with the glass beads and drying the mixture in the oven. Once dried, the samples were watered by capillary rise. This procedure does not allow the fulfillment of several conditions, which are necessary to study the samples by means of our conceptual model: all samples must have the same amount of water, the mucilage concentration should not vary depending on its position in the sample, and the mucilage need to be homogeneously distributed in the pores and at their surface. The addition of a controlled quantity of water to the glass beads and thorough homogenization of the samples appear therefore as the method of choice. Additional application of a suction to get rid of the air bubbles and to drain the samples to a pendular bridge state could be considered in a next experiment, given this method does not modify the spatial distribution of mucilage in the samples.

4.3. Influence of the mucilage concentration on the R_1 and the R_2 for all glass beads

The ESEM images (Fig. 2) suggest the organization of the polymer in the pore space depends on the particle size. Derivation of the polymeric network effect $G^{*}_{1,2,B}$ from R_1 and R_2 for each particle size would enable verification of this aspect and its effect on the relaxation rate. For this, R_1 and R_2 were plotted as a function of the mucilage concentration for each particle size. The slope corresponds to the polymeric network effect $G^{*}_{1,2,B}$ according to Eq. (6). The linear relationships between $R_{1,2}$ and the mucilage concentration were analysed for each particle size by means of the statistical parameters listed in Table 2.

R_1 increased with increasing mucilage concentration for GB2000, GB350 and GB150, and decreased with increasing mucilage concentration for GB55. For R_1 , R^2 and the significance of the proportional relationship (Pearson R , p) decreased from GB2000 to GB150. R_2 increased with increasing mucilage concentration for all particles. For R_2 , the significance of the proportional relationship decreased for GB55.

The decrease of R_1 for GB55-mucilage despite the increase of the mucilage concentration may come from the formation of bigger pores, either due to a disturbance because of the multiplication of the air bubbles or to a distortion of the pores originated by the mucilage itself.

The polymeric network effects on R_1 ($G^{*}_{1,B}$) (Fig. 5a) and on the R_2 ($G^{*}_{2,B}$) (Fig. 5b) were plotted against the particle diameter. Values of $G^{*}_{1,2,B}$ in pure mucilage were from Brax et al. (2018). $G^{*}_{2,B}$ was higher than $G^{*}_{1,B}$ for pure mucilage. $G^{*}_{1,B}$ for glass beads comprised between 150 and 2000 μm was similar to $G^{*}_{1,B}$ for pure mucilage, but $G^{*}_{1,B}$ for GB55 was negative. The particle size affected $G^{*}_{1,B}$ differently than $G^{*}_{2,B}$: $G^{*}_{2,B}$ was similar to $G^{*}_{2,B}$ for pure mucilage and then increased with decreasing particle size until GB150. $G^{*}_{2,B}$ dropped for GB55.

Combination with the previous results suggests that $G^{*}_{1,2,B}$ does not only reflect the polymeric network effect but results from a distortion of

the pores. The negative value of $G^{*}_{1,B}$ for GB55 shows that this distortion affects R_1 more than the polymeric network effect does. The behavior of $G^{*}_{2,B}$ indicates that R_2 is more sensitive to the polymeric network than R_1 . Indeed, transverse relaxation depends on direct interactions between the spins of the water protons and the ones of the polymer protons without the energy transfer required for longitudinal relaxation (Belton et al., 1988).

The increase of $G^{*}_{2,B}$ with decreasing pore size probably corresponds to the rearrangement of the polymer in a stiffer network, as illustrated in Fig. 6. In Fig. 6b, the inter-particle pore is several times larger than the pores formed by the pure mucilage (Fig. 6a): the network organization of the free polymer and of the polymer trapped in big pores changes little. Fig. 6b could schematize GB2000-mucilage. In Fig. 6c, decreasing inter-particle pore affects more and more the organization of the polymer network: the polymer rearranges to form smaller pores. Rearrangement of the polymer network leads to the increase of R_2 . The drop of $G^{*}_{2,B}$ for GB55 is linked with the distortion of the pores, but also suggests that the opposite effect took place for very small particles: the low concentration of polymer per pores combined with the pore smallness prevents the organization of the polymer in a network (Fig. 6d).

4.4. Influence of the mucilage concentration on the surface relaxivity and the matrix confinement effect

In order to investigate how the mucilage concentration affects the surface relaxivity and the bulk relaxation, R_1 and R_2 were expressed as a function of the inverse of the GB diameter (Eq. (6)). The statistical values (supporting information) indicated the linear relationship between R_1 , R_2 and the reciprocal GB diameter were significant for all mucilage concentrations. According to Eqs. (2), (3) and (6), the slope corresponds to $\beta\rho_{1,2,WP}$ for GB-water and to $\beta(\rho_{1,2,WP} + \rho_{1,2,c})$ for GB-mucilage: The slope captures the influence of the mucilage concentration on the surface relaxivity coupled with the pore size proportional factor β and was plotted against the mucilage concentration in Fig. 7.

The values of $\beta\rho$ for R_1 lowered with increasing mucilage concentration, while the values of $\beta\rho$ for R_2 stayed similar over the concentration range of mucilage.

Previous observations (Figs. 2–5) suggested an increase of the pore size for the smallest particles at higher mucilage concentrations. This would imply a drop of the pore size proportional factor β for the smallest particles (Eq. (3)). The overall $\beta\rho_{1,2}$ would be then subjected to two opposite trends with higher mucilage concentrations: increase of $\rho_{1,2}$ and decrease of β . In Fig. 7, the decrease of β seems to influence the longitudinal $\beta\rho_1$ stronger than the transverse $\beta\rho_2$, for which both trends seem to be balanced. These results suggest that ρ_2 is more sensitive than ρ_1 to the gel effect. The results also propose that the acceleration of the surface relaxation identified by Brax et al. (2018) might not be significant to detect and describe mucilage in porous medium: isolation of ρ from β was not possible and the variation of ρ was shielded by the decrease of β .

According to Eq. (6), the y-intercepts of R_1 and of R_2 as a function of the reciprocal GB diameter correspond to the bulk relaxation rates $1/T_{1,2,B,WP}$ for GB-water and $1/T_{1,2,B,GP}$ for GB-mucilage. The bulk relaxation rates are expressed by $1/T_{1,2,BW}$ for GB-water and by $1/T_{1,2,B} + G_{1,2,B} \cdot c_{muc} + X_{1,2,MC}$ for GB-mucilage (Eqs. (2), (3) and (6)). They were plotted against the mucilage concentration in Fig. 8. R_1 and R_2 of pure mucilage were described by $1/T_{1,2,BW} + G_{1,2,B} \cdot c_{muc}$ (Eq. (1)) and were plotted on Fig. 8 to highlight $G^{*}_{1,2,B}$ and $X_{1,2,MC}$ in porous media.

The slopes for GB-mucilage, ($G^{*}_{1,B} = 0.23 \pm 0.04 \text{ s}^{-1}\cdot\text{wt}\%^{-1}$ and $G^{*}_{2,B} = 0.60 \pm 0.06 \text{ s}^{-1}\cdot\text{wt}\%^{-1}$) were higher than the slopes for pure mucilage ($G^{*}_{1,B} = 0.10 \pm 0.00 \text{ s}^{-1}\cdot\text{wt}\%^{-1}$ and $G^{*}_{2,B} = 0.41 \pm 0.00 \text{ s}^{-1}\cdot\text{wt}\%^{-1}$). The same trend was observed for the y-intercepts of GB-mucilage ($1/T_{1,BW} + X_{1,MC} = 0.42 \pm 0.03 \text{ s}^{-1}$ and $1/T_{2,BW} + X_{2,MC} = 0.47 \pm 0.04 \text{ s}^{-1}$) and pure mucilage ($1/T_1$

Table 2
Statistical values characterizing the linear relationship between the R_1 or the R_2 and the mucilage concentration for all particle sizes.

		GB2000	GB350	GB150	GB55
R_1	Pearson R	0.96	0.88	0.59	-0.93
	R^2	0.92	0.78	0.35	0.86
	p-Value	3.99E-10	1.29E-05	9.89E-03	2.25E-07
R_2	Pearson R	0.97	0.95	0.94	0.68
	R^2	0.94	0.91	0.89	0.47
	p-Value	4.31E-11	4.44E-08	3.94E-09	3.51E-03

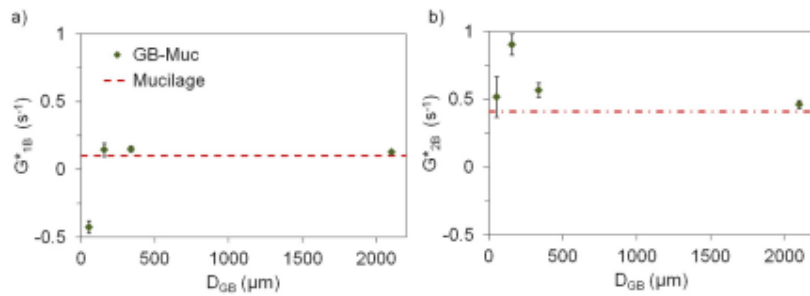


Fig. 5. Polymeric network effect G^*_{1B} (a) and G^*_{2B} (b) affected by the particle sizes.

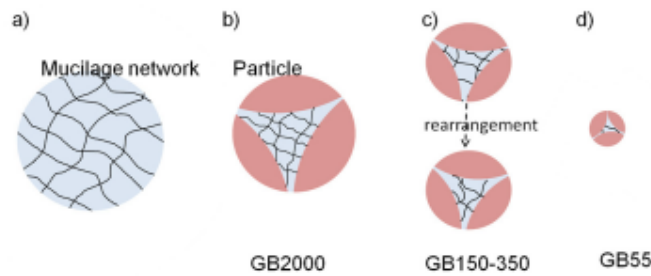


Fig. 6. Schematic representation of the rearrangement of the polymer network according to the porosity.

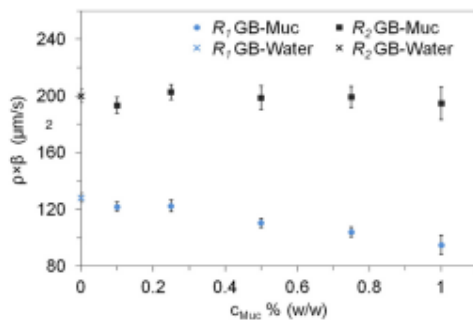


Fig. 7. Influence of the mucilage concentration on the surface relaxivity coupled with the pore size proportional factor for R_2 and R_1 .

$BW = 0.38 \pm 0.00 \text{ s}^{-1}$ and $1/T_2 \text{ BW} = 0.41 \pm 0.00 \text{ s}^{-1}$), which implies that the matrix confinement effect $X_{1,2 \text{ MC}}$ is larger than zero.

These results suggest that the polymeric network in porous GB medium affects proton relaxation stronger than the polymeric network in free mucilage. This observation is explained by the spider-web effect, translated by an increase of rigidity of the polymer strands in the porous medium: while polymer strands do not have volume restriction in the

free mucilage, the walls of the particles restrict the elongation of the polymer strands in a porous medium. These walls also serve as a frame for the polymer porous network, thus conferring rigidity to the polymer strands. The spider-web effect is translated by an increase of $G^*_{1,2}$ with the mucilage concentration and by $X_{1,2 \text{ MC}}$ larger than zero.

Finally, our conceptual model describing the gel effect on the NMR parameters offers a quantitative analysis of the shift of the relaxation rate due to the presence of mucilage in porous media. The interpretation of results showed a pore-size specific organization of the polymeric network, which suggested that the gel effect on further soil properties also depends on the particle size. A similar concept was presented by Kroener et al. (2018), who found that the effect of chia seed mucilage on saturated hydraulic conductivity was particle size specific.

In a next step, the method should be applied to root exudates and mucilages and to soil samples with increasing complexity regarding pore size distribution and organic matter content. A further challenge is also to develop the detection and characterization of mucilage when present as a biohydrogel phase in the soil medium. The change of mucilage properties after drying and rewetting also needs to be understood, given experiments showed that the rewetting of biohydrogel phases in soil leads to a change of the macroscopic properties (Buchmann et al., 2015a).

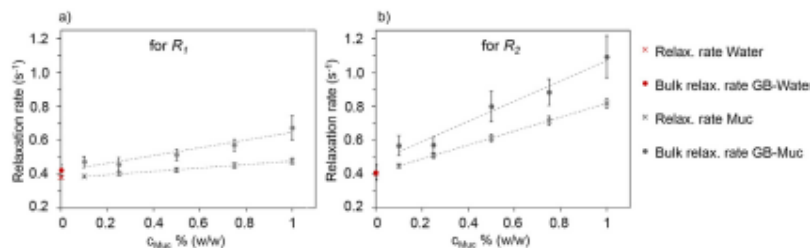


Fig. 8. Influence of the mucilage concentration on the longitudinal (a) and transverse (b) bulk relaxation in porous media.

Table 3

Summary of the several gel effects investigated in this paper.

Gel effect	Cause	Translated by	Significant?
Accelerated surface relaxation	Chemico-physical interactions between water protons and polymer	$\rho_{CP} > \rho_{WP}$, but ρ could not be isolated from	No
Accelerated bulk relaxation	Chemico-physical interactions between water protons and polymer	$\frac{1}{T_{1,2,R/GP}} > \frac{1}{T_{1,2B/WP}}$	Yes
Polymer network effect	Polymer organization in the pore space	$G^*_{1,2}$	Yes, depends on particle size and mucilage concentration
Spider-web effect	Rigidity of the polymer network in the pore space > in the free polymer	$G^*_{1,2}$ $X_{1,2,AC} > 0$	Yes

5. Conclusion

In conclusion, the combination of ^1H NMR and ESEM images showed that the organization of the mucilage network depends on the particle size. The *polymeric network effect* was stronger in the porous medium of particles between 150 and 350 μm and dropped for very fine and very coarse particles. Accordingly, it would be interesting to measure the hydraulic conductivity at several mucilage concentrations and investigate a correlation between the water mobility measured with ^1H NMR and the hydraulic conductivity.

Slow R_1 and fast R_2 suggested a distortion of the pores for the smaller glass beads at high mucilage concentrations, which needs to be verified by additional experiments. This alteration from our defined samples helps to highlight and to discriminate between several gel effects and their relative influence on longitudinal and transverse relaxation (Table 3). *Accelerated surface relaxation* is not validated as a significant gel effect, as both R_1 and R_2 seem to be more affected by the pore distortion than by the increase of the surface relaxivity ρ related to the gel effect. On the contrary, *accelerated bulk relaxation* is a significant gel effect: it is composed of the *polymeric network effect*, which carries information about the concentration of mucilage in the pore and organization of the polymer network in the pore. The *accelerated bulk relaxation* also brings to evidence a *spider-web effect*, which attests the additional rigidity of the polymer network due to its strands spanned in the pore space, as opposed to unattached and loose strands in the free gel. Finally, the transverse bulk relaxation was more affected by these gel effects than the longitudinal relaxation.

Acknowledgement

The authors wish to thank the DFG (German Research Foundation) for funding within the project MUCILAGE (SCHA840/20).

Appendix A. Supplementary data

Supplementary data to this article can be found online at <https://doi.org/10.1016/j.geoderma.2019.01.013>.

References

- Ahmed, M.A., Kroener, E., Holz, M., Zarebanadkouki, M., Carminati, A., 2014. Mucilage exudation facilitates root water uptake in dry soils. *Funct. Plant Biol.* 41, 1129. <https://doi.org/10.1071/FP13330>.
- Ahmed, M.A., Kroener, E., Benard, P., Zarebanadkouki, M., Kaestner, A., Carminati, A., 2016. Drying of mucilage causes water repellency in the rhizosphere of maize: measurements and modelling. *Plant Soil* 407, 161–171. <https://doi.org/10.1007/s11104-015-2749-1>.
- Albalasmeh, A.A., Ghezzehei, T.A., 2014. Interplay between soil drying and root exudation in rhizosphere development. *Plant Soil* 374, 739–751. <https://doi.org/10.1007/s11104-013-1910-y>.
- Alexander, A.L., McCreery, T.T., Barrette, T.R., Gmitro, A.F., Unger, E.C., 1996. Microbubbles as novel pressure-sensitive MR contrast agents. *Magn. Reson. Med.* 35, 801–806. <https://doi.org/10.1002/mrm.1910350603>.
- Bayer, J.V., Jaeger, F., Schaumann, G.E., 2010. Proton nuclear magnetic resonance (NMR) relaxometry in soil science applications. *Open Magn. Reson. J.* 3, 15–26.
- Belton, P.S., Hills, B.P., Raimbault, E.R., 1988. The effects of morphology and exchange on proton NMR relaxation in agarose gels. *Mol. Phys.* 63, 825–842.

- Brax, M., Buchmann, C., Schaumann, G.E., 2017. Biohydrogel induced soil–water interactions: how to untangle the gel effect? A review. *J. Plant Nutr. Soil Sci.* 180, 121–141. <https://doi.org/10.1002/jpln.201600453>.
- Brax, M., Buchmann, C., Schaumann, G.E., 2018. Effect of mucilage on water properties in the rhizosphere monitored by ^1H -NMR relaxometry. *Microporous Mesoporous Mater.* 269, 47–50. <https://doi.org/10.1016/j.micromeso.2017.07.044>. (Proceedings of the 13th International Bologna Conference on Magnetic Resonance in Porous Media (MRPML3)).
- Brownstein, K.R., Tarr, C.E., 1979. Importance of classical diffusion in NMR studies of water in biological cells. *Phys. Rev. A* 19, 2446.
- Buchmann, C., Schaumann, G.E., 2017. Effect of water entrapment by a hydrogel on the microstructural stability of artificial soils with various clay content. *Plant Soil* 414, 181–198. <https://doi.org/10.1007/s11104-016-3110-z>.
- Buchmann, C., Bentz, J., Schaumann, G.E., 2015a. Intrinsic and model polymer hydrogel-induced soil structural stability of a silty sand soil as affected by soil moisture dynamics. *Soil Tillage Res.* 154, 22–33. <https://doi.org/10.1016/j.still.2015.06.014>.
- Buchmann, C., Meyer, M., Schaumann, G.E., 2015b. Characterization of wet aggregate stability of soils by H-NMR relaxometry. *Magn. Reson. Chem.* 53, 694–703. <https://doi.org/10.1002/mrc.4147>.
- Butler, J., Reeds, J., Dawson, S., 1981. Estimating solutions of first kind integral equations with nonnegative constraints and optimal smoothing. *SIAM J. Numer. Anal.* 18, 381–397. <https://doi.org/10.1137/0718025>.
- Capitani, M.J., Corzo-Rios, L.J., Chel-Guerrero, L.A., Betancur-Ancona, D.A., Nolasco, S.M., Tomás, M.C., 2015. Rheological properties of aqueous dispersions of chia (*Salvia hispanica* L.) mucilage. *J. Food Eng.* 149, 70–77. <https://doi.org/10.1016/j.jfoodeng.2014.09.043>.
- Carminati, A., 2012. A model of root water uptake coupled with rhizosphere dynamics. *Vadose Zone J.* 11, 0. <https://doi.org/10.2136/vzj2011.0106>.
- Carminati, A., Vetterlein, D., 2013. Plasticity of rhizosphere hydraulic properties as a key for efficient utilization of scarce resources. *Ann. Bot.* 112, 277–290. <https://doi.org/10.1093/aob/mcs262>.
- Carminati, A., Schneider, C.L., Moradi, A.B., Zarebanadkouki, M., Vetterlein, D., Vogel, H.-J., Hildebrandt, A., Weller, U., Schüler, L., Oswald, S.E., 2011. How the rhizosphere may favor water availability to roots. *Vadose Zone J.* 10, 988–998. <https://doi.org/10.2136/vzj2010.0113>.
- Chenu, C., 1993. Clay-or sand-polysaccharide associations as models for the interface between micro-organisms and soil: water related properties and microstructure. *Geoderma* 56, 143–156.
- Chui, M.M., Phillips, R.J., McCarthy, M.J., 1995. Measurement of the porous microstructure of hydrogels by nuclear magnetic resonance. *J. Colloid Interface Sci.* 174, 336–344.
- Codd, S.L., Vogt, S.J., Hornemann, J.A., Phillips, A.J., Maneval, J.E., Romanenko, K.R., Hansen, L., Cunningham, A.B., Seymour, J.D., 2011. NMR relaxation measurements of biofoaming in model and geological porous media. *Org. Geochem.* 42, 965–971. <https://doi.org/10.1016/j.orggeochem.2011.03.014>. (Applications and developments of magnetic resonance techniques in Geosciences).
- Davit, Y., Iltis, G., Debenest, G., Veran-Tissotres, S., Wildenschild, D., Gerino, M., Quintard, M., 2011. Imaging biofilm in porous media using X-ray computed microtomography. *J. Microsc.* 242, 15–25. <https://doi.org/10.1111/j.1365-2818.2010.03432.x>.
- Degrassi, A., Toffanin, R., Paoletti, S., Hall, L.D., 1998. A better understanding of the properties of alginate solutions and gels by quantitative magnetic resonance imaging (MRI). *Carbohydr. Res.* 306, 19–26.
- Dougherty, R., Kunzelmann, K.-H., 2007. Computing local thickness of 3D structures with ImageJ. *Microsc. Microanal.* 13, 1678–1679. <https://doi.org/10.1017/S1431927607074430>.
- Dunn, K.-J., Bergman, D.J., LaTorraca, G.A., 2002. Nuclear Magnetic Resonance: Petrophysical and Logging Applications. Pergamon, New York.
- Fyfe, C.A., Blazek, A.I., 1997. Investigation of Hydrogel Formation from Hydroxypropylmethylcellulose (HPMC) by NMR Spectroscopy and NMR Imaging Techniques. *Macromolecules* 30. <https://doi.org/10.1021/ma970076o>.
- Godefroy, S., Korb, J.-P., Fleury, M., Bryant, R.G., 2001. Surface nuclear magnetic relaxation and dynamics of water and oil in macroporous media. *Phys. Rev. E* 64, 021605. <https://doi.org/10.1103/PhysRevE.64.021605>.
- Gregory, P.J., 2006. Roots, rhizosphere and soil: the route to a better understanding of soil science? *Eur. J. Soil Sci.* 57, 2–12. <https://doi.org/10.1111/j.1365-2389.2005.00778.x>.
- Helliwell, J.R., Sturrock, C.J., Grayling, K.M., Tracy, S.R., Flavel, R.J., Young, L.M., Whalley, W.R., Mooney, S.J., 2013. Applications of X-ray computed tomography for examining biophysical interactions and structural development in soil systems: a

- review. *Eur. J. Soil Sci.* **64**, 279–297. <https://doi.org/10.1111/ejss.12028>.
- Hills, B.P., 1992. The proton exchange cross-relaxation model of water relaxation in biopolymer systems. *Mol. Phys.* **76**, 489–508.
- Hills, B.P., Godward, J., Debaty, M., Barras, L., Satrio, C.P., Ouwerx, C., 2000. NMR studies of calcium induced alginate gelation. Part II. The internal bead structure. *Magn. Reson. Chem.* **38**, 719–728.
- Jaeger, F., Grohmann, E., Schaumann, G.E., 2006. ^1H NMR Relaxometry in natural humus soil samples: insights in microbial effects on relaxation time distributions. *Plant Soil* **280**, 209–222. <https://doi.org/10.1007/s11104-005-3035-4>.
- Jaeger, F., Shebegolikhina, A., Van As, H., Schaumann, G.E., 2010. Proton NMR relaxometry as a useful tool to evaluate swelling processes in peat soils. *Open Magn. Reson. J.* **3**, 27–45.
- Kazanskii, K.S., Dubrovskii, S.A., 1992. Chemistry and physics of “agricultural” hydrogels. In: *Polyelectrolytes Hydrogels Chromatographic Materials*. Springer, Berlin Heidelberg, pp. 97–133.
- Keating, K., Knight, R., 2006. A laboratory study to determine the effect of iron oxides on proton NMR measurements. *Geophysics* **72**, E27–E32. <https://doi.org/10.1190/1.2399445>.
- Kirkland, C.M., Hiebert, R., Phillips, A., Grunewald, E., Walsh, D.O., Seymour, J.D., Codd, S.L., 2015. Biofilm detection in a model well-bore environment using low-field NMR. *Groundw. Monit. Remediat.* **35**, 36–44. <https://doi.org/10.1111/gwmr.12117>.
- Kleinberg, R.L., 1996. Utility of NMR T2 distributions, connection with capillary pressure, clay effect, and determination of the surface relaxivity parameter ρ_2 . *Magn. Reson. Imaging* **14**, 761–767.
- Kleinberg, R.L., Kenyon, W.E., Mitra, P.P., 1994. Mechanism of NMR relaxation of fluids in rock. *J. Magn. Reson. A* **108**, 206–214.
- Kroener, E., Zarebanadkouki, M., Kaestner, A., Carminati, A., 2014. Nonequilibrium water dynamics in the rhizosphere: how mucilage affects water flow in soils. *Water Resour. Res.* **50**, 6479–6495. <https://doi.org/10.1002/2013WR014756>.
- Kroener, E., Holz, M., Zarebanadkouki, M., Ahmed, M., Carminati, A., 2018. Effects of mucilage on rhizosphere hydraulic functions depend on soil particle size. *Vadose Zone J.* **17**.
- Kulkarni, R., Tuller, M., Fink, W., Wildenschild, D., 2012. Three-dimensional multiphase segmentation of X-ray CT data of porous materials using a Bayesian Markov random field framework. *Vadose Zone J.* **11**. <https://doi.org/10.2136/vzj2011.0082>.
- Li, B., Ding, D., Wang, Y., Sun, P., Ma, J., He, B., 1999. NMR characterization of absorbed water in equilibrium swollen hydrogel P(AM-NaA). *J. Appl. Polym. Sci.* **72**, 1203–1207. [https://doi.org/10.1002/\(SICI\)1097-4628\(19990531\)72:9<1203::AID-APP9>3.0.CO;2-R](https://doi.org/10.1002/(SICI)1097-4628(19990531)72:9<1203::AID-APP9>3.0.CO;2-R).
- Lüsse, S., Arnold, K., 1998. Water binding of polysaccharides: NMR and ESR studies. *Macromolecules* **31**, 6891–6897. <https://doi.org/10.1021/ma971869d>.
- Mao, R., Tang, J., Swanson, B.G., 2001. Water holding capacity and microstructure of gellan gels. *Carbohydr. Polym.* **46**, 365–371. [https://doi.org/10.1016/S0144-8617\(00\)00337-4](https://doi.org/10.1016/S0144-8617(00)00337-4).
- Meiboom, S., Gill, D., 1958. Modified spin-echo method for measuring nuclear relaxation times. *Rev. Sci. Instrum.* **29**, 688–691. <https://doi.org/10.1063/1.1716296>.
- Meyer, M., Buchmann, C., Schaumann, G.E., 2018. Determination of quantitative pore-size distribution of soils with ^1H NMR relaxometry. *Eur. J. Soil Sci.* **69**, 393–406. <https://doi.org/10.1111/ejss.12548>.
- Mirhej, M.E., 1965. Proton spin relaxation by paramagnetic molecular oxygen. *Can. J. Chem.* **43**, 1130–1138.
- Mitchell, J., Chandrasekera, T.C., Johns, M.L., Gladden, L.F., Fordham, E.J., 2010. Nuclear magnetic resonance relaxation and diffusion in the presence of internal gradients: the effect of magnetic field strength. *Phys. Rev. E Stat. Nonlinear Soft Matter Phys.* **81**, 026101. <https://doi.org/10.1103/PhysRevE.81.026101>.
- Naveed, M., Brown, L.K., Raffan, A.C., George, T.S., Bengough, A.G., Roose, T., Sinclair, I., Koebnick, N., Cooper, L., Hackett, C.A., Hallett, P.D., 2017. Plant exudates may stabilize or weaken soil depending on species, origin and time. *Eur. J. Soil Sci.* **68**, 806–816. <https://doi.org/10.1111/ejss.12487>.
- Sanderlin, A.B., Vogt, S.J., Grunewald, E., Bergin, B.A., Codd, S.L., 2013. Biofilm detection in natural unconsolidated porous media using a low-field magnetic resonance system. *Environ. Sci. Technol.* **47**, 997–992. <https://doi.org/10.1021/es3040686>.
- Schindelin, J., Arganda-Carreras, I., Frise, E., Kaynig, V., Longair, M., Pietzsch, T., Preibisch, S., Rueden, C., Saalfeld, S., Schmid, B., Tinevez, J.-Y., White, D.J., Hartenstein, V., Eliceiri, K., Tomancak, P., Cardona, A., 2012. Fiji: an open-source platform for biological-image analysis. *Nat. Methods* **9**, 676–682. <https://doi.org/10.1038/nmeth.2019>.
- Schlüter, S., Sheppard, A., Brown, K., Wildenschild, D., 2014. Image processing of multiphase images obtained via X-ray microtomography: a review. *Water Resour. Res.* **50**, 3615–3639. <https://doi.org/10.1002/2014WR015256>.
- Shapiro, Y.E., 2011. Structure and dynamics of hydrogels and organogels: an NMR spectroscopy approach. *Prog. Polym. Sci.* **36**, 1184–1253. <https://doi.org/10.1016/j.propolymsci.2011.04.002>.
- Song, Y.-Q., Venkataraman, L., Hürlimann, M.D., Flaum, M., Frulla, P., Straley, C., 2002. T1–T2 correlation spectra obtained using a fast two-dimensional Laplace inversion. *J. Magn. Reson.* **154**, 261–268. <https://doi.org/10.1006/jmre.2001.2474>.
- Song, Y.-Q., Carneiro, G., Schwartz, L.M., Johnson, D.L., 2014. Experimental identification of diffusive coupling using 2D NMR. *Phys. Rev. Lett.* **113**, 235503. <https://doi.org/10.1103/PhysRevLett.113.235503>.
- Sutherland, I., 2001. Biofilm exopolysaccharides: a strong and sticky framework. *Microbiology* **147**, 3–9. <https://doi.org/10.1099/00221287-147-1-3>.
- Todoruk, T.R., Langford, C.H., Kantzas, A., 2003. Pore-scale redistribution of water during wetting of air-dried soils as studied by low-field NMR relaxometry. *Environ. Sci. Technol.* **37**, 2707–2713.
- Tristán-Vega, A., García-Pérez, V., Aja-Fernández, S., Westin, C.-F., 2012. Efficient and robust nonlocal means denoising of MR data based on salient features matching. *Comput. Methods Prog. Biomed.* **105**, 131–144. <https://doi.org/10.1016/j.cmpb.2011.07.014>.
- Venkataraman, L., Song, Y.-Q., Hürlimann, M.D., 2002. Solving Fredholm integrals of the first kind with tensor product structure in 2 and 2.5 dimensions. *IEEE Trans. Signal Process.* **50**, 1017–1026. <https://doi.org/10.1109/78.995059>.
- Void, R.L., Waugh, J.S., Klein, M.P., Phelps, D.E., 1967. Measurement of Spin Relaxation in Complex Systems.
- Zarebanadkouki, M., Kim, Y.X., Moradi, A.B., Vogel, H.-J., Kaestner, A., Carminati, A., 2012. Quantification and modeling of local root water uptake using neutron radiography and deuterated water. *Vadose Zone J.* **11**, vzj2011.0196. <https://doi.org/10.2136/vzj2011.0196>.
- Zickenrott, I.-M., Woche, S.K., Bschmann, J., Ahmed, M.A., Vetterlein, D., 2016. An efficient method for the collection of root mucilage from different plant species—a case study on the effect of mucilage on soil water repellency. *J. Plant Nutr. Soil Sci.* **179**, 294–302. <https://doi.org/10.1002/jpln.201500511>.

*5. GEL FORMATION MECHANISM AND GEL PROPERTIES
CONTROLLED BY Ca^{2+} IN CHIA SEED MUCILAGE AND MODEL
SUBSTANCES*

Gel formation mechanism and gel properties controlled by Ca²⁺ in chia seed mucilage and model substances

Mathilde Brax¹, Gabriele Ellen Schaumann¹, and Dörte Diehl^{1*}

¹ University Koblenz-Landau, Institute for Environmental Sciences, Group of Environmental and Soil Chemistry, Fortstrasse 7, 76829 Landau, Germany

Abstract

Polygalacturonic acid (PGA) is considered as a model substance for mucilage to study mucilage–soil interactions, assuming that the gel formation mechanism of mucilage is comparable to the one of PGA. However, some studies question the accepted hypothesis, which states that, like for PGA, this mechanism relies on cross-links between uronic acid and calcium for mucilage. The aim of this study was therefore to understand the influence of the abundance and degree of esterification of uronic acids and the influence of calcium on the gel formation mechanism in mucilage as compared to model substances.

The mucilage used was from chia seeds, as it is easily available in great quantity and has gel properties shared by root mucilage. Results reported here demonstrate that, while the gel formation mechanism of PGA relied on specific cross-links with calcium and led to heterogeneous gels, low-methoxy pectin (LMP) formed homogeneous calcium gels also characterized by non-specific ionic interactions with calcium. On the contrary, despite similar uronic acid content to LMP, chia seed mucilage was mostly governed by weak electrostatic interactions between entangled polymer chains, which conferred the gel poor water retention. Addition of calcium reduced repulsion and molecular expansion, resulting in a reduction of the water content in chia seed mucilage. Finally, the discrepancies between PGA, LMP and chia seed mucilage discredit the use of PGA as model for chia seed mucilage. Comparison with root mucilage is still needed. This study offers the keys for further mechanistic understanding on the influence of mucilage on soil properties.

Key words: biohydrogel / cation–polymer interactions / mucilage / mucilage model substance / rhizosphere / water mobility

Accepted November 05, 2018

1 Introduction

Root mucilage has been acknowledged to affect biological processes (Knee et al., 2001; Ahmed et al., 2014) and to modulate physical properties of the rhizosphere (Czames et al., 1999; Traoré et al., 2000). Numerous studies used polygalacturonic acid (PGA) as a model substance for root mucilage to determine its influence on soil properties (Zhang et al., 2008; Barré and Hallett, 2009; Mimmo et al., 2009; Peng et al., 2011). Mucilage's fast degradation rate (Van Veelen et al., 2018) and in particular its time-consuming production and associated small yields (Ahmed et al., 2015; Zickenrott et al., 2016) indeed required the use of model substances (Brax et al., 2017). The choice of PGA as a model for mucilage is based on the high content of uronic acid measured in maize mucilage (Morel et al., 1986) and on the similarities between mucilage and the calcium polygalacturonate network formed on garlic roots visualized with transmission and scanning electron microscopy (Gessa and Deiana, 1992, 1990).

Yet, the uronic acid content in mucilage varies strongly depending on the plant and the growing conditions: Bacic et al. (1986) measured 3 wt% (based on the total polysac-

charide content) of uronic acid in *Zea mays* L. grown under axenic conditions, whereas in another study Morel et al. (1986) measured 22 wt% for the same plant under the same growing conditions and 34 wt% for the same plant but grown under non-sterile conditions. An uronic acid content of even 48 wt% was measured for 3-days old cress seedlings mucilage (Ray et al., 1988). Despite the variations in the uronic acid content, all these studies agree that mucilage consists with over 90% of its dry mass in polysaccharides. Thus, the supramolecular structure of the mucilage polymer consists mostly of neutral sugars and of varying contents of uronic acids.

Despite their low concentration in soil, uronic acids are suggested to play a crucial role in the supramolecular structure of biohydrogels and in their interactions with soil. Gel properties of acidic polysaccharides highly depend on abundance and degree of esterification of uronic acids, as well as on the ionic composition of the surrounding solution (Grasdalen et al., 1988; Garnier et al., 1993). Non-esterified and deprotonated uronic acids may link to the soil surface or form ionic cross-



*Correspondence: D. Diehl; e-mail: diehl@uni-landau.de

links with multivalent cations of the surrounding soil solution (Morel et al., 1987; de Kerchove and Elimelech, 2007). Root mucilage, having less uronic acids than PGA, contains less and more scattered negative charges than PGA. Moreover, the degree of methyl esterification of uronic acids in root mucilage has not been measured yet. Arabidopsis seed mucilage shows a degree of esterification of over 30% (Voiniciuc et al., 2013). This suggests that also in root mucilage some uronic acids are esterified, which would reduce the negative charge of the polymer even more.

Discrepancies between PGA and mucilage concerning number, distribution, and screening of uronic acids could lead to fundamental differences in the self-organization processes of these polymers and consequently in their interactions with soil particles. For example, Morel et al. (1987) found that PGA adsorption to heavy metals and clay surfaces was due to the formation of salts and complexes between carboxylic groups and cations. On the contrary, they showed that ionic binding through carboxylic groups was not the prevalent mechanism for maize mucilage. The results obtained by Watt et al. (1993) also question ionic binding through carboxylic groups as adsorption mechanism for root mucilage, as the neutralization of anionic sites in root cap mucilage with cationic dyes did not affect soil binding by mucilage. Both studies proposed that the hydroxyl groups of the terminally branched neutral sugars participate to the binding mechanism of mucilage to soil.

Clarification of the chemical interactions between mucilage and its environment, e.g., metal cations and soil particles, first necessitates a clearer understanding of the governing self-organization processes in mucilage itself. To our best knowledge, while research has been done on model substances (Mimmo et al., 2003, 2009), no study has yet either investigated the gelling mechanism of mucilage and its dependence on cross-linking cations, or compared it with gel properties such as water content, water binding or water retention.

The objective of the present study is to understand the influence of the abundance and degree of esterification of uronic acids, as well as the influence of calcium as cross-linking ion from the soil solution on the gel formation mechanism in natural mucilage as compared to selected model substances. We further aim to establish a relationship between the observed gel formation mechanisms and the resulting gel properties. Thereby, we identify the gel network defined by network stiffness and pore size measured by ¹H NMR relaxometry, and the hydrogel properties characterized by water content, water mobility and water retention in this work (Fig. 1).

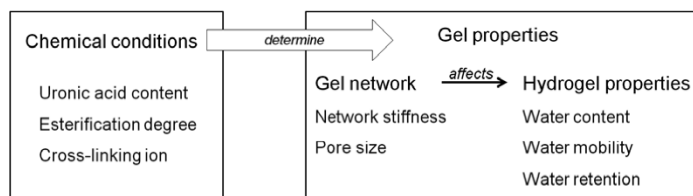


Figure 1: Relationship between chemical conditions and gel properties.

We hypothesize that the gel formation mechanism and the resulting properties of mucilage depend on the interactions between uronic acid and calcium, and thus that they are not comparable to those of PGA due to discrepancies in their respective uronic acid contents. To proof this hypothesis, links between chemical conditions, gel formation mechanism and gel properties were drawn for mucilage and its model substances with the following hypotheses:

1. The capacity of mucilage and its model substances to bind calcium decreases with decreasing uronic acid content and with increasing degree of esterification.
2. Gels with high calcium content tend to form many specific cross-links, which induce a stiff network and small pores.
3. Gels with low calcium content are rather governed by non-specific ionic interactions and form only few cross-links with calcium, which induce only a weak network with large pores.
4. We further hypothesize that the higher the gel bound calcium content is, the lower the water content and water mobility but the higher the capacity of water retention are.

In order to investigate the relationships between chemical properties of the polymers, cross-linking ion and gel properties, polygalacturonic acid (PGA), low-methoxy pectin (LMP), and high-methoxy pectin (HMP) were the three substances differing in uronic acid content and degree of esterification investigated as model. Due to the experimental difficulty to isolate substantial amounts from root mucilage (Zickenrott et al., 2016), chia seed mucilage (*Salvia hispanica* L.) was used as natural mucilage: it is easily available in great quantities and shares gel properties such as viscosity relevant to seed, root and microbial exudates in soils (Read and Gregory, 1997; Sutherland, 2001; Ahmed et al., 2015; Capitani et al., 2015). All substances were dialyzed against several concentrations of CaCl₂-solutions. Thereafter, gel yield, calcium content, and water content were measured to determine the effect of the calcium concentration in the dialysis solution on the gel formation and gel swelling. To further characterize the hydrogel properties, water retention was quantified by dehydration over sand and water mobility was measured with proton nuclear magnetic resonance (¹H NMR) relaxometry to characterize the hydrogel properties.

2 Theoretical background

2.1 NICA and Donnan models

Interactions between polyelectrolytes and calcium can be specific and nonspecific (Benedetti et al., 1996). Specific binding involves coordinative interactions between calcium and galacturonate residues (Grant et al., 1973). The NICA model describes gels formed by these specific interactions between a cation and negatively charged surface functional groups (Kinniburgh et al., 1996). In this case, the junction zones, i.e., the zone where two chains are linked together (Jarvis, 1984), are described by the egg-box model (Rees and Welsh, 1977). This model suggests that helical chains strongly associate by the specific sequestration and binding of calcium

ions. Low degree of esterification of the polysaccharide, high uronic acid content and long unsubstituted galacturonic backbone favour specific surface speciation of calcium with the polymer (Kinniburgh et al., 1996; Tibbitts et al., 1998). Nonspecific interactions between the uncharged functional groups or the hydroxyl groups of polyelectrolytes and calcium are governed by electrostatic forces and can be described by the Donnan model (Benedetti et al., 1996; Kinniburgh et al., 1996). In order to preserve the overall electroneutrality in Donnan gels, more mobile ions from the surrounding solution penetrate into the gel phase than are released back from the gel into the surrounding solution (Benedetti et al., 1996). Thus, a potential difference between the gel and the surrounding solution, the 'Donnan potential', is built, which holds the ions inside the 'Donnan volume' that surrounds the charged polyelectrolyte gel (Koopal et al., 2005). In this case, the junction zones are less spatially defined and rather embrace zones of dense electrostatic interactions (Skouri et al., 1995). Swelling of a polyelectrolyte is determined by a balance between the gel rigidity that restricts swelling and the osmotic 'Donnan pressure' of free ions that promotes swelling of the gel (Rubinstein et al., 1996). Specific calcium binding is related to cross-links formation and gel stiffness (Tibbitts et al., 1998), and thus reduces the gel elasticity and swelling. In contrast, nonspecific electrostatic interactions increase the swelling pressure with increasing charge of the polyelectrolytes and decreasing salt concentration in the surrounding solution (Benedetti et al., 1996; Rubinstein et al., 1996).

2.2 Characterization of water entrapment in hydrogels by ¹H NMR relaxometry

In the field of nuclear magnetic resonance, water mobility is defined by the translational mobility and the rotational correlation time of the water protons measured with the proton relaxation time (Belton, 1997). This one corresponds to the time required by the hydrogen spins to re-reach equilibrium conditions within a static magnetic field after excitation by high frequency pulse. It varies according to various interactions between the spin system and its surrounding environment (Meiboom and Gill, 1958). Water in close interaction to the polymer chains exchanges rapidly with free water trapped in the hydrogel network, so that the water protons observed relaxation time is the weighted average of both (Průšová et al., 2013). There are several pathways of proton relaxation, nevertheless proton exchange between labile polysaccharide protons and water protons is thought to be the main relaxation mechanism in water-polysaccharide systems (Shapiro, 2011): the chemical structure of the polysaccharide influences proton relaxation. The non-exchangeable protons are not considered to contribute to the measured signal due to the rapidity of their signal decay and to their very small contribution to the overall signal intensity (de Celis Alonso et al., 2010). Besides, rigidity of the polymer network implies a significant reduction of the water rotational correlation time (Belton, 1997; Lüsse and Arnold, 1998). The concentration of the cross-linking agent affects the flexibility of the polymer chains and thus the average mobility of water (Dobies et al., 2005; de Celis Alonso et al., 2010). To sum up, proton relaxation in hydrogels is influenced by the chemistry of the poly-

mer, the flexibility of the network and by the pore size, which can be expressed by the relaxation rate (Brax et al., 2018).

3 Material and methods

3.1 Choice of the model substances

The α-1,4-linked-galacturonic acid sequences in pectin can be altered by 1,2-rhamnose units or other neutral sugars such as galactose or arabinose (Rees and Welsh, 1977). The galacturonic acids are partially esterified with methyl groups, and the degree of esterification is a measure of the extent of substitution. Low-methoxy pectin (LMP) and high-methoxy pectin (HMP) are distinguished by their degree of esterification inferior to 50% and higher than 50%, respectively. The gelation mechanism of pectin depends on its degree of esterification: LMP forms ionic gels with calcium, while gelation of HMP requires a drop of the water activity (through addition of glucose) to promote electrostatic interactions between the polymer chains (Oakenfull, 1991). The high uronic acid content of polygalacturonic acid (PGA) as well as the low degree of esterification of LMP and the high degree of esterification of HMP make these polymers suitable model substances to compare them with a natural mucilage obtained from chia seeds.

3.2 Chia seed mucilage extraction

Chia seed mucilage was extracted by following the method described by Ahmed et al. (2014) with some modifications. Distilled water was added slowly to chia seeds under constant stirring so that the seed-to-water ratio was 1:10 (w/w). Mucilage excretion reaches a steady state after 30 min (De la Paz Salgado-Cruz et al., 2013), so that after being kept 30 min at room temperature, chia seed mucilage was extracted by vacuum filtration using stainless sieves of 500 and 100 μm successively. The collected mucilage was further freeze-dried.

3.3 Total uronic acid content

Total uronic acid content was determined by the m-hydroxybiphenyl method (Blumenkrantz and Asboe-Hansen, 1973). In order to keep the absorbance measurements within the range of Lambert and Beer's law, polymer solutions were used in a concentration of 0.015% (w/w).

3.4 Gel formation

The hydrogels were formed by dialysis of the polymer against CaCl₂-solutions. The idea behind this method was to simulate the diffusion of calcium ions from the soil solution into the gel phase built by mucilage around the roots. For this, 0.15% (w/w) solutions of PGA (polygalacturonic acid, 95%, enzymatic, Sigma, Germany), LMP (low methoxy pectin, potassium salt from citrus fruit, 20–34% esterified, Sigma, Germany) and HMP (high methoxy pectin, potassium salt from citrus fruit, 55–70% esterified, Sigma, Germany), and 0.14% (w/w) freeze-dried chia seed mucilage were prepared. According to the literature, the concentration of 0.15% (w/w)

PGA corresponds to the concentration of the exuded root mucilage (Mimmo et al., 2003). In order to ensure complete dissolution, the HMP solution was heated up to 60°C, while drops of 10M KOH were added to the PGA solution, which was further acidified to pH 5 with 33% HCl after complete dissolution. In addition, chia seed mucilage was dialysed for 48 h against distilled water to remove all dissolved ions before the dialysis against CaCl₂.

The CaCl₂ concentration in the 2 L dialysis solution ([CaCl₂]_{dialyse}) was set between 0.5 mM and 10 mM, which corresponds to the natural range of calcium concentration in soil solution. The pH of the dialysis solution was adjusted to 5 with a 10 M KOH solution or 33% HCl. A volume of 20 mL of the PGA, LMP, HMP, and mucilage solutions were transferred into plastic cylinders (4.0 cm · 2.8 cm) closed on both sides with dialysis tubing (MWCO 12,000–14,000) and immersed into the dialysis solution. After 48 h, the samples were washed three times by dialysis against distilled water, which was renewed every 24 h. This way, the calcium in the gels could be considered as bound (Morel et al., 1986). Six replicates were treated for each CaCl₂ concentration.

3.5 Gel dehydration

The gels were dehydrated smoothly over sand by the same procedure as described by Buchmann et al. (2015) in order to avoid the artefacts related to harsh dehydration conditions (Brax et al., 2017). For this, the dialysis tubing was removed and replaced by a nylon mesh on one side of the cylinder. The cylinders were set for dehydration in jam glasses filled with 80 g acid washed coarse quartz sand (630–200 nm, Quarzwerke GmbH, Germany). Three replicates were placed openly in the jam glasses for 10 min to drain the free water not trapped in the hydrogel structure, while the other three replicates were further dehydrated for 4 h. The dehydration was stopped by closing the lower side of the cylinder with a cap. The gel yield of the polymers was calculated out of the ratio between the dry mass of the polymer in the gel and the dry mass of the polymer originally injected in the dialysis tubing and expressed in percent.

3.6 ¹H NMR-relaxometry

3.6.1 Measurement conditions

¹H NMR measurements of the transverse relaxation time (T₂) were performed with a Minispec MQ (Bruker, Germany) at a magnetic field of 0.176 T. Transverse relaxation decay was obtained by applying the Carr-Purcell-Meiboom-Gill (CPMG) pulse sequence (Meiboom and Gill, 1958). The echo time and the recycle delay were kept constant at 0.3 ms and 10 s respectively, while echoes, scan numbers, and gains were adapted for each sample.

3.6.2 Determination of gel volume with ¹H NMR relaxometry

For more precision, the volume of entrapped water in the gels was calculated from the signal intensity at t = 0 and gain 75

(SI_{t=0; 75}) after calibrating the NMR device (Jaeger et al., 2009). As the samples were measured at several gains x, SI_{t=0; 75} was calculated with Eq. (1) and Eq. (2):

$$SI_{t=0; 75}^{1/4} = \frac{SI_{t=0; x}}{F \cdot 75} \quad (1)$$

$$F^{1/4} = \frac{SI_{t=0; x}}{SI_{t=0; x-1}} \quad (2)$$

F is the gain correction factor obtained by measuring the SI_{t=0} of a known amount of water at several gains. The volume of the gels was then calculated by means of the linear regression between SI_{t=0; 75} and the water content.

3.6.3 Determination of relaxation rate

The T₂ measurements were reduced to 200 points with MATLAB (R2008b). To calculate the relaxation time T_{2,i} of the water protons in the gels, each CPMG decay was fitted with mono-, bi- or tri-exponential decay functions according to Eq. (3):

$$SI_{t=0}^{1/4} = \sum_{i=1}^X A_i \exp\left(-\frac{t}{T_{2,i}}\right) \quad (3)$$

Origin 7.5 SR7 was used to fit the experimental data with exponential decay functions and to analyse the fits with statistical parameters. The exponential multiplicity was chosen after examining the Chi-square value c² and the residuals, and also after consideration of several criteria to give the data physical sense (Průšová et al., 2013): the relaxation time had to be superior to zero, the total amplitude had to be superior to zero but inferior to the maximal amplitude of the exponential decay. The distribution of the residuals had to be homogeneous. In case of a multi-exponential relaxation, the difference between the relaxation times T_{2,A}, T_{2,B} or T_{2,C} had to be greater than 100 ms. Further processing of the data to calculate the relaxation rates was done with Excel.

3.7 Cation analysis

A fraction of each gel was taken, weighed (ultra micro Sartorius SE2, Germany), and oven-dried for 24 h at 105°C. The dried samples were weighed and put in microwave tubes with 500 mL distilled 65% HNO₃ and 1.5 mL ultrapure 33% HCl. The microwave (MarsXpress, CEM GmbH, Germany) digestion program performed consisted of heating until 200°C over a temperature ramp for 15 min and then in constant heating at 200°C for 40 min. The digests were subsequently analyzed by inductively coupled plasma optical emission spectrometry (ICP-OES, Agilent 720 Series, Germany). Calcium, Mg, Na, and K contents were measured for three subreplicates for several gels in order to determine the variability of the cation concentration inside the gels. Calcium content was calculated out of the ratio between the calcium in each gel and the dry mass of the polymer, while the water content resulted from the ratio between the water in each gel and the dry mass of the polymer.

4 Results and discussion

4.1 Uronic acid content

Table 1 shows the total and the free (i.e., non-esterified) uronic acid contents expressed in weight percent of the dry mass (wt%) and the degree of esterification. As a reference, PGA (polygalacturonic acid) consists uniquely of free uronic acids. Total uronic acid contents in LMP (low methoxy pectin) and HMP (high methoxy pectin) were only 22–5 wt% and 31–5 wt%, respectively, as the heterogeneous backbone of pectin is also constituted of neutral sugars. With 23–2 wt%, the total uronic acid content in chia seed mucilage was in good agreement with the data reported by Timilsena et al. (2015) and Lin et al. (1994). The total uronic acid content in mucilage was also similar to the total uronic acid content of LMP. According to the producer, a fraction of the uronic acids in LMP and HMP are methyl esterified: free uronic acid contents in LMP and HMP were 15–18 wt% and 9–14 wt%, respectively, so they had much smaller amounts of negatively charged sites available for calcium cross-links than PGA. In the following experiments, mucilage was used with a dry mass of 0.14 wt%, so that its total uronic acid content was the same than the one in 0.15 wt% LMP.

The measured total uronic acid weight equivalents of chia seed mucilage and LMP in this study are in good agreement with the values published for other kinds of mucilage, e.g., 11.5 wt% and 4 wt% for wheat and cowpea mucilage, respectively (Moody et al., 1988), 13 wt% for pea mucilage (Knee et al., 2001), and 7 and 27 wt% in soybean root mucilage (Timotiwi and Sakurai, 2002). However, the uronic acid weight equivalent of PGA is far above these values, what already now questions PGA's suitability as a model substance for root mucilage.

Table 1: Measured total and calculated free uronic acid content expressed in weight percent of the dry mass (wt%) and degree of esterification (%) of polygalacturonic acid (PGA), low methoxy pectin (LMP), high methoxy pectin (HMP), and chia seed mucilage (Mucilage) samples.

	Total uronic acid (wt%)	Degree of esterification (%)	Free uronic acid (wt%)
PGA	100	0	100
LMP	22–5	20–34	15–18
HMP	31–5	55–70	9–14
Mucilage	23–2	n.d.	n.d.

4.2 Effect of CaCl₂ dialysis on gel formation

4.2.1 High methoxy pectin

According to the described procedure, the cylinders containing the HMP solution were set on sand for 10 min dehydration to remove the free water after the dialysis against calcium.

However, the whole HMP solution flowed through the nylon mesh for all [CaCl₂] concentrations. This shows that the water was not retained by a three-dimensional polymer network.

The high degree of esterification of HMP thus prevented the formation of ionic networks, as its gelling mechanism actually relies on physical forces and depends on polymer-polymer interactions (Endress, 1991). Although this result was predictable, it clearly shows that HMP is not an appropriate model substance for mucilage, as it requires heating and sucrose addition to form a gel.

4.2.2 Polygalacturonic acid

Focus is first given on gel yield, calcium content, and water content plotted against [CaCl₂]_{dialysis} analyzed depending on the polymer and the [CaCl₂]_{dialysis} at t₀. The gel yield of the polymer at t₀ expresses the efficacy with which the polymer strands formed a gel with calcium. PGA was, among the analyzed polymers, the most efficient in gel formation upon CaCl₂ dialysis with a gel yield that increased from 70 to 100% with [CaCl₂]_{dialysis} increasing from 0.5 to 2.5 mM. The gel yield remained at 100% for higher [CaCl₂]_{dialysis} (Fig. 2a). The increase of [CaCl₂]_{dialysis} from 0.5 to 2.5 mM only slightly increased the calcium content from 2.1 to 2.4 mmol mg⁻¹ (Fig. 2b) but doubled the amount of water retained in the gel from 0.16 to 0.33 g mg⁻¹ (Fig. 2c). Higher [CaCl₂]_{dialysis} neither increased the calcium content nor the water content. The Ca/COO ratio indicates how many calcium atoms per carboxylate group of the uronic acids are fixed in the gel structure. In the egg-box model, one calcium atom forms ionic bonds with two carboxylate groups, what corresponds to a Ca/COO ratio of 0.5. The Ca/COO ratio for Ca-PGA was constant at 0.40–0.03 in the range of deviation for all [CaCl₂]_{dialysis}. Although the gel yield of PGA was higher than the one of LMP or mucilage, the water content in the Ca-PGA gels was much lower than in the Ca-LMP and Ca-mucilage gels (Fig. 2c).

The gel yields suggest that a calcium concentration in the dialysis solution below 2.5 mM was not sufficient to bind all PGA polymer chains together. According to the results, all polymer strands became involved in a 3D-network and formed a gel saturated with calcium at 2.5 mM and higher [CaCl₂]_{dialysis}. The slightly lower Ca/COO ratio than suggested by the egg-box model could be due to the steric hindrance or shielding of some uronic acids, preventing their binding to calcium. The low water content despite a high gel yield indicates that strong surface speciation of calcium with PGA, e.g., by the egg-box model, limits the swelling of the gel due to the multitude of cross-links between the chains (de Kerchove and Elimelech, 2007). This supports the assumption that the homogeneity of PGA's backbone and the high specificity of galacturonic acid to calcium binding led to the formation of strong NICA gels by PGA with calcium.

4.2.3 Low methoxy pectin

The gel yield of LMP increased from 14 to 40% between 0.5 and 5 mM [CaCl₂]_{dialysis} and stayed constant for 5 and 10 mM

[CaCl₂]_{dialysis} (Fig. 2a). On the contrary, calcium treatment of LMP effectively changed the calcium and water content in the Ca-LMP gels: between 0.5 and 2.5 mM [CaCl₂]_{dialysis}, the calcium content in Ca-LMP increased strongly from 1.7 to 2.8 mmol mg⁻¹ and the water content quadrupled from 0.5 to 1.9 g mg⁻¹. Higher ionic strength led to a slight decrease of the calcium content to 2.4 mmol mg⁻¹ but to a strong drop of the water content to 0.7 g mg⁻¹. The high calcium content in Ca-LMP gels is surprising, as the lower uronic acid weight equivalent and the partial esterification of the uronic acids suggested a lower specificity of LMP than PGA for calcium. The Ca/COO ratio of Ca-LMP was correspondingly far above the ideal 0.5 predicted by the egg-box model: it increased from 1.8 to over 3 between 0.5 and 2.5 mM [CaCl₂]_{dialysis}.

Reason for the low gel yield of LMP could be an inhomogeneous distribution and esterification of the uronic acids on the LMP backbones, leading to highly esterified and nearly neutral strands unable to form a gel with calcium. Other reasons are the drop of probability for the free uronic acids to form efficient calcium cross-links due to their smaller number, associated with the steric hindrance of the polymer backbone, restraining the possibilities of an overlapping of different polymer chains (Garnier et al., 1993). The high Ca/COO ratio could be caused by a change in the number of free uronic acids in the gel after 10 min dehydration due to a selective depletion of polymers with a low number of free uronic acids, and consequently due to an underestimation of the remaining free uronic acid content. However, considering that the total loss (60% loss for 40% gel yield) is due to neutral sugars, would result in a maximal 2.5 fold overestimation of Ca/COO ratio only that is 1.25. The Ca/COO ratio of Ca-LMP being above 1.8 indicates that most of the calcium is not bound specifically but non-specifically to the polymer, building an electrostatic potential characteristic for Donnan gels. Overall electrical neutrality is probably maintained by absorption of chloride anions by the gel.

Although the calcium content in the Ca-LMP gels is similar to the one measured in the Ca-PGA gels, the water content is several times higher than the one of Ca-PGA. The strong swelling and the high calcium content in Ca-LMP indicate that the formation of the polymer network is driven by the osmotic pressure of free ions acting to swell the gel (Rubinstein et al., 1996). Thus, in contrast to PGA, the interactions between LMP as polyelectrolyte and calcium are mostly nonspecific and governed by electrostatic forces rather than by specific cross-links (Benedetti et al., 1996; Kinniburgh et al., 1996). Electrostatic interactions are mainly controlled by the ionic strength, which deeply modifies the behaviour of polyelectrolyte gels: at low salt concentrations, the chains are strongly stretched at swelling equilibrium (Skouri et al., 1995). The addition of salt reduces the swelling of polyelectrolyte gels, as it produces a screening of the interactions

and a rearrangement of the chains as long as the cross-linking degree is not too high (Skouri et al., 1995; Rubinstein et al., 1996). Rearrangement, involving shrinking of the Ca-LMP gel network, explains the drop of the water content upon dialysis at high ionic strength.

4.2.4 Mucilage

Chia mucilage already contained calcium and formed a gel without additional calcium addition. Washing of chia mucilage from the mobile cations upon dialysis against distilled water resulted in a gel yield of 44%. All cations did not diffuse out of mucilage upon dialysis against water, as it still contained 0.07 – 0.02 mmol mg⁻¹ Mg, 0.07 – 0.03 mmol mg⁻¹ K, and 0.01 – 0.01 mmol mg⁻¹ Na. Upon calcium dialysis, the gel yield of mucilage increased to 75% independently of the [CaCl₂]_{dialysis} (Fig. 2a). Although the gel yield of mucilage was significantly higher than the one of LMP, the calcium content in mucilage remained very low in contrast to those measured for Ca-PGA and Ca-LMP (Fig. 2b). Still, the calcium content increased with increasing [CaCl₂]_{dialysis} from 0.06 mmol mg⁻¹ with no calcium addition to 0.22 mmol mg⁻¹ at the highest [CaCl₂]_{dialysis}. The water content of mucilage was with 1.2 g mg⁻¹ after dialysis against water significantly higher than for PGA for all [CaCl₂]_{dialysis} and for LMP at low [CaCl₂]_{dialysis}. The water content of mucilage dropped upon calcium treatment and decreased slightly from 0.81 to 0.67 g mg⁻¹ with increasing ionic strength (Fig. 2c).

The increase of the gel yield of Ca-mucilage upon calcium addition suggests that polymer strands that were little or not involved into the gel polymeric network before calcium addition, integrated the gel network due to new interactions with the added calcium. Given that K, Mg, and Na ions were not washed away upon dialysis against distilled water, these ions also interact with the polymer, probably by participating to the

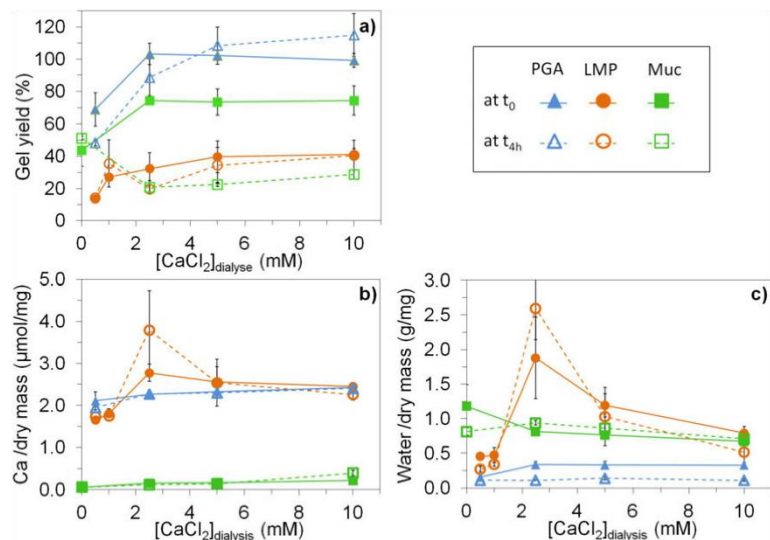


Figure 2: Gel yield of the polymers (a), calcium content (b), and water content (c) of Ca-PGA, Ca-LMP and Ca-mucilage gels after 10 min (t₀) and 4 h (t_{4h}) dehydration for all CaCl₂ dialysis concentrations ([CaCl₂]_{dialysis}).

swelling of the polyelectrolyte. Similarly to Ca-LMP, the water content in mucilage decreased at high ionic strength, referring to a rearrangement of the structure due to shielding charge effects: without counter ions, negative charges produce strong intermolecular repulsion forces and thus an expanded molecule. The addition of counter ions decreases the repulsion and molecule expansion. Shielding effects of calcium have already been observed for chia mucilage and mucilage gum of *Opuntia ficus indica* (Medina-Torres et al., 2000; Capitani et al., 2015), as they caused a decrease of the viscosity due to the contraction of the polysaccharide molecule. Still, the shielding effect of calcium ions have a stronger impact on the water content of Ca-LMP gels than of Ca-mucilage, what suggests that the mucilage polymer backbone is less charged than the one of LMP. Interestingly, the decrease of the water content at high ionic strength was not followed by an increase of the calcium content in Ca-LMP and mucilage gels: higher ionic strength induced a rearrangement of the gel network, which resisted washing, but did not lead to an increase of the calcium content in the gels.

As mucilage had a total uronic acid content similar to LMP, the comparatively very low calcium content in mucilage reveals a low specificity of mucilage for calcium and points out the quasi non-availability of uronic acids for calcium interactions. This suggests that the gel formation mechanism of mucilage does not only rely on interactions with calcium, but principally on the entanglement of the polymer chains via intermolecular forces between the polymer chains such as hydrogen bonding and electrostatic interactions.

4.3 Influence of absorbed calcium on water content and water mobility in the gels

4.3.1 General trends

The water content increased with the calcium content for Ca-PGA and Ca-LMP gels (Fig. 3a). In contrast, for Ca-mucilage, even the small increase observed for the calcium content reduced the water content. Ca-mucilage and Ca-LMP showed only mono-exponential CPMG decays, thus, were characterized by only one relaxation rate (Fig. 3b–c). In contrast, Ca-PGA gels displayed bi- and tri-exponential CPMG decays and were characterized by two or three relaxation rates and, thus, two or three water populations (Fig. 4). Except a small increase from 1.65 to 1.81 s⁻¹ for Ca-LMP at low calcium content, the relaxation rate decreased with increasing water and calcium contents for Ca-PGA and Ca-LMP gels, revealing increasing network flexibility and/or pore sizes (Fig. 3b–c). The relaxation rates of mucilage with and without calcium addition were independent from the water and the calcium contents. All in the range of 0.5 s⁻¹, they were smaller than the relaxation rates of Ca-LMP at similar water contents (Fig. 3b).

The relationship between water and calcium content for PGA and LMP showed that the absorption of calcium promotes gel formation and thus swelling for these gels. On the contrary, decrease of water content with increasing calcium uptake in mucilage highlights the decrease of molecular repulsion and molecule expansion due to calcium addition. The slight increase of the relaxation rate for Ca-LMP with the increase of the calcium content at low values reveals a reduction of the network flexibility and/or pore sizes, which probably results from specific interactions between the uronic acids and calcium as the first step of Ca-LMP gel formation. Decrease of the relaxation rate with increasing calcium content expresses the stretching of the polymer chains upon swelling for Ca-LMP and Ca-PGA, as the gel network either forms bigger pores and/or becomes thinner and more flexible, what reduces the relaxation possibilities of the water protons (de Celis Alonso et al., 2010).

The relaxation rate pattern also reflects the chemistry of each polymer, given that the main relaxation mechanism in gels is the proton exchange between water and polysaccharide (Hills et al., 1991). LMP has less exchangeable protons than PGA due to its smaller uronic acid content and a degree of esterification superior to 0%. Therefore, LMP should reveal shorter relaxation rates than PGA. The number of exchangeable protons in mucilage is unknown, but its very short relaxation rate suggests that most uronic acids in mucilage are esterified or shielded. Indeed, methyl ester groups restrict the mobility of water but not to the extent of dipolar or hydrogen-bonded groups, which induce long relaxation rates (Kerr and Wicker, 2000).

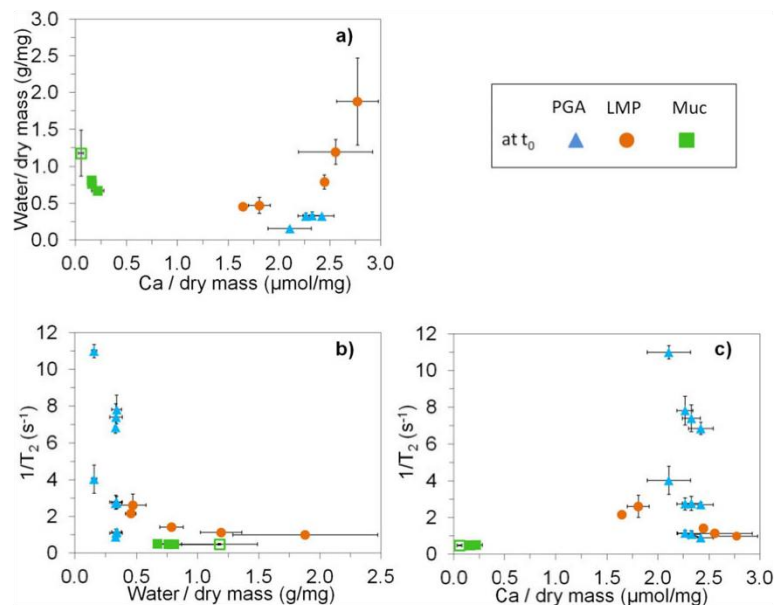


Figure 3: Water content expressed as a function of the calcium content (a), relaxation rate 1/T₂ plotted against the water content (b), and against the calcium content (c) for Ca-PGA, Ca-LMP and Ca-mucilage gels at t₀.

4.3.2 Mobility of water in Ca-PGA and Ca-LMP gels

Analysis of the amount of water corresponding to each relaxation rate gives information about the distribution of water between different environments (Fig. 4a). The three relaxation rates ($1/T_{2A}$, $1/T_{2B}$, $1/T_{2C}$) indicate the presence of water fractions differing in mobility. At t_0 , the water fraction A characterized by $1/T_{2A} > 6.7 \text{ s}^{-1}$ was the same for all Ca-PGA gels, whereas the water fraction B characterized by $2.5 \text{ s}^{-1} < 1/T_{2B} < 4 \text{ s}^{-1}$ jumped from 1.3 mL for the gels formed at 0.5 mM $[\text{CaCl}_2]_{\text{dialysis}}$ to values above 6 mL for the gels formed at higher $[\text{CaCl}_2]_{\text{dialysis}}$. The third water fraction C with a short $1/T_{2C} < 1.25 \text{ s}^{-1}$ did not exceed 2 mL and decreased with increasing $[\text{CaCl}_2]_{\text{dialysis}}$.

While the values of the relaxation rate in Ca-PGA account for the rigidity of the polymer network and the pore size, its multimodal distribution rather expresses the heterogeneity of the Ca-PGA gels. Combination of the results from Figs. 1 and 4 suggests a two-step formation of Ca-PGA gels with increasing concentration of calcium ions available for bonding: the first step corresponds to the creation of a type A network, and the second step to the creation of type B and C networks. The potential for type A network formation is already fully exploited at the lowest $[\text{CaCl}_2]_{\text{dialysis}}$ of 0.5 mM, because the amount of water in fraction A is independent from further increase of $[\text{CaCl}_2]_{\text{dialysis}}$. The long relaxation rate $1/T_{2A}$ reveals strongly reduced water mobility for water fraction A, which indicates the formation of a dense and stiff polymer network due to manifold calcium cross-links. In contrast, type B network swells with increasing $[\text{CaCl}_2]_{\text{dialysis}}$ up to the point at which it fully reaches its potential number of calcium cross-links. Building of type B network probably corresponds to the 30% increase of the gel yield. The strong swelling of type B network for the gels formed at 0.5 mM and 2.5 mM $[\text{CaCl}_2]_{\text{dialysis}}$ is traded by the drop of the corresponding $1/T_{2B}$ from 4 to 2.7 s^{-1} and explained by the making of new cross-links between the free polymer strands and the high number of available calcium ions. Further increase of $[\text{CaCl}_2]_{\text{dialysis}}$ does not affect the amount of water in fraction B. The shorter $1/T_{2B}$ than $1/T_{2A}$ indicates a looser and less dense network in the fraction B than in fraction A. The $1/T_{2C}$ water fraction appears only in gels formed at 2.5 mM and higher $[\text{CaCl}_2]_{\text{dialysis}}$ and is characterized by very short relaxation rates. This suggests the formation of several sub-gel units, which bridge the gaps between the smaller $1/T_{2A}$ and $1/T_{2B}$ gel structures. Also the $1/T_{2C}$ network probably fully reaches its potential number of calcium cross-links or non-specific calcium interactions during the formation at 2.5 mM $[\text{CaCl}_2]_{\text{dialysis}}$. Out of these results, it is not clear if the calcium content is higher in the $1/T_{2C}$ water fraction and thus leads to strong swelling, or if it is too low to generate network formation.

High affinity between polymer chains and their solvent leads to an extension of the polymer chains and swelling of the gel (Tibbitts et al., 1998). Yet, the high specificity of PGA for calcium leads to rash binding, as the PGA chains first dimerize through strong and specific associations between uronic

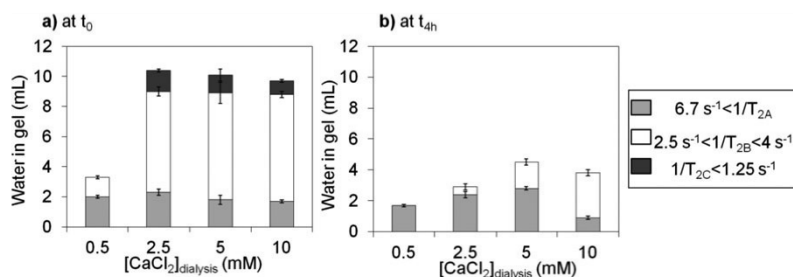


Figure 4: Amount of water in each $1/T_2$ water fraction of Ca-PGA gels respective to the dialysis concentrations after 10 min (t_0) (a) and after 4 h (t_{4h}) (b) of dehydration.

acids and divalent cations (Jarvis, 1984; de Kerchove and Elimelech, 2007). This rash binding does not give the polymer chains involved in binding time to arrange in extended formations and results in the agglomeration of the polymer around the cross-linking agents and thus limited swelling. Therefore, fraction A probably corresponds to the gel formed by specific interactions with calcium. Once the negative charges on the PGA chains are shielded by ionic interactions with calcium, the chains or chain associations still possessing some mobility rearrange to an energetic favourable conformation, which induces swelling. This second step corresponds to dimer-dimer aggregation and is rather driven by hydrogen bonding and Van der Waals interactions (Morris et al., 1982; Seale et al., 1982; de Kerchove and Elimelech, 2007). The denser regions are linked by chains holding together by electrostatic interactions, creating intermediate zones characterized by higher water mobility, in which the polymer backbone is less rigid and the chains more scattered (Skouri et al., 1995). Fractions B and C should then correspond to the formation of such zones.

In comparison to Ca-PGA, the density and stiffness of the Ca-LMP polymer network formed by calcium-uronic acid interactions is limited due to steric hindrance of the backbone and to the low speciation of calcium at the LMP surface. According to the literature, Ca-LMP gel formation mechanism should follow the same two-step process as the one of Ca-PGA gels (Gilsenan et al., 2000). Thus, the decrease of Ca-LMP relaxation rate from 2.6 to 1.4 s^{-1} should correspond to the second step involving dimer-dimer aggregation and swelling. However, the monomodal relaxation in Ca-LMP gels in our study indicates a homogeneous polymer network. Yet, in comparison to PGA, the weaker specificity of LMP with calcium induces a slower network formation and a higher mobility of the polymer chains. These aspects enable a massive rearrangement of the Ca-LMP network, leading to an energetic favorable conformation and a homogeneous network. The junction zones between the chains in Ca-LMP are probably less spatially defined than in Ca-PGA, and rather surround zones of dense electrostatic interactions (Skouri et al., 1995).

4.4 Gel dehydration

4.4.1 Polygalacturonic acid

Finally, all gels were submitted to 4 hours dehydration over sand to investigate how the chemical conditions, the gel for-

mation mechanism and the properties of the swollen gels affected the water retention.

Ca-PGA gel formed at 0.5 mM [CaCl₂]_{dialysis} kept its calcium and water content constant upon dehydration, but the gel yield dropped from 70% to 50% (Fig. 2). Drop of the gel yield at constant water and calcium content indicates a loss of gel (water + calcium + polymer). Ca-PGA gel formed at 0.5 mM [CaCl₂]_{dialyse} mostly lost gel of the B fraction (Fig. 4b), as it was probably made up of polymer strands only involved in a loose PGA-Ca-PGA network. On the contrary, the Ca-PGA gels formed at higher [CaCl₂]_{dialysis} did not lose relevant amounts of polymer during the dehydration, as their gel yields at t_0 and t_{4h} were similar within the standard deviation range (Fig. 2a). However, the water content of the PGA-gels formed at higher [CaCl₂]_{dialysis} dropped from 0.3 to 0.1 g mg⁻¹, whereas the calcium content remained constant (Fig. 2b–c). The sole drop of the water content indicates a loss of water by the Ca-PGA gels upon dehydration, which is confirmed in Fig. 4b: upon dehydration, the B and C fractions disappeared largely and entirely, while the water content in the A fraction varied only little. Thus, type A network holds water better than type B or C network.

Finally, type B and C networks characterized by high relaxation rates do not effectively retain water against dehydration. These observations corroborate with those from Belton (1997) and from Mao et al. (2001), who related the microstructure of gellan-calcium gels with their water retention. Mao et al. (2001) showed that small pores (here characterized by short $1/T_{2A}$) were formed independently from the calcium concentration and had a thin web structure providing high capillary forces. On the contrary, the formation of bigger pores, characterized by low capillary forces, were dependent on the calcium concentration (here B and C fractions).

4.4.2 Low-methoxy pectin

Gel yield, calcium and water contents of Ca-LMP gels stayed constant upon dehydration in the range of standard deviation (Fig. 2).

As Ca-LMP gels did not lose polymer during the dehydration, calcium interactions with the polymers were strong enough to mostly withstand dehydration. This supports the hypothesis of a homogeneous Ca-LMP gel formation. Similarly to Ca-PGA, the existence of small pores with high capillary forces characterized by high relaxation rates explains the high water retention of the Ca-LMP gels formed at 0.5 and 1.0 mM [CaCl₂]_{dialysis}. However, the high water retention of the Ca-LMP gels formed at [CaCl₂]_{dialysis} > 2.5 mM and characterized by high water content rather originates from the high osmotic pressure in the gels due to high calcium content. The high water retention reveals the capacity of a network made of non-specific ionic interactions to retain great amounts of water. This shows that the electrostatic forces between the polymer chains and calcium are strong enough to prevent the collapse of the polymer structure, as opposed to those in fractions $1/T_{2B}$ and $1/T_{2C}$ for Ca-PGA. These results show that the water retention in polyelectrolytes

depends on both, the pore size and the osmotic pressure within the gel (Belton, 1997).

4.4.3 Mucilage

Upon dehydration, mucilage without calcium addition kept the same gel yield within the standard deviation, whereas its water content dropped (Fig. 2a–c). In contrast, mucilage treated with calcium maintained its water content upon dehydration, while the gel yield decreased from 75 to 22% upon dehydration.

Drop of the water content upon dehydration in mucilage not treated with calcium can be related to the big pores and low osmotic pressure (due to the very low cation content) in the gel. The fact that calcium-treated mucilage lost gel upon dehydration, but that mucilage not treated with calcium did not, suggests that the reorganization of the mucilage network due to calcium absorption renders the gels less resistant to dehydration. Calcium absorption probably created zones of intensive interactions around the calcium ions, but also hindered polymer-polymer interactions in other zones: polymers not involved in interactions with calcium then flowed away during the dehydration.

4.5 Relations between chemical conditions, gel formation mechanism and gel properties

Our results bring out the close relations existing between the chemical conditions, the gel formation mechanism, and the properties of the resulting gels. However, we found that the capacity of a polymer to bind calcium does not decrease with decreasing uronic acid content as proposed in hypothesis 1, as PGA and LMP had similar calcium content: the term bind requires more precise description, namely what kind of binding. In Ca-PGA gels, the specific bonds formed between calcium and the uronic acids are schematized by the egg-box model (Fig. 5). They created a heterogeneous gel characterized by fractions with small pores of high stiffness, which had low water content and high water retention, and by fractions with the opposite properties (Fig. 5): the rash Ca-PGA network formation and the stiffness of its network did not allow the polymer strands to arrange in a homogeneous, energetically favourable network. On the contrary, in Ca-LMP gels, most of the absorbed calcium was involved in nonspecific ionic interactions with the polymer chains, what allowed the gels to swell very strongly and their networks to rearrange to create homogeneous gels (Fig. 5). These findings refute hypotheses 2 and 3, as the specific and nonspecific interactions of the polymers with calcium rather depended on the uronic acid content and esterification degree than on the calcium content. Despite their high water content and high water mobility, the Ca-LMP gels resisted dehydration because of their high osmotic pressure. These conclusions also refute hypothesis 4, as high water retention was not only caused by high capillary forces as in Ca-PGA, but was also due to high osmotic pressure as in Ca-LMP. Surprisingly, even though mucilage had similar uronic acid content to LMP, it had much lower calcium content than LMP. The gelling mechanism of mucilage rather relied on non-ionic electrostatic interactions

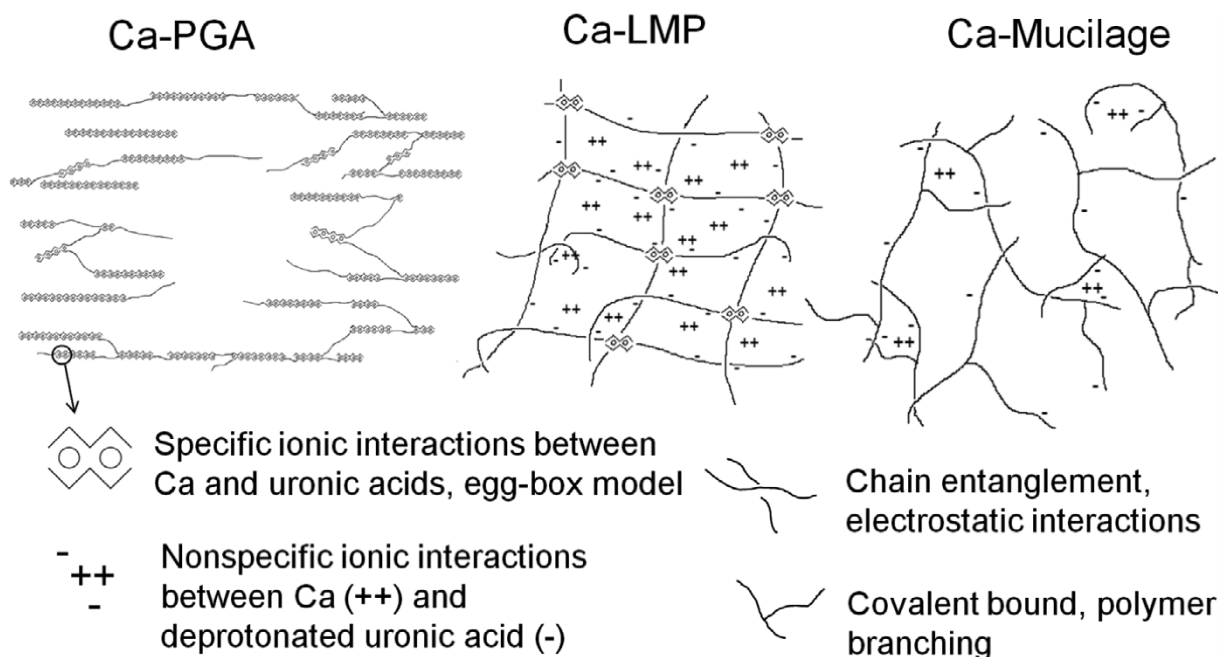


Figure 5: Schematic representation of Ca-PGA, Ca-LMP and Ca-mucilage gel networks.

between entangled polymer chains, which conferred mucilage high water content and mobility, but lower water retention than Ca-LMP also due to low osmotic potential (Fig. 5). A high degree of esterification of the uronic acids in mucilage or a regularity of their distribution on the polymer backbone could explain the differences between the gel formation mechanism of LMP and mucilage. Another reason could be a high degree of branching of the mucilage polymers, which would hinder coordinative interactions between several chains and favorize chain entanglements. Still, mucilage behaved as a weak polyelectrolyte upon calcium absorption, as it shrunk due to reduction of the molecular repulsion and molecule expansion.

5 Conclusion

Finally, PGA and LMP prove as non-suitable model substances for chia seed mucilage due to diverging gel formation mechanisms and gel properties. Thus, abundance of uronic acid and their degree of esterification in mucilage should be of first consideration before attributing the changes of the physical properties in the rhizosphere to calcium cross-links between uronic acids of mucilage and soil particles or ions in solution.

A deep understanding of the gel-specific properties of root mucilage is needed to resolve the physico-chemical processes leading to changes of the rhizosphere properties. A model substance such as chia seed mucilage should have comparable physical or chemical properties to its associated substance root mucilage. Therefore, the next steps are the study of the chemical composition and of the physico-chemical properties of root mucilage from several plants, and the subsequent comparison with chia seed mucilage.

Acknowledgments

The authors wish to thank the DFG (German Research Foundation) for funding within the project MUCILAGE (SCHA849/20).

References

- Ahmed, M. A., Holz, M., Woche, S. K., Bachmann, J., Caminati, A. (2015): Effect of soil drying on mucilage exudation and its water repellency: a new method to collect mucilage. *J. Plant Nutr. Soil Sci.* 178, 821–824.
- Ahmed, M. A., Kroener, E., Holz, M., Zarebanadkouki, M., Caminati, A. (2014): Mucilage exudation facilitates root water uptake in dry soils. *Funct. Plant Biol.* 41, 1129–1137.
- Bacic, A., Moody, S. F., Clarke, A. E. (1986): Structural analysis of secreted root slime from maize (*Zea mays* L.). *Plant Physiol.* 80, 771–777.
- Barré, P., Hallett, P. D. (2009): Rheological stabilization of wet soils by model root and fungal exudates depends on clay mineralogy. *Eur. J. Soil Sci.* 60, 525–538.
- Belton, P. S. (1997): NMR and the mobility of water in polysaccharide gels. *Int. J. Biol. Macromol.* 21, 81–88.
- Benedetti, M. F., Van Riemsdijk, W. H., Koopal, L. K. (1996): Humic substances considered as a heterogeneous Donnan gel phase. *Environ. Sci. Technol.* 30, 1805–1813.
- Blumenkrantz, N., Asboe-Hansen, G. (1973): New method for quantitative determination of uronic acids. *Anal. Biochem.* 54, 484–489.
- Brax, M., Buchmann, C., Schaumann, G. E. (2017): Biohydrogel induced soil-water interactions: how to untangle the gel effect? A review. *J. Plant Nutr. Soil Sci.* 180, 121–141.
- Brax, M., Buchmann, C., Schaumann, G. E. (2018): Effect of mucilage on water properties in the rhizosphere monitored by ¹H-NMR relaxometry. *Micropor. Mesopor. Mat.* 269, 47–50.

- Buchmann, C., Bentz, J., Schaumann, G. E. (2015): Intrinsic and model polymer hydrogel-induced soil structural stability of a silty sand soil as affected by soil moisture dynamics. *Soil Till. Res.* 154, 22–33.
- Capitani, M. I., Corzo-Ríos, L. J., Chel-Guerrero, L. A., Betancur-Ancona, D. A., Nolasco, S. M., Tomás, M. C. (2015): Rheological properties of aqueous dispersions of chia (*Salvia hispanica* L.) mucilage. *J. Food Eng.* 149, 70–77.
- Czarnes, S., Hiller, S., Dexter, A. R., Hallett, P. D., Bartoli, F. (1999): Rootsoil adhesion in the maize rhizosphere: the rheological approach. *Plant Soil* 211, 69–86.
- de Celis Alonso, B., Rayment, P., Ciampi, E., Ablett, S., Marciari, L., Spiller, R. C., Norton, I. T., Gowland, P. A. (2010): NMR relaxometry and rheology of ionic and acid alginate gels. *Carbohydr. Polym.* 82, 663–669.
- De la Paz Salgado-Cruz, M., Calderón-Domínguez, G., Chanona-Pérez, J., Farrera-Rebollo, R. R., Méndez-Méndez, J. V., Díaz-Ramírez, M. (2013): Chia (*Salvia hispanica* L.) seed mucilage release characterisation. A microstructural and image analysis study. *Ind. Crop. Prod.* 51, 453–462.
- de Kerchove, A. J., Elimelech, M. (2007): Formation of polysaccharide gel layers in the presence of Ca²⁺ and K⁺ ions: measurements and mechanisms. *Biomacromolecules* 8, 113–121.
- Dobies, M., Kusmia, S., Jurga, S. (2005): ¹H NMR and rheological studies of the calcium induced gelation process in aqueous low methoxyl pectin solutions. *Acta Phys. Pol. Ser. A* 108, 33–46.
- Endress, H.-U. (1991): Nonfood Uses of Pectin, in Walter, R. H. (ed.): *The Chemistry and Technology of Pectin*. Academic Press, San Diego, CA, USA, pp. 251–268.
- Garnier, C., Axelos, M. A., Thibault, J.-F. (1993): Phase diagrams of pectin-calcium systems: Influence of pH, ionic strength, and temperature on the gelation of pectins with different degrees of methylation. *Carbohydr. Res.* 240, 219–232.
- Gessa, C., Deiana, S. (1990): Fibrillar structure of Ca polygalacturonate as a model for a soil-root interface. *Plant Soil* 129, 211–217.
- Gessa, C., Deiana, S. (1992): Ca-polygalacturonate as a model for a soil-root interface. *Plant Soil* 140, 1–13.
- Gilsenan, P. M., Richardson, R. K., Morris, E. R. (2000): Thermally reversible acid-induced gelation of low-methoxy pectin. *Carbohydr. Polym.* 41, 339–349.
- Grant, G. T., Morris, E. R., Rees, D. A., Smith, P. J. C., Thom, D. (1973): Biological interactions between polysaccharides and divalent cations: the egg-box model. *FEBS Lett.* 32, 195–198.
- Grasdalen, H., Einar Bakøy, O., Larsen, B. (1988): Determination of the degree of esterification and the distribution of methylated and free carboxyl groups in pectins by ¹H-NMR spectroscopy. *Carbohydr. Res.* 184, 183–191.
- Hills, B. P., Cano, C., Belton, P. S. (1991): Proton NMR relaxation studies of aqueous polysaccharide systems. *Macromolecules* 24, 2944–2950.
- Jaeger, F., Bowe, S., Van As, H., Schaumann, G. E. (2009): Evaluation of ¹H NMR relaxometry for the assessment of pore-size distribution in soil samples. *Eur. J. Soil Sci.* 60, 1052–1064.
- Jarvis, M. C. (1984): Structure and properties of pectin gels in plant cell walls. *Plant Cell Environ.* 7, 153–164.
- Kerr, W. L., Wicker, L. (2000): NMR proton relaxation measurements of water associated with high methoxy and low methoxy pectins. *Carbohydr. Polym.* 42, 133–141.
- Kinniburgh, D. G., Milne, C. J., Benedetti, M. F., Pinheiro, J. P., Filius, J., Koopal, L. K., Van Riemsdijk, W. H. (1996): Metal ion binding by humic acid: application of the NICA-Donnan model. *Environ. Sci. Technol.* 30, 1687–1698.
- Knee, E. M., Gong, F.-C., Gao, M., Teplitski, M., Jones, A. R., Foxworthy, A., Mort, A. J., Bauer, W. D. (2001): Root mucilage from pea and its utilization by rhizosphere bacteria as a sole carbon source. *Mol. Plant. Microbe Interact.* 14, 775–784.
- Koopal, L. K., Saito, T., Pinheiro, J. P., Van Riemsdijk, W. H. (2005): Ion binding to natural organic matter: General considerations and the NICA-Donnan model. *Colloids Surf. A.* 265, 40–54.
- Lin, K.-Y., Daniel, J. R., Whistler, R. L. (1994): Structure of chia seed polysaccharide exudate. *Carbohydr. Polym.* 23, 13–18.
- Lüsse, S., Arnold, K. (1998): Water binding of polysaccharides—NMR and ESR studies. *Macromolecules* 31, 6891–6897.
- Mao, R., Tang, J., Swanson, B. G. (2001): Water holding capacity and microstructure of gellan gels. *Carbohydr. Polym.* 46, 365–371.
- Medina-Torres, L., Brito-De La Fuente, E., Torrestiana-Sanchez, B., Kathain, R. (2000): Rheological properties of the mucilage gum (*Opuntia ficus indica*). *Food Hydrocoll.* 14, 417–424.
- Meiboom, S., Gill, D. (1958): Modified spin-echo method for measuring nuclear relaxation times. *Rev. Sci. Instrum.* 29, 688–691.
- Mimmo, T., Marzadori, C., Francioso, O., Deiana, S., Gessa, C. E. (2003): Effects of aluminum sorption on calcium-polygalacturonate network used as soil-root interface model. *Biopolymers* 70, 655–661.
- Mimmo, T., Marzadori, C., Gessa, C. E. (2009): Does the degree of pectin esterification influence aluminium sorption by the root apoplast? *Plant Soil* 314, 159–168.
- Moody, S. F., Clarke, A. E., Bacic, A. (1988): Structural analysis of secreted slime from wheat and cowpea roots. *Phytochemistry* 27, 2857–2861.
- Morel, J. L., Andreux, F., Habib, L., Guckert, A. (1987): Comparison of the adsorption of maize root mucilage and polygalacturonic acid on montmorillonite homoionic to divalent lead and cadmium. *Biol. Fertil. Soils* 5, 13–17.
- Morel, J. L., Mench, M., Guckert, A. (1986): Measurement of Pb²⁺, Cu²⁺ and Cd²⁺ binding with mucilage exudates from maize (*Zea mays* L.) roots. *Biol. Fertil. Soils* 2, 29–34.
- Morris, E. R., Rees, D. A., Young, G. (1982): Chiroptical characterisation of polysaccharide secondary structures in the presence of interfering chromophores: Chain conformation of inter-junction sequences in calcium alginate gels. *Carbohydr. Res.* 108, 181–195.
- Oakenfull, D. G. (1991): *The Chemistry of High-Methoxyl Pectins*, in Walter, R. H. (ed.): *The Chemistry and Technology of Pectin*. Academic Press, San Diego, CA, USA, pp. 87–108.
- Peng, X., Hallett, P. D., Zhang, B., Hom, R. (2011): Physical response of rigid and non-rigid soils to analogues of biological exudates. *Eur. J. Soil Sci.* 62, 676–684.
- Průšová, A., Vergeldt, F. J., Kučenk, J. (2013): Influence of water content and drying on the physical structure of native hyaluronan. *Carbohydr. Polym.* 95, 515–521.
- Ray, T. C., Callow, J. A., Kennedy, J. F. (1988): Composition of root mucilage polysaccharides from *Lepidium sativum*. *J. Exp. Bot.* 39, 1249–1261.
- Read, D. B., Gregory, P. J. (1997): Surface tension and viscosity of axenic maize and lupin root mucilages. *New Phytol.* 137, 623–628.
- Rees, D. A., Welsh, E. J. (1977): Secondary and tertiary structure of polysaccharides in solutions and gels. *Angew. Chem. Int. Ed. Engl.* 16, 214–224.
- Rubinstein, M., Colby, R. H., Dobrynin, A. V., J oanny, J.-F. (1996): Elastic modulus and equilibrium swelling of polyelectrolyte gels. *Macromolecules* 29, 398–406.

- Seale, R., Morris, E. R., Rees, D. A. (1982): Interactions of alginates with univalent cations. *Carbohydr. Res.* 110, 101–112.
- Shapiro, Y. E. (2011): Structure and dynamics of hydrogels and organogels: An NMR spectroscopy approach. *Prog. Polym. Sci.* 36, 1184–1253.
- Skouri, R., Schosseler, F., Munch, J. P., Candau, S. J. (1995): Swelling and elastic properties of polyelectrolyte gels. *Macromolecules* 28, 197–210.
- Sutherland, I. W. (2001): The biofilm matrix—an immobilized but dynamic microbial environment. *Trend. Microbiol.* 9, 222–227.
- Tibbits, C. W., MacDougall, A. J., Ring, S. G. (1998): Calcium binding and swelling behaviour of a high methoxyl pectin gel. *Carbohydr. Res.* 310, 101–107.
- Timilsena, Y. P., Adhikari, R., Kasapis, S., Adhikari, B. (2015): Rheological and microstructural properties of the chia seed polysaccharide. *Int. J. Biol. Macromol.* 81, 991–999.
- Timotiwu, P. B., Sakurai, N. (2002): Identification of mono-, oligo-, and polysaccharides secreted from soybean roots. *J. Plant Res.* 115, 77–85.
- Traoré, O., Groleau-Renaud, V., Plantureux, S., Tubeileh, A., Boeuf-Tremblay, V. (2000): Effect of root mucilage and modelled root exudates on soil structure. *Eur. J. Soil Sci.* 51, 575–581.
- Van Veelen, A., Tourell, M. C., Koebernick, N., Pileio, G., Roose, T. (2018): Correlative visualization of root mucilage degradation using X-ray CT and NMRI. *Front. Environ. Sci.* 2018. DOI: <https://doi.org/10.3389/fenvs.2018.00032>.
- Voiniciuc, C., Dean, G. H., Griffiths, J. S., Kirchsteiger, K., Hwang, Y. T., Gillett, A., Dow, G., Western, T. L., Estelle, M., Haughn, G. W. (2013): FLYING SAUCER1 is a transmembrane RING E3 ubiquitin ligase that regulates the degree of pectin methylesterification in Arabidopsis seed mucilage. *Plant Cell* 25, 944–959.
- Watt, M., McCully, M. E., Jeffrey, C. E. (1993): Plant and bacterial mucilages of the maize rhizosphere: Comparison of their soil binding properties and histochemistry in a model system. *Plant Soil* 151, 151–165.
- Zhang, B., Hallett, P. D., Zhang, G. (2008): Increase in the fracture toughness and bond energy of clay by a root exudate. *Eur. J. Soil Sci.* 59, 855–862.
- Zickenrott, I.-M., Woche, S. K., Bachmann, J., Ahmed, M. A., Vetterlein, D. (2016): An efficient method for the collection of root mucilage from different plant species—A case study on the effect of mucilage on soil water repellency. *J. Plant Nutr. Soil Sci.* 179, 294–302.

6. INFLUENCE OF THE PHYSICO-CHEMICAL PROPERTIES OF ROOT MUCILAGE AND MODEL SUBSTANCES ON THE MICROSTRUCTURAL STABILITY OF SAND

This chapter contains the abstract and the manuscript version submitted to Biogeochemistry after the minor revisions required for acceptance. The numeration of the subchapters corresponds to the numeration figuring in the manuscript and the formatting to the one required by the journal.

Abstract

Root mucilage (RM), a soil-born biohydrogel, affects the physical stability of the rhizosphere. One reason for this is attributed to the present polysaccharides which contribute to the formation of aggregates by acting as interparticulate glue.

The aim of this study was to explore how physico-chemical properties of polymers of interparticulate gels influence this gluing and thus soil microstructural stability. We hypothesized that the microstructural stability of sand increases with the viscosity of the amended biohydrogel, which depends on the content of carbohydrate polymers and non-esterified uronic acids which themselves determine the amount of absorbed calcium.

Therefore, natural RM of maize and wheat were compared with higher viscous chia seed mucilage (SM) as a widely used model for RM, and with industrial pectin rich in uronic acids partially methylated.

Results showed that additionally to Ca binding by uronic acids, binding by proteins is a further possible mechanism of Ca adsorption in RM. Upon Ca addition, the viscosity increased upon intermolecular associations (pectin) and decreased upon suppression of intermolecular charge-charge repulsion (chia SM, maize RM). Amount of high-molecular weight material in the amendment affected strongly soil microstructural stability. Results further suggested the creation of gel micro-zones upon Ca addition, which increased the viscosity of interparticulate gel and sand microstructural stability.

Finally, the study outlines several physico-chemical mechanisms through which interactions between biotic (roots and seed) and abiotic components (mineral particles) influence soil structure, which control the water, air and nutrient flow through the rhizosphere and is, thus, an important soil quality parameter.

1. Introduction

Plant roots, bacteria, and fungi can modify the properties of their surrounding soil by exuding polysaccharidic substances (e.g., Barré and Hallett 2009; Naveed et al. 2017). These substances have a high water holding capacity and can absorb water in amounts above 90% of their own mass. The resulting gels have increased viscosity and the ability to swell and shrink. The term “gel effect” defines the biohydrogel-induced variations of soil properties (Brax et al. 2017), among which the stabilization of the soil structure is a significant one. Several pore-scale effects have been identified to explain the stabilization of the soil structure by biohydrogels: In the wet state,

stronger binding between soil particles due to a gluing effect leads to an increased cohesion of soil aggregates (e.g., Watt et al. 1993; Zhang et al. 2008). After drying and rewetting, reduction of the wetting rate, cementation, and increased polymer-particle surface contact enhance aggregate stability and reduce slaking (e.g., Orts William J. et al. 2007; Buchmann et al. 2015). Chemical interactions between biohydrogel and soil particles further affect soil structural stability (e.g., Barré and Hallett 2009; Buchmann et al. 2015). In general, it is expected that the exudation of mucilage by soil biota has similar effects on the soil structure as the already investigated biohydrogels. Variations of the soil structure induced by interactions between abiotic components (soil particles) and biotic components ultimately affects soil hydraulic properties such as water content, water retention and hydraulic conductivity (Kroener et al. 2018). Still, the exact relations between chemical properties of mucilage and the gel effects are unknown.

Well-defined model polymers such as polyacrylic acid for extracellular polymeric substances (EPS) are used for simplification of biohydrogel-soil systems and enable the focus on already complex pore-scale processes (Mayer et al. 1999; Barré and Hallett 2009). Polygalacturonic acid (PGA) has been widely used as model substance for root mucilage (RM) (e.g., Zhang et al. 2008; Albalasmeh et al. 2013). It has an uronic acid content of 100 wt% (based on the total polysaccharide content). Accordingly, PGA forms a gel by specific ionic bonding between deprotonated uronic acid and calcium (Grant et al. 1973). Such gels are governed by strong and specific interactions and form hard and brittle gels (de Kerchove and Elimelech 2007).

RM polysaccharides are composed of neutral sugars and uronic acids and are made responsible for the gelling properties of RM. The presence of uronic acids in RM should additionally lead to the formation of ionic bonds with calcium from the soil solution or ions at the surface of soil particles (e.g., Zhang et al. 2008; Chen and Arye 2016). Only few studies reported the uronic acid content in RM, but it varies from 3 to 28 wt% (based on the total polysaccharide content) in maize RM (e.g., Morel et al. 1986; Watanabe et al. 2008) to values less than 5 wt% in barley and maize exudates (Naveed et al. 2017). Such low contents of uronic acid in RM question the ability of RM to stabilize the gel *via* ionic bounds with calcium. For example, chia seed mucilage (SM) has an uronic acid content of 23 wt% (Timilsena et al. 2015) and it forms gels characterized by the entanglement of different chains by physical cross-links (Capitani et al. 2015; Brax et al. 2019b). Physical cross-links result from non-specific interactions between uncharged functional groups and from electrostatic interactions between uncharged functional groups and ions.

In contrast to its well-defined polymer analogues, root mucilage has a more complex chemical composition regarding the types and composition of carbohydrates (e.g., Fedeniuk and Biliaderis 1994; Read et al. 2003). Therefore, the understanding is still scarce about how the viscosity of biohydrogels affects pore-scale stabilization mechanisms, which lead to an increase of soil structural stability and ultimately to variations in the water flow in the soil profile.

Although chia SM has been widely used as RM analogue (e.g., Kroener et al. 2014; Benard et al. 2018), little is known about the extent to which chia SM forms gels of similar structure and properties as RM, and which effects of chia SM on soil are comparable to those of RM. Recent results showed that the viscosity of chia SM and maize and barley root exudates differed and that chia SM had the highest viscosity (Naveed et al., 2017). This highlights the need to understand the relationships between chemical composition and physico-chemical properties of RM from several plants and to compare them to model substances like chia SM.

The properties of a biohydrogel are controlled by its chemical composition and by the structural arrangement of the polymers, which depends on the physico-chemical forces at play between the chains (Brax et al. 2017, 2019b). Therefore, one aim of this study was to explore how chemical properties, particularly uronic acid content and Ca absorption capacity, of several RMs affect their physical gel properties, like viscosity, in comparison to other gels suggested to be models of RM. The second aim was to understand how these composition-property relationships found for RM and other substances affect gel-induced pore-scale properties, i.e., microstructural stability of artificial soils, differently. The following hypotheses were formulated in order to help achieving these aims:

1. Calcium absorption by RM increases with the content of non-esterified uronic acid constituting the backbone of RM.
2. The viscosity of RM increases with the content of carbohydrate polymers.
3. Absorption of calcium by RM increases the viscosity of RM.
4. The microstructural stability of sand amended with RM increases with the viscosity of RM, whether or not treated with calcium.

Beside chia SM, low-methoxy pectin (LMP) was chosen as a possible model substance for RM because it has a lower uronic acid content than PGA, and its partial methyl esterification may better model the processes occurring in RM (Mimmo et al. 2008). RM was collected from wheat and maize young roots as they differ in their rheological properties. For chemical characterization, calcium absorption, carbohydrate and uronic acid contents were measured. The viscosity was measured in samples with and without Ca addition and the same preparations were mixed with glass beads and coarse sand to measure their effect on the microstructural stability of artificial soils.

2. Materials and methods

2.1 Collection of mucilage

Collection of maize and wheat root mucilage (RM). Maize and wheat RM were extracted as described by Holz et al. (2018) using an aeroponic method. For this, wheat (*Triticum aestivum* cv. Julius) and maize (*Zea mays*) seeds were surface-sterilized in hydrogen peroxide (10%) for 10 min, rinsed thoroughly with distilled water and spread on a stainless steel mesh (mesh size 2 mm). The meshes (36 × 52 cm) were mounted in PE boxes (37 × 53 × 27 cm top). Both were rinsed with 10% H₂O₂ beforehand to inhibit microbial activity. The PE boxes were filled up to 12 cm with distilled water. The meshes were fixed at 22 cm from the bottom of the boxes. Each box contained one aquarium heater set at 23°C (25 Watt, EHEIM) and two air diffusers (Long-Long 25 cm) connected to an air pump to ensure ~100% air humidity. The seeds were grown 3 days in the dark, before mucilage was collected from the young roots under vacuum suction once a day for the next 2-3 days. RM was sieved through a 100 µm mesh and freeze-dried. Freeze-drying was essential in order to re-dissolve all substances at the same defined concentration.

Extraction of chia seed mucilage (SM). Chia seeds (*Salvia hispanica* L.) were added to distilled water (1:20 w/w ratio), mixed thoroughly for 2 min and kept for 30 min at room temperature until

mucilage excretion reached a steady state (Salgado-Cruz et al. 2013). Chia SM was extracted under vacuum filtration through a 500 μm sieve, sieved through 100 μm mesh to remove seed rests. The filtered and freshly extracted chia seed mucilage had a concentration of 0.12 ± 0.00 wt% and was finally freeze-dried.

2.2 Dialysis and chemical characterization of RM and its model substances

Dialysis was conducted as described in Brax et al. (2019b) with some modifications: Freeze-dried maize, wheat, and chia mucilage as well as low-methoxy pectin (LMP, citrus pectin, esterification degree 32-38%, galacturonic acid content 85%, Herbstreith & Fox KG, Germany) were separately mixed with water at a concentration of 0.05 wt% (500 mg/L) and let rest for 24 hours until complete dissolution. The concentration was set at 0.05 wt%. The prepared samples (20 mL) were transferred into a plastic cylinder (4 \times 2.8 cm) previously closed on one side with dialysis tubing (molecular weight cut-off: 12,000-14,000). Dialysis tubing was then fixed on the open end of the cylinder and immersed for 24 h in distilled water to remove the dissolved cations. The first subset of the samples was analysed for TOC, CHNS, and dry mass (Figure 1). The second subset was dialyzed against a 5 mM CaCl_2 -solution adjusted to pH 5 using KOH and HCl. After 48 h, the samples were washed three times by dialysis against distilled water, which was renewed every 24 h. The calcium contained in the gels, therefore, was considered bound (Morel et al. 1986). The second subset was analyzed for the cations (Figure 1). All samples were prepared in triplicate.

The molecular weight cut-off of the dialysis tubing corresponds to 67 ± 5 linked uronic acid molecules: The molecules which could diffuse out of the dialysis tubes were not the long polymer chains suspected to be involved in the gelling of the RM and its model substances. Thus, the total carbon (TC) ratio corresponding to the ratio of total carbon measured for the samples after the dialysis (TC_{dial}) and before the dialysis ($\text{TC}_{\text{initial}}$) gives an indication about the amount of high molecular weight (HMW) material (Table 1).

Total organic carbon (TOC) was measured *via* multiNC 2100S (Analytic Jena, Germany) (Figure 1) with the non-purgeable organic carbon (NPOC) method. Calibration was done using potassium hydrogen phthalate (Merck, Darmstadt, Germany).

Elemental nitrogen and carbon content was determined as weight percentage of the freeze-dried material (Vario micro cube, Elementar Analysensysteme GmbH, Germany) and used to obtain the C:N ratios.

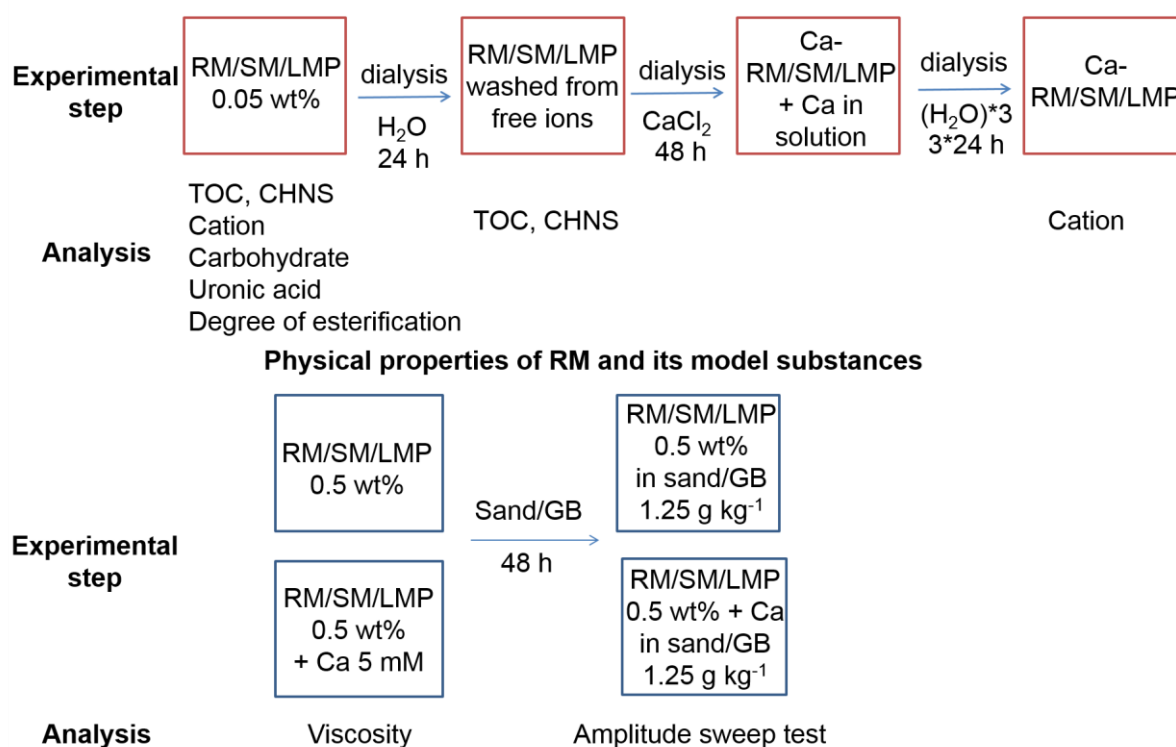


Fig. 1 Overview over the treatment procedures of root mucilage (RM), seed mucilage (SM) and low-methoxy pectin (LMP) and their corresponding physico-chemical analyses.

Cation analysis was obtained from 1 mL sample digested with 0.5 mL 33% HCl and 1.5 mL 65% HNO₃ in a microwave by a 15 min heating ramp followed by constant heating at 200°C for 40 min. The digests were subsequently analysed by inductively coupled plasma optical emission spectrometry (ICP-OES, Agilent 720 Series, Germany) for the metals Ca, Mg, Na and K.

Total uronic acid content in wt% of the dry mass was determined according to the modified phenylphenol method of Blumenkrantz (1973) improved by Filisetti-Cozzi and Carpita (1991) for a reduced browning of neutral sugars. The principle of the phenylphenol method is the formation of chromogens by the reaction of hydrolysed uronic acid with meta-hydroxydiphenyl. For this, 40 μL of 4 M sulfamic acid-potassium sulfamate (pH 1.6) was added to 400 μL of sample solution. After mixing, 2.4 mL of concentrated H₂SO₄ containing 12.5 mM sodium tetraborate was added. After boiling for 20 min and cooling with an ice bath, 80 μL of a solution of 0.15 wt% *m*-hydroxybiphenyl in 0.5 wt% NaOH was added. The tubes were incubated for 15 min at room temperature before absorption at 525 nm was measured (UV-Vis Spectrometer specord 50, Analytik Jena, Germany). Calibration curve was measured with standard solutions of polygalacturonic acid (PGA, 95%, enzymatic, Sigma, Germany) between 5-125 mg L⁻¹, so that the measured quantity of uronic acid was given in PGA weight equivalent.

Galacturonic acid was not the only uronic acid found in root exudates (Naveed et al. 2017). As not all uronic acids have the same absorption coefficient, a correction factor was calculated for several uronic acids and expressed in the errors given in Figure 3a: The absorption coefficient of PGA was divided by the absorption coefficients of mannuronic ($a_{\text{PGA}}/a_{\text{UA}}=0.88$), irudonic ($a_{\text{PGA}}/a_{\text{UA}}=0.92$) and glucuronic ($a_{\text{PGA}}/a_{\text{UA}}=1.50$) acid obtained from Blumenkrantz and Asboe-Hansen (1973). The product of the measured PGA weight equivalents and of the lowest

correction factor of mannuronic acid corresponded to the lower possible uronic acid concentration in the sample, and vice-versa of glucuronic acid to the higher possible concentration.

Degree of esterification (DE) was calculated out of the ratio between the methanol content released by base hydrolysis of the esterified uronic acids and the total uronic acid content measured by colorimetry (McFeeters and Armstrong 1984). Methanol released from base hydrolysis of uronic acid methyl esters was measured by gas chromatography. For this, the samples were dissolved in water to give a 10 mg/mL solution and 1.5 mL citric acid, 0.1 M NaCl buffer (pH 5) was added to 1 mL of sample solution. The total volume was 2.5 mL and the final concentration of citric acid 5 mM. Further, 200 μ L of 1.0 M NaOH was added, the samples were sonicated for 5 min and let rest overnight. The next day, 300 μ L of 82.5 mM citric acid solution was added to lower the pH to 7 for GC analysis. The samples were measured with a GC-FID (Varian CP-3800, Varian Inc, Palo Alto, USA) equipped with a 60 m TR-FAME column (Thermo Fisher Scientific, Waltham, USA). A sample volume of 1 μ L was injected at 150°C with a 1/10 split ratio. Carrier gas was nitrogen at a constant flow of 0.7 mL min⁻¹. The oven was programmed for 0.2 min at 50°C, a ramp with 20°C min⁻¹ to 130°C and holding for 3 min at 130°C. The DE is given for the lowest and for the highest possible uronic acid content (Figure 3b).

Total carbohydrate content was measured with the phenol-sulphuric acid method established by Dubois (1956). This method is based on the dehydration of hydrolyzed saccharides to furfural derivatives during their reaction with concentrated sulfuric acid. The reaction of furfural derivatives with phenol forms coloured complexes, which absorb in the UV-Vis spectrum (Dubois et al. 1956). A volume of 1 mL sample solution was mixed with 40 μ L phenol-water reagent (57 wt%), 2.5 mL concentrated H₂SO₄ were quickly added and the mixture was vortexed. After at least 15 min at room temperature, absorption was measured at 490 nm with the same UV-Vis Spectrometer as previously. Calibration curve was measured with standard solutions of glucose (5-70 mg L⁻¹). Amount of glucose weight equivalent was also measured for another set of 50 mg L⁻¹ standard solutions consisting of glucose-PGA mixtures (5-45; 25-25; 45-5 mg L⁻¹) for comparison.

As not all sugars have the same absorption coefficient, a correction factor was calculated similarly to the uronic acid for several sugars. For this, the total sugar content was measured as glucose equivalent for 50 mg L⁻¹ standard solutions of fructose (99%, Alfa Aesar), galactose (98.5%, Dr. Ehrenfester), xylose (99.5%, Dr. Ehrenfester), PGA and the previously described pectin. The correction factor was the ratio between the real sugar content (50 mg L⁻¹) and the sugar content measured as glucose equivalent. The product of the measured glucose equivalent and of the highest correction factor corresponded to the highest possible total sugar concentration in the samples).

2.3 Physical characterization

Root mucilage and model substance preparation for the physical characterization was performed in distilled water at a higher concentration of 0.5 wt% (5.00 g/L) than for the chemical analysis (Figure 1). For the calcium-treated samples, the same quantity of sample was dissolved in half the volume of distilled water, and the other half of the volume was added as a 10 mM CaCl₂ solution resulting in 0.5 wt% in 5 mM CaCl₂ solution.

Viscosity of RM and its model substances was measured using a MCR 102 rheometer (Anton Paar, Ostfildern, Germany) with a parallel-plate measuring system (25 mm diameter). Flow curve

measurements were conducted at 20°C with a measurement gap of 250 µm and a shear rate of 0.01 - 600 s⁻¹.

Preparation of amended artificial soils was performed at 0.5 wt%, a middle value for the dry mass of RM collected with the aeroponic method (Zickenrott et al. 2016). Amendment of soil with this RM concentration aims to characterize processes taking place close to the root interface. Glass beads (338 ± 44 µm) and a coarse quartz sand (grain size: 0.2% 2000-630 µm, 94.9% 630-200 µm, and 4.9% 200-63 µm, Quarzwerke GmbH, Weferlingen) were used as artificial soils. In order to limit bacterial degradation of RM, the artificial soils were successively washed with 2 M HCl solution and distilled water and were oven-dried at 105°C for 24 h prior to the experiments. The samples were prepared by homogeneously mixing the artificial soils with wheat and maize RM, chia SM, and LMP and by adjusting them to their maximal water content of 25 wt%. Final concentration of the different samples was 1.25 g dry RM or model substance per kg soil. The adjusted concentration was in the range of EPS in deciduous forest and permanent grassland as estimated by Chenu (1995), but significantly less than the 4.6 g dry root exudate (kg dry soil)⁻¹ applied by Naveed et al. (2017).

Amplitude sweep measurement were conducted to determine the microstructural stability of the samples using the same rheometer and geometry as described for the viscosity measurements. Water-saturated conditions were used to minimize the effects of water menisci forces, hence the structural stability of the non-amended artificial soils directly depended on the solid-solid friction between mineral particles as a function of soil texture (Buchmann and Schaumann 2017). Microstructural stability was described by the yield stress for both non-treated artificial soils and treated with RM of wheat and maize, chia SM, pectin and glucose (Figure 6). The measurements were carried out at 20°C (regulated by a Peltier unit) under the following conditions: Plate gap was set to 2 mm throughout the measurements with deformation γ increasing from 0.001-100% in logarithmic scale for a total of 33 measurement points. Frequency was kept constant at 0.681 Hz. Results were presented as yield stress τ (peak elastic stress), which typically represents the onset of soil microstructural collapse (Naveed et al. 2017).

2.4 Environmental scanning electron microscopy (ESEM)

Small amounts of each amended soil were immersed into liquid nitrogen and directly after transferred in the freeze-drier. Shock-freezing the samples aimed to reduce as much as possible changes in the structure of the polymer network (Brax et al. 2019a). ESEM images of these samples were taken with a FEI Quanta 250 ESEM (FEI Company Hillsboro, United States) under low vacuum with chamber pressures between 60 and 80 Pa. A large field detector was used with an acceleration voltage between 12.5 and 15 kV.

2.4 Statistical analyses

Mean values and standard deviations were calculated for all parameters. Differences between the mucilage types (type) in chemical and physical parameters (Table 1, Figure 2, 3a, 4, 5a and 6), the effect of Ca addition (treatment) on viscosity of mucilage (H3, Figure 5a) and on the yield stress of glass beads and sand amended with these substances (H4, Figures 6), and the effect of substrate type (glass beads or sand) on the yield stress were tested with linear mixed effect models with random intercept from replicate measurements using the packages nlme and car (R core team, 2018) including interaction only when it was significant. The model was accepted to sufficiently describe the data if the Shapiro-Wilk normality test and Levene test of the residuals

resulted in a $p > 0.05$. The effect of a factor was considered significant when the anova test of one model with and one model without the respective factor (null model) resulted in a p -value < 0.05 (Winter 2013). In order to meet model assumptions, data of uronic acid content, viscosity, and yield stress were transformed logarithmically. Significant differences between types and treatments were marked with different letters (Table 1, Figures 2, 3a, 5a, and 6). Finally, to test the hypothesized relationships between Ca absorption and content of non-esterified uronic acid (H1), and \ln (viscosity) and polymer content (H2), as well as the dependence of yield stress on \ln (viscosity) and polymer content (H4), linear regression analyses were performed for Figure 3b, Figures 5b, and 7a-b weighed by the reciprocal standard deviation of the parameters using the package stats of the statistical software R (R core team, 2018). Correlation and strength of the relationship between the data are described by the coefficient of determination r^2 and the significance (p -value) of the slope.

3. Results and discussion

3.1 Chemical composition of mucilage and analogues

The ratio of total carbon content after and before dialysis differs significantly between the substance types ($p = 3.8 \cdot 10^{-11}$) and shows that low methoxy pectin (LMP) as a high molecular weight (HMW) polymer did not lose significant amounts of carbon upon dialysis (Table 1). In contrast, chia seed mucilage (SM) lost about 25% of its initial total carbon upon dialysis, whereas maize and wheat root mucilage (RM) lost 49% and 59%, respectively. The C/N ratio after water dialysis (Table 1) reveals that LMP and chia SM had a significantly lower N content than wheat and maize RM ($p < 1.6 \cdot 10^{-6}$ for all).

Table 1 Mean and standard deviation of the ratio of total carbon after water dialysis TC_{dial} with respect to initial total carbon $TC_{initial}$ and C/N ratio after water dialysis in maize and wheat root mucilage (maize RM, wheat RM), chia seed mucilage (chia SM) and low-methoxy pectin (LMP). Both were significantly affected by the mucilage type ($p = 3.8 \cdot 10^{-11}$ and $2.6 \cdot 10^{-10}$ for TC ratio and C/N, respectively). Significant differences are marked by different letters in brackets.

	Wheat RM	Maize RM	Chia SM	LMP
TC_{dial} / TC_{raw}	0.45 ± 0.04 (a)	0.62 ± 0.01 (b)	0.74 ± 0.05 (c)	0.96 ± 0.03 (d)
C/N	6.6 ± 0.4 (a)	11.3 ± 1.1 (a)	70.8 ± 7.6 (b)	79.8 ± 4.5 (b)

The concentrations of Na, K, Mg and Ca in the samples were measured before dialysis and after dialysis against 5 mM $CaCl_2$ solution (Figure 2). Whereas the commercially purified citrus pectin (LMP) was nearly free of cations before dialysis, RM of maize and wheat and chia SM contained $250 \pm 40 \mu\text{mol mL}^{-1}$ K (Figure 2a). In contrast to the RM of maize and wheat that contained no relevant amounts of other cations, significantly higher Ca and Mg contents of $160 \pm 4 \mu\text{mol mL}^{-1}$ were found in chia SM ($p < 8.5 \cdot 10^{-17}$ and $3.6 \cdot 10^{-12}$ for Ca and Mg, respectively). After dialysis, Na, K, and Mg were either washed out or replaced by Ca for all samples (Figure 2b). This indicates the affinity of maize and wheat RM and of chia SM to Ca^{2+} . The highest amount of bound Ca was found in LMP with $948 \pm 23 \mu\text{mol mL}^{-1}$ followed by chia SM with $666 \pm 36 \mu\text{mol mL}^{-1}$

¹ ($p = 9.4 \cdot 10^{-17}$), which exceeded the occupied charge before dialysis. In contrast, with a Ca content of $83 \pm 8 \mu\text{mol mL}^{-1}$ for maize and wheat RM, Ca dialysis did not result in a complete saturation of all charges that had been occupied before dialysis (Figure 2b).

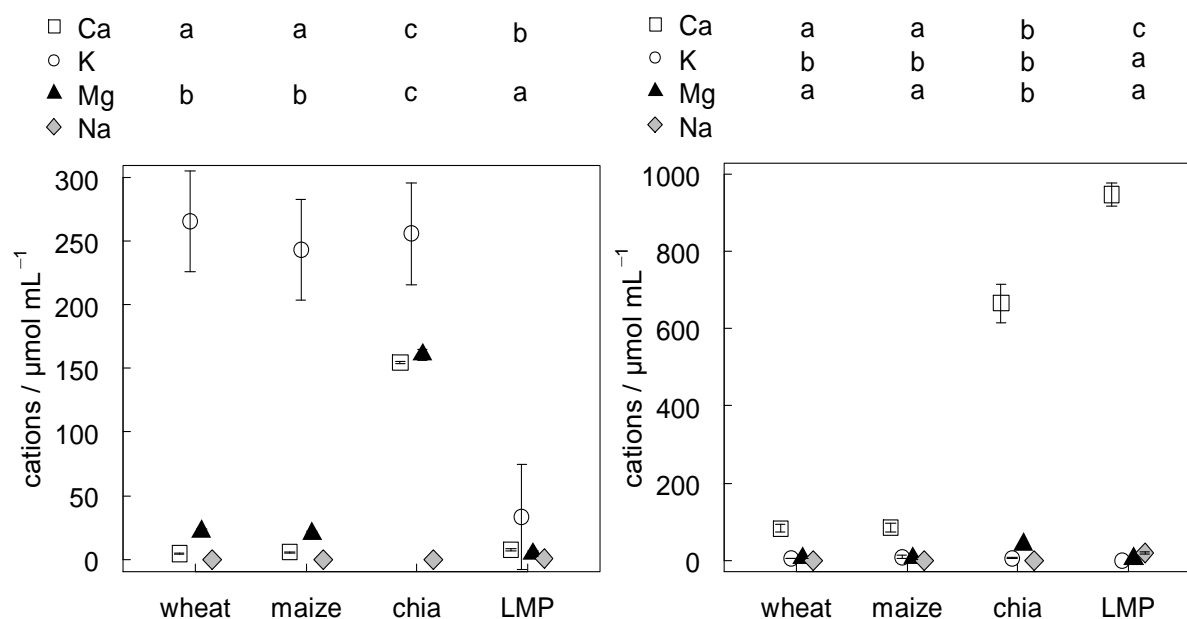


Fig. 2 Initial cation content (a) and bound cation content after calcium treatment (b) in maize and wheat root mucilage, chia seed mucilage and in low-methoxy pectin (LMP) was significantly affected by the mucilage type for the initial Ca ($p = 4 \cdot 10^{-24}$) and Mg content ($p = 1.8 \cdot 10^{-17}$) and for the Ca ($p = 3.7 \cdot 10^{-14}$), K ($p = 4.5 \cdot 10^{-4}$), and Mg content ($p = 2.8 \cdot 10^{-10}$) after Ca treatment. Error bars show standard deviation. Different letters beside the legend symbols indicate significant mucilage type specific differences in the respective cation. Where letters are missing, model assumptions were not met.

The uronic acid content in the different substances varied (Figure 3a) significantly ($p = 2.1 \cdot 10^{-31}$). With $81 \pm 6 \text{ wt\%}$ galacturonic acid equivalent (GalA eq) LMP verified the information provided by the manufacturer (85%). The uronic acid content in chia SM was with $39 \pm 4 \text{ wt\%}$ GalA eq (almost half of the one in LMP) significantly lower ($p = 5.3 \cdot 10^{-9}$) whereas only $4 \pm 1 \text{ mg L}^{-1}$ GalA eq was measured for maize RM and no uronic acid was detected in wheat RM (Figure 3a). As several types of uronic acid are present in mucilage (Naveed et al. 2017) and due to their various absorption coefficients, mannuronic acid (ManA eq) and glucuronic acid equivalents (GluA eq) were also represented in Figure 3a. The degree of esterification (DE) measured for LMP was between $21 \pm 1\%$, which is below the one given by the producer (32-38%). The DE of maize RM was $43 \pm 0\%$, whereas the DE of chia SM was 8 ± 1 thus remarkably lower. The concentration of bound Ca in the different substances after Ca dialysis plotted against the content of non-esterified PGA equivalent (Figure 3b) resulted in a significant weighted linear regression with an intercept of $82.6 \pm 4.8 \cdot 10^{-5} \mu\text{mol mL}^{-1}$ ($p = 3.3 \cdot 10^{-13}$) and a slope of $16.8 \pm 2.6 \mu\text{mol mL}^{-1} \text{ wt\%}^{-1}$ ($p = 0.033$, $r^2 = 0.9557$). Therefore, the concentration of bound Ca was significantly greater than zero at the y-intercept and significantly increased with the content of non-esterified uronic acid.

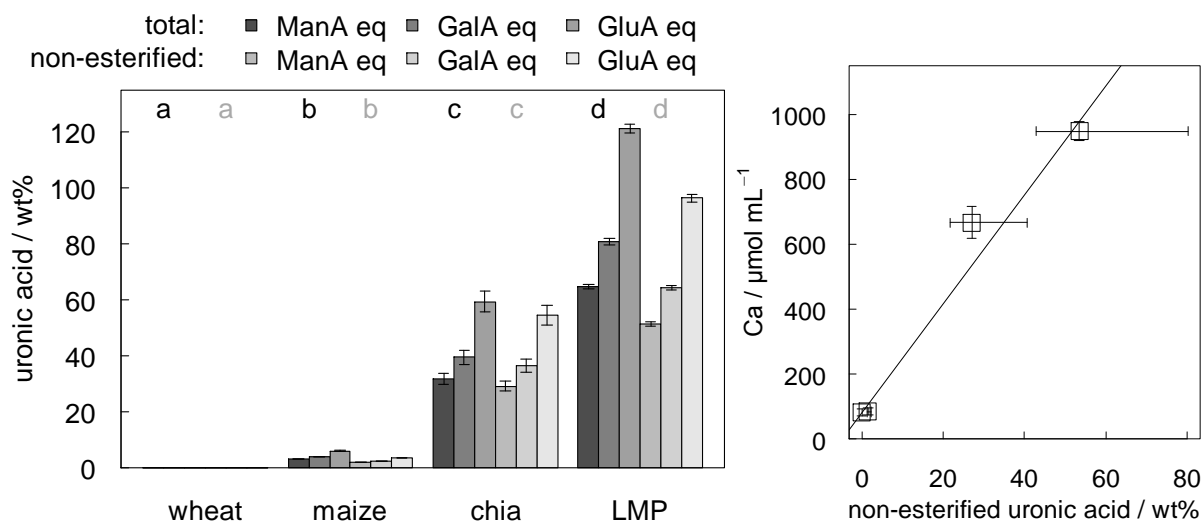


Fig. 3 Content of total and of non-esterified uronic acid as mannuronic acid (MaA), galacturonic acid (GalA), and glucuronic acid (GluA) equivalent in wt% of the dry mass in maize and wheat root mucilage, chia seed mucilage, and in low-methoxy pectin (LMP) (a) were both significantly affected by the mucilage type ($p = 2.1 \cdot 10^{-31}$). Error bars show standard deviation and different letters of the same grayscale indicate significant differences. Correlation between the non-esterified galacturonic acid content and the bound Ca concentration after calcium treatment was with an intercept of $82.6 \pm 4.7 \cdot 10^{-5}$ ($p = 3.3 \cdot 10^{-13}$) and a slope of 16.8 ± 2.6 ($p = 0.0224$) significant ($r^2 = 0.9557$) (b). Horizontal error bars represent mannuronic (lower) and glucuronic (upper) acid equivalents.

Chia SM had the highest carbohydrate content ($p = 2.7 \cdot 10^{-5}$) with 35 ± 2 wt% glucose equivalent (Gluc eq) and maize and wheat RM showed similar values ($p = 0.897$) around only 7.5 ± 1 wt% Gluc eq (Figure 4a). In addition to glucose, various neutral and acidic carbohydrates are present in mucilage (Naveed et al. 2017) and affect the absorption coefficient. A correction factor (i.e., ratio of sugars to glucose equivalent) was measured for several carbohydrates (Table 2). As LMP had the highest correction factor, the carbohydrate content equivalent to LMP was also represented in Figure 4. To prove the influence of uronic acids on the absorption coefficient, three standard solutions consisting of glucose-PGA mixtures (5-45, 25-25, and 45-5 mg L⁻¹) were prepared for comparison. The correction factors (i.e., the ratio of sugars to glucose equivalent) increased from 1.1 (5-45 mg L⁻¹) to 1.6 (25-25 mg L⁻¹) and 2.2 (45-5 mg L⁻¹), accordingly to the increase of the fraction of PGA in the solution.

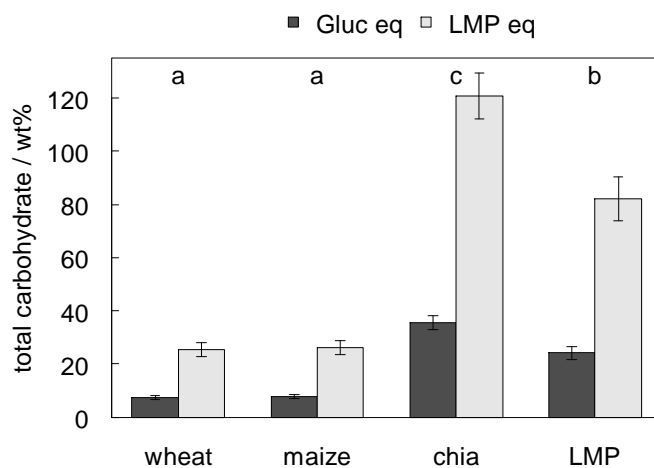


Fig. 4 Total carbohydrate content as glucose equivalent (Glu eq) and LMP equivalent (LMP eq) in maize and wheat root mucilage, chia seed mucilage and in low-methoxy pectin (LMP) in wt% of the dry mass was significantly affected by the mucilage type ($p = 3.4 \cdot 10^{-11}$). Error bars show standard deviation and significant differences are indicated by different letters.

Table 2 Mean and standard deviation of the correction factor (i.e., ratio of sugars to glucose equivalent) of various carbohydrates measured for the glucose calibration curve.

Substance	Glucose	Galactose	Fructose	Xylose	PGA	LMP
Correction factor	1.0	1.3±0.0	1.5±0.1	1.1±0.0	2.5±0.2	3.4±0.3

3.2 Suitability of the Dubois total carbohydrate method for mucilage

The analytical accuracy of the Dubois method for samples rich in uronic acid such as chia SM or LMP was low, as the correction factor measured for LMP involved correction bars over three times the experimental value measured for the total sugar content (Figure 4). The reason is that neutral sugars, uronic acids, and amino sugars show different chemical reactivity with the derivatization reagent. Therefore, the absorption coefficient of uronic acids typically ranges between 30% and 40% of the one of neutral sugars, whereas amino sugars do not react at all (Mecozzi 2005; Liebezeit and Behrends 2007). Although not indicated by the manufacturer, the potential presence of amino sugars in LMP was suggested by the high nitrogen content (Table 1) and would explain why the correction factor for LMP is higher than that for PGA. The calibration with glucose despite the dependence of the absorption coefficient on the type of sugar leads to an underestimation of the total carbohydrate (Albalasmeh et al. 2013). This shows that the Dubois method is inappropriate to measure and compare the total carbohydrate content in RM and analogue substances, which potentially contain amino sugars and uronic acids. An alternative method involves the hydrolysis of the polysaccharides and the derivatisation of their constituent monosaccharides to volatile compounds allowing analysis using gas chromatography (Osborn et al. 1999; Bacilio-Jiménez et al. 2003).

3.3 The chemical composition of root mucilage differs from its analogues

Wheat and maize RM contained higher amounts of low molecular weight (LMW) substances than chia SM and the purified citrus pectin LMP. Osborn et al. (1999) also found that a majority of neutral sugars in crude maize RM is present as glucose monomer. One explanation is that roots profit from the exudation of microbially easily degradable monosaccharides improving symbiosis with soil bacteria and fungi (Angers and Caron 1998).

The content of uronic acid in chia SM was slightly higher than the data reported by Timilsena et al. (2015) and Lin et al. (1994). The content of uronic acid measured) and the one in maize RM was in good agreement with the value measured by Bacic et al. (1986) in *Zea Mays L.* grown under axenic conditions. Low amounts of uronic acid below 4.5 wt% of the dry mass were also measured for barley and maize root exudates (Naveed et al. 2017). In contrast to our results, 11.5 wt% uronic acids were measured in wheat root mucilage (Moody et al. 1988). One reason for this discrepancy could be that the seed variety used by Moody et al. (1988) was from another cultivar (cv Condor) than ours (Julius). Furthermore, the growth procedure and extraction procedures are not standardized, which complicates the comparison and interpretation of

published results. In contrast to chia SM and LMP, the low amounts of uronic acid measured for RM in this study and in the literature suggest that the interactions between the polymers in RM and the resulting gel properties of RM are not only governed by uronic acids.

Whereas chia SM seems to mostly consist of uronic acids and neutral sugars, the low carbohydrate content and uronic acid content in maize and wheat RM suggest that there is only a small amount of polymeric substances in RM of this study, which is partly verified by the high carbon loss during dialysis of wheat and maize RM. Another reason could be the presence of other types of polymers such as proteins (Fedeniuk and Biliaderis 1994; Knee et al. 2001), and phospholipids (Read et al. 2003), which have already been found in RM. The small C/N ratio for RM suggests indeed the presence of amino sugars or of proteins in RM (Bacic et al. 1986; Knee et al. 2001).

3.4 Calcium adsorption in mucilage relies on free uronic acids - but not only

The lower amount of HMW material in wheat and maize RM than in chia SM and LMP resulted in a reduced solid concentration after dialysis, which alone can explain the reduced amount of absorbed Ca. However, the positive correlation between non-esterified uronic acid and bound Ca in Figure 3b indicates that Ca binding occurs mostly by interactions with free uronic acids according to hypothesis 1. In addition, further Ca binding mechanisms are suggested by the positive y-intercept as it indicates calcium absorption also in the absence of free uronic acid. This is particularly relevant for wheat and maize RM, which contained zero and near to zero free uronic acids and still adsorbed Ca. One possible mechanism supported by the low C/N ratio is the absorption of Ca by proteins probably also present in RM (Dudev and Lim 2004). An alternative mechanism was suggested by Morel et al. (1987) and Watt et al. (1993), who found that binding of RM to soil and clay materials occurs through hydroxyl and amino groups of RM rather than by ionic binding with free uronic acids. These considerations underline the necessity to take into account proteins and phospholipids as additional constituents of RM to evaluate the composition-property relationship in RM, as these compounds affect ionic binding to calcium and probably the viscosity of mucilage.

3.5 Rheology of root mucilage and analogues

The flow curves (Brax 2019) of all RM and analogues showed a shear-thinning behaviour indicated by the decrease of the viscosity with increasing shear rate and caused by the alignment of the randomly positioned polymer chains in the flow direction resulting in less interaction among adjacent chains (Koocheki et al. 2013). We examined the viscosity of the samples at a medium shear rate of 107 s^{-1} to differentiate between the strength of the interactions between the polymers, and thus to compare potentially different gel formation mechanisms. The different samples (0.5 wt%) including one of glucose reveal a significantly different viscosity ($p = 2 \cdot 10^{-17}$). Without additional calcium, the viscosity increased in the following order (Figure 5a): glucose \approx ($p = 0.0628$) wheat RM $<$ ($p = 6.7 \cdot 10^{-12}$) maize RM $<$ ($p = 4.9 \cdot 10^{-8}$) LMP \ll ($p = 2.5 \cdot 10^{-14}$) chia SM. The viscosity of glucose and wheat RM were between 1 and 2 mPa·s and thus only slightly higher than that of water, which is 1 mPa·s at 20°C. In contrast, the viscosity of chia SM was with $128 \pm 4.5 \text{ mPa}\cdot\text{s}$ much higher than that of maize RM and LMP in the range of 10 mPa·s ($p = 2.3 \cdot 10^{-16}$ and $2.5 \cdot 10^{-14}$, respectively). Upon calcium addition, the viscosity of LMP increased to $116 \pm 12 \text{ mPa}\cdot\text{s}$ ($p = 1.0 \cdot 10^{-16}$), whereas the one of chia SM and maize RM decreased to $73 \pm 0.4 \text{ mPa}\cdot\text{s}$ ($p = 3.0 \cdot 10^{-6}$) and $2 \pm 0.1 \text{ mPa}\cdot\text{s}$ ($p = 6.2 \cdot 10^{-13}$), respectively. The viscosity of wheat RM also increased slightly to $2 \pm 0.4 \text{ mPa}\cdot\text{s}$ upon Ca addition ($p = 2.7 \cdot 10^{-3}$). The partly opposite

effects of Ca on the viscosity of the different samples are reflected in the statistical model by a significant interaction of treatment and mucilage type ($p = 4.7 \cdot 10^{-23}$). Probably, other mucilage type specific factors oppositely influence the viscosity of the gels at different Ca concentrations.

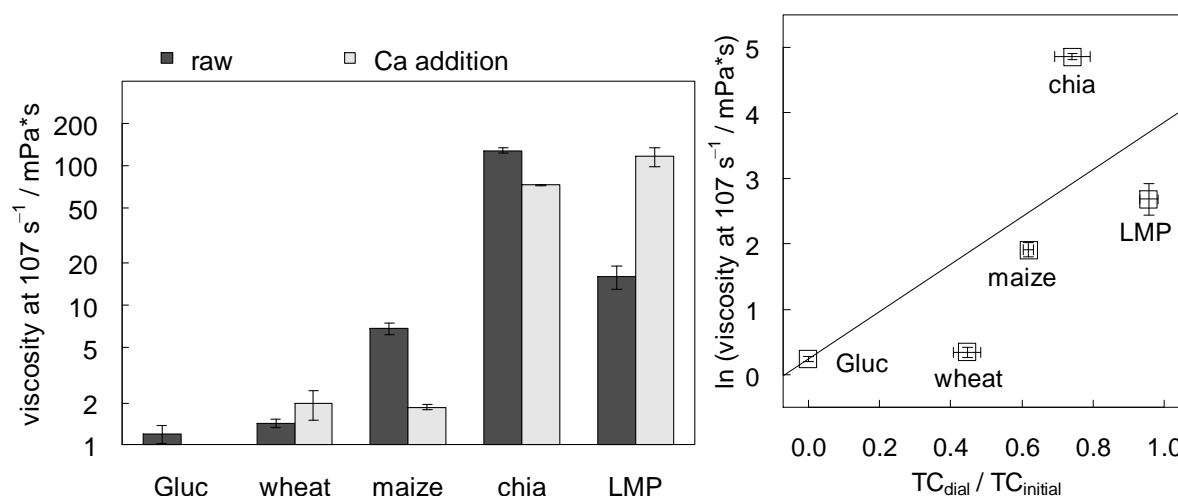


Fig. 5 Viscosity at a shear rate of 107 s^{-1} measured for 0.5 wt% glucose (Gluc), wheat and maize root mucilage, chia seed mucilage and low-methoxy pectin (LMP) dissolved in pure water (raw) and enriched in calcium (Ca addition) was significantly affected by mucilage type ($p = 5.8 \cdot 10^{-35}$), by Ca treatment ($p = 2.89 \cdot 10^{-22}$) and by the interaction of both ($p = 4.7 \cdot 10^{-23}$) (a). Different letters indicate significant differences. Correlation between the $\ln(\text{viscosity})$ at a shear rate of 107 s^{-1} and the TC ratio (total carbon ratio after and before dialysis $\text{TC}_{\text{dial}} / \text{TC}_{\text{initial}}$) for glucose, RM, and its analogues dissolved in water revealed a significant intercept of 0.24 ± 0.02 ($p = 0.0011$) and a significant slope of 3.58 ± 1.12 ($p = 0.0492$, $r^2 = 0.7737$) (b).

Therefore, the viscosity at a shear rate of 107 s^{-1} of glucose, RM, and its analogues was also plotted against the TC ratio of the respective substances (Figure 5b). The TC ratio value for glucose was assumed to be 0, as the molar mass of glucose is much smaller than the molecular weight cut-off (MWCO) of the dialysis tubing. The logarithmic values of the viscosity significantly increase with the TC ratio ($r^2 = 0.7737$, $p = 0.0492$).

3.6 Various factors determine the viscosity of root mucilage and analogues

3.6.1 Molecular weight and charge affect polymer interactions

As glucose is a monomeric carbohydrate, friction forces between the glucose molecules are not relevant and its viscosity is similar to the one of water. Internal frictions between polymer molecules increase the viscosity which explains the increase of viscosity with the TC ratio and thus with the amount of polymeric material (Mezger, T. G. 2014). The lower viscosity of LMP than of chia SM in water despite the higher amount of HMW material results from the negatively charged free uronic acids distributed on the polymer chains of LMP. Those repel each other and thereby reduce the internal friction giving LMP the viscosity of a viscous liquid. In contrast, the viscosity of chia SM was the one of a weak viscoelastic gel and comparable to literature results (Medina-Torres et al. 2000; Capitani et al. 2015). Its viscosity was attributed to molecular interactions between the polymer chains, which include electrostatic interactions and hydrogel bonding (Medina-Torres et al. 2000). Such interactions are characteristic for polyelectrolyte gels (Skouri et al. 1995; Rubinstein et al. 1996). Weak positive molecular interactions between the polymer chains could also induce the viscosity in maize RM, which was in good accordance to

earlier studies (Read and Gregory 1997; Read et al. 1999) and comparable to that of LMP, although maize RM had less HMW material than LMP. This suggests that strong attractive forces between the molecules in maize RM compensated for the smaller amount of interacting polymers.

Although wheat and maize RM had similar carbohydrate and non-esterified uronic acid contents, wheat RM was less viscous than maize RM and its viscosity was similar to the one of barley root exudate (Naveed et al. 2017). One reason could be the smaller amount of polymeric material in wheat RM than in maize RM leading to fewer molecular interactions between the polymer chains. This result supports hypothesis 2, which supposed that the viscosity increases with the content of polysaccharide derived sugars, as long as the type of polymers do not differ.

3.6.2 Calcium connects or contracts polymers with opposite effects on viscosity

Calcium-treatment of LMP induced a strong increase of its viscosity due to intermolecular associations between calcium and deprotonated uronic acids (Axelos et al. 1991). Finally, hypothesis 3, which supposed that interactions with calcium increase the viscosity of RM and analogues, was only valid for LMP. In contrast, for polyelectrolyte gels, addition of positive ions results in a drop in the viscosity. It induces the suppression of intermolecular charge-charge repulsion and results in the contraction of the polysaccharide molecules through complexation with the added ions. This leads to a drop of the friction forces between the polymer chains and thus reduces the viscosity (Koocheki et al. 2013). This mechanism explains the decrease of the viscosity of chia SM upon calcium treatment (Capitani et al. 2015) and may also explain the one of maize RM as it behaved similarly.

The suggested presence of proteins in RM could also increase the viscosity. For example, glycoproteins are recognized for their high-water binding and gel-formation properties (Fincher et al. 1983), and could additionally influence the gel properties of maize RM. The slightly increased viscosity of wheat RM with calcium addition could result from calcium-binding proteins such as arabinogalactan or other glycoproteins, also possibly present in RM (Knee et al. 2001; Timotiwu and Sakurai 2002).

3.6 Mechanical and visual microstructure of mucilage - model soil systems

The yield stress obtained from rheological measurements of the glass bead samples increased in the order of the following amendments: wheat RM \sim ($p = 0.452$) maize RM \sim ($p = 0.105$) chia SM $<$ ($p = 7.5 \cdot 10^{-4}$) LMP (Figure 6). Generally, the yield stress was by $\sim 58 \pm 20$ Pa higher for sand than for the glass beads ($p = 0.0016$). Calcium addition increased significantly the yield stress of the amended glass beads ($p = 9.9 \cdot 10^{-9}$) by $\sim 47 \pm 15$ Pa and of the amended sand samples ($p = 9.2 \cdot 10^{-13}$) by $\sim 114 \pm 44$ Pa. For the glass beads, calcium addition had the strongest effect on the yield stress of LMP-amended samples ($\sim 68 \pm 12$ Pa, $p = 6.5 \cdot 10^{-5}$). In sand, calcium addition to maize RM-, chia SM- and LMP-amended samples led to a similar increase of the yield stress by $\sim 132 \pm 31$ Pa ($p = 5.3 \cdot 10^{-8}$).

6 Influence of the physico-chemical properties of root mucilage and model substances on the microstructural stability of sand

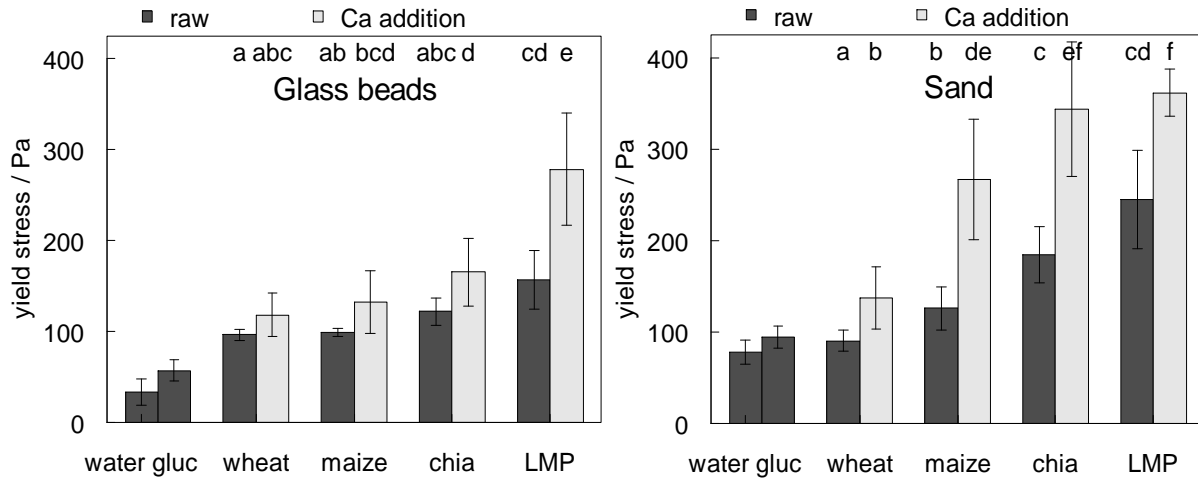


Fig. 6 Yield stress of saturated glass beads and sand amended with distilled water, 0.5 wt% glucose (Gluc), wheat and maize root mucilage, chia seed mucilage and low-methoxy pectin (LMP) in water (raw) and enriched in calcium (Ca addition) were both significantly affected by the mucilage type ($p = 1.1 \cdot 10^{-5}$ and $2.3 \cdot 10^{-9}$ for glass beads and sand) and by the Ca treatment ($p = 9.9 \cdot 10^{-9}$ and $9.2 \cdot 10^{-23}$, respectively). Different letters indicate significant differences. In addition, yield stress of amended sand was significantly higher than of glass beads ($p = 0.0016$).

The yield stress of the sand samples amended with the different substances raw and enriched in calcium was plotted against the viscosity (Figure 7a). A general positive trend ($r^2 = 0.582$, $p = 0.0277$) was observed between the yield stress of the amended samples and the logarithmic values of the viscosity of the amendments, but some spike values and the low coefficient of determination suggest that beside the viscosity of the amendment, other factors influence the yield stress. For example, the viscosity of wheat and maize RM treated with calcium does not differ significantly ($p = 0.633$), but the yield stress of sand amended with maize RM and calcium is nearly double as high as the one of sand amended with wheat RM and calcium ($p = 9.3 \cdot 10^{-5}$).

The yield stress of the sand samples amended with the raw substances was plotted against their respective TC ratio (Figure 7b) which corresponds to the ratio of total carbon measured for the substances after (TC_{dial}) and before dialysis ($TC_{initial}$). The yield stress significantly increased with increasing TC ratio of the amendments ($r^2 = 0.9665$, $p = 0.0169$) and thus with increasing amount of large molecules in the amending substances.

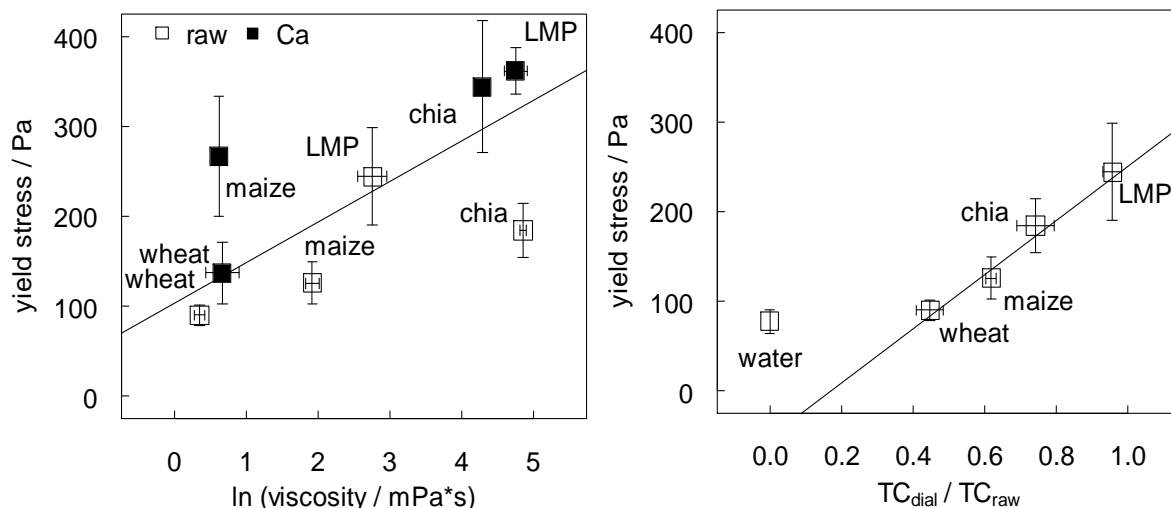


Fig. 7 Correlation between the yield stress and \ln (viscosity) for sand amended with RM and its analogues prepared in water or enriched in calcium revealed an intercept of 103 ± 54 ($p = 0.195$) and a significant slope of 45.1 ± 15.6 ($p = 0.0277$, $r^2 = 0.582$) **(a)**. Correlation between the yield stress and the TC ratio (total carbon ratio after and before dialysis $TC_{dial} / TC_{initial}$) for sand amended with water, RM and its analogues prepared in water revealed an intercept of -51.4 ± 24.9 ($p = 0.1751$) and a significant slope of 302 ± 40 ($p = 0.0169$, $r^2 = 0.9665$) **(b)**. Error bars represent standard deviations.

The interparticulate network of freeze-dried natural mucilage in sand varies between chia SM (Figure 8a), maize RM (Figure 8b) and wheat RM (Figure 8c). Chia SM had relatively thick and long strands covering the surface of the sand particles and extending over several particles. Maize RM formed thinner strands than chia SM but the inset shows that it also extended into the pore space. Interparticulate wheat RM was difficult to spot with the ESEM. Still, strands linking two particles were found and pictured on Figure 8c. In general, the quantity of polymeric material observed with the ESEM in amended sand decreased from chia SM, to maize RM and wheat RM. One reason could be the decreasing quantity of HMW compounds for these substances revealed by their TC ratio, as small molecules are not visible here.

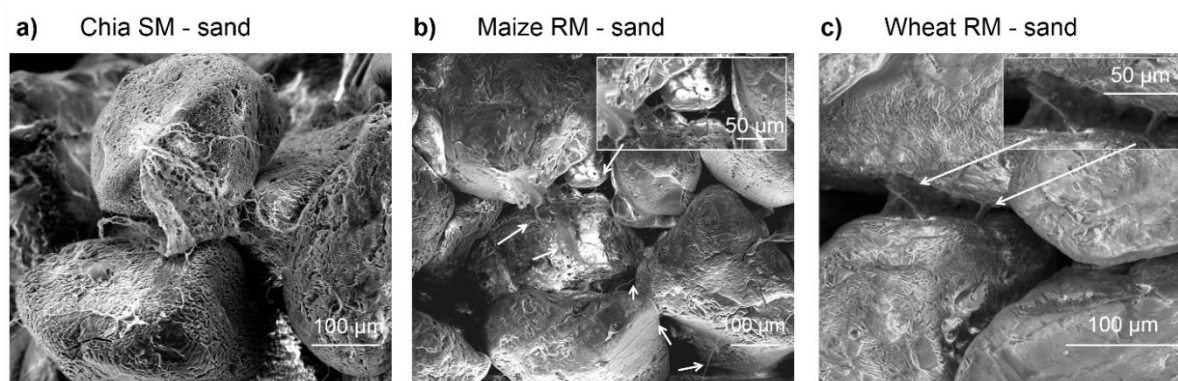


Fig. 8 ESEM pictures of sand amended with 0.5 wt% chia seed mucilage (SM) **(a)**, maize **(b)** and wheat root mucilage (RM) **(c)** prepared in water with a dry mass concentration of $1.25 \text{ g dry substance kg}^{-1}$ sand after shock-freezing with N_2 (l) and freeze-drying.

3.8 Various physico-chemical factors influence microstructural stability

3.8.1 How mucilage properties may compensate for surface roughness effects

The non-uniform shape and roughness of the sand particles severely affect particle-particle friction and increase soil microstructural stability. This explains the about two times higher yield stress for sand than for glass beads in water and glucose solution.

The very similar yield stress of untreated and glucose-treated samples shows that neutral species with the viscosity of water do not particularly affect soil microstructural stability. As suggested by hypothesis 4, the microstructural stability generally increases with the viscosity of the different substances. Yet, raw LMP stabilized sand stronger than chia SM, although its viscosity was lower. It is rather unlikely that LMP or chia SM interacted chemically differently with the inert silicate surface of the glass beads and sand. One explanation is that the higher amount of HMW material in LMP increased the amount of interparticle bridges between sand and LMP in comparison to sand and chia SM, thus increasing interparticle adhesion forces and soil particle interconnectivity (e.g., Markgraf et al. 2012; Buchmann and Schaumann 2017). The high amount of HMW substances could also lead to the formation of thicker bridges as observed for sand

treated with chia SM in comparison to sand treated with maize RM, which would also positively influence the microstructural stability.

Interparticulate strands were also observed in sand amended with wheat RM and may explain why wheat RM, despite its low viscosity, positively affected the microstructural stability of the glass beads as much as maize RM. The similar values for the microstructural stability of glass beads and sand amended with wheat RM indicate that the gluing effect of wheat RM compensated the missing stabilizing roughness effect in the glass beads but did not add to the stabilizing roughness effect in the sand. In contrast, the additional stabilizing effect measured for sand amended with maize RM could be due to the higher amount of polymeric material in maize RM than wheat RM.

3.8.2 Calcium treatment increases microstructural stability of all samples

The increase of the microstructural stability of LMP and wheat RM amended samples upon calcium addition results from the increase of the viscosity of LMP and wheat RM upon calcium addition. This is consistent with hypothesis 4, which predicted the increase of the yield stress with the increase of the viscosity of the amendment. In contrast to that, the microstructural stabilizing effect of maize RM and chia SM increased although their viscosity decreased upon calcium addition due to the contraction of the polymers. These polymeric clumps may be characterized by thicker polymer strands governed by strong molecular interactions. They would create micro-zones in the gel, which would locally possess a higher viscosity than the bulk gel. In the pore space, these micro-zones could increase the viscosity of the interparticulate gel and thus lead to an increased microstructural stability in the soil samples. An alternative explanation to this “micro-viscosity effect” of interparticulate gel could be that the Ca in maize RM and chia SM was distributed on the polymer surfaces and, thereby, available for bridges between mucilage and the surfaces of the glass beads and sand grains. These additional bridges may also have increased microstructural stabilization.

3.8.3 “Spider-web effect” due to hard boundaries in the pore space

The discrepancy between viscosity and stabilizing effect of the last examples indicates that interparticulate gels probably have different properties than bulk gels due to the constraint of hard boundaries. Only few studies have already dealt with the properties of gels under the constraint of hard boundaries, which is most probably due to the difficulty to characterize such gels. Marcombe et al. (2010) developed a theory showing that gels restricted by boundaries swell in an inhomogeneous way. Near the boundary between the gel and a solid surface, the gel is constrained, and the swelling ratio is lower than that of a free gel. This theory is consistent with the findings of an earlier study (Brax et al. 2019a), in which lower water mobility was measured in interparticulate chia SM than in freely swollen chia SM using $^1\text{H-NMR}$ relaxometry. The authors suggested that the polymer network in an interparticulate gel behaves similarly to a spider-web: Polymer strands spanned into the pore space increase the rigidity of the polymer network as opposed to unattached polymer strands in the free gel. In the present study, calcium bridges between chia SM or maize RM and the surface of the particles, and additional cross-linkage between polymer strands upon calcium addition could increase the spider-web effect and thus the microstructural stability.

3.9 How similar is root mucilage to its analogues and other soil-born gels

The amount of free uronic acid, amount of HMW material, calcium absorption and the change of the viscosity upon calcium absorption differed strongly between LMP and the two analyzed RM. LMP appears therefore as an inappropriate substance to model the chemical and physical properties of RM. Despite weaker gel properties and varying molecular composition of their HMW substances including the possible presence of proteins or amino acids and the almost absence of free uronic acid in maize RM, chia SM and maize RM seem to possess similar molecular interactions upon calcium enrichment. As chia SM has a higher viscosity than maize RM for the same dry mass concentration in gel, dilute chia SM may be an appropriate model substance to model the viscosity of maize RM. But the results presented here should not be generalized to all RM, as maize and wheat RM did not show the same behaviour upon calcium enrichment. Yet, further physico-chemical data characterizing the composition and type of polymer present in RM are needed to clear the mechanisms at play. For example, the protein content, the hydrodynamic volume, and the molecular weight of the polymer chains also affect viscosity and cation absorption (Axelos et al. 1991; MacDougall et al. 1996).

4. Conclusions

The present study highlights how plant roots and seeds may alter their closely surrounding environment by exudation of mucilage that in the presence of calcium significantly stabilizes the microstructure of mineral particles and by this improves storage, availability and transport of water, nutrients and air. The strong mucilage type specific differences especially in Ca absorption and changes in viscosity upon Ca treatment might be related to the respective plant specific environmental requirements. However, they complicate conclusions on the mechanisms of the observed microstructural stabilization. Thus, model substances cannot replace the analysis of a large variety of root mucilage types in order to better understand their structure-property relationship and classify their behaviour in soil. Moreover, amount and acidity of polysaccharides alone proved to be insufficient to describe structure-property relationships in different root and seed mucilage types. Indications suggest that also other substances e.g., proteins and lipids, are involved and a more specific HMW compounds characterization is needed to draw composition-property profiles. Furthermore, soil microstructural stabilization by mucilage was not directly related to the viscosity of the bulk gels. Thus, other possible mechanisms like a “spider-web effect” due to hard boundary constraints and a “micro-viscosity effect” of interparticulate gel, which increases the rigidity of the polymer network inside the pore space, have to be considered.

5. Literature

- Albalasmeh AA, Berhe AA, Ghezzehei TA (2013) A new method for rapid determination of carbohydrate and total carbon concentrations using UV spectrophotometry. *Carbohydrate Polymers* 97:253–261. doi: 10.1016/j.carbpol.2013.04.072
- Angers DA, Caron J (1998) Plant-induced Changes in Soil Structure: Processes and Feedbacks. *Biogeochemistry* 42:55–72. doi: 10.1023/A:1005944025343

- Axelos MAV, Lefebvre J, Qiu C-G, Rao MA (1991) CHAPTER 11 - Rheology of Pectin Dispersions and Gels. In: Walter RH (ed) *The Chemistry and Technology of Pectin*. Academic Press, San Diego, pp 227–250
- Bacic A, Moody SF, Clarke AE (1986) Structural Analysis of Secreted Root Slime from Maize (*Zea mays* L.). *Plant Physiol* 80:771–777
- Bacilio-Jiménez M, Aguilar-Flores S, Ventura-Zapata E, et al (2003) Chemical characterization of root exudates from rice (*Oryza sativa*) and their effects on the chemotactic response of endophytic bacteria. *Plant and Soil* 249:271–277. doi: 10.1023/A:1022888900465
- Barré P, Hallett PD (2009) Rheological stabilization of wet soils by model root and fungal exudates depends on clay mineralogy. *European Journal of Soil Science* 60:525–538. doi: 10.1111/j.1365-2389.2009.01151.x
- Benard P, Zarebanadkouki M, Carminati A (2018) Impact of Pore-Scale Wettability on Rhizosphere Rewetting. *Front Environ Sci* 6:. doi: 10.3389/fenvs.2018.00016
- Blumenkrantz N, Asboe-Hansen G (1973) New method for quantitative determination of uronic acids. *Analytical biochemistry* 54:484–489
- Brax M (2019) Influence of the physico-chemical properties of root mucilage and model substances on the microstructural stability of sand. Mendeley data v1. doi: 10.17632/x9nhyrfm42.1
- Brax M, Buchmann C, Schaumann GE (2017) Biohydrogel induced soil–water interactions: how to untangle the gel effect? A review. *J Plant Nutr Soil Sci* 180:121–141. doi: 10.1002/jpln.201600453
- Brax M, Buchmann C, Schaumann GE (2018) Effect of mucilage on water properties in the rhizosphere monitored by ¹H-NMR relaxometry. *Microporous and Mesoporous Materials* 269:47–50. doi: 10.1016/j.micromeso.2017.07.044
- Brax M, Köhne M, Kroener E, Schaumann GE (2019a) Potential of NMR relaxometry to unravel the properties of mucilage in several pore sizes. *Geoderma* 340:269–278. doi: 10.1016/j.geoderma.2019.01.013
- Brax M, Schaumann GE, Diehl D (2019b) Gel formation mechanism and gel properties controlled by Ca²⁺ in chia seed mucilage and model substances. *Journal of Plant Nutrition and Soil Science* 182:92–103. doi: 10.1002/jpln.201800430
- Buchmann C, Meyer M, Schaumann GE (2015) Characterization of wet aggregate stability of soils by H-NMR relaxometry. *Magn Reson Chem* 53:694–703. doi: 10.1002/mrc.4147
- Buchmann C, Schaumann GE (2017) Effect of water entrapment by a hydrogel on the microstructural stability of artificial soils with various clay content. *Plant Soil* 414:181–198. doi: 10.1007/s11104-016-3110-z
- Buchmann C, Schaumann GE (2018) The contribution of various organic matter fractions to soil–water interactions and structural stability of an agriculturally cultivated soil. *Journal of Plant Nutrition and Soil Science* 181:586–599. doi: 10.1002/jpln.201700437
- Capitani MI, Corzo-Rios LJ, Chel-Guerrero LA, et al (2015) Rheological properties of aqueous dispersions of chia (*Salvia hispanica* L.) mucilage. *Journal of Food Engineering* 149:70–77. doi: 10.1016/j.jfoodeng.2014.09.043
- Chang I, Im J, Lee S-W, Cho G-C (2017) Strength durability of gellan gum biopolymer-treated Korean sand with cyclic wetting and drying. *Construction and Building Materials* 143:210–221. doi: 10.1016/j.conbuildmat.2017.02.061
- Chang I, Im J, Prasadhi AK, Cho G-C (2015) Effects of Xanthan gum biopolymer on soil strengthening. *Construction and Building Materials* 74:65–72. doi: 10.1016/j.conbuildmat.2014.10.026

- Chen F, Arye G (2016) Effect of lipid/polysaccharide ratio on surface activity of model root mucilage in its solid and liquid states. pp EPSC2016-6099
- Chenu C (1995) Extracellular Polysaccharides: An interface Between Microorganisms and Soil Constituents. In: Environmental Impacts of Soil Component Interactions: Land Quality, Natural and Anthropogenic Organics. CRC Press, Boca Raton, FL, pp 217–233
- de Kerchove AJ, Elimelech M (2007) Formation of polysaccharide gel layers in the presence of Ca²⁺ and K⁺ ions: measurements and mechanisms. *Biomacromolecules* 8:113–121. doi: 10.1021/bm060670i
- Delattre C, Pierre G, Laroche C, Michaud P (2016) Production, extraction and characterization of microalgal and cyanobacterial exopolysaccharides. *Biotechnology Advances* 34:1159–1179. doi: 10.1016/j.biotechadv.2016.08.001
- Dubois M, Gilles KA, Hamilton JK, et al (1956) Colorimetric method for determination of sugars and related substances. *Analytical Chemistry* 28:350–356
- Dudev T, Lim C (2004) Monodentate versus Bidentate Carboxylate Binding in Magnesium and Calcium Proteins: What Are the Basic Principles? *J Phys Chem B* 108:4546–4557. doi: 10.1021/jp0310347
- Fatehi H, Abtahi SM, Hashemolhosseini H, Hejazi SM (2018) A novel study on using protein based biopolymers in soil strengthening. *Construction and Building Materials* 167:813–821. doi: 10.1016/j.conbuildmat.2018.02.028
- Fedeniuk RW, Biliaderis CG (1994) Composition and Physicochemical Properties of Linseed (*Linum usitatissimum* L.) Mucilage. *J Agric Food Chem* 42:240–247. doi: 10.1021/jf00038a003
- Filissetti-Cozzi TMCC, Carpita NC (1991) Measurement of uronic acids without interference from neutral sugars. *Analytical Biochemistry* 197:157–162. doi: 10.1016/0003-2697(91)90372-Z
- Fincher GB, Stone BA, Clarke AE (1983) Arabinogalactan-Proteins: Structure, Biosynthesis, and Function. *Annual Review of Plant Physiology* 34:47–70. doi: 10.1146/annurev.pp.34.060183.000403
- Flemming H-C, Wingender J (2010) The biofilm matrix. *Nat Rev Micro* 8:623–633. doi: 10.1038/nrmicro2415
- Goh KKT, Matia-Merino L, Chiang JH, et al (2016) The physico-chemical properties of chia seed polysaccharide and its microgel dispersion rheology. *Carbohydrate Polymers* 149:297–307. doi: 10.1016/j.carbpol.2016.04.126
- Grant GT, Morris ER, Rees DA, et al (1973) Biological interactions between polysaccharides and divalent cations: The egg-box model. *FEBS Letters* 32:195–198. doi: 10.1016/0014-5793(73)80770-7
- Holz M, Leue M, Ahmed MA, et al (2018) Spatial Distribution of Mucilage in the Rhizosphere Measured With Infrared Spectroscopy. *Front Environ Sci* 6:. doi: 10.3389/fenvs.2018.00087
- Knee EM, Gong F-C, Gao M, et al (2001) Root Mucilage from Pea and Its Utilization by Rhizosphere Bacteria as a Sole Carbon Source. *MPMI* 14:775–784. doi: 10.1094/MPMI.2001.14.6.775
- Koocheki A, Taherian AR, Bostan A (2013) Studies on the steady shear flow behavior and functional properties of *Lepidium perfoliatum* seed gum. *Food Research International* 50:446–456. doi: 10.1016/j.foodres.2011.05.002
- Kroener E, Holz M, Zarebanadkouki M, et al (2018) Effects of mucilage on rhizosphere hydraulic functions depend on soil particle size. *Vadose Zone Journal* 17:
- Kroener E, Zarebanadkouki M, Kaestner A, Carminati A (2014) Nonequilibrium water dynamics in the rhizosphere: How mucilage affects water flow in soils. *Water Resources Research* 50:6479–6495. doi: 10.1002/2013WR014756

- Lembre P, Lorentz C, Martino PD (2012) Exopolysaccharides of the Biofilm Matrix: A Complex Biophysical World. *The Complex World of Polysaccharides*. doi: 10.5772/51213
- Liebezeit G, Behrends B (2007) Determination of amino acids and carbohydrates. In: *Methods of Seawater Analysis*. Wiley-Blackwell, pp 541–555
- Lin K-Y, Daniel JR, Whistler RL (1994) Structure of chia seed polysaccharide exudate. *Carbohydrate Polymers* 23:13–18. doi: 10.1016/0144-8617(94)90085-X
- MacDougall AJ, Needs PW, Rigby NM, Ring SG (1996) Calcium gelation of pectic polysaccharides isolated from unripe tomato fruit. *Carbohydrate Research* 293:235–249. doi: 10.1016/0008-6215(96)00197-8
- Marcombe R, Cai S, Hong W, et al (2010) A theory of constrained swelling of a pH-sensitive hydrogel. *Soft Matter* 6:784–793. doi: 10.1039/B917211D
- Markgraf W, Watts CW, Whalley WR, et al (2012) Influence of organic matter on rheological properties of soil. *Applied Clay Science* 64:25–33. doi: 10.1016/j.clay.2011.04.009
- Mayer C, Moritz R, Kirschner C, et al (1999) The role of intermolecular interactions: studies on model systems for bacterial biofilms. *Int J Biol Macromol* 26:3–16
- McFeeters RF, Armstrong SA (1984) Measurement of pectin methylation in plant cell walls. *Anal Biochem* 139:212–217
- Mecozzi M (2005) Estimation of total carbohydrate amount in environmental samples by the phenol–sulphuric acid method assisted by multivariate calibration. *Chemometrics and Intelligent Laboratory Systems* 79:84–90. doi: 10.1016/j.chemolab.2005.04.005
- Medina-Torres L, Brito-De La Fuente E, Torrestiana-Sanchez B, Katthain R (2000) Rheological properties of the mucilage gum (*Opuntia ficus indica*). *Food Hydrocolloids* 14:417–424. doi: 10.1016/S0268-005X(00)00015-1
- Mezger, T. G. (2014) *The Rheology Handbook*. Vincentz Network, Hannover
- Mimmo T, Marzadori C, Gessa CE (2008) Does the degree of pectin esterification influence aluminium sorption by the root apoplast? *Plant Soil* 314:159–168. doi: 10.1007/s11104-008-9715-0
- Moody SF, Clarke AE, Bacic A (1988) Structural analysis of secreted slime from wheat and cowpea roots. *Phytochemistry* 27:2857–2861. doi: 10.1016/0031-9422(88)80676-9
- Morel JL, Andreux F, Habib L, Guckert A (1987) Comparison of the adsorption of maize root mucilage and polygalacturonic acid on montmorillonite homoionic to divalent lead and cadmium. *Biol Fert Soils* 5:13–17. doi: 10.1007/BF00264339
- Morel JL, Mench M, Guckert A (1986) Measurement of Pb²⁺, Cu²⁺ and Cd²⁺ binding with mucilage exudates from maize (*Zea mays* L.) roots. *Biol Fert Soils* 2:29–34. doi: 10.1007/BF00638958
- Naveed M, Brown LK, Raffan AC, et al (2017) Plant exudates may stabilize or weaken soil depending on species, origin and time. *Eur J Soil Sci* 68:806–816. doi: 10.1111/ejss.12487
- Orts William J., Roa-Espinosa Aicardo, Sojka Robert E., et al (2007) Use of Synthetic Polymers and Biopolymers for Soil Stabilization in Agricultural, Construction, and Military Applications. *Journal of Materials in Civil Engineering* 19:58–66. doi: 10.1061/(ASCE)0899-1561(2007)19:1(58)
- Osborn HMI, Lochey F, Mosley L, Read D (1999) Analysis of polysaccharides and monosaccharides in the root mucilage of maize (*Zea mays* L.) by gas chromatography. *Journal of Chromatography A* 831:267–276. doi: 10.1016/S0021-9673(98)00935-2
- Read DB, Bengough AG, Gregory PJ, et al (2003) Plant roots release phospholipid surfactants that modify the physical and chemical properties of soil. *New Phytologist* 157:315–326. doi: 10.1046/j.1469-8137.2003.00665.x

- Read DB, Gregory PJ (1997) Surface tension and viscosity of axenic maize and lupin root mucilages. *The New Phytologist* 137:623–628
- Read DB, Gregory PJ, Bell AE (1999) Physical properties of axenic maize root mucilage. *Plant and Soil* 211:87–91. doi: 10.1023/A:1004403812307
- Rubinstein M, Colby RH, Dobrynin AV, Joanny J-F (1996) Elastic Modulus and Equilibrium Swelling of Polyelectrolyte Gels. *Macromolecules* 29:398–406. doi: 10.1021/ma9511917
- Salgado-Cruz M de la P, Calderón-Domínguez G, Chanona-Pérez J, et al (2013) Chia (*Salvia hispanica* L.) seed mucilage release characterisation. A microstructural and image analysis study. *Industrial Crops and Products* 51:453–462. doi: 10.1016/j.indcrop.2013.09.036
- Skouri R, Schosseler F, Munch JP, Candau SJ (1995) Swelling and Elastic Properties of Polyelectrolyte Gels. *Macromolecules* 28:197–210. doi: 10.1021/ma00105a026
- Timilsena YP, Adhikari R, Kasapis S, Adhikari B (2015) Rheological and microstructural properties of the chia seed polysaccharide. *International Journal of Biological Macromolecules* 81:991–999. doi: 10.1016/j.ijbiomac.2015.09.040
- Timotiwiu PB, Sakurai N (2002) Identification of mono-, oligo-, and polysaccharides secreted from soybean roots. *J Plant Res* 115:77–85. doi: 10.1007/s102650200012
- Watanabe T, Misawa S, Hiradate S, Osaki M (2008) Characterization of root mucilage from *Melastoma malabathricum*, with emphasis on its roles in aluminum accumulation. *New Phytologist* 178:581–589. doi: 10.1111/j.1469-8137.2008.02397.x
- Watt M, McCully ME, Jeffree CE (1993) Plant and bacterial mucilages of the maize rhizosphere: Comparison of their soil binding properties and histochemistry in a model system. *Plant Soil* 151:151–165. doi: 10.1007/BF00016280
- Winter, B. (2013). Linear models and linear mixed effects models in R with linguistic applications. arXiv:1308.5499. [<http://arxiv.org/pdf/1308.5499.pdf>]
- Zhang B, Hallett PD, Zhang G (2008) Increase in the fracture toughness and bond energy of clay by a root exudate. *European Journal of Soil Science* 59:855–862. doi: 10.1111/j.1365-2389.2008.01045.x
- Zickenrott I-M, Woche SK, Bachmann J, et al (2016) An efficient method for the collection of root mucilage from different plant species—A case study on the effect of mucilage on soil water repellency. *J Plant Nutr Soil Sci* 179:294–302. doi: 10.1002/jpln.201500511

7. SYNTHESIS AND CONCLUSIONS

7.1. Possibilities, limits and outlook of mucilage detection in soil with ^1H NMR relaxometry

There is a range of methods that enable to characterize the effect of gel phases on soil properties. Those methods are listed in the review paper (chapter 2). Still, the detection of these gel phases remains complicated and no method is alone sufficient to detect and characterize these gel phases in soil. Reason for this is the low attenuation contrast between gel-associated water and water confined in soil pores (chapter 2). In this work, a methodical detection of gel phases in soil with ^1H NMR relaxometry was investigated and a validation of the results obtained is proposed by the combination of ^1H NMR relaxometry with imaging techniques (chapters 3-4).

Presence of gel phases originating from microbial or from plant origin in soil pores is traduced by a shift of the relaxation time to shorter values (*Jaeger et al.*, 2006; *Sanderlin et al.*, 2013). As a result, NMR relaxometry methods enabling the distinction of gel phases in soil are the ratio of the longitudinal by the transverse relaxation time (*Jaeger et al.*, 2010) and the subtraction of the transverse and longitudinal relaxation rate (chapter 3). For the same pore size, these methods give different values for pores filled with water and pores filled with gel. Yet, rearrangement of the mucilage network according to the pore sizes in soil and to mucilage concentration complicates the quantification of mucilage in porous soil. A solution is to characterize the various arrangements of the gel polymer network in the pore space with the ESEM after shock-freezing and freeze-drying of the samples (chapter 4). As a result, a first qualitative assessment can be made on the effect of the rearrangement of the polymer network on the NMR relaxation times and rates (chapter 4).

Still, identification of gel phases in undefined soil samples remains uncertain as various parameters (pore size, paramagnetic species in the soil solution) can also induce shifts of the relaxation time, which themselves affect the ratio or the subtraction of the aforementioned relaxation parameters. Notably, the exudation of mucilage as a gel may affect the size of soil pores: Swelling of soil organic matter results in an expansion of small pores (*Schaumann et al.*, 2005; *Todoruk et al.*, 2003), what renders the evaluation of the pore size with ^1H NMR relaxometry unreliable (*Meyer et al.*, 2018). A solution to overcome this problem is the combination of ^1H NMR relaxometry with *in-situ* imaging techniques measuring the pore size such as μCT (chapter 4). It still requires a thorough method development, but the relaxation time distribution obtained with ^1H NMR relaxometry can be compared with the pore size distribution obtained with μCT (Figure 7.1). In the future, each relaxation time range could be associated to exact corresponding pore size range measured with μCT . The ratio or subtraction of relaxation times or rates attributed to each pore size range would then give information about the presence of gel phases (Figure 7.1).

In real soils, environmental factors such as swelling of soil particles, ions from the soil solution possibly affecting the properties of interparticulate gel or paramagnetic impurities further complicate the detection of gel phases as they additionally affect the relaxation of water protons. A solution to detect gel phases in such soils is to measure the self-diffusion coefficient of water D additionally to the relaxation time (Figure 7.1).

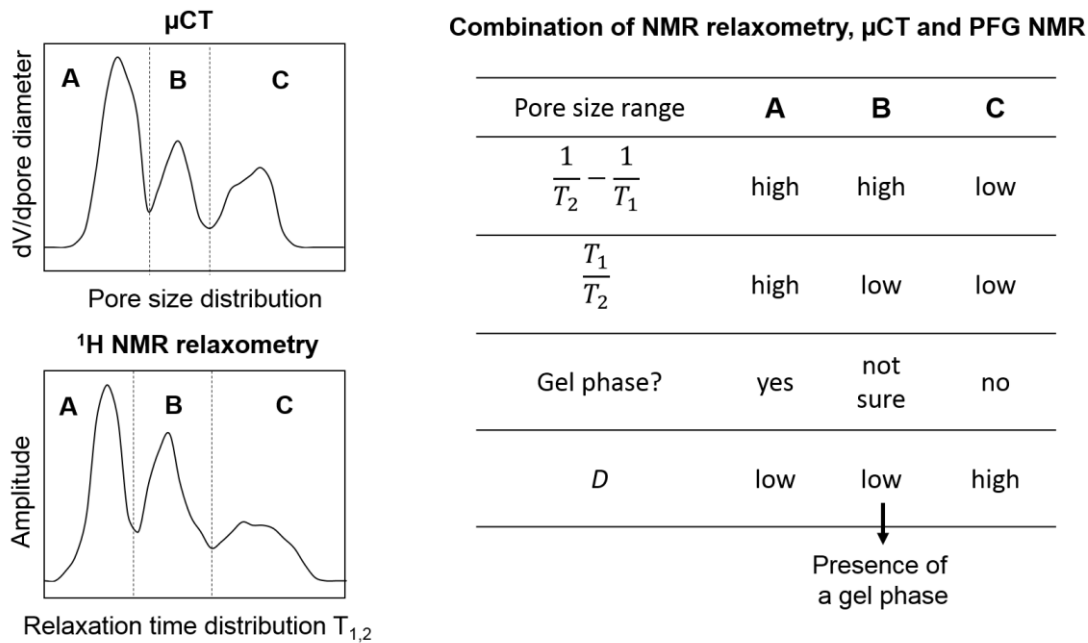


Figure 7.1. Combination of ^1H NMR relaxometry, μCT and PFG NMR to detect gel phases in soil.

D measured with pulsed field gradient (PFG) NMR characterizes the translational mobility of the water molecules, which is also affected by gel phases in soil (Jaeger *et al.*, 2010). Our measurements of the self-diffusion coefficient of water in mucilage and in mucilage-glass beads mixtures (Annex chapter 8.3) were little promising, as they did not differ strongly from those of water and water-glass beads mixtures. The reason is experimental as too short values were taken for the diffusion time Δ : With our instrument, measurement of D with values of Δ greater than 50 ms did not provide acceptable results. Study of D in biohydrogels require a very long Δ from 10 to 1000 ms (Götz and Hinrichs, 2008). Already exciting results have been obtained with Δ values between 200 and 500 ms from D - T_2 correlation measurements of biofilm growth in porous media (Herrling *et al.*, 2017; Vogt *et al.*, 2013). The combination of both parameters enhances the quality of the information, as pure water could be distinguished from biofilm in undefined porous media. Still, the authors emphasize the need of further development of this correlation method for reliable detection of biofilm in soil.

7.2. A stepwise approach to explain the gel effect: from the mucilage polymers to soil physical properties

Figure 1.4 in the introduction presented the stepwise strategy of the MUCILAGE project to clarify the relevance of mucilage for root water uptake. The experimental studies performed in this thesis aimed at resolving the following steps: **a** properties of “free” mucilage, **b** gel properties of mucilage in the pore space and partly **c** consequences on soil physical properties. In Table 7.1, the results are summarized in an upscaling design. The factors identified in this thesis as affecting the gel effects of mucilage can be of physical nature (soil particle size, hard boundary constraint in chapters 3,4,6) and of chemical nature (gel concentration, amount of free uronic acids and of HMW material, presence of calcium in chapters 5,6). They can have consequences on the molecular (governed by chemical forces) and supramolecular scale (governed by chemical and physical forces) on the properties of mucilage. Molecular consequences relate to interactions

such as a high Ca absorption due to a high content of free uronic acids of the polymer (chapter 5). Supramolecular structures describe several polymer molecules interacting via chemical or physical forces. Consequences on the supramolecular structure can be the rearrangement of the polymer chains due to a physical constraint such as soil pore size (chapter 4), or due to a chemical factor, for example the coiling of the polymer chains due to intermolecular charge-charge repulsion coming from the presence of Ca as studied in chapters 5 and 6. Hence, molecular properties of the polymer chains, their supramolecular arrangement and the physical properties of the resulting gel are closely bound: A high uronic content leads to a plurality of calcium bridges between the polymer chains, which can increase viscosity and water retention (chapter 5). Further, although if it was not studied here, the ability of polymer chains to rearrange according to soil particle size or to the concentration of mucilage as found in chapter 4 probably depends on the elasticity of the network, which itself varies according to the chemical properties of the polymer. Indeed, a gel, whose formation mechanism relies on Ca bridges between polymers with high amounts of uronic acids, is stiff and brittle in comparison to a gel, whose polymers are linked through less strong intermolecular interactions (Van der Waals forces, hydrogen bonding).

In Table 7.1, the various factors listed in the first column and their molecular and supramolecular consequences reported in the second column affect the properties of the free gel and of the interparticulate gel network figuring in the third column. Those include strength, microviscosity and organization of the polymer network in the interparticulate space. The properties of interparticulate gels are specifically addressed in the next subchapter 7.3. Variations of soil water mobility (characterized by longitudinal and transversal relaxation) and of soil microstructural stability result from the various properties of the interparticulate gel network and are reported in column 4 (chapters 3-4-6). Further soil properties affected by the gel effect are investigated in several other studies and summarized in column 5, in particularly in the studies published by our project partners. For example, in addition to the decrease of the water mobility measured for all particle sizes, the increasing mucilage concentration decreases the saturated hydraulic conductivity of sandy soil (*Kroener et al.*, 2014). The additional resistance to water flow inside the pores is attributed to the increased frictions between the water molecules and the mucilage network (*Kroener et al.*, 2018). Thus, the upscaling presented in Table 7.1 from right to left illustrates the importance to clear processes at play in gel at the molecular scale to fully understand the resulting “macroscopic” soil properties.

Table 7.1. Summary of the factors affecting the various gel effects of mucilage in the pore space, and how they affect soil physical properties in the rhizosphere.

Factors affecting the gel effects of mucilage (<i>example</i>)	Molecular and supramolecular consequences	Properties of free gel and of IGN*	Gel effect on soil properties found in this work	Further soil properties affected by the gel effect
Soil particle size (<i>type of soil</i>)	Rearrangement of polymer chains (Chap.4)	↑ Strength of IGN for middle-sized particles, ± Organization of IGN in the pore (Chap.4)	↓ Water mobility for middle-sized particles (Chap.4)	↓ Hydraulic conductivity for middle-sized particles, ± Water retention (<i>Kroener et al., 2018</i>)
Hard boundary constraint (<i>soil pore walls</i>)	IGN grips at the surface of the particles (Chap.4-6)	↑ Strength of IGN as a contrast to free gel, Unhomogeneous distribution of IGN in the pore space (Chap.4-6)	↓ Water mobility (Chap.3-4), ↑ Friction between soil particles and ↑ Microstructural stability (Chap.6)	± Mucilage distribution during drying (<i>Benard et al., 2018</i>)
↑ Gel concentration (<i>distance from roots, plant species...</i>)	↑ Polymer network, Rearrangement of polymer chains, ↑ Frictions between polymer chains (Chap.3-4)	↑ Strength of IGN (Chap.4)	↓ Water mobility (Chap.4)	↓ Hydraulic conductivity, ↑ Water retention (<i>Kroener et al., 2014</i>), ↓ Pore-scale wettability (<i>Benard et al., 2018</i>)
↑ Free uronic acids (<i>plant species, root or seed mucilage</i>)	Gel formation mechanism, ↑ Ca adsorption, ± Viscosity and ± Water retention of free gel (Chap.5-6)	± Viscosity and ± Water retention of free gel, ± Strength of IGN, ± Microviscosity of IGN (Chap.5-6)	± Microstructural stability (Chap.6)	↑ Affinity with clay materials, pH dependent (<i>Morel et al., 1987</i>)
↑ HMW material (<i>plant species, root or seed mucilage</i>)	↑ Polymeric network, ↑ Frictions between polymer chains, (Chap. 6)	↑ Viscosity of free gel, ↑ Strength of IGN, ↑ Microviscosity of IGN (Chap. 6)	↑ Microstructural stability (Chap. 6)	Indirectly linked with measured viscosity, ↑ Microstructural stability (<i>Naveed et al., 2017</i>)
Presence of Ca (<i>soil solution, soil particle surface</i>)	± Ca bridges between polymer chains, ± Intermolecular charge-charge repulsion (Chap. 5-6)	± Viscosity of free gel, ↑ Microviscosity and ↑ strength of IGN, Ca bridges between particle surface and polymer (Chap. 5-6)	↑ Microstructural stability (Chap. 6)	Not found

* IGN: Interparticulate gel network; ↓ decreases; ↑ increases; ± affects but depends on further parameters

In particularly, the influence of the chemical properties of mucilage on its chemical interactions with soil particles belongs in Table 7.1 and should be given more scientific attention in the future. Indeed, studies concerning soil amendment with non-ionic soil-borne polymers such as xanthan, dextran or scleroglucan report various results in comparison to studies evaluating soil properties after amendment with PGA (*Chenu and Guérif, 1991; Czarnes et al., 2000*). The authors attribute these differences to various bond energies between polymers and soil particles. Still, the binding mechanisms between mucilage and soil particles are unclear. Several studies considered that the binding of mucilage to soil particles occurs similarly to PGA through ionic binding with the deprotonated uronic acids of mucilage, thus leading to edge-face bonding with clay particles (*Mikutta et al., 2004; Peng et al., 2011; Zhang et al., 2008*). The little content of uronic acid in mucilage associated to their partial esterification may unvalidate this mechanism. Binding of soil particles to the hydroxyl groups of terminally branched neutral sugars in mucilage suggested by Morel et al. (1987) and Watt et al. (1993) may be an acceptable mechanism. Consequences of the binding mechanism of mucilage on soil physical properties are also unclear. For polymers making non-ionic chemical bounds with soil particles, physical binding through enmeshing of soil particles within interparticulate polymer network may be more relevant than chemical binding for their contribution to soil properties. In this case, the effectiveness of mucilage to modify soil properties is likely to mostly reside in properties such as size, conformation of the polymers, hydration and viscosity of the gel (*Akhtar et al., 2018*).

7.3. Bringing together the three main interparticulate gel properties

As a contrast to bulk or free gel, this thesis showed that gel properties vary for interparticulate gel located in small soil pores. Interparticulate gel should be considered as micro-zones of gel distributed in the pores with specific properties. As a result, it is necessary to consider the properties of interparticulate gel in contrast to those of free gel to assess the gel effect on soil properties. Out of the findings in chapters 5 and 6 and the summary in Table 7.1, three main interparticulate gel properties are identified: the spider-web effect, the polymer network effect and the microviscosity effect (Table 7.2).

Table 7.2. The three interparticulate gel properties in the pore space and their description.

Interparticulate gel properties	Description	Acknowledged consequences
Spider-web effect	Restriction of elongation of the polymer chains due to grip of the polymer network to the surface of soil particles	↑ Water retention ↓ Water mobility, ↓ Saturated hydraulic conductivity ↑ Microstructural stability (Chap. 4-6) (<i>Kroener et al., 2018</i>)
Polymer network effect	Organization of the network in the pore space dependent on the environment	± Water mobility ± Saturated hydraulic conductivity (Chap. 4) (<i>Kroener et al., 2018</i>)
Microviscosity effect	Increased viscosity of gel micro-zones	↑ Microstructural stability (Chap. 6)

Spider-web effect

According to the spider-web effect found in chapter 4, the walls of soil particles restrict the elongation of the polymer strands and serve as a frame for the polymer network. This way, interparticulate polymer network can be compared to a spider-web attached to tree branches or grasses, whose mechanical properties combine high tensile strength with extensibility (Gosline *et al.*, 1986). This enables the spider-web to absorb a large amount of energy before breaking. Without this frame, the spider-web would collapse and lose these properties. In soil, the spider-web effect also increases the strength of the polymer network of interparticulate gel as a contrast to free gel (chapter 4).

As mentioned in the last subchapter, the binding mechanism between polymer and soil particle is unclear for mucilage. Stronger connections could result from Ca bridges between a negative-charged particle surface, divalent calcium and negative-charged or negatively polarized mucilage molecules. Weak connections could result from electrostatic forces between the surface and the mucilage molecule. The forces controlling the grip of the polymer network on the soil particle surface may affect the strength of the spider-web effect. For example, stronger bridges would strengthen the spider-web effect and probably enhance the already altered soil physical properties.

The spider-web effect has several consequences on soil physical properties. The frictions between the network and the water molecules decrease the water mobility in the pores, decrease the saturated hydraulic conductivity and increase water retention. The tensile strength of the network increases the microstructural stability of soil particles. The diffusion of solutes being reduced in gels (Muhr and Blanshard, 1982), a further little explored consequence of the spider-web effect may be to affect the transport of solutes from and to the roots by decreasing the coefficient of diffusion.

Polymer network effect

The effect of the available pore space on the organization of the polymer network was named the polymer network effect in chapter 4. The polymer network can organize itself to form thick or thin strands, small or big pores and to be continuous or not from one side of the pore to the other. The variability of such organization is enabled by the flexibility of the polymer network, which can rearrange according for example to the space it is allocated in the pore.

As a consequence, the extent of gel-induced soil properties varies with the organization of the polymer network. The polymer network effect can explain the variation of the water mobility and of the hydraulic conductivity in function of soil particle size for the same concentration of mucilage: The water mobility is stronger hindered in middle pores (particle size between 150 and 350 μm) than in large and small pores (particle size over 2000 μm and smaller than 55 μm respectively) (chapter 4). Similarly, the saturated hydraulic conductivity is lower for fine sand (particle size between 60 and 500 μm) than for coarse and silty soil (particle size >500 μm and <20 μm respectively) (Kroener *et al.*, 2018). One explanation may come from the size of the meshes formed by the polymer network, which can be measured by imaging the polymer network with the ESEM after shock-freezing and freeze-drying of the samples. In free or bulk freeze-dried mucilage, the meshes are in the range of 5 to 10 μm (Annex chapter 8.3). In comparison, the pore size formed by glass beads with a particle diameter of 350 μm measured by μCT is between 30 and 100 μm (chapter 4, annex chapter 8.4). Thus, in soil pores larger than 10 times the mesh size formed by the polymer network in the free gel, the organization of the interparticulate polymer

network may be little affected by the pore size and the constraint of hard boundaries. In soil pores smaller than 3 times the mesh size formed by the polymer network in the free gel, the low concentration of polymer per pores and possibly repulsion forces between the polymer strands may prevent the organization of the polymer into a network. In soil pores between 3 and 10 times the mesh size formed by the polymer network in the free gel, the polymer network may rearrange to form a network with smaller meshes. As a result, the water mobility and the saturated hydraulic conductivity are stronger affected in the middle-sized pores, as the increased strength and rigidity of the polymer network increase friction forces with water molecules.

Microviscosity effect

The microviscosity effect discussed in chapter 6 suggests that the viscosity of free gels is not equivocal to the viscosity of micro-zones in the gels as the polymer chains are differently organized in interparticulate gel in contrast to free gel. Measurement of this microviscosity is a challenge as it may differ on the scala at which the material is characterized. As an example, polymer chains in maize root mucilage and chia seed mucilage coil and contract upon calcium addition (chapter 6). The resulting viscosity of the free gel decreases due to a drop of frictions forces between all polymer chains. Yet, the viscosity of the micro-zones in the gel may rather be affected by the strong interactions between polymer chains and calcium and thus increases. To test the microviscosity effect, microscale viscosity measurements realized with the atomic force microscope (AFM) should be compared with standard macroscopic viscosity measurements of the free gel.

Finally, the microviscosity effect could be related to the spider-web effect, as an increased tensile strength of the polymer network probably induces an increase of the microviscosity. As a result, increased microviscosity and tensile strength of interparticulate gel should result in a higher microstructural stability of the soil particles. Further consequences of the microviscosity effect on soil physical properties have not been investigated until now, but they may be similar to those of the spider-web effect.

7.4. Significance of the physico-chemical composition of mucilage on the rhizosphere microstructural and hydraulic properties

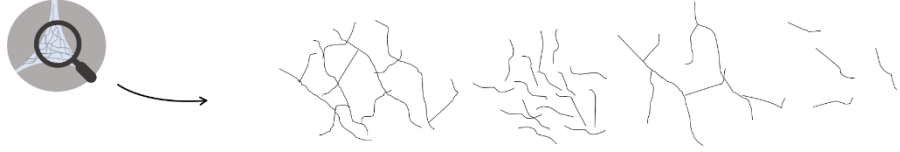
Role of the physico-chemical composition of mucilage for soil moisture dynamics

Figure 7.2 schematizes the possible relationships between the polymer networks of mucilage, the physico-chemical properties of the mucilage polymers, the properties of the corresponding gels and the gel effect on the physical properties of the rhizosphere. On the contrary to what has been hypothesized in the literature (*Gessa and Deiana, 1992; Mimmo et al., 2008; Peng et al., 2011*), the gel formation mechanisms of chia seed and of root mucilage are not only governed by specific ionic interactions between calcium and deprotonated uronic acids as described by the egg-box model for PGA (chapter 5). It rather relies on nonspecific interactions between the polymer chains and the ions of the surrounding solution, as well as on non-ionic electrostatic interactions between the polymer chains leading to chain entanglement (chapter 5). As schematized in Figure 7.2, the gel effect of mucilage are therefore suspected to depend strongly on the amount of polymer in mucilage as well as on the length and configuration of the chains.

The extent to which interparticulate gel properties affect soil physical properties, in particularly soil microstructural stability, varies strongly with the physico-chemistry of mucilage (chapter 6).

Indeed, the mechanical properties of the interparticulate polymer network of winter wheat and maize root mucilage, chia seed mucilage and low-methoxy pectin are greatly affected by an increase of the quantity of HMW material in these substances (chapter 6). The length of the polymer chains and the strength of interactions within the network characterized by the gel formation mechanism are further factors affecting gel properties (*Martin, 1971*), and are thus suggested to change interparticulate gel properties and affect the gel effect on soil physical properties (chapter 6). Still, these factors have been little studied until now.

Possible polymer networks of mucilage



Physico-chemical properties of the mucilage polymers	Length polymer chains	++	-	++	-
	HMW content	++	++	-	-
	Interactions strengthes	++	+	+	-
Interparticulate gel properties	Spider-web effect	++	+	+	-
	Polymer network effect	++	+	-	-
	Microviscosity effect	++	+	+	-
Physical properties of the rhizosphere	Water content	++	+	+	-
	Water retention	++	++	+	-
	Hydraulic conductivity	--	-	-	-
	Microstructural stability	++	+	+	-

Figure 7.2. Potential influences of various physico-chemical properties of mucilage on soil physical properties.

Chapter 4 demonstrated the relationships between the spider-web effect, the polymer network effect and soil water mobility and suggested that the variations measured for the water mobility explain the increased water retention and decreased saturated hydraulic conductivity measured in Kroener et al. (2018). Although if chapter 6 outlines the relationships between polymer network, physico-chemical properties of mucilage, microviscosity effect and microstructural stability of the rhizosphere, these connections remain to be done for rhizosphere water content, water retention and hydraulic conductivity.

To link the results found in this work with previsions on root water uptake, interparticulate gel properties could be integrated into numerical simulations describing water moisture dynamics. For example, the Ohnesorge number (equation 7.1) describes the break-up of liquid jets and depends on the viscosity, density and surface tension of the liquid.

$$O_h = \frac{\mu}{\sqrt{\rho\sigma r}} \quad 7.1$$

As soil dries, mucilage becomes stiffer and its viscosity determines the spatial configuration of the liquid phase (*Benard et al., 2018*). Surface tension opposes to stretching and as drying progresses, it eventually causes the break up of the liquid bridge. Viscosity opposes to the stretching of the bridge an prevents break up. Therefore, according to the Ohnesorge number, mucilage increased viscosity and smaller surface tension in comparison to water contribute to

the perennity of the hydraulic bridge connecting roots and soil particles upon drying thus preventing or delaying root desiccation (*Benard et al.*, 2018). For a better understanding of rhizosphere moisture dynamics of various plants, the Ohnesorge number should be calculated for various root mucilage by taking into account the interparticulate effects modifying the properties measured for the free gels. In the future, this could lead to a better engineering and management of the culture of crops under water scarcity.

From the point of view of the plant

The final interdisciplinary aim of “mucilage research” is to clear the relationships between the chemico-physical properties of mucilage, its effect on soil and the needs of the plants. If it is to act as an efficient water reservoir as suggested by Carminati et al. (2011), root mucilage needs to engender a strong spider-web effect, which resists environmental changes, as suggested by Table 7.2 and Figure 7.2. Additionally, root mucilage needs a high water retention capacity to act as a water reservoir. The high water retention measured for chia seed mucilage over several Ca concentrations (chapter 5) hence suggests that if it possesses similar properties, the gel capsule formed by mucilage at the root tip would survive under various soil solutions.

A further function of mucilage for the plant could be to enhance the diffusion of nutrients to the roots due to the higher water content of the rhizosphere in comparison to the bulk soil over several matric potentials (*Kroener et al.*, 2014; 2018). In this case, the chemistry of mucilage may also play a role. Whereas free uronic acids immobilize metal cations through specific ionic interactions (*Mimmo et al.*, 2003), nonspecific ionic interactions between ions and the mucilage molecule may favorize the diffusion of nutrients across the interface through the cell membrane (*Mimmo et al.*, 2008).

An exciting research field, which requires close interdisciplinary work, is the attribution of the properties of various mucilage to the special needs of their respective plants. Indeed, mucilage reveals itself quite plural in its properties and its gel effects: Chapter 6 outlines the various properties of maize and winter wheat mucilage; Barley rhizodeposits were shown to behave as surfactants by drying the rhizosphere at smaller suctions, whereas maize root deposits behave as hydrogels that hold water in the rhizosphere (*Naveed et al.*, 2019). Why would mucilage of various plant species have various properties, if it is not to answer to the special needs of their plant? As one possible hint, viscosity could be related to the plant physiological properties. For example, maize is a plant which grew originally in the desert. The high viscosity of maize root mucilage could have served the needs of a plant growing in a dry environment as it enhances soil-root contact over negative water potentials (*Naveed et al.*, 2019).

7.5. Soil-born gel phases, a strategy of nature?

To be relevant for soil properties, the gel effect and thus mucilage should persist over several days. Yet, information about the becoming of mucilage in the rhizosphere is missing. As it is mostly composed of sugars, mucilage is an attractive source of energy for bacteria and may be quickly degraded. It is not clear how fast mucilage is mineralized by microorganisms: *in vitro* experiments showed that the HMW compounds in mucilage were used as sole C source for growth of rhizosphere bacteria (*Knee et al.*, 2001). High soil moisture leads to nearly total degradation of mucilage after 15 days, whereas drought suppresses mucilage mineralization (*Ahmed et al.*, 2018). Still, mucilage being relatively quickly degraded in real soil, the study of mucilage decomposition and its effect on pore-scale processes is relevant for soil properties and

root-water uptake. For example, the increase of microbial biomass in soil resulting from mucilage degradation (*Ahmed et al.*, 2018) could lead to the replacement of the gel phase “mucilage” by a bacterial biofilm or EPS, which also forms a gel phase. The question is then how EPS-induced gel effects do vary in contrast to those induced by mucilage.

A recent hypothesis is that the gel properties of mucilage and EPS are similar, so that both gels induce similar pore-scale processes (chapter 5; *Benard et al.*, 2018). The gel formation mechanism of EPS also relies on electrostatic and nonspecific interactions (*Sutherland*, 2001). EPS have a large water holding capacity, they alter soil matrix structure and connectivity of pore space and modify the surface tension and viscosity (*Zheng et al.*, 2018). The high viscosity of EPS and mucilage is responsible for the formation of thin filaments and interconnected thin lamellae that span through the soil matrix maintaining the continuity of the liquid phase across the pore space even during severe drying (*Benard et al.*, 2019; *Volk et al.*, 2016). Although not to the same extent, EPS and mucilage have comparable gel effects on soil properties as similarly to mucilage, EPS increases soil structural stability (*Watt et al.*, 1993), soil water content and soil water retention (*Chenu*, 1993; *Rosenzweig et al.*, 2012), and decreases saturated hydraulic conductivity (*Baveye et al.*, 1998; *Volk et al.*, 2016). EPS also induces water repellency once dried, depending on the bacterial strain (*Schaumann et al.*, 2007).

Additionally to roots and bacteria, earthworms and fungi also exude a viscous polysaccharidic material, but which has been little researched until now (*Caesar-Tonthat*, 2002; *Zhang et al.*, 2016). As the gel effect comes from the presence of HMW material in the form of polysaccharides in mucilage and EPS, the polysaccharidic exudates of earthworms and fungi may also have a gel effect similar to mucilage and EPS on soil properties. Therefore, the production of gel phases by various entities in soil may be a strategy of nature to modulate soil physical properties where and when needed. Although the extent of the gel effect may vary according to the soil types, exuding species and further environmental conditions, the gel effect may be general for soil-born exudates showing gel properties. As a result, the concept of gel effect induced by mucilage in the pore space and its effect on soil properties studied for chia seed mucilage, low-methoxy pectin, maize and winter wheat root mucilage on glass beads and sand (chapters 3-4-5-6) may be applied for all soil-born gel phases. This way, the concepts and tools developed in this thesis and reported in the literature bring us a step forward to answer further questions concerning the gel effect on soil properties.

8. REFERENCES

- Ahmed, M. A., Kroener, E., Holz, M., Zarebanadkouki, M., Carminati, A. (2014): Mucilage exudation facilitates root water uptake in dry soils. *Funct. Plant Biol.* 41, 1129.
- Ahmed, M. A., Holz, M., Woche, S. K., Bachmann, J., Carminati, A. (2015): Effect of soil drying on mucilage exudation and its water repellency: a new method to collect mucilage. *J. Plant Nutr. Soil Sci.* 1–4.
- Ahmed, M. A., Sanaullah, M., Blagodatskaya, E., Mason-Jones, K., Jawad, H., Kuzyakov, Y., Dippold, M. A. (2018): Soil microorganisms exhibit enzymatic and priming response to root mucilage under drought. *Soil Biol. Biochem.* 116, 410–418.
- Akhtar, J., Galloway, A. F., Nikolopoulos, G., Field, K. J., Knox, P. (2018): A quantitative method for the high throughput screening for the soil adhesion properties of plant and microbial polysaccharides and exudates. *Plant Soil* 428, 57–65.
- Albalasmeh, A. A., Ghezzehei, T. A. (2014): Interplay between soil drying and root exudation in rhizosheath development. *Plant Soil* 374, 739–751.
- Almdal, K., Dyre, J., Hvidt, S., Kramer, O. (1993): What is a 'gel'? *Makromol. Chem. Macromol. Symp.* 76, 49–51.
- Andry, H., Yamamoto, T., Irie, T., Moritani, S., Inoue, M., Fujiyama, H. (2009): Water retention, hydraulic conductivity of hydrophilic polymers in sandy soil as affected by temperature and water quality. *Journal of Hydrology* 373, 177–183.
- Bacic, A., Moody, S. F., Clarke, A. E. (1986): Structural Analysis of Secreted Root Slime from Maize (*Zea mays* L.). *Plant Physiol.* 80, 771–777.
- Bacilio-Jiménez, M., Aguilar-Flores, S., Ventura-Zapata, E., Pérez-Campos, E., Bouquelet, S., Zenteno, E. (2003): Chemical characterization of root exudates from rice (*Oryza sativa*) and their effects on the chemotactic response of endophytic bacteria. *Plant Soil* 249, 271–277.
- Bais, H. P., Weir, T. L., Perry, L. G., Gilroy, S., Vivanco, J. M. (2006): The role of root exudates in rhizosphere interactions with plants and other organisms. *Annu. Rev. Plant Biol.* 57, 233–266.
- Barré, P., Hallett, P. D. (2009): Rheological stabilization of wet soils by model root and fungal exudates depends on clay mineralogy. *European Journal of Soil Science* 60, 525–538.
- Bayer, J. V., Jaeger, F., Schaumann, G. E. (2010): Proton nuclear magnetic resonance (NMR) relaxometry in soil science applications. *Open Magn. Reson. J.* 3, 15–26.
- Baveye, P., Vandevivere, P., Hoyle, B. L., DeLeo, P. C., Lozada, D. S. de (1998): Environmental Impact and Mechanisms of the Biological Clogging of Saturated Soils and Aquifer Materials. *Crit. Rev. Environ. Sci. Technol.* 28, 123–191.
- Belton, P. S. (1997): NMR and the mobility of water in polysaccharide gels. *Int. J. Biol. Macromol.* 21, 81–88.
- Benard, P., Zarebanadkouki, M., Carminati, A. (2018): Impact of Pore-Scale Wettability on Rhizosphere Rewetting. *Front. Environ. Sci.* 6.
- Benard, P., Zarebanadkouki, M., Hedwig, C., Holz, M., Ahmed, M. A., Carminati, A. (2018): Pore-Scale Distribution of Mucilage Affecting Water Repellency in the Rhizosphere. *Vadose Zone Journal* 17.
- Benard, P., Zarebanadkouki, M., Carminati, A. (2019): Physics and hydraulics of the rhizosphere network. *J. Plant Nutr. Soil Sci.* 182, 5–8.
- Bentz, J. (2018) Der Einfluss räumlich heterogener Grenzflächenspannungsverteilungen auf den kapillaren Aufstieg (Master Thesis).

- Buchmann, C., Bentz, J., Schaumann, G. E. (2015a): Intrinsic and model polymer hydrogel-induced soil structural stability of a silty sand soil as affected by soil moisture dynamics. *Soil Tillage Res.* 154, 22–33.
- Buchmann, C., Meyer, M., Schaumann, G. E. (2015b): Characterization of wet aggregate stability of soils by H-NMR relaxometry. *Magn. Reson. Chem.* 53, 694–703.
- Buchmann, C., Schaumann, G. E. (2017): Effect of water entrapment by a hydrogel on the microstructural stability of artificial soils with various clay content. *Plant Soil* 414, 181–198.
- Buchmann, C., Schaumann, G. E. (2018): The contribution of various organic matter fractions to soil–water interactions and structural stability of an agriculturally cultivated soil. *J. Plant Nutr. Soil Sci.* 181, 586–599.
- Brax, M., Buchmann, C., Schaumann, G. E. (2018): Effect of mucilage on water properties in the rhizosphere monitored by ¹H-NMR relaxometry. *Microporous Mesoporous Mater.* 269, 47–50.
- Brax, M., Schaumann, G. E., Diehl, D. (2019): Gel formation mechanism and gel properties controlled by Ca²⁺ in chia seed mucilage and model substances. *J. Plant Nutr. Soil Sci.* 182, 92–103.
- Brownstein, K. R., Tarr, C. E. (1979): Importance of classical diffusion in NMR studies of water in biological cells. *Phys. Rev. A* 19, 2446.
- Caesar-Tonthat, T. C. (2002): Soil binding properties of mucilage produced by a basidiomycete fungus in a model system. *Mycological Research* 106, 930–937.
- Callaghan, P. T., Coy, A., Halpin, T. P. J., MacGowan, D., Packer, K. J., Zelaya, F. O. (1992): Diffusion in porous systems and the influence of pore morphology in pulsed gradient spin-echo nuclear magnetic resonance studies. *J. Chem. Phys.* 97, 651–662.
- Capitani, M. I., Corzo-Rios, L. J., Chel-Guerrero, L. A., Betancur-Ancona, D. A., Nolasco, S. M., Tomás, M. C. (2015): Rheological properties of aqueous dispersions of chia (*Salvia hispanica* L.) mucilage. *J. Food Eng.* 149, 70–77.
- Carminati, A., Moradi, A. B., Vetterlein, D., Vontobel, P., Lehmann, E., Weller, U., Vogel, H.-J., Oswald, S. E. (2010): Dynamics of soil water content in the rhizosphere. *Plant Soil* 332, 163–176.
- Carminati, A., Schneider, C. L., Moradi, A. B., Zarebanadkouki, M., Vetterlein, D., Vogel, H.-J., Hildebrandt, A., Weller, U., Schüler, L., Oswald, S. E. (2011): How the Rhizosphere May Favor Water Availability to Roots. *Vadose Zone Journal* 10, 988–998.
- Carminati, A., Vetterlein, D. (2013): Plasticity of rhizosphere hydraulic properties as a key for efficient utilization of scarce resources. *Ann. Bot.* 112, 277–290.
- Carminati, A., Zarebanadkouki, M., Kroener, E., Ahmed, M. A., Holz, M. (2016): Biophysical rhizosphere processes affecting root water uptake. *Ann. Bot.*
- Chaboud, A., Rougier, M. (1984): Identification and Localization of Sugar Components of Rice (*Oryza sativa* L.) Root Cap Mucilage. *Journal of Plant Physiology* 116, 323–330.
- Chenu, C., Guérif, J. (1991): Mechanical Strength of Clay Minerals as Influenced by an Adsorbed Polysaccharide. *Soil Sci. Soc. Am. J.* 55, 1076–1080.
- Chenu, C. (1993): Clay-or sand-polysaccharide associations as models for the interface between micro-organisms and soil: water related properties and microstructure. *Geoderma* 56, 143–156.
- Chenu, C., Roberson, E. B. (1996): Diffusion of glucose in microbial extracellular polysaccharide as affected by water potential. *Soil Biology and Biochemistry* 28, 877–884.
- Codd, S. L., Vogt, S. J., Hornemann, J. A., Phillips, A. J., Maneval, J. E., Romanenko, K. R., Hansen, L., Cunningham, A. B., Seymour, J. D. (2011): NMR relaxation measurements of biofouling in model and geological porous media. *Org. Geochem.* 42, 965–971.
- Czarnes, S., Hallett, P. D., Bengough, A. G., Young, I. M. (2000): Root- and microbial-derived mucilages affect soil structure and water transport. *Eur. J. Soil Sci.* 51, 435–443.

- de Celis Alonso, B., Rayment, P., Ciampi, E., Ablett, S., Marciani, L., Spiller, R. C., Norton, I. T., Gowland, P. A. (2010): NMR relaxometry and rheology of ionic and acid alginate gels. *Carbohydr. Polym.* 82, 663–669.
- Dunn, K.-J., Bergman, D. J., LaTorraca, G. A. (2002): Nuclear magnetic resonance: petrophysical and logging applications. Pergamon, New York.
- Finzi, A. C., Abramoff, R. Z., Spiller, K. S., Brzostek, E. R., Darby, B. A., Kramer, M. A., Phillips, R. P. (2015): Rhizosphere processes are quantitatively important components of terrestrial carbon and nutrient cycles. *Global Change Biology* 21, 2082–2094.
- Gessa, C., Deiana, S. (1990): Fibrillar structure of Ca polygalacturonate as a model for a soil-root interface. *Plant Soil* 129, 211–217.
- Gessa, C., Deiana, S. (1992): Ca-polygalacturonate as a model for a soil-root interface. *Plant Soil* 140, 1–13.
- Ghanem, M. E., Han, R.-M., Classen, B., Quetin-Leclercq, J., Mahy, G., Ruan, C.-J., Qin, P., Pérez-Alfocea, F., Lutts, S. (2010): Mucilage and polysaccharides in the halophyte plant species *Kosteletzkya virginica*: Localization and composition in relation to salt stress. *J. Plant Physiol.* 167, 382–392.
- Godefroy, S., Korb, J.-P., Fleury, M., Bryant, R. G. (2001): Surface nuclear magnetic relaxation and dynamics of water and oil in macroporous media. *Phys. Rev. E* 64, 021605.
- Goh, K. K. T., Matia-Merino, L., Chiang, J. H., Quek, R., Soh, S. J. B., Lentle, R. G. (2016): The physico-chemical properties of chia seed polysaccharide and its microgel dispersion rheology. *Carbohydr. Polym.* 149, 297–307.
- Gosline, J. M., DeMont, M. E., Denny, M. W. (1986): The structure and properties of spider silk. *Endeavour* 10, 37–43.
- Götz, J., Hinrichs, R. (2008): Diffusion and Relaxation in Gels, in: Webb, G. A. (ed.): Modern Magnetic Resonance. Springer Netherlands, pp. 1713–1719.
- Gregory, P. J. (2006): Roots, rhizosphere and soil: the route to a better understanding of soil science? *Eur. J. Soil Sci.* 57, 2–12.
- Haichar, F. el Z., Santaella, C., Heulin, T., Achouak, W. (2014): Root exudates mediated interactions belowground. *Soil Biol. Biochem.* 77, 69–80.
- Hallett, P. D., Gordon, D. C., Bengough, A. G. (2003): Plant influence on rhizosphere hydraulic properties: direct measurements using a miniaturized infiltrometer. *New Phytol.* 157, 597–603.
- Herrling, M. P., Weisbrodt, J., Kirkland, C. M., Williamson, N. H., Lackner, S., Codd, S. L., Seymour, J. D., Guthausen, G., Horn, H. (2017): NMR investigation of water diffusion in different biofilm structures. *Biotechnol. Bioeng.* 114, 2857–2867.
- Hills, B. P., Cano, C., Belton, P. S. (1991): Proton NMR relaxation studies of aqueous polysaccharide systems. *Macromolecules* 24, 2944–2950.
- Hills, B. P., Godward, J., Debatty, M., Barras, L., Saturio, C. P., Ouwere, C. (2000): NMR studies of calcium induced alginate gelation. Part II. The internal bead structure. *Magn. Reson. Chem.* 38, 719–728.
- Hiltner, L. (1904): Über nevere Erfahrungen und Probleme auf dem Gebiet der Boden Bakteriologie und unter besonderer Berücksichtigung der Grundung und Broche. *Arb. Deut Landw Ges Berl.* 98, 59–78.
- Hinsinger, P., Plassard, C., Jaillard, B. (2006): Rhizosphere: A new frontier for soil biogeochemistry. *Journal of Geochemical Exploration* 88, 210–213.
- Holz, M., Leue, M., Ahmed, M. A., Benard, P., Gerke, H. H., Carminati, A. (2018): Spatial Distribution of Mucilage in the Rhizosphere Measured With Infrared Spectroscopy. *Front. Environ. Sci.* 6.

- Hotchkiss, A. T., Savary, B. J., Cameron, R. G., Chau, H. K., Brouillette, J., Luzio, G. A., Fishman, M. L. (2002): Enzymatic modification of pectin to increase its calcium sensitivity while preserving its molecular weight. *J. Agric. Food Chem.* 50, 2931–2937.
- Jaeger, F., Grohmann, E., Schaumann, G. E. (2006): ¹H NMR Relaxometry in natural humous soil samples: Insights in microbial effects on relaxation time distributions. *Plant and Soil* 280, 209–222.
- Jaeger, F., Shchegolikhina, A., Van As, H., Schaumann, G. E. (2010): Proton NMR relaxometry as a useful tool to evaluate swelling processes in peat soils. *Open Magn. Reson. J.* 3, 27–45.
- Jones, D. L., Nguyen, C., Finlay, R. D. (2009): Carbon flow in the rhizosphere: carbon trading at the soil–root interface. *Plant Soil* 321, 5–33.
- Kazanskii, K. S., Dubrovskii, S. A. (1992): Chemistry and physics of “agricultural” hydrogels, in: *Polyelectrolytes Hydrogels Chromatographic Materials*. Springer Berlin Heidelberg, pp. 97–133.
- Kimmich, R. (2012): *NMR: tomography, diffusometry, relaxometry*. Springer Science & Business Media.
- Kirkland, C. M., Herrling, M. P., Hiebert, R., Bender, A. T., Grunewald, E., Walsh, D. O., Codd, S. L. (2015): In Situ Detection of Subsurface Biofilm Using Low-Field NMR: A Field Study. *Environ. Sci. Technol.* 49, 11045–11052.
- Kirtil, E., Oztop, M. H., Sirijariyawat, A., Ngamchuachit, P., Barrett, D. M., McCarthy, M. J. (2014): Effect of pectin methyl esterase (PME) and CaCl₂ infusion on the cell integrity of fresh-cut and frozen-thawed mangoes: An NMR relaxometry study. *Food Res. Int.* 66, 409–416.
- Kleinberg, R. L. (1999): Nuclear Magnetic Resonance, in: *Methods in the Physics of Porous Media*. Series: Experimental Methods in the Physical Sciences, ISBN: 9780124759824. Elsevier, vol. 35, pp. 337–385.
- Knee, E. M., Gong, F.-C., Gao, M., Teplitski, M., Jones, A. R., Foxworthy, A., Mort, A. J., Bauer, W. D. (2001): Root Mucilage from Pea and Its Utilization by Rhizosphere Bacteria as a Sole Carbon Source. *Mol. Plant. Microbe Interact.* 14, 775–784.
- Kravtchenko, T. P., Voragen, A. G. J., Pilnik, W. (1992): Analytical comparison of three industrial pectin preparations. *Carbohydr. Polym.* 18, 17–25.
- Kroener, E., Zarebanadkouki, M., Kaestner, A., Carminati, A. (2014): Nonequilibrium water dynamics in the rhizosphere: How mucilage affects water flow in soils. *Water Resour. Res.* 50, 6479–6495.
- Kroener, E., Ahmed, M. A., Carminati, A. (2015): Roots at the percolation threshold. *Phys. Rev. E* 91, 042706.
- Kroener, E., Holz, M., Zarebanadkouki, M., Ahmed, M., Carminati, A. (2018): Effects of mucilage on rhizosphere hydraulic functions depend on soil particle size. *Vadose Zone Journal* 17.
- Lin, K.-Y., Daniel, J. R., Whistler, R. L. (1994): Structure of chia seed polysaccharide exudate. *Carbohydr. Polym.* 23, 13–18.
- Liu, J., Shi, B., Jiang, H., Bae, S., Huang, H. (2009): Improvement of water-stability of clay aggregates admixed with aqueous polymer soil stabilizers. *Catena* 77, 175–179.
- Marcombe, R., Cai, S., Hong, W., Zhao, X., Lapusta, Y., Suo, Z. (2010): A theory of constrained swelling of a pH-sensitive hydrogel. *Soft Matter* 6, 784–793.
- Martin, J. P. (1971): Decomposition and binding action of polysaccharides in soil. *Soil Biol. Biochem.* 3, 33–41.
- McCully, M. E. (1999): ROOTS IN SOIL: Unearthing the Complexities of Roots and Their Rhizospheres. *Annu. Rev. Plant Physiol. Plant Mol. Biol.* 50, 695–718.
- McCully, M. E., Boyer, J. S. (1997): The expansion of maize root-cap mucilage during hydration. 3. Changes in water potential and water content. *Physiol. Plant.* 99, 169–177.

- McNear Jr., D. H. (2013): The Rhizosphere - Roots, Soil and Everything In Between. *Nat. Educ. Knowl.* 4.
- Metzner, R., Eggert, A., van Dusschoten, D., Pflugfelder, D., Gerth, S., Schurr, U., Uhlmann, N., Jahnke, S. (2015): Direct comparison of MRI and X-ray CT technologies for 3D imaging of root systems in soil: potential and challenges for root trait quantification. *Plant Methods* 11, 17.
- Meyer, M., Buchmann, C., Schaumann, G. E. (2018): Determination of quantitative pore-size distribution of soils with ^1H NMR relaxometry. *European Journal of Soil Science* 69, 393–406.
- Mimmo, T., Marzadori, C., Francioso, O., Deiana, S., Gessa, C. E. (2003): Effects of aluminum sorption on calcium-polygalacturonate network used as soil-root interface model. *Biopolymers* 70, 655–661.
- Mimmo, T., Marzadori, C., Gessa, C. E. (2008): Does the degree of pectin esterification influence aluminium sorption by the root apoplast? *Plant Soil* 314, 159–168.
- Morel, J. L., Mench, M., Guckert, A. (1986): Measurement of Pb^{2+} , Cu^{2+} and Cd^{2+} binding with mucilage exudates from maize (*Zea mays* L.) roots. *Biol. Fertil. Soils* 2, 29–34.
- Moody, S. F., Clarke, A. E., Bacic, A. (1988): Structural analysis of secreted slime from wheat and cowpea roots. *Phytochemistry* 27, 2857–2861.
- Moradi, A. B., Carminati, A., Vetterlein, D., Vontobel, P., Lehmann, E., Weller, U., Hopmans, J. W., Vogel, H.-J., Oswald, S. E. (2011): Three-dimensional visualization and quantification of water content in the rhizosphere. *New Phytologist* 192, 653–663.
- Morel, J. L., Andreux, F., Habib, L., Guckert, A. (1987): Comparison of the adsorption of maize root mucilage and polygalacturonic acid on montmorillonite homoionic to divalent lead and cadmium. *Biol Fert Soils* 5, 13–17.
- Muhr, A. H., Blanshard, J. M. V. (1982): Diffusion in gels. *Polymer* 23, 1012–1026.
- Muñoz, L. A., Cobos, A., Diaz, O., Aguilera, J. M. (2012): Chia seeds: Microstructure, mucilage extraction and hydration. *J. Food Eng.* 108, 216–224.
- Naveed, M., Brown, L. K., Raffan, A. C., George, T. S., Bengough, A. G., Roose, T., Sinclair, I., Koebernick, N., Cooper, L., Hackett, C. A., Hallett, P. D. (2017): Plant exudates may stabilize or weaken soil depending on species, origin and time. *Eur J Soil Sci* 68, 806–816.
- Naveed, M., Ahmed, M. A., Benard, P., Brown, L. K., George, T. S., Bengough, A. G., Roose, T., Koebernick, N., Hallett, P. D. (2019): Surface tension, rheology and hydrophobicity of rhizodeposits and seed mucilage influence soil water retention and hysteresis. *Plant Soil*.
- Nguyen, C. (2003): Rhizodeposition of organic C by plants: mechanisms and controls. *Agronomie* 23, 375–396.
- Oades, J. M. (1978): Mucilages at the Root Surface. *J. Soil Sci.* 29, 1–16.
- Osborn, H. M. I., Lochey, F., Mosley, L., Read, D. (1999): Analysis of polysaccharides and monosaccharides in the root mucilage of maize (*Zea mays* L.) by gas chromatography. *Journal of Chromatography A* 831, 267–276.
- Oswald, S. E., Tötze, C., Haber-Pohlmeier, S., Pohlmeier, A., Kaestner, A. P., Lehmann, E. (2015): Combining Neutron and Magnetic Resonance Imaging to Study the Interaction of Plant Roots and Soil. *Phys. Procedia* 69, 237–243.
- Pemorading, X., Hallett, P. D., Zhang, B., Horn, R. (2011): Physical response of rigid and non-rigid soils to analogues of biological exudates. *Eur. J. Soil Sci.* 62, 676–684.
- Pieterse, C. M. J., Jonge, R. de, Berendsen, R. L. (2016): The Soil-Borne Supremacy. *Trends Plant Sci.* 21, 171–173.
- Průšová, A., Vergeldt, F. J., Kučerík, J. (2013): Influence of water content and drying on the physical structure of native hyaluronan. *Carbohydr. Polym.* 95, 515–521.

- Rabbi, S. M. F., Tighe, M. K., Flavel, R. J., Kaiser, B. N., Guppy, C. N., Zhang, X., Young, I. M. (2018): Plant roots redesign the rhizosphere to alter the three-dimensional physical architecture and water dynamics. *New Phytol.* 219, 542–550.
- Ray, T. C., Callow, J. A., Kennedy, J. F. (1988): Composition of Root Mucilage Polysaccharides from *Lepidium sativum*. *J. Exp. Bot.* 39, 1249–1261.
- Read, D. B., Gregory, P. J. (1997): Surface tension and viscosity of axenic maize and lupin root mucilages. *New Phytol.* 137, 623–628.
- Read, D. B., Gregory, P. J., Bell, A. E. (1999): Physical properties of axenic maize root mucilage. *Plant Soil* 211, 87–91.
- Read, D. B., Bengough, A. G., Gregory, P. J., Crawford, J. W., Robinson, D., Scrimgeour, C. M., Young, I. M., Zhang, K., Zhang, X. (2003): Plant roots release phospholipid surfactants that modify the physical and chemical properties of soil. *New Phytol.* 157, 315–326.
- Rosenzweig, R., Shavit, U., Furman, A. (2012): Water Retention Curves of Biofilm-Affected Soils using Xanthan as an Analogue. *Soil Science Society of America Journal* 76, 61.
- Sanderlin, A. B., Vogt, S. J., Grunewald, E., Bergin, B. A., Codd, S. L. (2013): Biofilm detection in natural unconsolidated porous media using a low-field magnetic resonance system. *Environ. Sci. Technol.* 47, 987–992.
- Sasse, J., Martinoia, E., Northen, T. (2018): Feed Your Friends: Do Plant Exudates Shape the Root Microbiome? *Trends Plant Sci.* 23, 25–41.
- Schaumann, G. E., Hobbey, E., Hurraß, J., Rotard, W. (2005): H-NMR Relaxometry to monitor wetting and swelling kinetics in high organic matter soils. *Plant Soil* 275, 1–20.
- Schaumann, G. E., Braun, B., Kirchner, D., Rotard, W., Szewzyk, U., Grohmann, E. (2007): Influence of biofilms on the water repellency of urban soil samples. *Hydrol. Process.* 21, 2276–2284.
- Schaumann, G. E., Bertmer, M. (2014): Soil-Water Interactions, in: Emagres: NMR Spectroscopy: A Versatile Tool for Environmental Research. John Wiley & Sons, Ltd., Chichester, UK, pp. 291–303.
- Sealey, L. J., McCully, M. E., Canny, M. J. (1995): The expansion of maize root-cap mucilage during hydration. 1. Kinetics. *Physiol. Plant.* 93, 38–46.
- Shannon, T. M., Steer, M. W. (1984): The root cap as a test system for the evaluation of Golgi Inhibitors: I. Structure and dynamics of the secretory system and response to solvents. *J. Exp. Bot.* 35, 1697–1707.
- Sposito, G. (2013): Green Water and Global Food Security. *Vadose Zone J.* 12.
- Ström, A., Ribelles, P., Lundin, L., Norton, I., Morris, E. R., Williams, M. A. K. (2007): Influence of Pectin Fine Structure on the Mechanical Properties of Calcium–Pectin and Acid–Pectin Gels. *Biomacromolecules* 8, 2668–2674.
- Sutherland, I. (2001): Biofilm exopolysaccharides: a strong and sticky framework. *Microbiol. Read. Engl.* 147, 3–9.
- Timilsena, Y. P., Adhikari, R., Kasapis, S., Adhikari, B. (2015): Rheological and microstructural properties of the chia seed polysaccharide. *Int. J. Biol. Macromol.* 81, 991–999.
- Todoruk, T. R., Langford, C. H., Kantzas, A. (2003): Pore-scale redistribution of water during wetting of air-dried soils as studied by low-field NMR relaxometry. *Environ. Sci. Technol.* 37, 2707–2713.
- Traoré, O., Groleau-Renaud, V., Plantureux, S., Tubeileh, A., Boeuf-Tremblay, V. (2000): Effect of root mucilage and modelled root exudates on soil structure. *Eur. J. Soil Sci.* 51, 575–581.
- van Veelen, A., Tourell, M. C., Koebernick, N., Pileio, G., Roose, T. (2018): Correlative Visualization of Root Mucilage Degradation Using X-ray CT and MRI. *Front. Environ. Sci.* 6.

- Vogt, S. J., Sanderlin, A. B., Seymour, J. D., Codd, S. L. (2013): Permeability of a growing biofilm in a porous media fluid flow analyzed by magnetic resonance displacement-relaxation correlations. *Biotechnol. Bioeng.* 110, 1366–1375.
- Volk, E., Iden, S. C., Furman, A., Durner, W., Rosenzweig, R. (2016): Biofilm effect on soil hydraulic properties: Experimental investigation using soil-grown real biofilm. *Water Resour. Res.* 52, 5813–5828.
- Watanabe, T., Misawa, S., Hiradate, S., Osaki, M. (2008): Characterization of root mucilage from *Melastoma malabathricum*, with emphasis on its roles in aluminum accumulation. *New Phytol.* 178, 581–589.
- Watt, M., McCully, M. E., Jeffree, C. E. (1993): Plant and bacterial mucilages of the maize rhizosphere: Comparison of their soil binding properties and histochemistry in a model system. *Plant Soil* 151, 151–165.
- Zhang, B., Hallett, P. D., Zhang, G. (2008): Increase in the fracture toughness and bond energy of clay by a root exudate. *Eur. J. Soil Sci.* 59, 855–862.
- Zhang, D., Chen, Y., Ma, Y., Guo, L., Sun, J., Tong, J. (2016): Earthworm epidermal mucus: Rheological behavior reveals drag-reducing characteristics in soil. *Soil and Tillage Research* 158, 57–66.
- Zheng, W., Zeng, S., Bais, H., LaManna, J. M., Hussey, D. S., Jacobson, D. L., Jin, Y. (2018): Plant Growth-Promoting Rhizobacteria (PGPR) Reduce Evaporation and Increase Soil Water Retention. *Water Resour. Res.* 54, 3673–3687.
- Zickenrott, I.-M., Woche, S. K., Bachmann, J., Ahmed, M. A., Vetterlein, D. (2016): An efficient method for the collection of root mucilage from different plant species—A case study on the effect of mucilage on soil water repellency. *J. Plant Nutr. Soil Sci.* 179, 294–302.

9. ANNEXES

9.1. List of abbreviations

AFM	Atomic force microscope
Ca-PGA	Calcium polygalacturonate
D	Self-diffusion coefficient of water
EPS	Exopolysaccharides
ESEM	Environmental scanning electron microscope
HMP	High methoxy pectin
HMW	High molecular weight
LMP	Low methoxy pectin
LMW	Low molecular weight
μ CT	Micro-computed tomography
NMR	Nuclear magnetic mesonance
PFG	Pulsed field gradient
PGA	Polygalacturonic acid

9.2. Picturing the network of “free” chia seed mucilage

0.1 wt% chia seed mucilage was produced following the procedure described in chapter 4 after extraction and freeze-drying of fresh gel. Drying of the gel prior to its picturing with the ESEM was also similar to the steps pursued with the glass beads in chapter 4.

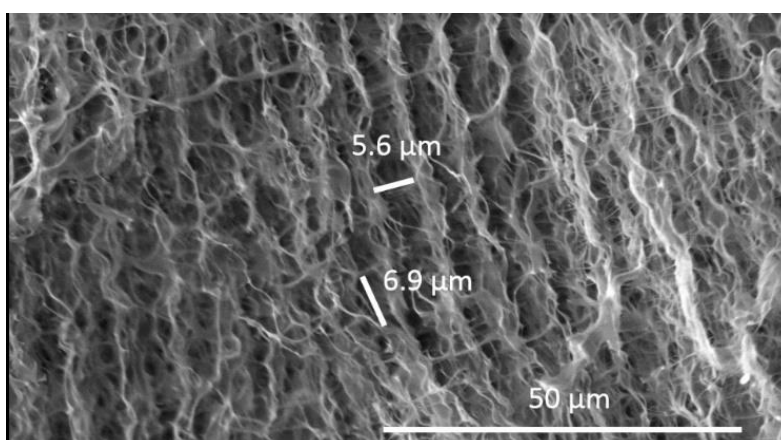


Figure 9.1. ESEM picture of chia seed mucilage network from a 0.1 wt% gel shock-frozen with N_2 (l) and then freeze-dried.

9.3. Supporting information of chapter 4

The formatting of the references in this annex corresponds to the formatting imposed by Geoderma.

Theoretical background about longitudinal and transverse relaxation

A ^1H -NMR relaxometry experiment involves exciting the nuclear magnetic moment of the protons by application of an RF pulse at the Larmor frequency and measuring the protons relaxation kinetics. Relaxation is a process by which the spins return to equilibrium, a state in which the populations of energy levels are predicted by the Boltzmann distribution, and in which no transverse magnetization or coherence is present in the system (Callaghan, 1993). Therefore, relaxation involves two processes: spin transitions between energy levels and transverse magnetization decaying to zero. The local transverse magnetic fields, which cause these energetic transitions, are often due to interactions of spins with one another or with the environment and oscillate close to the Larmor frequency. Thus, longitudinal or spin-lattice relaxation depends mainly on the interaction of the spins with their environment and describes how effective interactions between the spin system and the environment are in exchanging magnetic energy (Callaghan, 1993). Transverse relaxation destroys the coherence, or the transverse magnetization generated by the RF pulse, by destroying the alignment of the individual contributions. There are two mechanisms: 1) make the vectors jump to new positions at random, which requires transitions also causes longitudinal relaxation; 2) make the vectors get out of step with one another as a result of them precessing at different Larmor frequencies. This second mechanism is the dephasing of the spins due to local field inhomogeneity and variable molecular interactions (Callaghan 1993).

Comparison 1D and 2D measurements

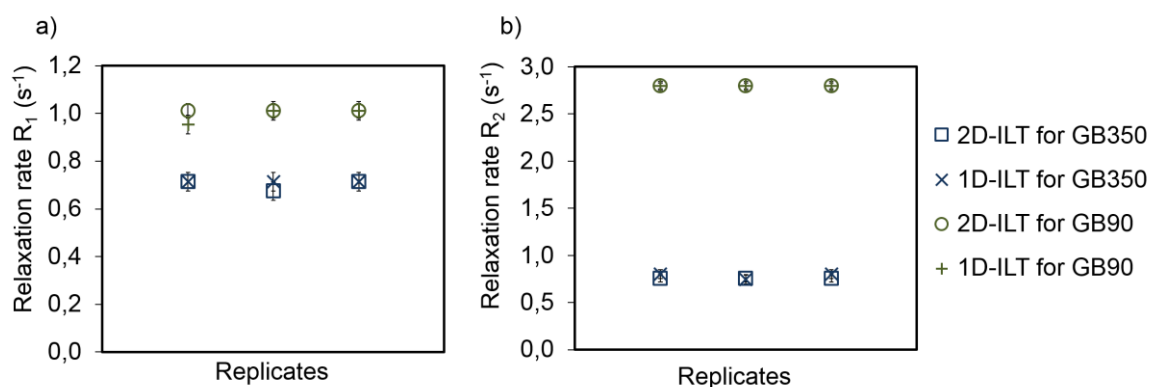


Figure 9.2. Comparison of the longitudinal relaxation rate (R_1) and transverse relaxation rate (R_2) obtained with 1D-ILT from conventional IR and CPMG pulse sequences with R_1 and R_2 obtained with 2D-ILT from T_1 - T_2 correlation measurement for GB350 and GB90 saturated with water.

X-ray computed microtomography of GB55

The inner spatial structure of GB55 mixed respectively with water, 0.1wt% and 1.0wt% mucilage was analyzed by μCT with the same conditions as for GB350 described in the article. Since the GB55 were too small to be segmented in a reliable way, their size distribution was not considered.

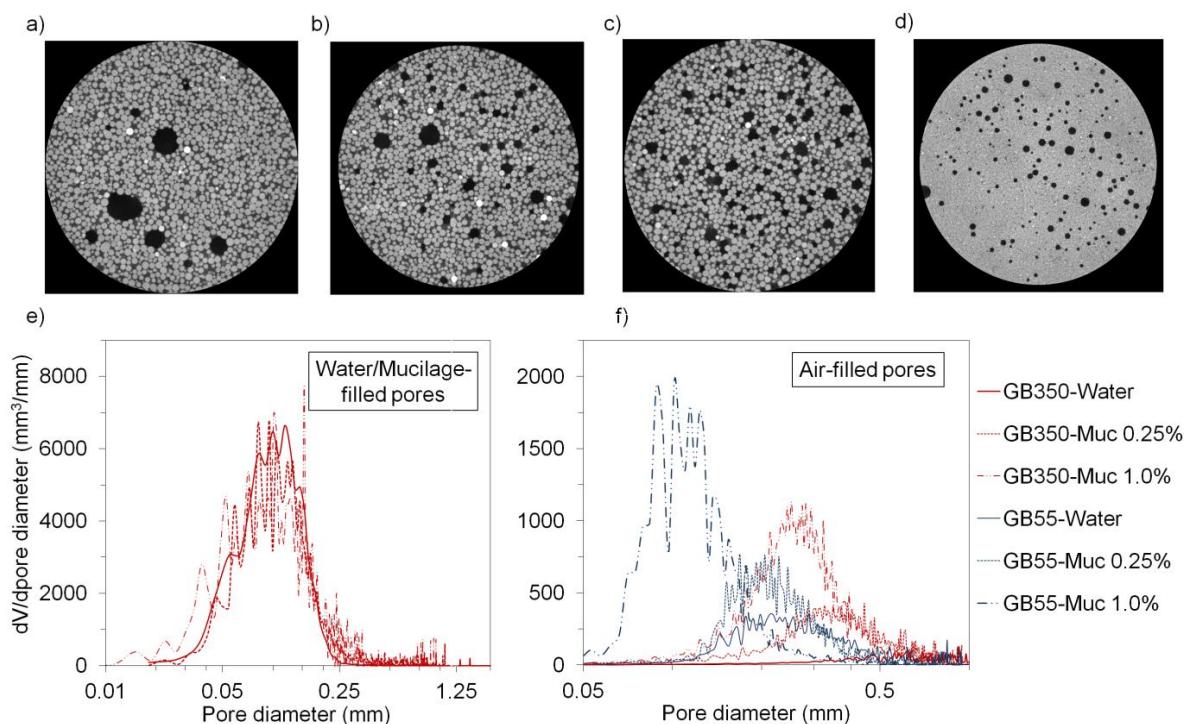


Figure 9.3. μ CT images of GB350 mixed with water (a), mucilage 0.25% (b), mucilage 1.0% (c) and of GB55 mixed with water (d). Volumetric pore size distribution of water- and mucilage-filled pores in GB350 (e), and volumetric air bubbles size distribution in GB55 and GB350 (f) in 2000 mm³ samples.

μ CT images were scanned for GB350 and for GB55 mixed with water, mucilage 0.25 wt%, and mucilage 1.0 wt%. The μ CT images (Figure 9.3a-d) show two-dimensional cuts from GB350 mixed with water (Figure 9.3a), mucilage 0.25 wt% (Figure 9.3b) and mucilage 1.0 wt% (Figure 9.3c), and a two-dimensional cut from GB55 mixed with water (Figure 9.3d). The gray value distribution allowed the segmentation between the glass beads (light gray spheres) and the pore space (dark gray and black area). The white dots might represent mineral impurities, which are denser than glass. Both dark gray, water could not be distinguished from mucilage due to their very similar density (Metzner et al., 2015). From Figure 9.4a to c the number of air bubbles (dark spheres) multiplied and their diameter decreased. The μ CT parameters did not permit to distinguish the particles from water in Figure 9.4d due to the limits of resolution, though the air bubbles were big enough and showed a sufficient contrast to be measured.

Statistical values characterizing the linear relationships between R_1/R_2 and the reciprocal glass beads diameter for all mucilage concentrations

Table 9.1. Statistical values characterizing the linear relationships between R_1/R_2 and the reciprocal glass beads diameter for all mucilage concentrations.

Mucilage concentration		0	0.1	0.25	0.50	0.75	1
R_1	pearson R	1.00	1.00	0.99	0.99	0.99	0.98
	R ²	0.99	0.99	0.99	0.98	0.99	0.96
	p-value	1.5E-11	3.4E-12	3.3E-10	2.2E-09	2.4E-11	2.0E-07
R_2	pearson R	1.00	1.00	1.00	0.99	0.99	0.98
	R ²	0.99	0.99	0.99	0.98	0.99	0.97

p-value	1.4E-11	1.5E-11	3.0E-11	2.2E-09	1.5E-10	4.1E-08
---------	---------	---------	---------	---------	---------	---------

Water self-diffusion coefficient measured with pulse field gradient (PFG)-NMR

Material and methods

PFG-NMR measurements were performed with a Bruker Minispec MQ (Bruker, Karlsruhe, Germany) at a magnetic field strength of 0.176 T using the standard application “Diffusio” provided by Bruker BioSpin (Bruker, Karlsruhe, Germany). A linear magnetic field gradient G ($T\ m^{-1}$) was aligned during the 1H -NMR relaxometry measurement to determine the self-diffusion coefficients D ($m^2\cdot s^{-1}$) (Stejskal and Tanner, 1965). The NMR spin-echo signal intensity I at a given magnetic field strength B is described as

$$I = I_0 \cdot e^{-(b \cdot D)} \quad (1)$$

Where

$$b = (-\gamma \cdot G \cdot \delta)^2 \cdot \left(\Delta - \frac{\delta}{3} \right) \quad (2)$$

I_0 is the initial signal intensity without magnetic field gradient, γ is the nucleus specific gyromagnetic ratio of a proton (2.675×10^8 rad/T·s), G is the strength of the gradient pulses, δ is the duration of the field gradient pulse and Δ is the observation time between two applied gradient pulses. The measured loss in intensity directly results from the self-diffusion of water in the sample during the interval Δ (Stejskal and Tanner, 1965).

The pulse parameters were set at $\delta = 1$ ms and $\Delta = 10$ ms as in Buchmann and Schaumann (2017) and G varied between 0 and $1.6\ T\cdot m^{-1}$. The self-diffusion coefficient of water in the samples D was normalized to that of pure water D_0 . D/D_0 was measured after the T_1 - T_2 measurement described in the manuscript for the same samples.

Results and discussion

Figure 9.4 shows the normalized self-diffusion coefficient of water D/D_0 in chia mucilage at several concentrations.

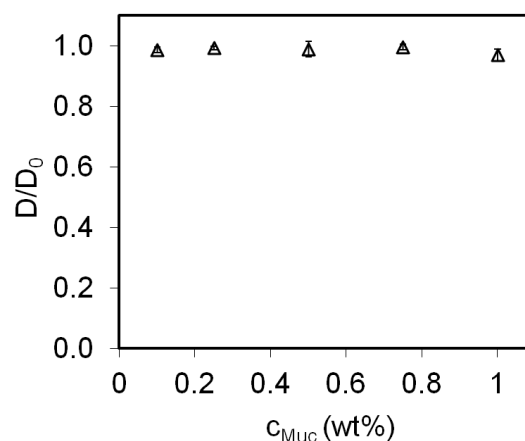


Figure 9.4. Self-diffusion coefficient of water D/D_0 in chia mucilage at several concentrations.

Surprisingly, the self-diffusion coefficient of water in chia mucilage equaled the one of pure water despite the increasing mucilage concentration. The principal reason is probably that the diffusion time $\Delta = 10$ ms was too short for the water molecules in chia mucilage to encounter the physical barriers of the polymer network (Hills et al., 2000). The D/D_0 of hydrogels is typically determined as a function of the diffusion time, which allows calculation of several parameters such as the critical pore radius or the tortuosity (Sen et al., 1994). Unfortunately, measurements of D/D_0 for Δ greater than 50 ms did not provide acceptable results using the available instrument.

Figure 9.5 shows the normalized self-diffusion coefficient of water D/D_0 in GB-Water and GB-Mucilage for several glass beads sizes and mucilage concentrations.

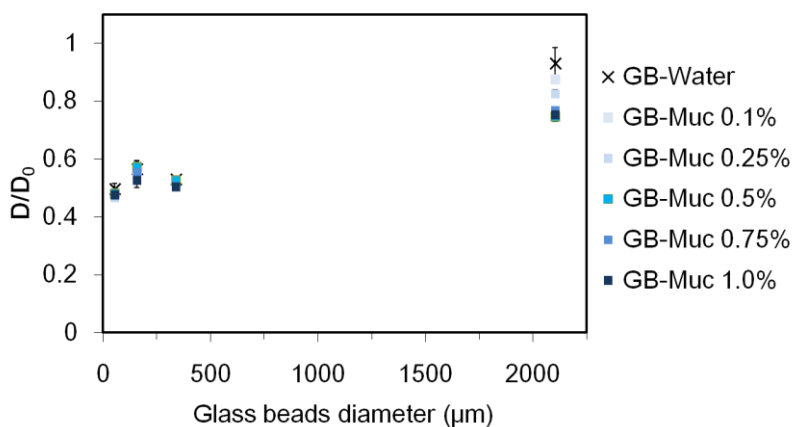


Figure 9.5. Self-diffusion coefficient of water D/D_0 in GB-Water and GB-Mucilage for several glass beads sizes and mucilage concentrations.

The D/D_0 decreases strongly from GB2000 to GB350 due to the reduction of the pore size, but remains around 0.5 for GB350, GB150 and GB50. Contrary to the D/D_0 of pure mucilage, the increasing concentration of mucilage affects the D/D_0 of GB2000. This is in accordance with the idea ventured in the manuscript that the properties of the mucilage network change in the porous system. Yet, mucilage concentration had little effect on the D/D_0 of the smallest glass beads. According to the manuscript, this could be related to the increase of the pore size of the smallest glass beads with the mucilage concentration.

All in all, the interpretation of the D/D_0 for GB-Mucilage remains difficult due to the complex processes happening at the pore-scale and to the up-to-now incomplete understanding and characterization of the D/D_0 of pure mucilage.

References

- Buchmann C., Schaumann G. E., (2017) Effect of water entrapment by a hydrogel on the microstructural stability of artificial soils with various clay content. *Plant Soil* 414:181–198.
- Butler, J., Reeds, J., Dawson, S., (1981) Estimating Solutions of First Kind Integral Equations with Nonnegative Constraints and Optimal Smoothing. *SIAM J. Numer. Anal.* 18, 381–397.

Callaghan P. T., (1993) Principles of nuclear magnetic resonance microscopy. Oxford University Press

Keating, K., Knight, R., 2006. A laboratory study to determine the effect of iron oxides on proton NMR measurements. *Geophysics* 72, E27–E32.

Metzner, R., Eggert, A., van Dusschoten, D., Pflugfelder, D., Gerth, S., Schurr, U., Uhlmann, N., Jahnke, S., 2015. Direct comparison of MRI and X-ray CT technologies for 3D imaging of root systems in soil: potential and challenges for root trait quantification. *Plant Methods* 11, 17.

Mitchell, J., Chandrasekera, T.C., Johns, M.L., Gladden, L.F., Fordham, E.J., 2010. Nuclear magnetic resonance relaxation and diffusion in the presence of internal gradients: the effect of magnetic field strength. *Phys. Rev. E Stat. Nonlin. Soft Matter Phys.* 81, 026101.

Sen, P.N., Schwartz, L.M., Mitra, P.P., 1994. Probing the structure of porous media using NMR spin echoes. *Magn. Reson. Imaging, Proceedings of the Second International Meeting on Recent Advances in MR Applications to Porous Media* 12, 227–230.

Stejskal, E.O., Tanner, J.E., 1965. Spin Diffusion Measurements: Spin Echoes in the Presence of a Time-Dependent Field Gradient. *J. Chem. Phys.* 42, 288–292.

10. CURRICULUM VITAE

Personal data

Date/Place of birth 27 April 1990 - Paris
 Nationality French
 Phone 0049 176 22 30 14 35
 Address Konrad-Adenauer Strasse 26
 76829 Landau in der Pfalz
 Germany
 e-Mail brax@uni-landau.de



Professional Experience

- Oct. 2014 – ongoing: **University of Koblenz-Landau (Germany)**
 Scientific staff in the groups of Prof. Dr. G. E. Schaumann / Environmental and Soil Chemistry
- July – Sept. 2013: **University of Bielefeld (Germany)**
 Internship in the group of Prof. Dr. H. Gröger / Biocatalysis in organic synthesis: Reactivity of the enzyme *Candida Antarctica* Lipase B with several amines under various reaction conditions.
- Oct. 2012 - April 2013: **University of Queensland – Brisbane (Australia)**
 Internship in the group of Prof. Dr. P. Bernhardt / Inorganic chemistry: Influence of the substituents of a conjugated bis-dithiocarbamate Schiff base ligand on the stabilisation of a trivalent copper complex.
- July - Sept. 2011: **University of Bielefeld (Germany)**
 Research assistant in the group of Prof. Dr. A. Godt / Organic and polymer chemistry: Synthesis of different precursors for polymer chemistry as part of the SFB 613 Project.
- June - July 2010: **University of Bielefeld (Germany)**
 Internship in the group of Prof. Dr. N. Sewald, supervised by Dr. Benedikt Sammet/ Organic chemistry: Several projects related to the synthesis of cryptophycine fragments.
- May - July 2008: **Eco-Tour Barahona (Dominican Republic)**
 Tourist guide (helping to supervise groups of ten people during excursions), logistic manager for the different excursion programs.

Education

- 2011 - 2014: **University of Bielefeld (Germany)**
- Master of Science in Chemistry, profile synthesis**
- Specialization in organic and inorganic chemistry
 - Topic of the master thesis: Synthesis of chiral alcohols *via* combination of Wacker oxidation and enzymatic reduction with superabsorber-supported catalysts
- 2008 - 2011: **University Paris–Diderot Paris VII (France) - University of Bielefeld (Germany)**
- French-German Bachelor degree in Chemistry sponsored by the UFA**
- 3 first semesters in Bielefeld, 3 last semesters in Paris
 - Topic of the bachelor thesis: Synthese eines durch Click Chemie funktionalisierbaren Bausteins für stäbchenförmige Moleküle und oligo-PPEs (oligo(para-phenyleneethynylene)s).
- 2007 - 2008: **University Paris IX Dauphine**
- Bachelor's degree in economics and management not continued because of a higher interest in scientific studies
- June 2007: **Lycée Sainte Marie de Neuilly (France)**
- French baccalaureate majoring in Sciences (mathematics, physics, chemistry)

Publications

Brax, M., Köhne, M., Kroener, E., Schaumann, G., Potential of NMR relaxometry to unravel the properties of mucilage in several model soils, *Geoderma*, **(in production)**.

Brax, M., Schaumann, G. E., Diehl, D., Gel formation mechanism and gel properties controlled by Ca²⁺ in chia seed mucilage and model substances, *J. Plant Nutr. Soil Sci.*, **(n.d)**, 0.

Brax, M., Buchmann, C., Schaumann, G. E., Effect of mucilage on water properties in the rhizosphere monitored by 1H-NMR relaxometry. *Microporous Mesoporous Mater.* **2018**, 269, 47–50.

Brax, M., Buchmann, C., Schaumann, G. E., Biohydrogel induced soil–water interactions: how to untangle the gel effect? A review. *J. Plant Nutr. Soil Sci.*, **2017**, 180, 121–141.

Bernhardt P.V., Brax M. A., England J., Farlow A. J., Hanson G. R., Yeng L. L., Mirza A. H., Wiegardt K., The trivalent copper complex of a bis-dithiocarbamate Schiff base: stabilization of Cu in three different oxidation states, *Inorg Chem.*, **2013**, 52 (3), 1650-1657.

Sammet B., Brax M., Sewald N., A two step synthesis of a key unit B precursor of cryptophycins by asymmetric hydrogenation, *Beilstein*, **2011**, 6, 243-245.

Oral presentations

Brax, M., Buchmann, C., Kenngott, K., Schaumann, G. E., Diehl, D., Role of sugars in the contribution of root exudates to soil structural stability, MicroSoil2018, Saint Loup Lamairé, France, June 2018.

Brax, M., Buchmann, C., Schaumann, G. E: Effect of mucilage on water properties in the rhizosphere monitored by ¹H-NMR relaxometry. MRPM 13, Bologna, Italy, September 2016.

Brax, M., Buchmann, C., Schaumann, G. E: The „gel effect“: effect of mucilage on water properties in the rhizosphere. Biohydrology Almeria, Spain, September 2016.

Brax, M., Köhne, M., Schaumann, G. E: Untangle soilwater-mucilage interactions with ¹H-NMR relaxometry. DBG Jahrestagung, Göttingen, Germany September 2017.

Brax, M., Buchmann, C., Schaumann, G. E: Untangle soil-water-mucilage interactions: ¹H NMR relaxometry is lifting the veil. EGU Vienna, Austria, April 2017.

Poster presentations

Schultze, N., Brax, M., Banfield, C., Dippold, M., Schaumann, G. E., Vetterlein, D., Young root mucilage of white lupine, field bean, winter wheat and maize: how does their chemical composition differ from each other? DBG Jahrestagung, Göttingen, Germany, September 2017.

Brax, M., Vetterlein, D., Carminati, A., Schaumann, G. E.: Characterization of water binding in a model mucilage using ¹H-NMR relaxometry. DBG Jahrestagung, München, Germany, September 2015.